Appendix A

Martin Bartholet, Christof Zwyssig, ”Permanent-Magnet Generators with Series Compensation, Diode Rectifier and DC/DC Converter for Wind Turbine Applications”, Chalmers tekniska högskola, Göteborg, Sverige, examensarbete, 2004.

THESIS FOR THE MASTER OF SCIENCE DEGREE

Permanent-Magnet Generators with Series Compensation, Diode Rectifier and DC/DC Converter for Wind Turbine Applications

Martin Bartholet and Christof Zwyssig

Department of Electric Power Engineering
CHALMERS UNIVERSITY OF TECHNOLOGY
Göteborg, Sweden 2004

Permanent-Magnet Generators with Series Compensation, Diode Rectifier and DC/DC Converter for Wind Turbine Applications

Martin Bartholet and Christof Zwyssig

© Martin Bartholet and Christof Zwyssig, 2004.

Technical Report No. 104E
Department of Electric Power Engineering
CHALMERS UNIVERSITY OF TECHNOLOGY
SE-412 96 Göteborg
Sweden
Telephone + 46 (0)31 772 1000

Chalmers Reproservice
Göteborg, Sweden 2004

Titel Permanentmagnetiserande generatorer med seriekompensation, diodlikriktare och DC/DC omvandlare för vindturbintillämpningar.
Title in english Permanent-magnet generators with series compensation, diode rectifier and DC/DC converter for wind turbine applications.
Författare/Author Martin Bartholet Christof Zwyssig
Utgivare/Publisher Chalmers Tekniska Högskola Institutionen för elteknik 412 96 Göteborg, Sverige
ISSN 1401-6184
Examensarbete/M.Sc. Thesis No. 104E
Ämne/Subject Kraftelektronik
Examinator/Examiner Ola Carlson
Datum/Date 20084-08-31

Tryckt av/Printed by Chalmers tekniska högskola 412 96 GÖTEBORG

Abstract

A wind turbine unit with direct current (DC) output is investigated in this thesis. It consists of a permanent-magnet synchronous generator (PMSG), series capacitors, a diode rectifier and a DC/DC converter. In order to experimentally verify the results obtained by calculation and simulation, a lab setup, including a DC/DC converter, is built. Simulation and measurement show good agreement, such that the models can be used for further research.

Series compensation and a diode rectifier in connection with a PMSG is analyzed and compared to other electrical systems considering power output. It is found to perform well for wind turbine applications and is a cheap and effective way of rectifying.

The DC/DC converter is investigated with respect to problems that arise when upscaling the wind turbine unit to higher power. It is found that the inductor has to be designed carefully and the stresses on the semiconductors might have to be limited with additional snubber circuits. Torque control of the PMSG by controlling the input current of the converter is realized.

For the Hönö test wind turbine, which is similar to the wind turbine unit with DC output, a new electrical configuration is proposed. Series instead of parallel compensation leads to a higher power output and lower losses at no and low load. Furthermore, the problem with overvoltage at low load is solved.

Acknowledgements

This work has been carried out at the Department of Electric Power Engineering at Chalmers University of Technology, Göteborg, Sweden from March to September 2004.

We would like to thank our supervisor, Assoc. Prof. Ola Carlson, and all the members of the department for help and input in all different areas of our thesis. We will also never forget the great time we spent together with you beside work.

A special thank goes to Prof. Dr. Johann W. Kolar of the Power Electronic Systems Laboratory, Swiss Federal Institute of Technology (ETH), Zurich, and Prof. Tore M. Undeland of the Department of Electric Power Engineering, Chalmers University of Technology, Göteborg, who made our thesis work at Chalmers possible.

Martin Bartholet and Christof Zwyssig
31st August 2004

Contents

Abstract **v**

Acknowledgements **vii**

Contents **ix**

1 Introduction **1**
1.1 DC in Wind Energy . . . 1
1.2 Possible Applications . . . 1
1.2.1 Offshore Wind Farms . . . 1
1.2.2 Wind Diesel Systems . . . 3
1.2.3 Wind Hydrogen Systems . . . 3
1.3 Wind Turbine Unit with DC Output . . . 4
1.3.1 Currently used Wind Turbine Configurations . . . 4
1.3.2 Generator and Rectifier Selection . . . 5
1.3.3 DC/DC Converter Selection . . . 6
1.3.4 Summary . . . 7
1.4 Outline of Thesis . . . 7

2 The Hönö Wind Turbine **9**
2.1 Blades . . . 9
2.2 Generator . . . 10
2.2.1 Resistance . . . 11
2.2.2 Back EMF . . . 11
2.2.3 Current Limit . . . 12
2.2.4 Inductance . . . 12
2.2.5 Summary of the Generator Data . . . 13
2.3 Electrical System . . . 14
2.4 Wind Turbine Controller . . . 15
2.5 Modelling . . . 16
2.5.1 Aerodynamical Model . . . 17
2.5.2 Mechanical Model . . . 17
2.5.3 Electrical Model . . . 17
2.5.4 Wind Turbine Controller . . . 18

3 Compensation **19**
3.1 Parallel Compensation . . . 19
3.2 Series Compensation . . . 21

4 Analysis of Different Electrical Systems for the Hönö Turbine **23**
4.1 Maximum Power . . . 23
4.2 Terminal Voltage . . . 24

4.3 DC Power . . . 27
4.4 No Load . . . 29
4.5 Simulation of the Full Model . . . 30
4.6 Proposed New Electrical Configuration . . . 31

5 DC/DC Converter 33
5.1 Inductor . . . 33
5.1.1 Parasitic Capacitance of the Inductor . . . 35
5.2 Current Controller . . . 36
5.3 Voltage and Current Measurement . . . 38
5.4 Overcurrent Protection . . . 39
5.5 Measurements . . . 39
5.5.1 Current and Voltage Stress on Inductor and Semiconductors . 39
5.5.2 Delays and Switching Transients . . . 42
5.5.3 Current Step . . . 47
5.6 Summary . . . 48

6 Experimental Lab Setup of a Wind Turbine Unit with DC Output 49
6.1 System Description . . . 49
6.1.1 DC Machine as Aerodynamic System . . . 49
6.1.2 PMSM . . . 49
6.1.3 Series Compensation . . . 50
6.1.4 Diode Rectifier . . . 51
6.1.5 Boost Converter . . . 51
6.1.6 Output Connection . . . 51
6.2 Modelling . . . 51
6.3 Comparing Simulation and Measurements . . . 52
6.3.1 DC Power . . . 52
6.3.2 Input Voltage . . . 52
6.4 Measurements for DC Link Application . . . 56

7 Conclusion 58
7.1 Future Work . . . 58

A Hönö - Electrical System 59

B Hönö - $C_p(\lambda)$ Values of the Blades 60

C Hönö - Model 61

D Hönö - Measurements 62

E Laboratory Setup - Overcurrent Protection 65

F Laboratory Setup - Simulink Model 67

References **70**

1 Introduction

1.1 DC in Wind Energy

In the past years there has been a lot of research and discussion on DC in power systems in general, and in connection with wind turbines in particular. There are several plans for large wind parks, mainly located offshore. For the usually long distance to the point of common coupling (PCC), high voltage direct current (HVDC) transmission can be favorable, because of the well known problem with capacitive current generation of long alternating current (AC) cables. With that, DC in the wind park down to the wind turbine may become interesting.

For small, isolated grids, wind-hybrid systems are a possibility, wind-diesel and wind-hydrogen being two examples. To be able to connect different power plants together, a DC link is a good solution [1]. Therefore, also the wind turbine should be able to feed into the DC link. An AC grid can be controlled and fed by an inverter.

For all the configurations discussed here, the common part is a wind turbine unit with a controllable DC output. The electrical part of such a unit consists of a generator, rectifier and possibly a DC/DC converter.

1.2 Possible Applications

1.2.1 Offshore Wind Farms

One of the reasons for DC in wind turbines is the trend to large offshore wind farms, where HVDC transmission becomes interesting. For a system that is frequently proposed the AC transmission is replaced by a HVDC connection. In variable speed tur-

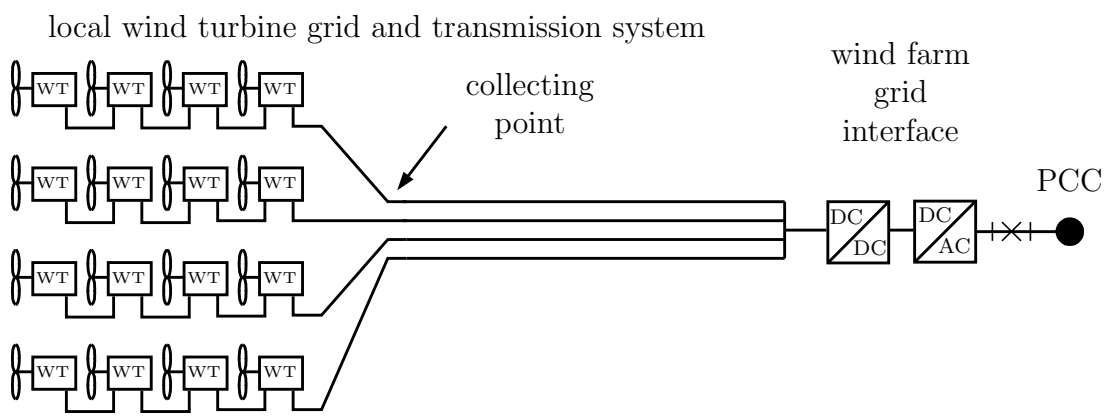

Fig. 1.1: Electrical system of the small DC wind park, adapted from [3].

bines, in connection with synchronous generators (usually direct-driven synchronous generators), a full AC-DC-AC converter is needed to connect the generator to the normal AC grid. Therefore, solutions have been proposed to directly connect wind turbines to a DC grid [2]. In that case only a rectifier is needed in the wind turbines.

The transmission is DC as well, and there is a single large inverter that feeds the power from the wind farm into the grid.

The first approach is to simply connect all wind turbine DC outputs. To feed into the mains a DC transformer and an inverter is needed (Fig. 1.1). This is referred to as the small DC wind park [3], and is considered for short distances to the PCC.

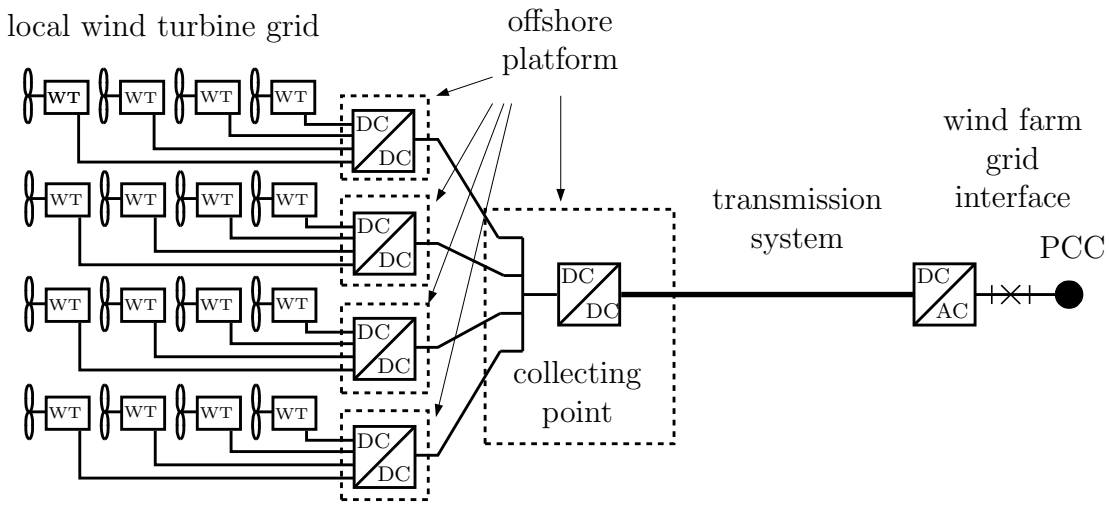

Fig. 1.2: Electrical system of the large DC wind park, adapted from [3].

The second approach has a long transmission and therefore needs a high voltage in order to have low losses. This is achieved by rising the wind turbine output voltage with one or several DC transformers before transmission (Fig. 1.2). This is referred to as the large DC wind park [3]. It has been analyzed with respect to cost, operation and faults [3, 4, 5].

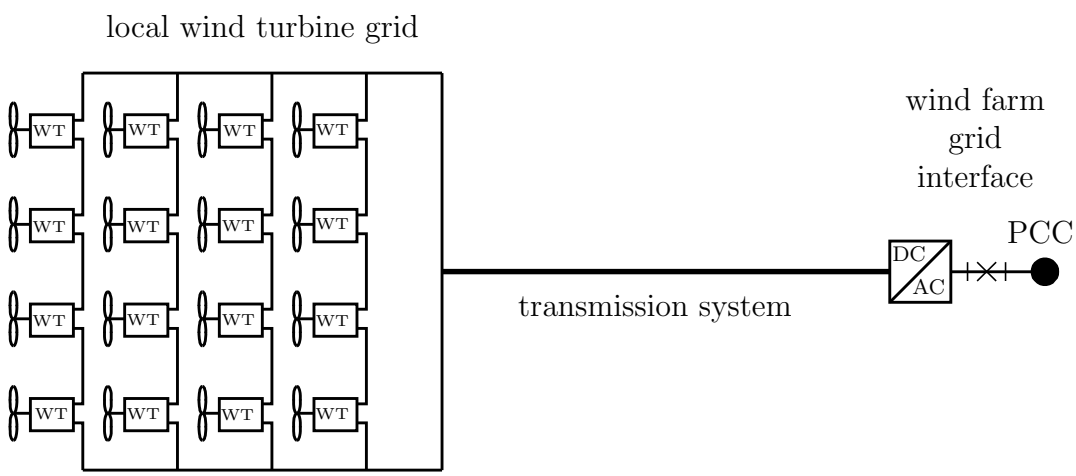

Fig. 1.3: Electrical system of the series DC wind park, adapted from [3].

Furthermore, there exists the idea of connecting the DC outputs of a certain

number of turbines in series to achieve a higher voltage for transmission [6]. This is referred to as the series DC wind park [3], (Fig. 1.3).

1.2.2 Wind Diesel Systems

For isolated grids, research has been conducted on wind-hybrid systems. One difficulty is that standard wind turbines are designed for a common connection to a large grid. High wind penetration therefore needs special attention concerning control of grid frequency and voltage. One possible solution is to install a DC link where the different power plants are connected. The AC grid is controlled by an inverter. One example is a hybrid system with a wind turbine and a diesel generator set (genset), which has been developed from the Svenska Högarna project [7]. The new system has a common DC link that can be fed by different power plants (Fig. 1.4). With this, the diesel generator does not have to operate at constant speed and can start quickly without synchronization, which keeps the number of engine starts down.

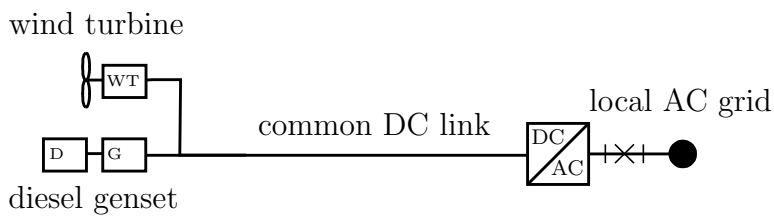

Fig. 1.4: Electrical system of a wind diesel system with DC link, adapted from [7].

1.2.3 Wind Hydrogen Systems

The drawback of a wind diesel system is that surplus wind energy in case of high wind speed can not be stored without additional energy storage. In recent years, wind hydrogen systems have been studied. Combining a wind turbine with an electrolyzer allows surplus wind energy to produce hydrogen. In case of low wind this can be used to produce electrical energy in fuel cells or gas turbines, but also for other applications such as heating or transportation. There are different ideas where these kind of systems can be used [8]:

- In local stand-alone systems with no grid connection, surplus wind energy may be used for hydrogen production
- In systems with a limited transmission capacity, e.g. at islands with a submarine cable to shore, or in areas with weak transmission, surplus wind energy may be used to produce hydrogen
- In systems where the portion of wind power integrated into the power system is already meeting system limits and more wind power may cause problems

for the power system operation. In this case, the increased wind power may be used for production of hydrogen.

A possible layout of a small stand-alone wind-hydrogen system consists of a wind turbine, battery storage, an electrolyzer, a compressor, a hydrogen storage tank and a demand for hydrogen used as a fuel for transportation (Fig. 1.5). Both electrolyzer and battery need DC, the hydrogen production is controlled by a DC/DC converter. Because of these requirements, the connection between the different parts of the system is a DC bus.

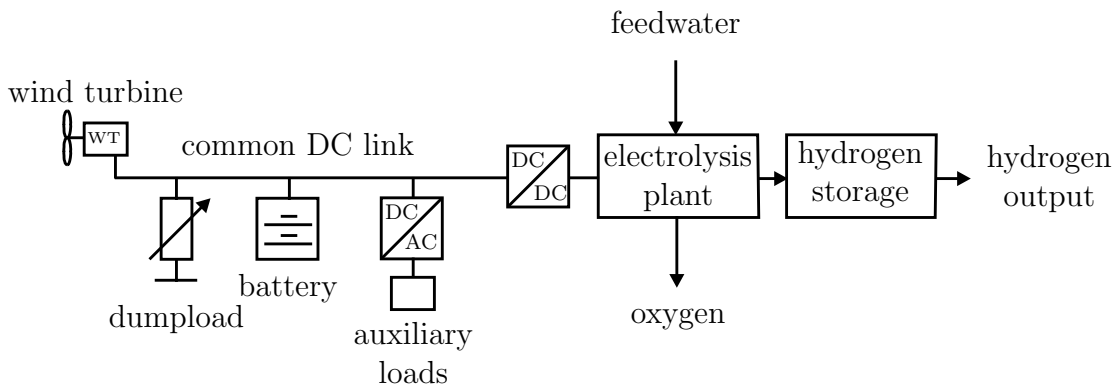

Fig. 1.5: Setup of an isolated wind hydrogen system, adapted from [8].

1.3 Wind Turbine Unit with DC Output

As mentioned in Chapter 1.1, the common part of all the configurations is a wind turbine unit with a controllable DC output. However, classical wind turbines are directly coupled to the AC grid.

1.3.1 Currently used Wind Turbine Configurations

There exist three state-of-the-art wind turbine configurations [9]:

Fixed Speed, Squirrel Cage Induction Generator The generator is coupled to the blades through a gearbox. The advantage is that a standard (mostly 1500 rpm) squirrel cage generator can be used. The disadvantages are the lower energy yield than variable speed turbines and the additional drive train and gearbox (cost, losses, maintenance).

Variable Speed, Doubly-Fed Induction Generator The generator is coupled to the blades through a gearbox. The stator is directly connected to the grid, whereas the rotor is connected to a converter. The advantage is that a standard doubly fed induction generator (mostly 1500 rpm) can be used and the optimal energy is captured due to variable speed. The disadvantages are the additional

drive train and gearbox (cost, losses, maintenance) and the converter (cost, losses).

Variable Speed, Direct-Driven Generator Here the generator is directly coupled to the blades. A full frequency converter is needed for connection to the grid. The advantages are to eliminate the disadvantages of the above. The disadvantages are the losses in the converter and the specially designed, large and heavy generator.

1.3.2 Generator and Rectifier Selection

All generators described in Chapter 1.3.1 produce AC. In the case of a DC output of the turbine, a rectifier is needed. That is an additional component in the first two configurations mentioned in Chapter 1.3.1, but one less in the last. This, in addition to economic reasons [10], is why the direct-driven generator becomes the preferred choice for a wind turbine unit with DC output. Different generator types have been analyzed and the permanent-magnet synchronous generator is found to be the best choice for this application [11]. Furthermore, four different rectifiers (Fig. 1.6) have been compared in connection with a direct-driven wind turbine generator [12]:

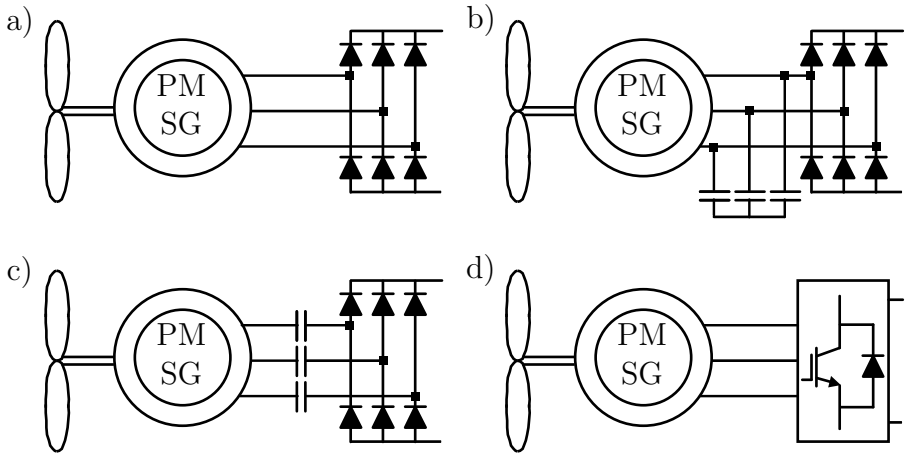

Fig. 1.6: The four compared rectifiers for a direct-driven permanent-magnet synchronous generator, a) plain diode rectifier, b) parallel (shunt) compensated diode rectifier, c) series compensated diode rectifier and d) transistor rectifier, adapted from [12].

Plain Diode Rectifier The advantages are the low losses and low cost. The disadvantage is that it keeps the terminal voltage in phase with the current, which leads, in connection with the large inductance of a direct-driven generator, to a low output power. Furthermore the DC voltage varies with generator speed and load.

Parallel (Shunt) Compensated Diode Rectifier To improve the performance of the above, shunt capacitors are introduced. They can be selected to maximize the rated power of the generator. The drawbacks are the reactive currents produced at no and low load and the decreasing compensation with increasing load, where the need for compensation increases as well.

Series Compensated Diode Rectifier To retain the advantages of the diode rectifier and overcome the disadvantages of parallel compensation, series compensation was designed. Because the capacitors are in series with the inductance of the generator, the compensation increases with the load, where also the need for compensation increases. For low speed the series compensation overcompensates. For wind turbine applications this is no problem, because low speed means low power [13].

Transistor Rectifier The transistor rectifier allows, in contrary to the other solutions, a full control over the generator current and flux linkage at all loads and speeds. It can also produce a constant DC voltage independent of the generator speed. The disadvantages are the higher losses in the rectifier and cost.

Plain and parallel compensated diode rectifiers are not suitable for wind turbine applications. The series compensated diode rectifier is found to be an interesting alternative to the transistor rectifier. It almost performs as well and will have less rectifier losses and may lead to a more cost effective system. Therefore, this rectifier is chosen in this work.

1.3.3 DC/DC Converter Selection

The series compensated diode rectifier is a passive setup. Therefore, a DC/DC converter is needed to have a control possibility. There are two main tasks:

1. **Input Current Control** The DC current is almost proportional to the torque in the generator. To run the turbine with the optimal tip speed ratio the wind turbine controller usually sets the torque reference, which then can be maintained by the current controller. This is the case in stall controlled wind turbines (no possibility to control the torque with pitching the blades) and in pitch controlled wind turbines when they are in optimal mode (pitch angle for maximal C_p).

2. **Output Voltage Control** The DC voltage after the rectifier varies with the generator speed. However, there are applications that need a stiff DC voltage. In that case the output voltage is controlled, the torque has to be controlled in another way. This can be done by controlling the output power of the wind turbine unit or by pitching the blades.

Different hard switching DC/DC converter topologies in connection with wind turbines have been investigated. For the two main tasks mentioned, the boost converter is the preferred choice if the transformation ratio is low [4, 14]. This is the case in this work because the main focus is on a wind turbine unit with DC output. A high transformation ratio is needed for DC transmission and large DC wind park layouts, which are analyzed in other works [3, 4, 5]. The boost converter has continuous input current, which requires a smaller capacitance between the diode rectifier and the converter compared to other converters with discontinuous input current. Furthermore, it can adjust a variable input voltage to a constant, higher output voltage over a large range.

1.3.4 Summary

The entire wind turbine unit used in this work consists of either stall or pitch controlled blades, a direct driven permanent magnet generator, series capacitors, diode rectifier, DC capacitor and a boost converter (Fig. 1.7). This system is

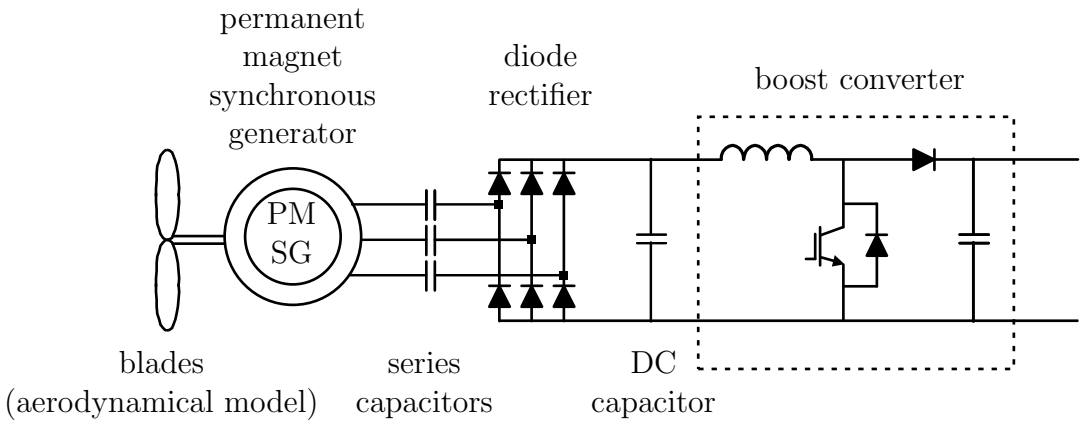

Fig. 1.7: The chosen configuration for the wind turbine unit with DC output.

analyzed with analytical calculations, simulations and measurements on a laboratory setup and the at Hönö wind turbine test station.

1.4 Outline of Thesis

In Chapter 2, all the information about the present system setup of the experimental wind turbine at the Hönö test station is gathered. This also includes measurements that have been carried out during the thesis.

Chapter 3 reviews the theory needed to analytically calculate currents, voltages and power for a compensated permanent-magnet generator with its single phase equivalent circuit.

For the Hönö wind turbine a new electrical configuration (series compensation) is proposed in Chapter 4. This is compared to the present, parallel compensated

setup with calculations, simulations and measurements.

In Chapter 5, the built DC/DC converter required for the wind turbine unit, introduced in Chapter 1, is described. The controller design, measurements and simulations are presented.

The lab setup of the wind turbine unit is described in Chapter 6. It includes a description of the different parts, modelling, simulation results and measurements. The setup is tested for different applications.

Finally, Chapter 7 draws conclusions and future work is suggested.

2 The Hönö Wind Turbine

The present experimental system at the Hönö test site is a variable speed, stall controlled wind turbine. It basically consists of a direct driven PMSG, parallel compensation, diode rectifiers, a DC link with electrical brake and a thyristor inverter.

2.1 Blades

The blades of the Hönö experimental wind turbine were manufactured at Gluelam A/S and LM Glasfiber A/S in Denmark [15], who also provided the $C_p(\lambda)$ characteristic (Fig. 2.1, Appendix B). The general equation for the mechanical power that

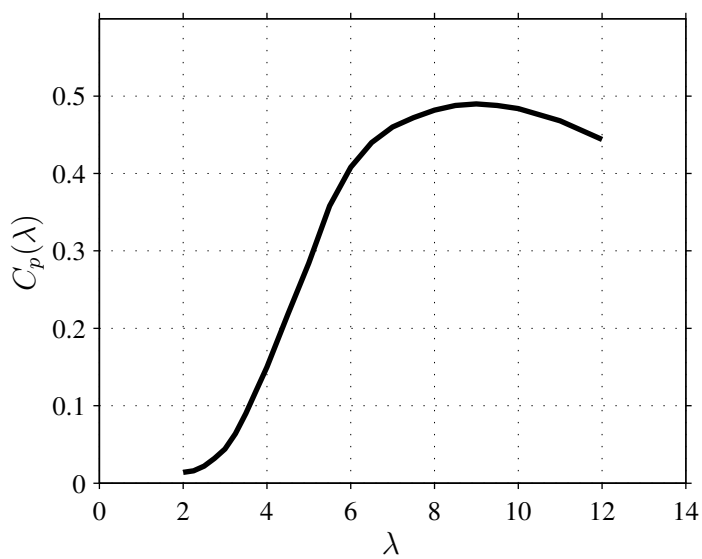

Fig. 2.1: $C_p(\lambda)$ characteristic of the Hönö wind turbine.

can be extracted from the wind is

$$P = 0.5\rho_{\text{air}} r^2 \pi C_p u^3, \tag{2.1}$$

where for the Hönö turbine

$\rho_{\text{air}} = 1.225\ \frac{\text{kg}}{\text{m}^3}$	air density;
$r = 6.75$ m	blade radius;
C_p	power coefficient;
u	wind speed ($\frac{\text{m}}{\text{s}}$).

With (2.1) and

$$\lambda = \frac{\omega_r r}{u} = \frac{n_r 2\pi r}{60u}, \tag{2.2}$$

where

λ tip speed ratio;
ω_r rotor angular frequency ($\frac{\text{rad}}{\text{s}}$);
u wind speed ($\frac{\text{m}}{\text{s}}$);
n_r rotor speed (rpm);

the optimal power for each rotor speed can be calculated:

$$P_{\text{optimal}} = 0.5\rho_{\text{air}} r^2 \pi C_{p,\text{optimal}} \left(\frac{n_r 2\pi r}{60\lambda_{\text{optimal}}} \right)^3, \tag{2.3}$$

where

$C_{p,\text{optimal}} = 0.49$ optimal power coefficient;
$\lambda_{\text{optimal}} = 9$ optimal tip speed ratio.

Furthermore, the maximum possible aerodynamic power is determined by calculating the power at a given rotor speed for the whole $C_p(\lambda)$ characteristic. This is done for different rotor speeds, and for each rotor speed the maximum value of the aerodynamical power is taken. In Fig. 2.2 both optimal and maximum aerodynamical power are illustrated.

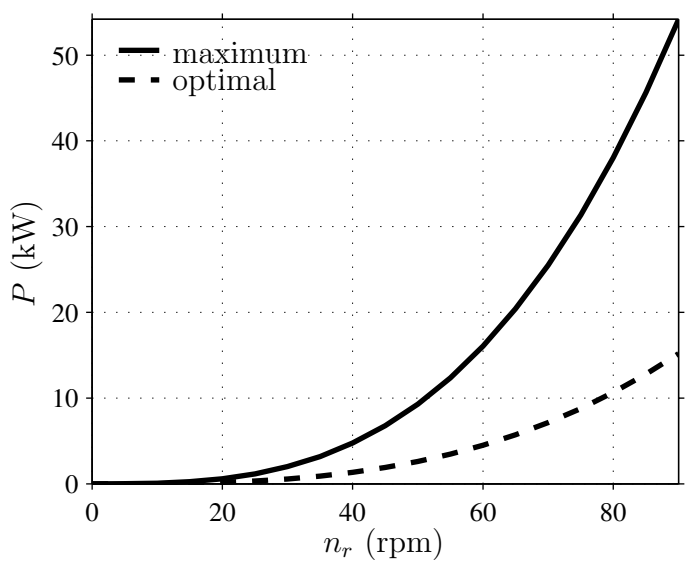

Fig. 2.2: Maximum and optimal aerodynamical power delivered by the Hönö blades.

The inertia of the blades is calculated to $J = 1600$ kgm^2. This is also the value taken for the whole drive train inertia in the mechanical model.

2.2 Generator

The generator at the Hönö test station is a 40 kW direct driven PMSG. The rotor has 24 pole-pairs and is designed with flux concentration. The magnet material is

ferrite. The whole generator has been tested in the laboratory [16]. Control and operation experience has been obtained at the Hönö test station [17]. The stator consists of 27 separate, concentrated windings. The equivalent circuit of one phase of the generator consists of an AC voltage source with an inductance and a resistor in series (Fig. 2.3).

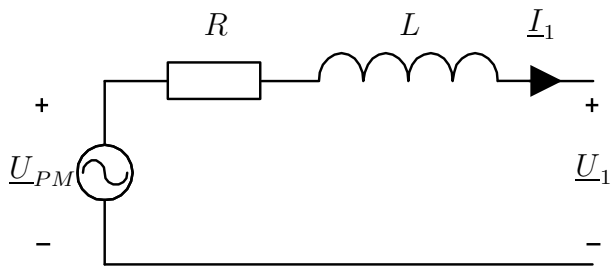

Fig. 2.3: Equivalent circuit for one phase of the Hönö generator.

2.2.1 Resistance

A DC measurement at stand still of the turbine has been made, which leads to a resistance of

$$R = \frac{U_{DC}}{I_{DC}} - R_L = 0.88\ \Omega \tag{2.4}$$

where

R	winding resistance;
$R_L = 0.4\ \Omega$	cable resistance.

2.2.2 Back EMF

Each stator coil of the generator was designed to give an open-circuit voltage of $U_{p,\text{rated}} = 211$ V at the rated speed of 75 rpm. With

$$U_{PM} = \sqrt{2}\pi f_s \psi_{PM} \tag{2.5}$$

and

$$f_s = f_r p = n_r p \frac{1}{60} \tag{2.6}$$

where

U_p	induced stator voltage;
f_s	stator frequency;
ψ_{PM}	permanent-magnet flux linkage;
f_r	rotor frequency (Hz);
n_r	rotor frequency (rpm);
$p = 24$	pole-pairs;

the induced voltage is proportional to the stator frequency (and therefore to the rotor speed):

$$U_p = k_1 f_s = k_2 n_r. \tag{2.7}$$

In order to get the fundamental component of the induced voltage, measurements on different coils at different speeds have been carried out. For the calculation Fast Fourier Transformation (FFT) within Matlab has been used. Time series of the measured voltage can be found in Appendix D. The measurements (Table 2.1) show a lower value for k_1 and k_2 compared to the theoretical values (211 V at $n_{r,\text{rated}} = 75$ rpm) at the design stage and earlier measurements [16]. Using the least square function on the different measurements leads to a fundamental component of the open loop voltage of $U_{p,r} = 192$ V at $n_{r,\text{rated}} = 75$ rpm).

	n_r (rpm)	f_s (Hz)	U_{PM} (V)	k_1 ($\frac{\text{V}}{\text{Hz}}$)	k_2 ($\frac{\text{V}}{\text{rpm}}$)	ψ_{PM} (Vs)
Coil 1	74.87	29.95	191.75	6.40	2.56	1.44
	59.93	23.97	154.74	6.46	2.58	1.45
	44.98	17.99	116.98	6.50	2.60	1.46
	29.99	12.00	77.76	6.48	2.59	1.46
Coil 2	74.93	29.97	190.84	6.37	2.55	1.43
	59.94	23.98	153.07	6.38	2.55	1.44
	44.95	17.98	115.28	6.41	2.56	1.44
	29.97	11.99	76.98	6.42	2.57	1.45
Coil 3	74.93	29.97	190.54	6.36	2.54	1.43
	59.98	23.99	152.08	6.34	2.54	1.43
	44.92	17.97	115.22	6.41	2.57	1.44
	29.88	11.95	76.49	6.40	2.56	1.44

Table 2.1: Open loop measurements for different speeds on different coils of the Hönö-Generator.

2.2.3 Current Limit

The highest possible continuous current without compensation is the short-circuit current

$$I_K = \frac{U_p}{X_d} = \frac{\sqrt{2}\pi f_s \psi_{PM}}{2\pi f_s L} = 7.72 \text{ A}. \tag{2.8}$$

In retardation mode (Section 2.4) the current in one phase was measured to be approximately 7.5 A. This is considered to do no harm to the generator and therefore the current limit I_l is set to this value.

2.2.4 Inductance

The inductance was estimated at the design stage to be 112 mH and measured in the lab to 119 mH. With these values the simulation results did not match the

measured DC power output. Therefore, new measurements have been undertaken at the Hönö test site. Measurements at (almost) standstill with an external source (transformer) lead to a inductance value of 100 to 110 mH, depending on the rotor position. But measurements at constant speeds with resistive and inductive loads on one single phase (Fig. 2.4) show different results (Fig. 2.5). With the measurements

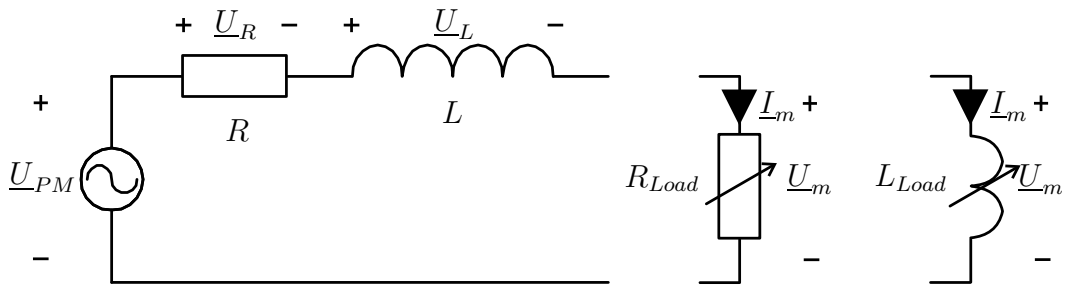

Fig. 2.4: Setup for measurements on a single phase with resistive and inductive load.

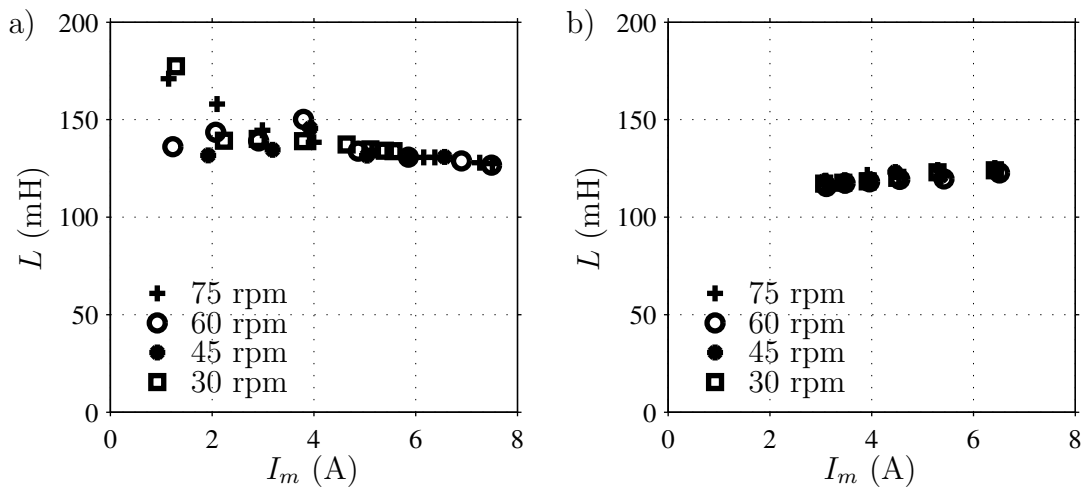

Fig. 2.5: Measurements for one single phase with a) resistive load, b) inductive load.

(U_m, I_m) and the knowledge of the induced voltage U_{PM} and the resistance R, the voltage over the inductance U_L can be calculated as function of the current for different speeds. This is done for resistive load (Fig. 2.6), because for a diode rectifier current and voltage also have to be in phase. With the least square method a value of $L = 132$ mH is found.

2.2.5 Summary of the Generator Data

All the generator data is collected in Table 2.2.

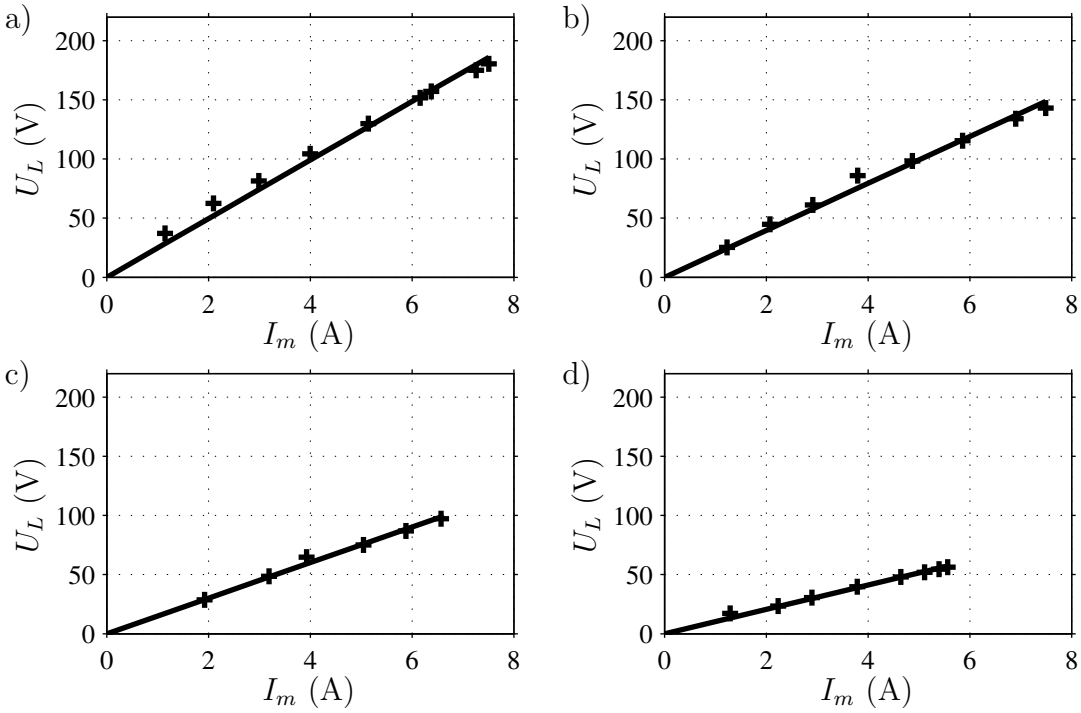

Fig. 2.6: Measurements on one single phase with resistive load and least square interpolation of voltage versus current through inductance. a) n = 75 rpm, b) n = 60 rpm, c) n = 45 rpm, d) n = 30 rpm.

Total		
rated power	P_{rated}	40 kW
number of modules	N	27
pole-pairs	p	24
rated speed	n_{rated}	75 rpm
Single Module		
rated power	P_{rated}	1.5 kW
rated voltage	$U_{p,\text{rated}}$	192 V
current limit	I_l	7.5 A
inductance	L	132 mH
resistance	R	0.88 Ω
rated stator frequency	$f_{s,\text{rated}}$	30 Hz
rated stator angular frequency	$\omega_{s,\text{rated}}$	188.5 $\frac{\text{rad}}{\text{s}}$
permanent-magnet flux linkage	ψ_{PM}	1.44 Vs

Table 2.2: Summary of the Hönö generator data.

2.3 Electrical System

Each of the 27 single phases described above is rectified with a diode rectifier. To compensate the large inductance of the generator, a capacitance C = 60 μF is placed

across the terminals on the AC side of the rectifier. This is called parallel (shunt) compensation. The modules then are arranged in two groups, one consisting of 13, the other one of 14 rectified single phases. Within the group they are connected in parallel to an electrolytic DC capacitor ($C_{DC} = 3300\ \mu$F). Then the two groups are connected in series to the DC link.

The connection to the grid is done by one smoothing inductor, a thyristor inverter and a transformer. In the DC link an electrical brake is added. This is for the case of control system failure or loss of grid. The whole electrical system including the single phase modules of the generator is shown in Appendix A.

2.4 Wind Turbine Controller

The control of the Hönö wind turbine is described in [17]. Due to the permanent-magnet generator, the diode rectifiers and stall control, only the DC-current can be controlled. The control scheme including the aerodynamical, electrical and mechanical model is shown in Fig. 2.7. The control can be divided into different modes of operation:

Standby The wind turbine is waiting for the right conditions to start up. When the cut-in wind speed is reached, a hydraulic systems spins the turbine up to 40 rpm where the wind forces take over. No load is applied below 50 rpm. Above that speed the control goes into ramp up mode.

Ramp up The load is softly increased. For a turbine speed higher than 55 rpm the control changes to optimal.

Optimal The DC current reference is set by the square of the rotor speed times a constant, in order to get the highest possible power for a given wind speed. When the rotor speed hits the reference speed set by the operator the controller goes into speed control mode.

Speed Control The speed is held constant to the reference speed with a PID-controller. If the turbine slows down below a adjustable level the mode changes back into optimal mode.

Retardation The speed of the turbine is slowed down in a controlled way. At high speed, the current is set to a given maximum generator torque. As the speed slows down the DC current reference is set down.

Voltage Control In order to prevent high voltages at optimal load, a voltage controller is always active. It sets a higher DC current reference if the DC voltage hits a limit. This leads to a lower DC voltage, but also a higher torque, which takes the wind turbine out of the optimal operation.

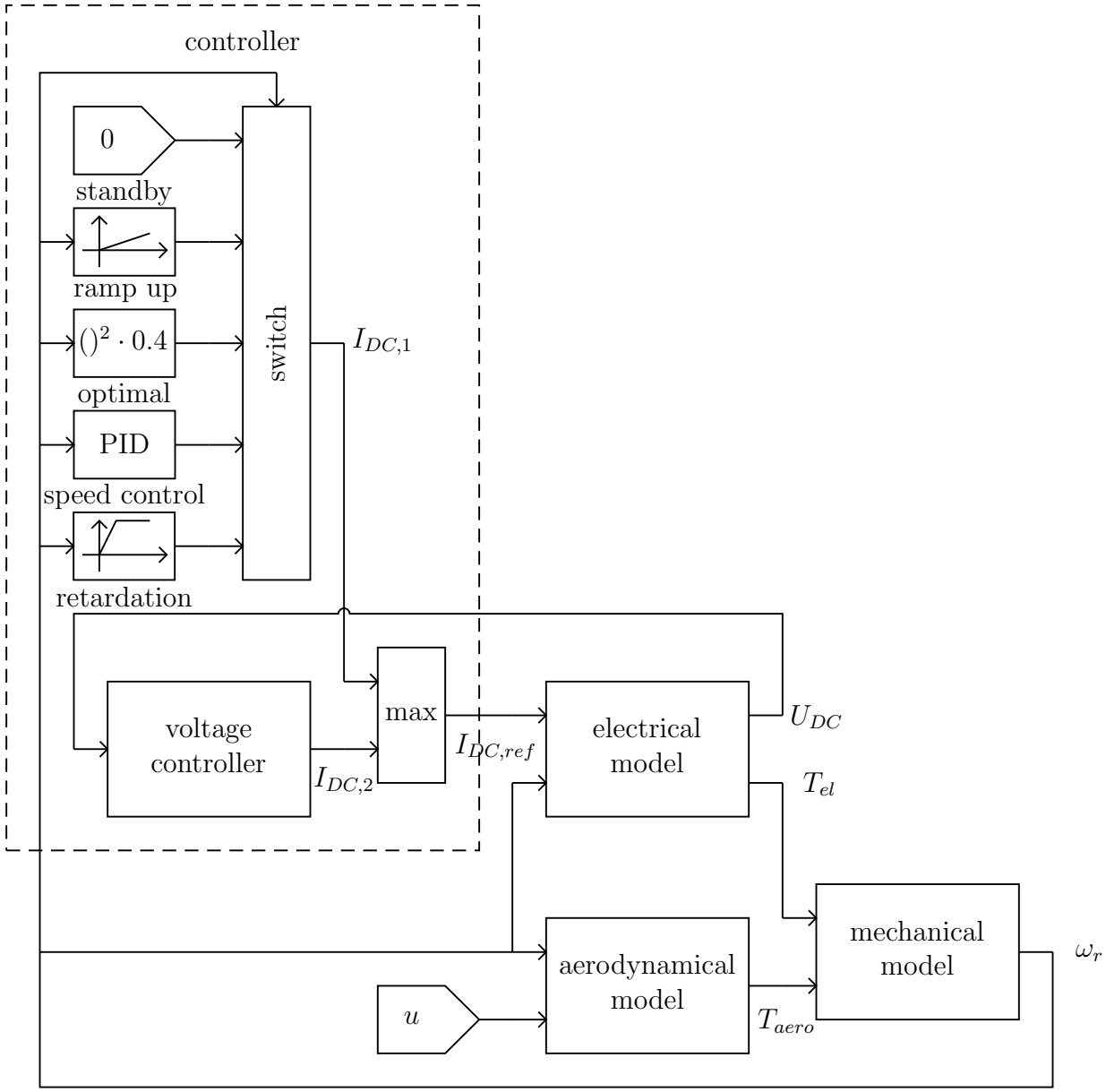

Fig. 2.7: Controller of the Hönö wind turbine.

2.5 Modelling

In order to evaluate different electrical configurations of the Hönö wind turbine, a model has been built in PSCAD/EMTDC. The full model consists of an aerodynamical, a mechanical, an electrical and a controller part (Fig. C.1). Simulations can be done with the full model or the electrical model only.

2.5.1 Aerodynamical Model

The aerodynamical model is based on Equation 2.1, where the $C_p(\lambda)$ characteristic is a look-up table with interpolation. The main inputs are the wind speed u (m/s) and the rotor angular frequency ω_r (rad/s). The aerodynamical Torque T_{aero} (Nm) is the output handed over to the mechanical model. Constant inputs are the blade radius r and the air density ρ_{air}.

2.5.2 Mechanical Model

The mechanical model consists of one dynamical expression

$$J\frac{d\omega_r}{dt} = T_{aero} - T_{el} \tag{2.9}$$

where

$J = 1600$ kgm^2	total inertia;
w_r	rotor angular frequency ($\frac{\text{rad}}{\text{s}}$);
T_{aero}	aerodynamical Torque (Nm);
T_{el}	electrical Torque (Nm).

The blades, drive train and rotor of the generator are considered to be stiff. The output of this model is the rotor angular frequency ω_r.

2.5.3 Electrical Model

The reference DC current $I_{DC,ref}$ and the rotor angular frequency ω_r are inputs to the electrical model. This consists of 27 single phase modules which are connected matching the Hönö setup (Appendix A). One single phase module is either parallel (Fig. 3.1) or series (Fig. 3.3) compensated. The inverter is modelled as a current source, controlled by the wind turbine controller output $I_{DC,ref}$. The electrical Torque T_{el} handed over to the mechanical model is calculated as

$$T_{el} = \frac{P_{DC} - P_{Cu}}{\omega_r} = \frac{U_{DC}I_{DC} - 27I_{AC,sp}^2 R}{\omega_r} \tag{2.10}$$

where

R	winding resistance;
P_{DC}	electrical power on the DC side;
P_{Cu}	copper losses;
ω_r	rotor angular frequency;
U_{DC}	DC voltage;
I_{DC}	DC current;
$I_{AC,sp}$	single phase current, rms;

which is considered to be accurate enough. Mechanical losses are not taken into account.

2.5.4 Wind Turbine Controller

The wind turbine controller is implemented according to the controller shown in Chapter 2.4, except the voltage controller. Without this, parallel and series compensation can be compared with regard to overvoltage problems.

3 Compensation

Direct driven permanent-magnet generators have a high stator inductance. In combination with a diode rectifier, there is the need for compensation in order to get higher rated and peak power for the electrical system [12]. Parallel (shunt) compensation has drawbacks that will be discussed further on in this section. An alternative to this is series compensation [13].

3.1 Parallel Compensation

Parallel (shunt) compensation means that a capacitor is placed across the terminals of the single phase equivalent circuit (Fig. 3.1). For the calculations, U_D and I_D, the voltage and current at the connection point to the diode rectifier, are considered to be in phase (Fig. 3.2). The generator current is calculated to

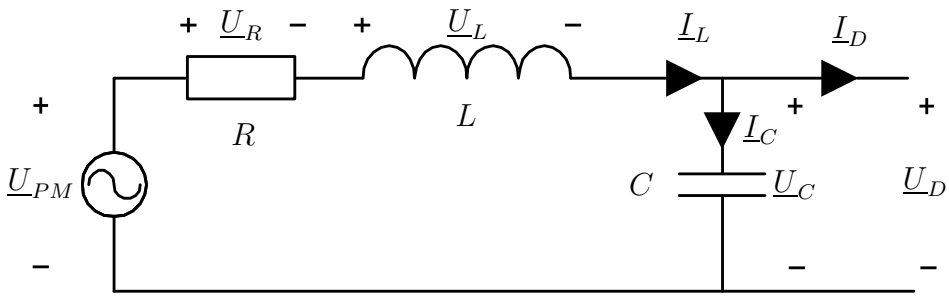

Fig. 3.1: Parallel compensation.

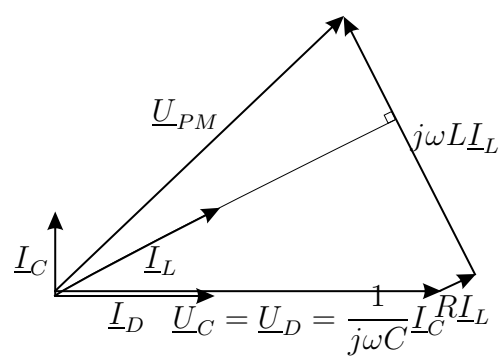

Fig. 3.2: The phasor diagram for parallel compensation.

$$\underline{I}_L = \underline{I}_C + \underline{I}_D \tag{3.11}$$
$$= j\omega C\underline{U}_D + \underline{I}_D \tag{3.12}$$
$$= j\omega C U_D + I_D. \tag{3.13}$$

Comparing the absolute values of right and left hand side leads to a terminal current of

$$I_D = \sqrt{I_L^2 - \omega^2 C^2 U_D^2} \tag{3.14}$$

and therefore the generator current as a function of its absolute value and the terminal voltage is

$$\underline{I}_L = j\omega C U_D + \sqrt{I_L^2 - \omega^2 C^2 U_D^2}. \tag{3.15}$$

When neglecting the resistance the generator voltage $\underline{U}_{PM}$ consists of

$$\underline{U}_{PM} = \underline{U}_L + \underline{U}_D \tag{3.16}$$

$$= j\omega L \underline{I}_L + U_D \tag{3.17}$$

$$= U_D(1 - \omega^2 LC) + j\omega L\sqrt{I_L^2 - \omega^2 C^2 U_D^2}. \tag{3.18}$$

Solving the absolute value of U_{PM}

$$U_{PM} = \sqrt{U_D^2(1 - \omega^2 LC)^2 + \omega^2 L^2 (I_L^2 - \omega^2 C^2 U_D^2)} \tag{3.19}$$

for U_D leads to

$$U_D = \frac{\sqrt{(I_L \omega L)^2 - U_{PM}^2}}{\sqrt{2\omega^2 LC - 1}}. \tag{3.20}$$

The output current of one module without resistor is

$$I_D = \sqrt{I_L^2 - (\omega C)^2 U_D^2} \tag{3.21}$$

$$= \sqrt{I_L^2 - (\omega C)^2 \frac{((I_L \omega L)^2 - U_{PM}^2)}{2\omega^2 LC - 1}} \tag{3.22}$$

Combining equation 3.20 and 3.22 results in an output power of

$$P_{out} = U_D I_D \tag{3.23}$$

$$= \frac{\sqrt{(I_L \omega L)^2 - U_{PM}^2}\sqrt{I_L^2 - \frac{(\omega C)^2 (I_L \omega L)^2 - U_{PM}^2}{2\omega^2 LC - 1}}}{\sqrt{2\omega^2 LC - 1}} \tag{3.24}$$

where I_L is the generator current.

For maximal power output the optimal current can be calculated with solving

$$\frac{dP_{out}}{dI_L} = 0 \tag{3.25}$$

for I_L. This leads to

$$I_L = \frac{U_{PM}\sqrt{1 - 2CL\omega^2 + 2C^2 L^2 \omega^4}}{L\omega\sqrt{2 - 4CL\omega^2 + 2C^2 L^2 \omega^4}}. \tag{3.26}$$

3.2 Series Compensation

The general drawback of parallel compensation is the high reactive power at low load and the relatively low peak power output [12]. A special drawback of this compensation at the Hönö turbine is the high terminal voltage at low load. The DC voltage has to be limited by a special voltage controller, which increases the DC current if the DC voltage gets too high. This takes the turbine out of the optimal control, which lowers the overall energy production. To overcome these drawbacks, series compensation (Fig. 3.3) is being investigated. Series compensation is not dependent on the load, but just on the rotor speed. The compensation then can be designed for rated speed. Full compensation means $\underline{I}_D$ is in phase with $\underline{U}_{PM}$ at rated speed, half compensation means half the voltage drop over L is being compensated (Fig. 3.4). The same calculations as for the parallel compensation can be done.

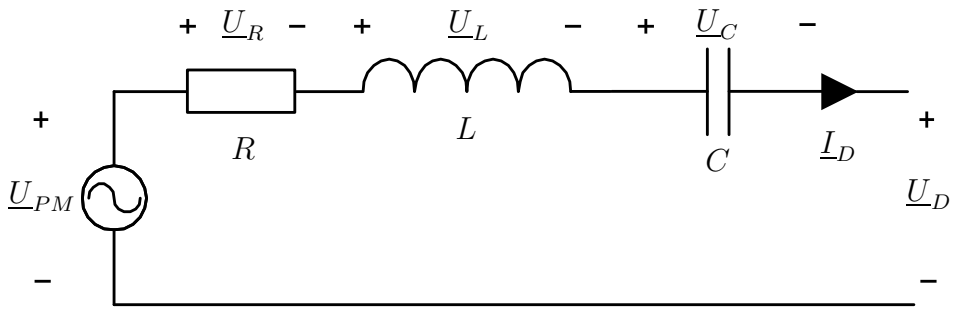

Fig. 3.3: Series compensation.

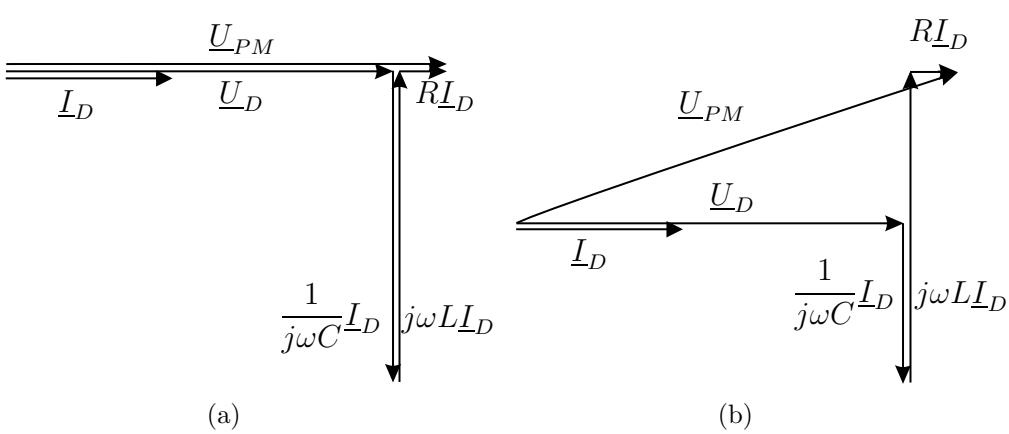

Fig. 3.4: The phasor diagram for series compensation. a) Full compensation, b) half compensation.

$$\underline{U}_{PM} = \underline{U}_R + \underline{U}_L + \underline{U}_C + \underline{U}_D \tag{3.27}$$

$$= \underline{I}_D R + \underline{I}_D j\omega L + \underline{I}_D \frac{1}{j\omega C} + \underline{U}_D \tag{3.28}$$

$$\underline{U}_D = U_D;$$
$$\underline{I}_D = I_D;$$

Comparing phase and magnitude gives

$$\varphi_{U,PM} = \arctan\left(\frac{I_D(\omega L - \frac{1}{\omega C})}{U_D + I_D R}\right) \tag{3.29}$$

and

$$U_{PM} = \sqrt{(U_D + I_D R)^2 + \left(I_D \omega L - I_D \frac{1}{\omega C}\right)^2}. \tag{3.30}$$

Solving (3.30) for U_D leads to

$$U_D = \sqrt{U_{PM}^2 - \left(I_D \omega L - I_D \frac{1}{\omega C}\right)^2} - I_D R \tag{3.31}$$

and when neglecting the resistor R, the output power is

$$P_{out} = U_D I_D = I_D \sqrt{U_{PM}^2 - \left(I_D \omega L - I_D \frac{1}{\omega C}\right)^2}. \tag{3.32}$$

To find the optimal current for maximum power, equation 3.32 is differentiated by I_D, which leads to:

$$\frac{dP_{out}}{dI_D} = \sqrt{U_{PM}^2 - \left(\omega L - \frac{1}{\omega C}\right)^2} - \frac{I_D^2 \left(\omega L - \frac{1}{\omega C}\right)^2}{\sqrt{U_{PM}^2 - I_D^2 \left(\omega L - \frac{1}{\omega C}\right)^2}}. \tag{3.33}$$

To get the dependence of I_D on ω one needs to set (3.33) equal to zero and solve it for I_D. Doing this leads to

$$I_D = \pm \frac{U_{PM} \omega C}{\sqrt{2 - 4\omega^2 LC + 2\left(\omega^2 LC\right)^2}}. \tag{3.34}$$

4 Analysis of Different Electrical Systems for the Hönö Turbine

The electrical system of the Hönö wind turbine consists, as described in Chapter 2, of the single phase modules of the generator, parallel (shunt) compensation and diode rectifiers. There are several drawbacks with this system. The compensation decreases with increasing load, which causes a relatively low peak power. Furthermore, the terminal voltage is not just dependent on the speed but also on the load. At low or no load there are high reactive currents which cause losses in the generator.

Series compensation was found to be the better choice for direct driven wind turbine generators with diode rectifiers [12]. This compensation is not dependent on the load, but just on the speed. It can be designed for rated speed, which is 75 rpm for the Hönö generator (Chapter 2). Full compensation means $\underline{I}_D$ in phase with $\underline{U}_{PM}$ at rated speed, half compensation means half the voltage drop over L is being compensated. For the Hönö generator this is

$$C_{\text{full}} = \frac{1}{\omega_{\text{rated}}^2 L} = 213\ \mu\text{F} \tag{4.35}$$

and

$$C_{\text{half}} = 2C_{\text{full}} = 426\ \mu\text{F} \tag{4.36}$$

where

$L = 132$ mH	inductance of one single phase module;
$\omega_{\text{rated}} = \frac{2\pi}{60} p n_{\text{rated}}$	rated electric angular frequency (rad/s);
$n_r = 75$ rpm	rated rotor frequency (rpm);
$p = 24$	pole-pairs.

To compare the present setup with the proposed new one, the performance of the Hönö wind turbine with both parallel and series compensation has been evaluated with analytical calculations, measurements and simulations in EMTDC with the electrical and full model.

4.1 Maximum Power

For parallel (3.24, 3.26) and series compensation (3.32, 3.34) the maximum mechanical power of the generator can be calculated for a current lower than or equal to a current limit (Chapter 2.2.3) of the generator. These values are compared with the ideal rectifier (sinusoidal current in phase with U_{PM}), non compensation and the maximum possible aerodynamical power (Fig. 2.2) at a given rotor speed (Fig. 4.1, 4.2, 4.3 and 4.4). The series compensation is designed for rated speed ($n_{\text{rated}} = 75$ rpm). The results show that the rotor speed must not be higher than 85 rpm for any rectifier if the current is limited to 7.5 A and the system should remain stable for any wind conditions. If the current can be higher there is unlimited power output for series compensation at rated speed (Fig. 4.1, 4.2, 4.3 and 4.4, a)). For parallel

compensation the power output is limited for every current (Fig. 4.1, 4.2, 4.3 and 4.4, b)).

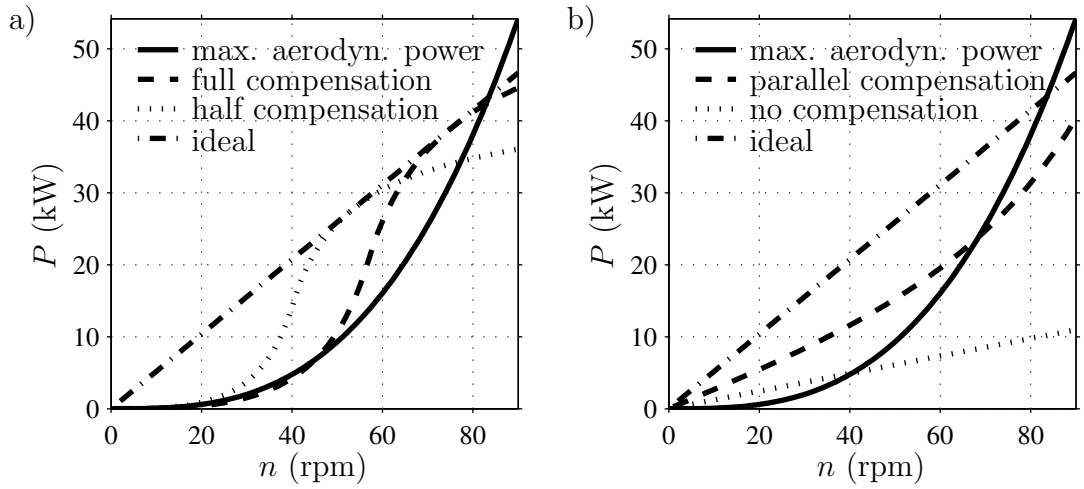

Fig. 4.1: Analytical calculation of the maximum mechanical power as a function of the rotor speed with a limited current of 7.5 A. a) Series compensation, b) parallel compensation and no compensation.

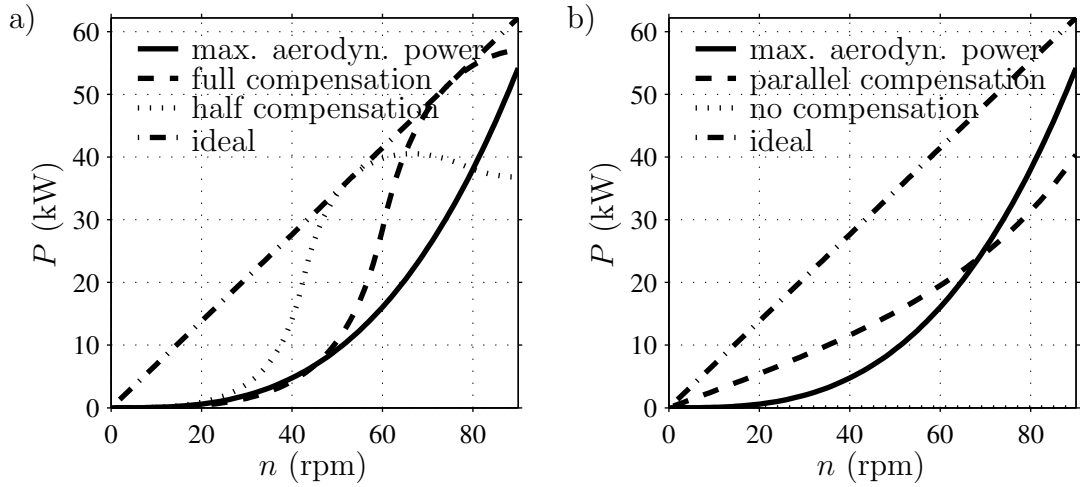

Fig. 4.2: Analytical calculation of the maximum mechanical power as a function of the rotor speed with a limited current of 10 A. a) Series compensation, b) parallel compensation and no compensation.

4.2 Terminal Voltage

The terminal voltage U_D of a single phase can be calculated for varying active power and different rotor speeds. For series compensation, solving (3.30) for I_D and

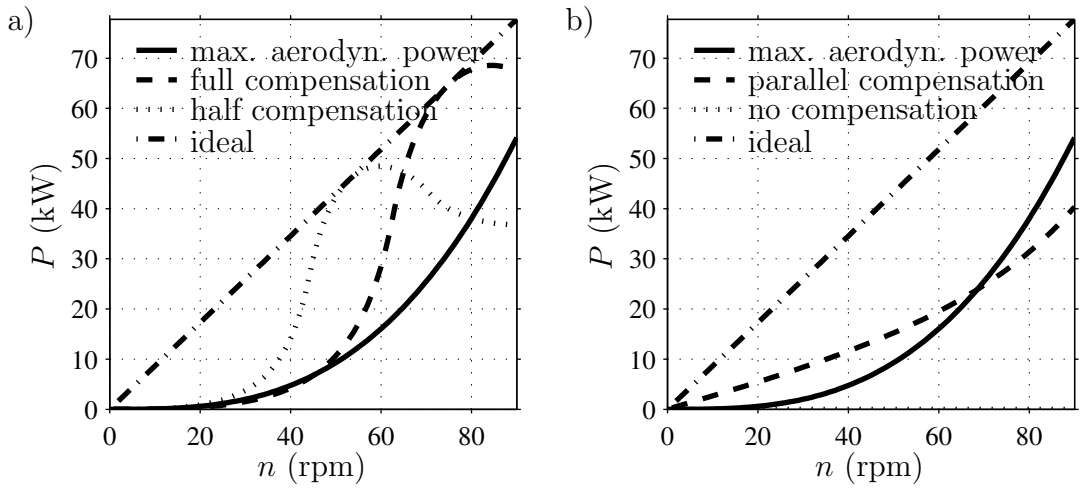

Fig. 4.3: Analytical calculation of the maximum mechanical power as a function of the rotor speed with a limited current of 12.5 A. a) Series compensation, b) parallel compensation and no compensation.

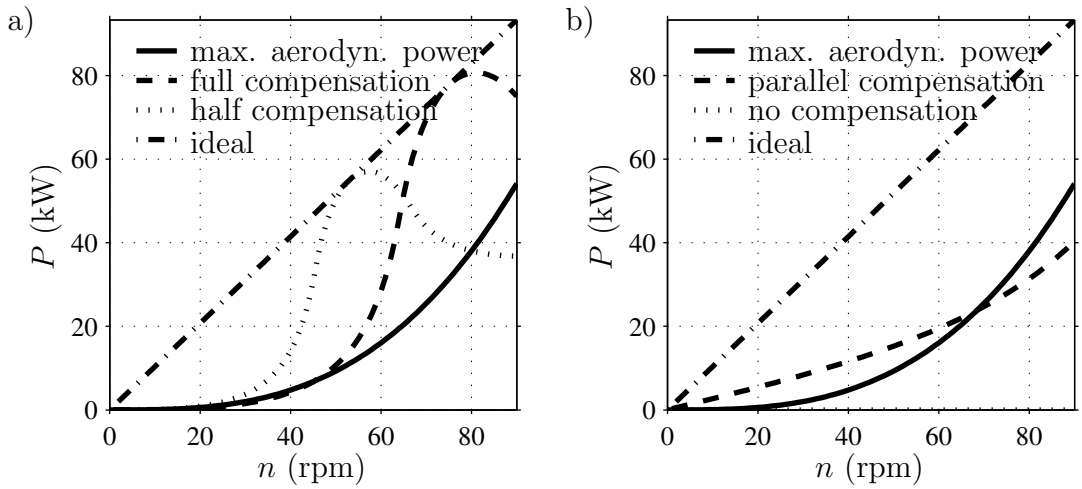

Fig. 4.4: Analytical calculation of the maximum mechanical power as a function of the rotor speed with a limited current of 15 A. a) Series compensation, b) parallel compensation and no compensation.

neglecting the resistance leads to

$$I_D = \frac{\sqrt{U_{PM}^2 - U_D^2}}{\omega L - \dfrac{1}{\omega C}} \tag{4.37}$$

which, with the power formula $P = U_D I_D$, results in

$$P = U_D \frac{\sqrt{U_{PM}^2 - U_D^2}}{\omega L - \dfrac{1}{\omega C}}. \tag{4.38}$$

Finally, (4.38) can be solved for U_D

$$U_D = \sqrt{\frac{C^2\omega^2 U_{PM}^2 + \sqrt{C^2\omega^2\left(-4\left(-1 + CL\omega^2\right)^2 P^2 + C^2\omega^2 U_{PM}^4\right)}}{2C^2\omega^2}} \tag{4.39}$$

to get the function $U_D = f(P, \omega)$. The same steps can be done for the parallel compensation which results in

$$U_D = \sqrt{\frac{U_{PM}^2 + \sqrt{-4L^2\omega^2\left(-1 + CL\omega^2\right)^2 P^2 + U_{PM}^4}}{2C^2\omega^2}} \tag{4.40}$$

for the parallel compensated single phase terminal voltage.

For parallel compensation the terminal voltage U_D is higher at low load (Fig. 4.5, a)) than for series compensation (Fig. 4.5, b)). At Hönö, the problem of

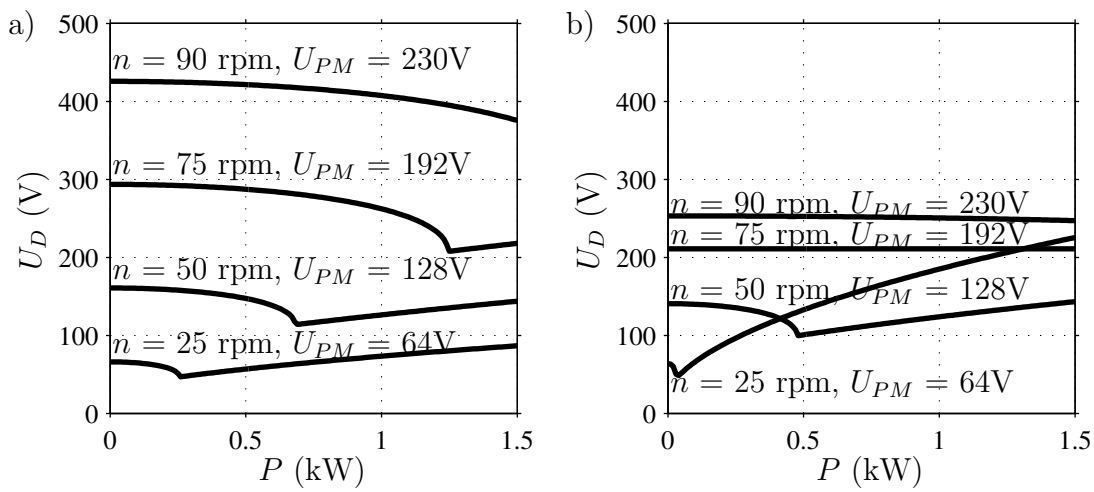

Fig. 4.5: Calculated terminal voltage of a single phase as function of the active power for different rotor speeds. a) Parallel compensation ($C_p = 60$ μF), b) series compensation ($C_s = C_{full} = 213$ μF).

high DC voltage occurs in optimal control operation, where the load is small. The terminal voltage for optimal power is lower for series compensation than for parallel compensation (Fig. 4.6).

To verify the calculated terminal voltages and to determine the DC voltage of the whole Hönö electrical system (Appendix A.1), simulations in PSCAD/EMTDC have

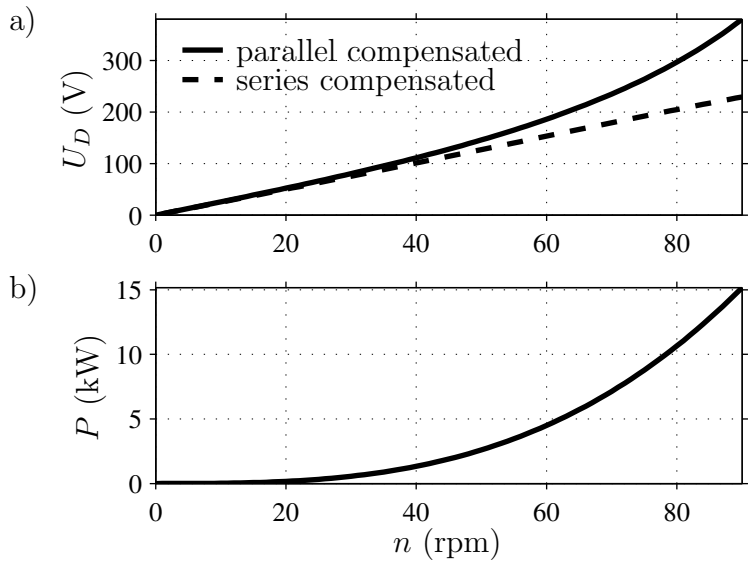

Fig. 4.6: Calculated terminal voltage of a single phase as function of the rotor speed for optimal power.

been undertaken. The whole simulation has been carried out for optimal control operation. In this mode the DC-current is directly controlled by the rotor speed (2.4). At the Hönö setup this is the case for 55 rpm $< n_r <$ stall speed, where stall speed can be adjusted by the operator. The results show that for parallel compensation both the terminal voltage U_D and the DC voltage U_{DC} are high due to the low load in optimal control (Fig. 4.7, a)). With series compensation both voltages are lower in the optimal control range (Fig. 4.7, b)). Furthermore, the optimal control range could be extended without risk of high over voltages. It also shows that the quadratic constant for optimal control is too high for parallel compensation, which leads to a lower C_p [17]. For series compensation the same quadratic constant value would lead to a higher, more optimal C_p.

4.3 DC Power

Another goal for the Hönö test station is to be able to get more power out of the generator. With parallel compensation there is always a maximum power output at a certain speed. This limits the operation area of the turbine, because the maximal generator power always has to be higher than the maximal aerodynamical power. If series compensation is installed instead, the power output at the speed the compensation is designed for is only limited by the current capability of the generator. To proof this, measurements and simulations have been carried out for different speeds with parallel (Fig. 4.8) and series (Fig. 4.9) compensation. The first measurements are taken from [16]. The measurements with series compensation have been made on one single module and the total DC current and DC power has been calculated

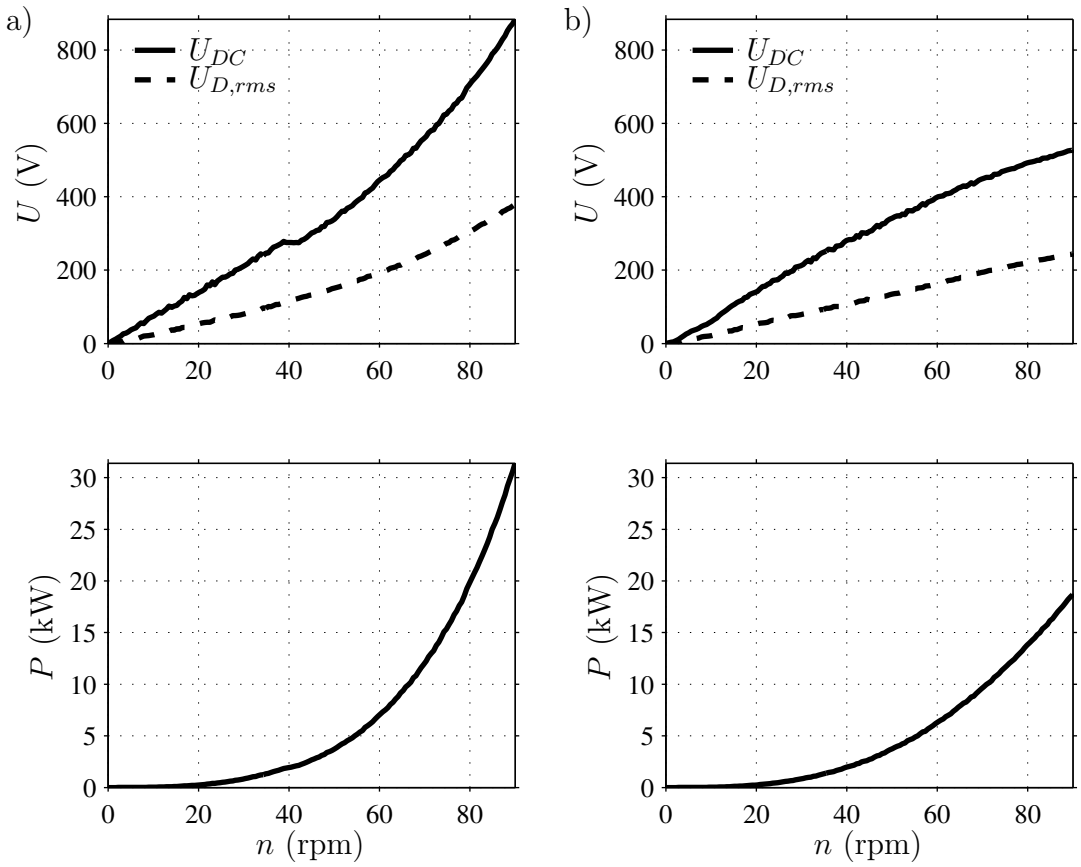

Fig. 4.7: Simulation of the electrical system of the Hönö generator. a) Parallel compensation, b) series compensation.

with

$$I_{DC} = 13.5 I_{DC,\text{single phase}} \tag{4.41}$$

and

$$P_{DC} = 27 I_{DC,\text{single phase}} U_{DC,\text{single phase}}. \tag{4.42}$$

Simulation and measurement show good agreement for both parallel and series compensation. It can be seen that the maximum output power at $n_r = 75.4$ rpm for parallel compensation is 34 kW, whereas for series compensation there is no maximal power for full compensation. Measurements could not be carried out for currents higher than the current limit of one single module ($I_l = 7.5$ A), because at the time it is unknown how much current the generator can exactly handle. There is the danger of demagnetizing the permanent magnets. To find out more about the magnetic flux, saturation and permanent magnets, FEM calculations are being done as part of a PhD thesis (Chapter 7).

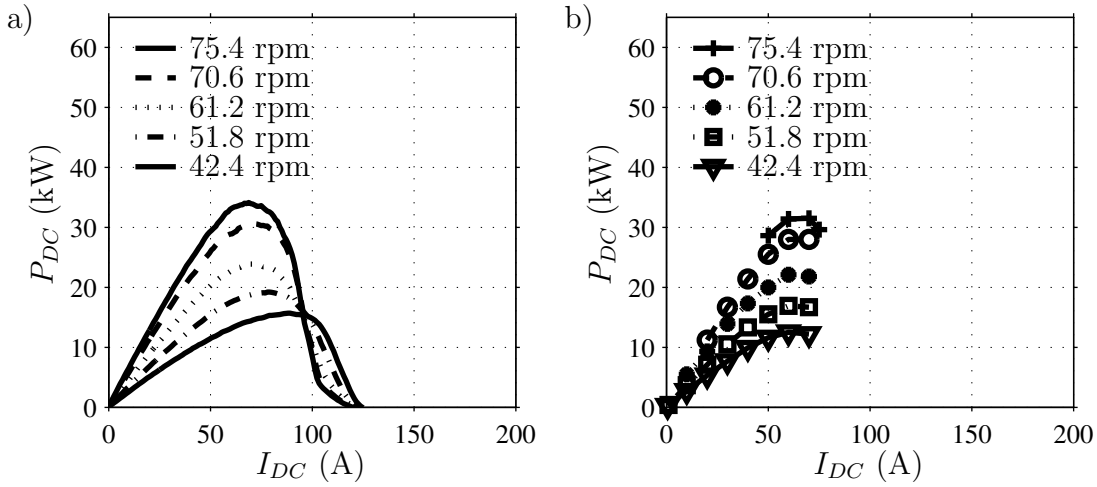

Fig. 4.8: DC power as a function of DC current for different speeds with parallel compensation. a) Simulation results, b) measurements.

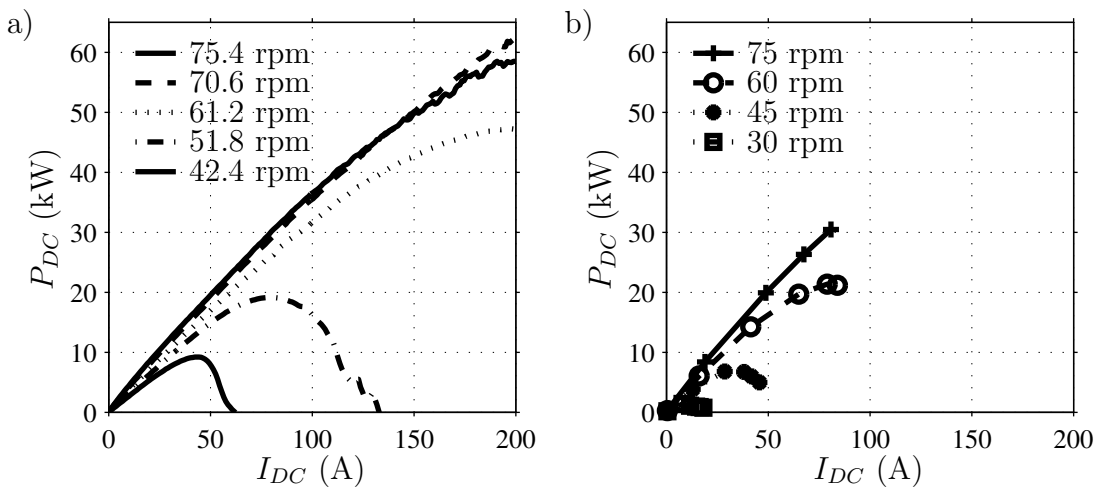

Fig. 4.9: DC power as a function of DC current for different speeds with full series compensation at 75 rpm. a) Simulation results, b) measurements.

4.4 No Load

A further advantage of the series compensation of a permanent-magnet generator is the no load or low load operation. With parallel compensation, there is already a current in the coils of the generator at no load. Looking at Figure 3.1 and considering $\underline{I}_D = 0$ the phase current can be calculated to

$$\underline{I}_L = \frac{\underline{U}_{PM}}{j\left(\omega L - \dfrac{1}{\omega C}\right) + R}, \tag{4.43}$$

which leads to an absolute current of

$$I_L = \frac{U_{PM}}{\sqrt{\left(\omega L - \frac{1}{\omega C}\right)^2 + R^2}}. \tag{4.44}$$

For example at nominal speed this leads to a current of $I_L = 3$ A. This leads to losses in the generator even at no load and low load. In comparison, for series compensation there is no current at no load (Fig. 3.3).

4.5 Simulation of the Full Model

Simulations of the full model have been run for a stall speed of 72 rpm and also 85 rpm. The first speed because there exist measurements to verify the model. The second one to see the advantage of series compensation with regard to power output. The measurements match the simulation results in case of the DC voltage and the rotor speed well. The simulation results for DC current and therefore DC power are higher than the measured ones. The reason for this is that just copper losses in the generator have been taken into account for the simulation. But especially mechanical losses have a big influence on the power output. For both parallel and series compensation in optimal operation of the wind turbine, the output power follows the optimal power output

$$P_{\text{optimal}} = 0.5\rho_{\text{air}} r^2 \pi C_{p,\text{optimal}} u^3, \tag{4.45}$$

where

$\rho_{\text{air}} = 1.225\ \frac{\text{kg}}{\text{m}^3}$	air density;
$r = 6.75$ m	blade radius;
$C_{p,\text{optimal}} = 0.49$	optimal power coefficient;
u	wind speed ($\frac{\text{m}}{\text{s}}$),

very well. When the speed is limited C_p decreases for increasing wind speed and the power output moves away form the optimal curve.

Also at a stall speed of 72 rpm there is an advantage of series compensation. The DC voltage is more constant and does not exceed 460 V (Fig. 4.10). As expected, the power output is the same for parallel and series compensation, the difference is the more constant DC voltage and the ability of handling higher speeds. With rising the stall speed the power output could be increased for higher wind speeds. Then series compensation is needed to still be able to operate safely.

Parallel compensation for a stall speed of 85 rpm is not stable anymore for windspeeds exceeding 11 m/s (Fig. 4.11). With series compensation the power output is increased. The limitation is the current capability of the generator. Further advantages of series compensation would be low generator losses at small load and more stable DC voltage.

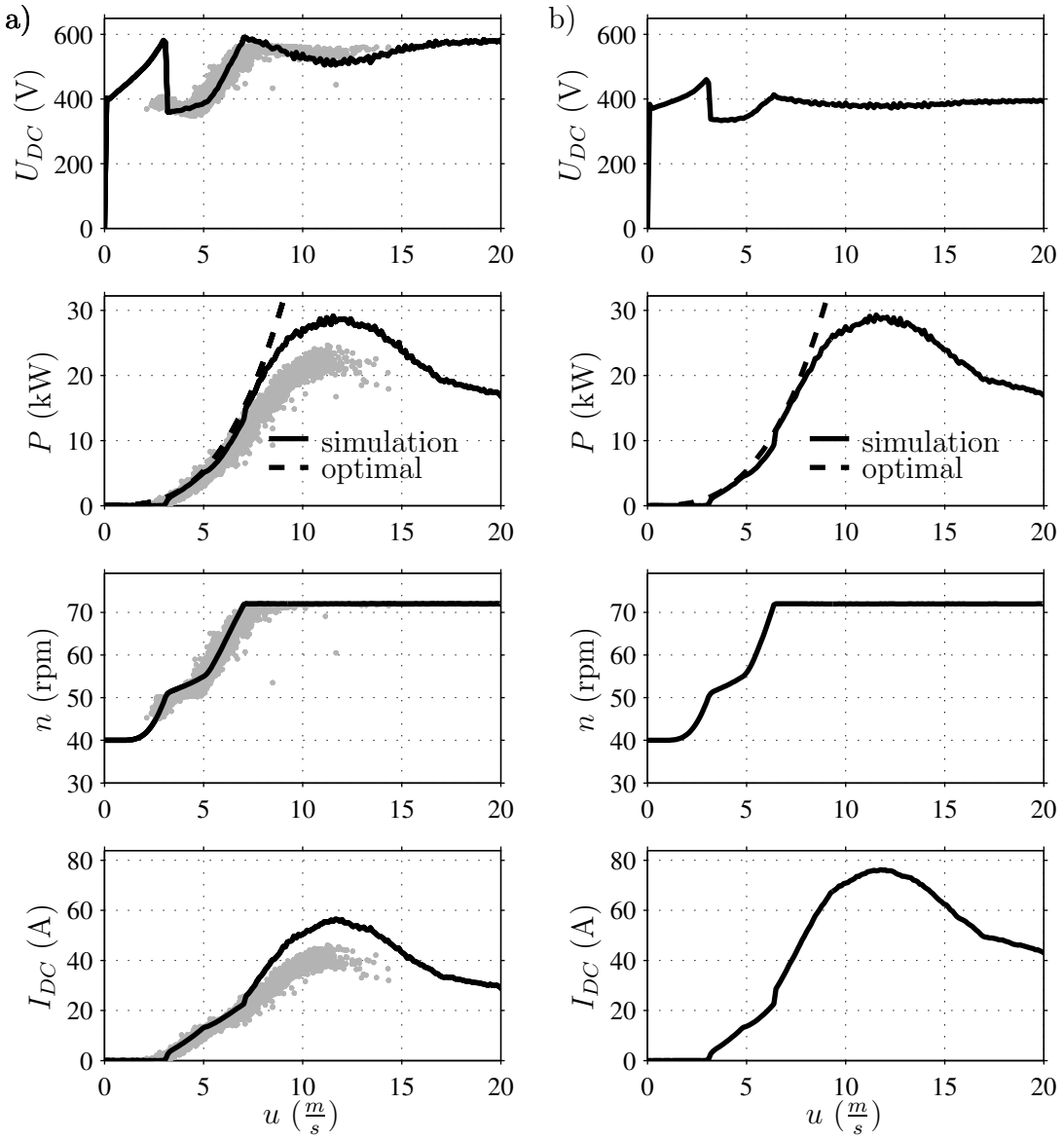

Fig. 4.10: Simulation of the whole Hönö model (aerodynamical, mechanical, electrical) with a stall speed of 72 rpm. a) Parallel compensation, simulation (black) and measurements (grey), b) series compensation.

4.6 Proposed New Electrical Configuration

The proposed new electrical system is series compensation. Full compensation for rated speed is recommended, which leads to a capacitance of 213 μF for each of the 27 phases. The new system solves the problem of overvoltages at high speed and low load. Furthermore, the losses at no and low load in the generator decrease. Also, if FEM calculations and information from the manufacturer show that the generator

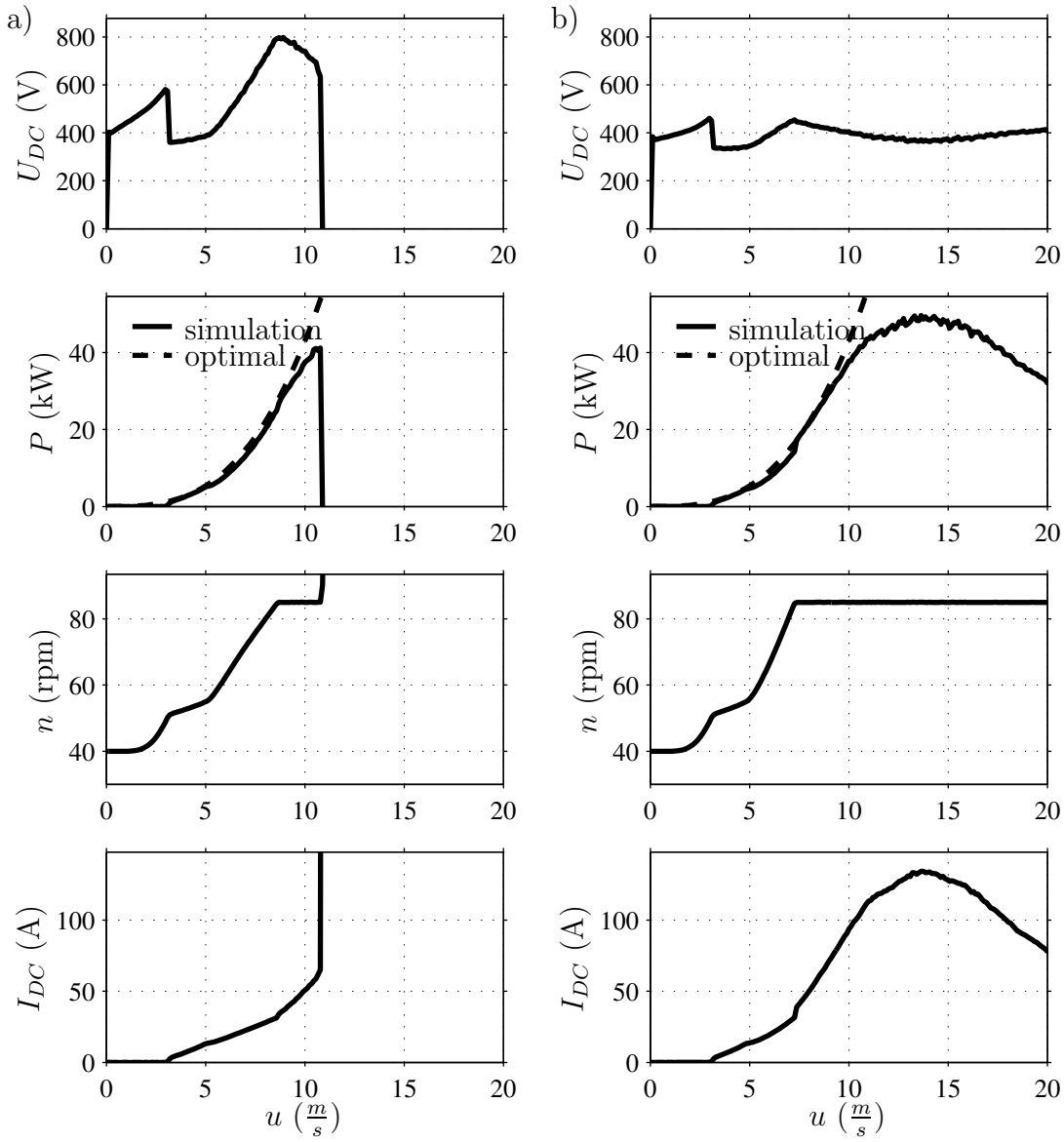

Fig. 4.11: Simulation of the whole Hönö model (aerodynamical, mechanical, electrical) with a stall speed of 85 rpm. a) Parallel compensation, b) series compensation.

can handle higher currents, there is the possibility of increasing the power output of the wind turbine by rising the stall speed.

5 DC/DC Converter

For a wind turbine unit as described in Chapter 1, a boost converter is needed to have a control possibility. It follows the diode rectifier and the output can be connected to different loads, for example a stiff DC link or a resistive load (Fig. 5.1).

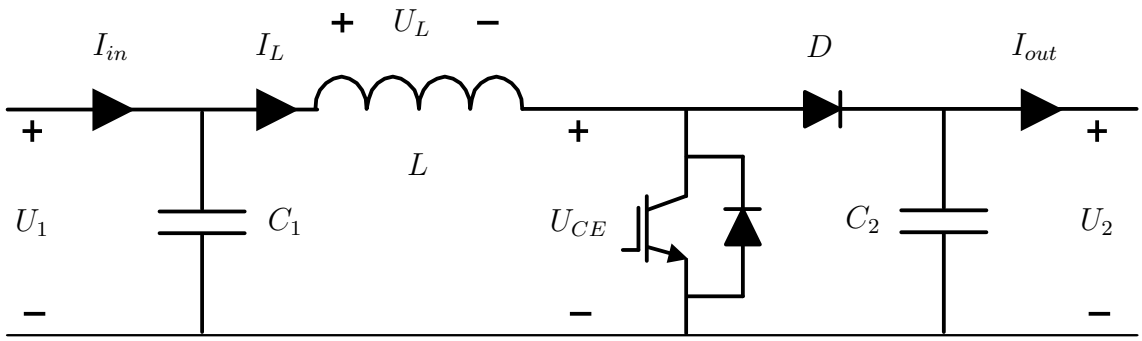

Fig. 5.1: Scheme of the boost converter.

To test a whole wind turbine unit, such a converter has been built. Both input and output capacitor have a capacitance of 1950 μF. The switch is realized with a Semikron IGBT module (SKM 400 GB 125 D). This module consists of one half-bridge (two in series connected IGBTs with antiparallel diodes). The freewheeling diode of the upper IGBT is used as boost diode D while the gate of that IGBT is connected to negative potential, U_{GE} = -8 V (Fig. 5.11). The inductor is described in more detail in section 5.1. In order to keep the connection of the IGBT module with the output capacitor C_2 as low inductive as possible it is realized with a stripline. The IGBT is switched with frequency of f_s = 10 kHz. The controller is implemented in dSpace.

5.1 Inductor

The inductor for the DC/DC-Converter is built with an iron-powder core having the data

frequency range	DC - 1 MHz;
geometry ($d_a \times d_i \times h$)	101.6 mm × 57.2 mm × 33 mm;
magnetics (l_e, A_e, V_e)	249 mm, 743 mm^2, 185280 mm^3;
A_L value	260 $\frac{\text{nH}}{\text{N}^2}$;
relative permeability (μ_r)	75.

To get the desired value L = 15 mH the inductor is designed with the standard theory [18]. The number of windings is calculated to

$$N = \sqrt{\frac{L}{A_L}} = 240, \tag{5.46}$$

which leads, with the maximal magnetic flux density $\hat{B} = 1$ T, to a maximal peak inductor current of

$$\hat{I} = \frac{\hat{H} l_e}{N} = \frac{\hat{B} l_e}{\mu_r \mu_0 N} = 11 \text{ A} \tag{5.47}$$

The copper wire has a diameter of $d = 2$ mm and the inductance is designed for a frequency of $f = 10$ kHz. Considering the skin effect this frequency leads to a penetration depth of

$$\delta = \sqrt{\frac{1}{\pi \sigma_{Cu} \mu_{Cu} f}} = 0.66 \text{ mm} \tag{5.48}$$

where

$$\begin{array}{ll} \sigma_{Cu} = \rho_{Cu}^{-1} = 5.8824 \cdot 10^7 \ \frac{1}{\Omega \text{m}} & \text{electric conductivity;} \\ \mu_{Cu} = \mu_0 = 4\pi \cdot 10^{-7} \ \frac{\text{Vs}}{\text{Am}} & \text{magnetic permeability;} \\ \rho_{Cu} = 1.7 \cdot 10^{-8} \ \Omega\text{m} & \text{electric resistance.} \end{array}$$

This leads to a current area of

$$A = 2\pi\delta \frac{d - \delta}{2} = 2.77 \text{ mm}^2 \tag{5.49}$$

and a maximal electric current density of

$$\hat{S} = \frac{\hat{I}}{A} = 3.97 \ \frac{\text{A}}{\text{mm}^2}. \tag{5.50}$$

With a mean turn length of approximately $l_{loop} = 0.14$ m the resistance of the inductor is calculated to

$$R_L = \rho_{Cu} \frac{N l_{\text{loop}}}{A} = 0.20 \ \Omega. \tag{5.51}$$

which leads to a maximal resistive power dissipation of

$$P_{Cu,max} = \hat{I} R_L = 24.95 \text{ W}. \tag{5.52}$$

The core losses are estimated with a data sheet of a similar iron powder material. The maximal peak-to-peak current ripple is $\Delta\hat{I} = 0.67$ A. This results in a maximum change of the magnetic flux density of

$$\Delta\hat{B} = \mu_r \mu_0 N \frac{\Delta\hat{I}}{l_e} = 56.40 \text{ mT}. \tag{5.53}$$

Furthermore, the power loss can now be calculated to $P_{\text{core},max} = 16.68$ W. The total maximal losses are therefore

$$P_{tot,max} = P_{\text{core},max} + P_{Cu,max} = 41.63 \text{ W}. \tag{5.54}$$

Measurements with the wound inductor have shown that the inductance slightly changes at a given switching frequency ($f_s = 10$ kHz) depending on the average current in the coil (Table 5.1).

Iavg (A)	3	3.5	4	4.5	5	5.5
L (mH)	13.2	15.7	14.39	14.51	15.63	17.19

Table 5.1: Measured boost inductance L.

5.1.1 Parasitic Capacitance of the Inductor

The main inductor of the boost converter has several layers of windings (Section 5.1). Therefore there is a large, parasitic, parallel capacitance (Fig. 5.2). This par-

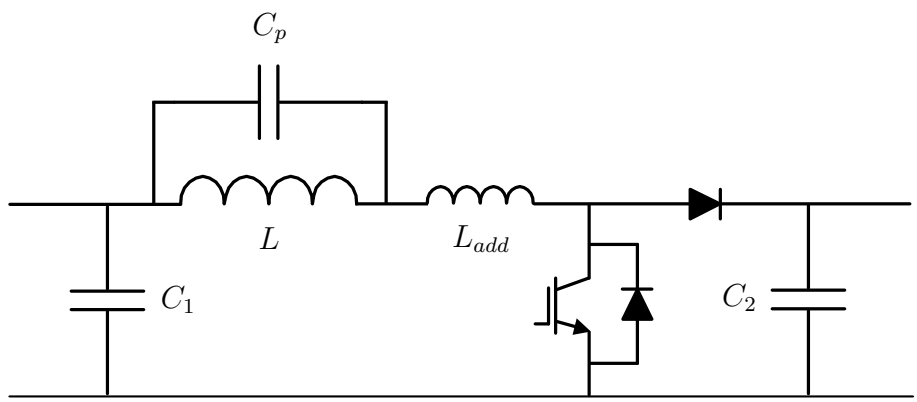

Fig. 5.2: Boost converter with parasitic capacitor C_p and additional inductor L_{add}.

asitic capacitance arises between neighboring windings as well as between winding and ground and results in a high frequency oscillation of the current just after the switching. Because this frequency is in the range of the switching operation (200-400 ns), the effects can not be simulated with ideal switches. With the normal setup (Fig. 5.1) there is a first big current spike (Fig. 5.3, a)). The assumption is made that with that current the parasitic capacitance C_p (Fig. 5.2) is charged/discharged. With

$$Q = \int I dt \tag{5.55}$$

and

$$C = \frac{Q}{U} \tag{5.56}$$

the parasitic capacitance is calculated to C = 585 pF. Looking at the oscillation (Fig. 5.3, a)) the inductance of the wiring can be calculated with

$$L_{\text{wiring}} = \frac{1}{C(2\pi f)^2} = 1.45\ \mu\text{H}, \tag{5.57}$$

which is realistic. Furthermore, a measurement with an additional, low capacitance, ferrite core inductor L_{add} (Fig. 5.2) in series with the main inductor is carried out

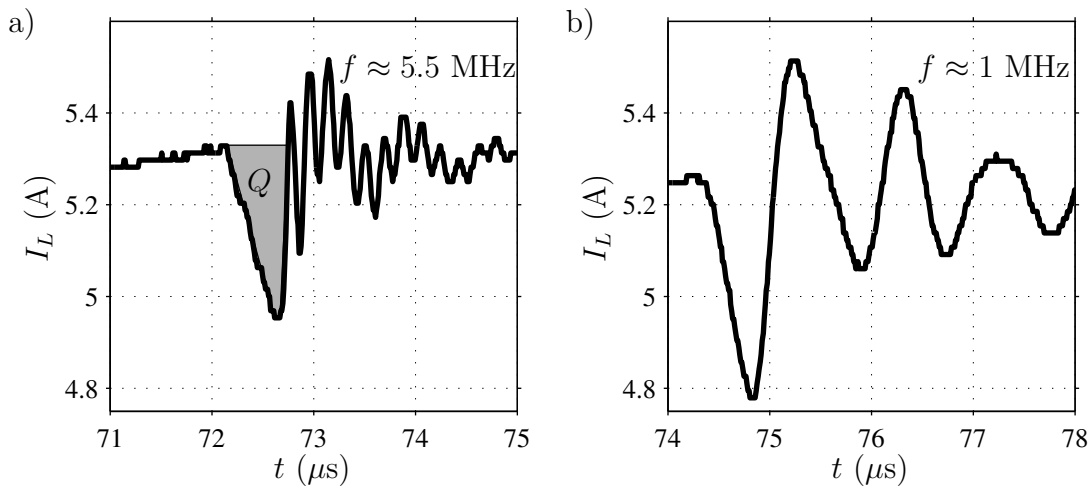

Fig. 5.3: Measurement of the current through the main inductor L. a) Normal setup, b) with additional, low capacitive inductor L_{add} in series.

(Fig. 5.3, b)). The additional inductance was 50 μH, so the wiring inductance can be neglected. With

$$C = \frac{1}{L_{add}(2\pi f)^2} \tag{5.58}$$

the capacitance is determined to 530 pF, which is in good agreement with the value calculated with Equation 5.56. These current spikes and oscillations are no problem for the converter in that power range. The current measurement for the control is always sampled in between the switching operation and therefore is not affected by these spikes. A possibility to avoid a large parasitic capacitance is to build the inductor with just one layer of windings or to use multi chamber windings.

5.2 Current Controller

The current controller is designed for a boost converter with constant input voltage, output capacitor and resistive load (Fig. 5.1). The controller parameters are found with bode plot analysis [19]. The current in the inductance can be controlled by a proportional integral (PI) controller:

$$d(s) = G_c(s)e(s) \tag{5.59}$$

where $e(s)$ is the error between the reference current and the actual coil current

$$e(s) = i_{\text{coil},ref}(s) - \tilde{i}_{\text{coil}}(s), \tag{5.60}$$

$G_c(s)$ is the transfer function of the PI-Controller

$$G_c(s) = k_p \left(1 + \frac{1}{sT_n}\right) \tag{5.61}$$

and $d(s)$ is the duty cycle for the switch.

The control-to-input-current transfer function $G_{id}(s)$ of the converter with resistive load (Fig. 5.1) is found through state-space averaging [20]. This leads to

$$G_{id}(s) = \frac{i(s)}{d(s)} = \frac{s\frac{U_2}{L} + \frac{1}{LC_2}\left(\frac{U_2}{R_{\text{out}}} + I_L(1-D)\right)}{s^2 + s\frac{1}{R_{\text{out}}C_2} + \frac{1}{LC_2}(1-D)^2} \tag{5.62}$$

where $i(s)$ is the inductor current and $d(s)$ is the duty-cycle. Fig. 5.4 shows this transfer function for the following parameters:

U_1	294.5 V;
U_2	375.1 V;
L	15 mH;
R_{out}	100 Ω;
C_2	1950 μF;
duty-cycle D	$\frac{(U_2 - U_1)}{U_2}$.

Thus it appears that the phase margin is never smaller than -90° and therefore

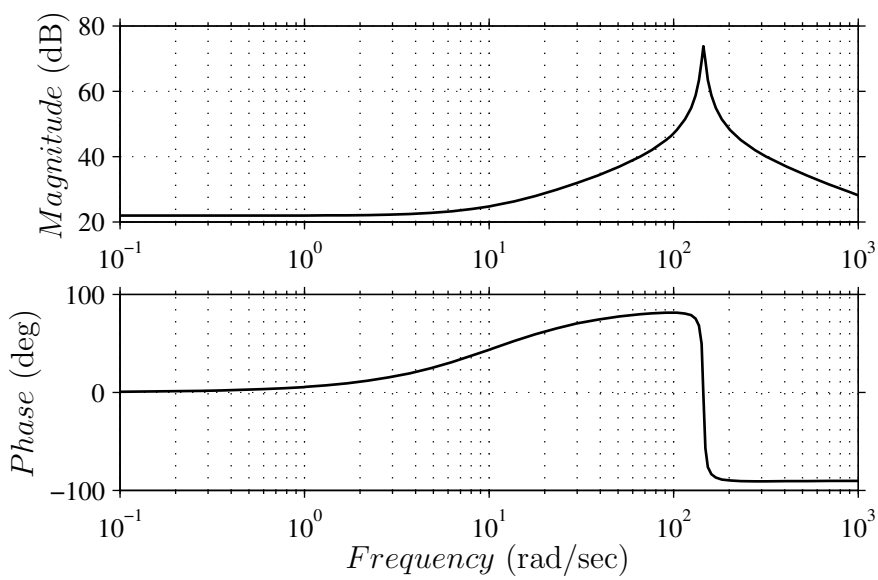

Fig. 5.4: Bode diagram of control-to-input-current transfer function $G_{id}(s)$.

the controller could be tuned very fast. Since the inertia of the drive train is high, the time constants for the whole system are quite large. Nevertheless, the current controller can have a wide bandwidth, whereas the wind turbine controller (which sets the reference current) has to be much slower. A too fast current controller will

try to compensate the current ripple caused by the diode rectifier, which is neither necessary nor desired. The control parameters (5.61) have been set to $Tn = 0.005$ and $kp = 0.15$. The resulting bode plot of the open loop transfer function is shown in Fig. 5.5. The closed loop bode plot shows a bandwidth of approximately $\omega_c = 3000$

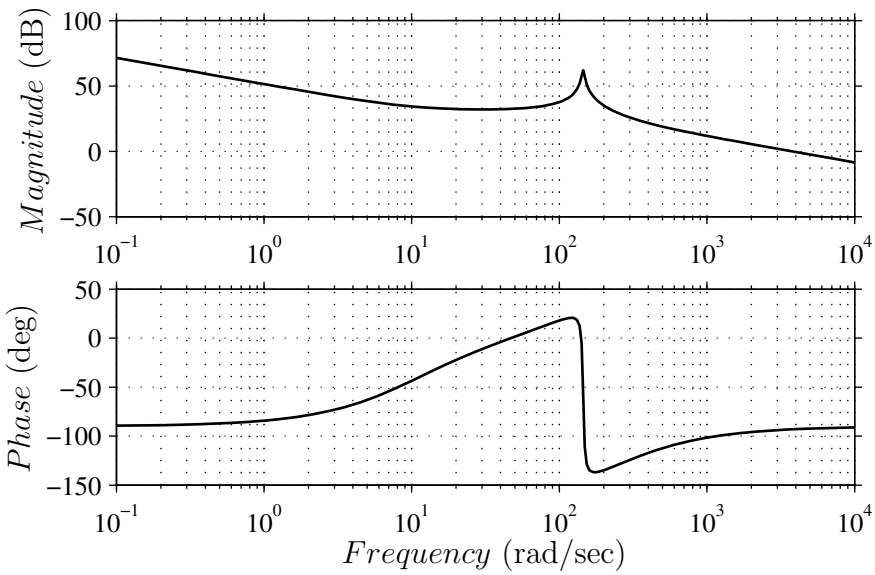

Fig. 5.5: Bode diagram of $G_c(s)G_{id}(s)$.

rad/s, which leads to a frequency of roughly $f_c = 500$ Hz (Fig. 5.6). For discrete systems the critical frequency is the sampling rate, because it can be modelled as a dead time with the value of the sampling time. The bandwidth of the controller is a factor 20 away from the switching frequency of the system, which leads to a stable controller. In order to use the controller in dSpace, it has to be implemented with discrete integrator blocks (Appendix F).

5.3 Voltage and Current Measurement

The voltage measurement is done with the measuring card "UMAT2.PCB", which has been developed at the Department of Electrical Engineering at Chalmers University of Technology. This card consists of each three independent channels to measure voltages and currents. The measured signals are connected to the dSpace system.

The currents are measured with LEM current transducers (LA100-S), which have a turns ration of 1:2000. The measurement wires are wrapped six times around the current sensors, such that the measured currents represents six times the actual currents. The output currents of the LEM modules flow through 100 Ω shunt resistors. The voltage across these resistors are then measured with the dSpace system.

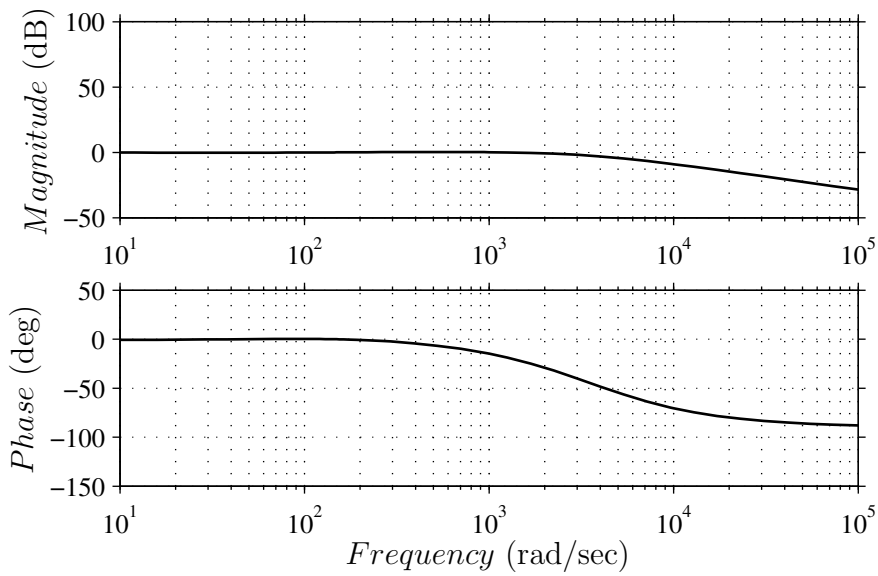

Fig. 5.6: Closed loop bode diagram.

Scaling all these, the voltages have to be multiplied by a factor of 200/6 in order to display the actual currents.

5.4 Overcurrent Protection

An overcurrent protection is built for the inductor current. It is realized as an analog circuit (Fig. E.1). No protection is implemented for the input and output current.

5.5 Measurements

5.5.1 Current and Voltage Stress on Inductor and Semiconductors

Of interest are the voltage across and the current through the inductor and the overvoltage across the IGBT due to the parasitic inductance of the stripline. Furthermore, the current through the semiconductors, especially the IGBT, would be important to know. The semiconductors could be chosen to match the current stresses and the losses could be measured. Because the diode D and the IGBT are built into one package and the output loop of the converter is realized with a stripline, the current through the semiconductors can not be measured. For the measurements the coil current is $I_L = 5$ A. The input voltage is set to $U_1 = 300$ V and the output voltage to $U_2 = 400$ V. The duty cycle is $d = 0.25$.

The PWM output signal of the dSpace DSP system shows a disturbance when the IGBT is switched (Fig. 5.7). The delay through the overcurrent protection logic and the drive circuit is clearly visible.

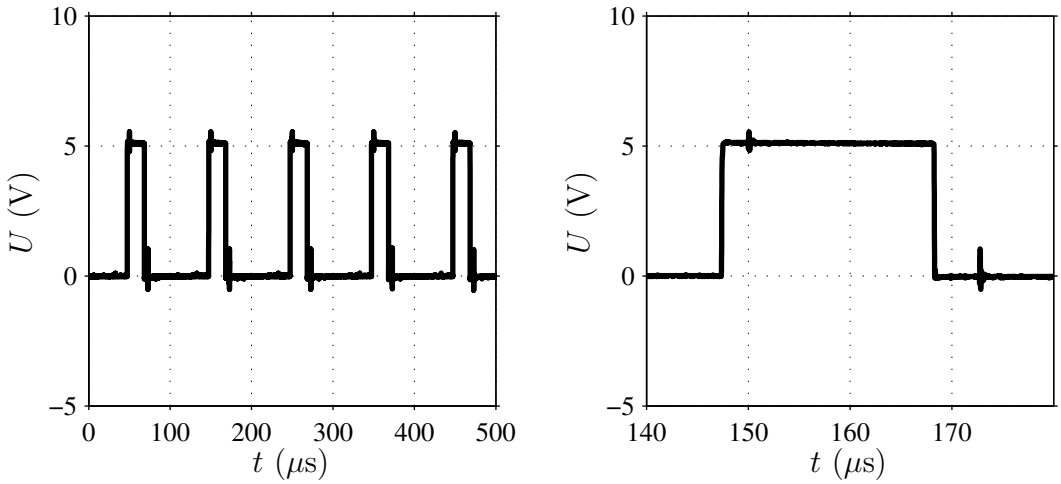

Fig. 5.7: dSpace PWM signal.

The voltage across the inductor shows an undershoot at turn off. This is due to the parasitic inductance of the stripline and possibly also an inductive behavior of the diode (Fig. 5.8).

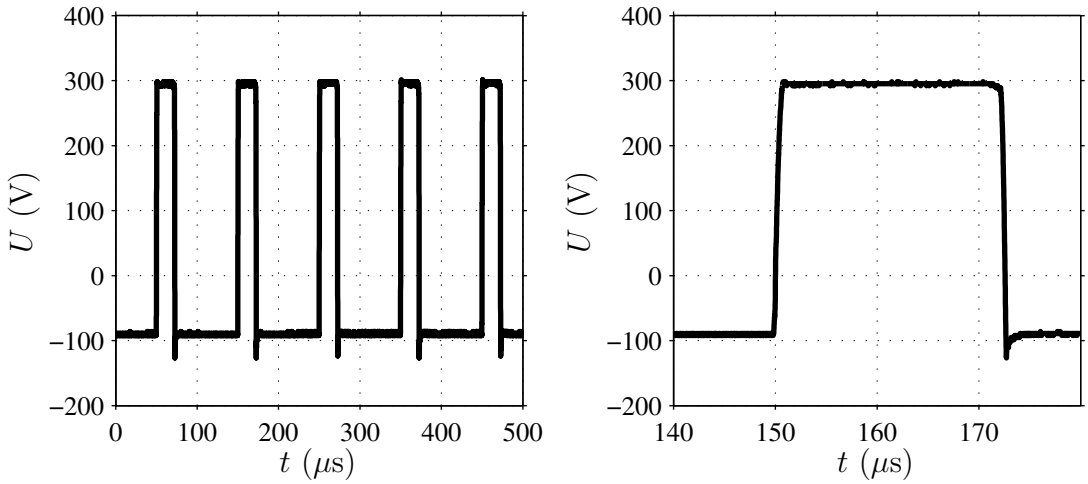

Fig. 5.8: Voltage over inductor at an average input current of 5A.

The current through the inductor has a quite large oscillation at the switching instants due to the parasitic capacitance (Fig. 5.9). There is an initial large current spike during the switching transients, where the main charging/discharging of the parasitic capacitor takes place. The following oscillation is between this capacitor and the wiring inductance.

With the standard setup of the driver ($R_G = 22\ \Omega$) the voltage across the IGBT has an overshoot at turn off of approximately 30 V, due to the parasitic inductance

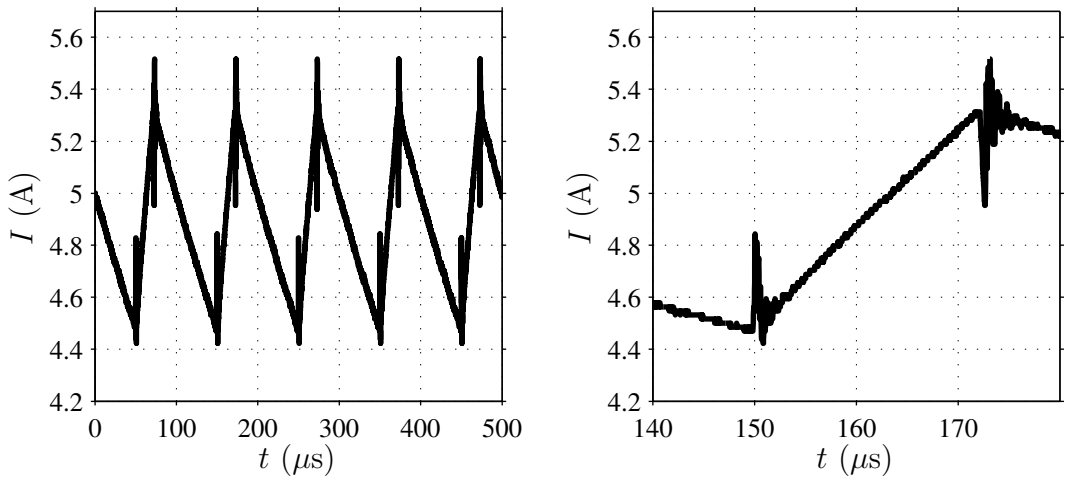

Fig. 5.9: Inductor current.

of the stripline ($\Delta U_{CE} = L_p \frac{di}{dt}$). Even with faster switching ($R_G = 7.8\ \Omega$) the overshoot is only 35 V (Fig. 5.10). Therefore there is no need for a snubber circuit, the stripline is low inductive enough. But for higher power, higher current boost converters this issue needs to be accounted for.

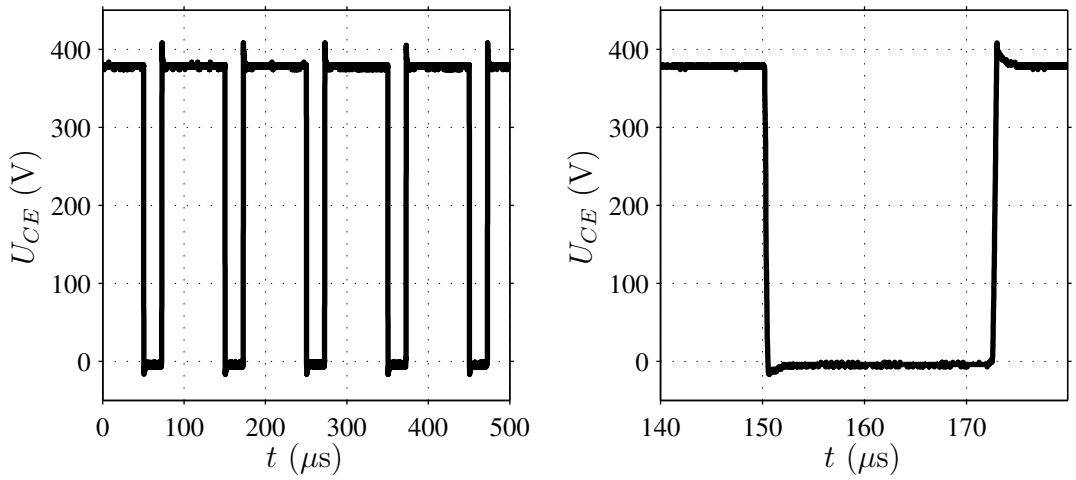

Fig. 5.10: Collector-emitter voltage U_{CE} at an inductor current of 5A, gate resistance $R_G = 7.8\ \Omega$.

5.5.2 Delays and Switching Transients

The delays of the gate driver and the switching transients for both turn on and turn off are analyzed. The transients are compared for two different gate resistors, $R_G = 22\ \Omega$ and $R_G = 7.8\ \Omega$. The measured voltages are (Fig. 5.11):

U_{dS}	dSpace PWM output signal;
U_{RG}	driver output voltage, before gate resistance;
U_{RG}	gate-emitter voltage;
U_{CE}	collector-emitter-voltage.

The delay of the signal through the overcurrent protection logic and the drive circuit

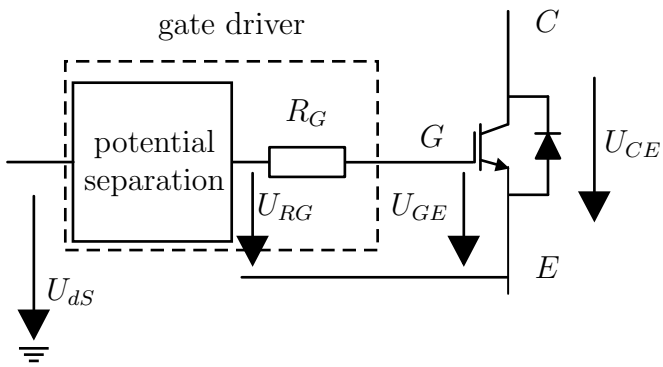

Fig. 5.11: IGBT with drive circuit.

with the potential separation is independent of the gate resistance. It is measured to be 1.67 μs for turn on (Fig. 5.14) and 1.60 μs for turn off (Fig. 5.15).

In contrary, the switching transients change with different gate resistances. For a lower resistance, the IGBT switches earlier and faster. The four voltages are shown for two periods for a gate resistance $R_G = 22\ \Omega$ (Fig. 5.12) and $R_G = 7.8\ \Omega$ (Fig. 5.13). The two resistances are compared for turn on (Fig. 5.14) and turn off (Fig. 5.15).

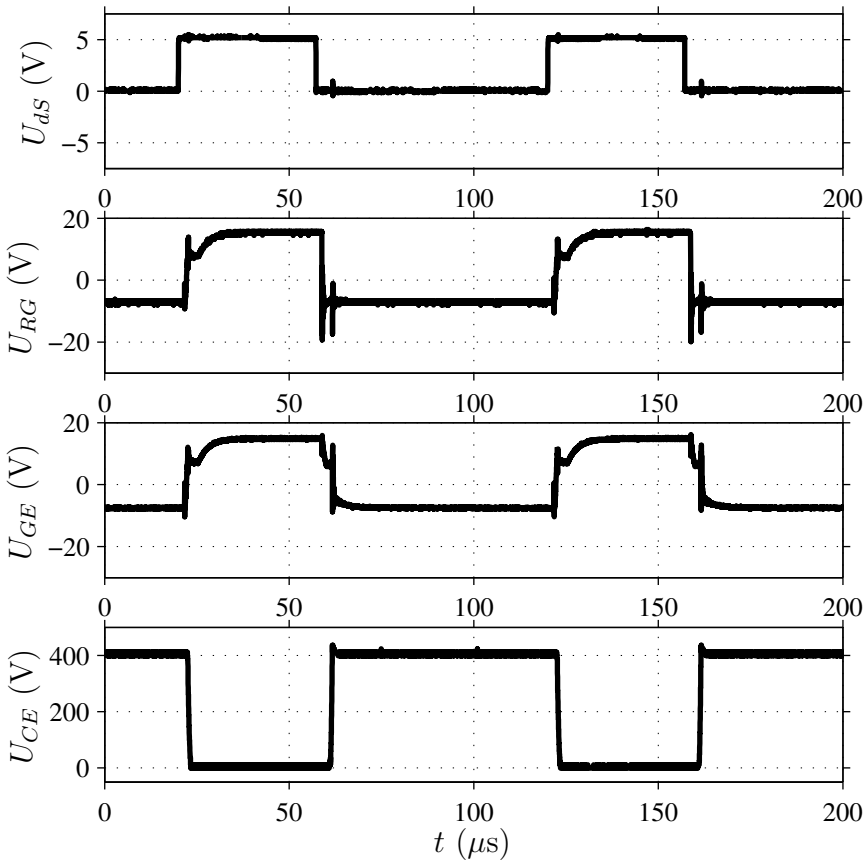

Fig. 5.12: U_{dS}, U_{RG}, U_{GE} and U_{CE} for $R_G = 22\ \Omega$.

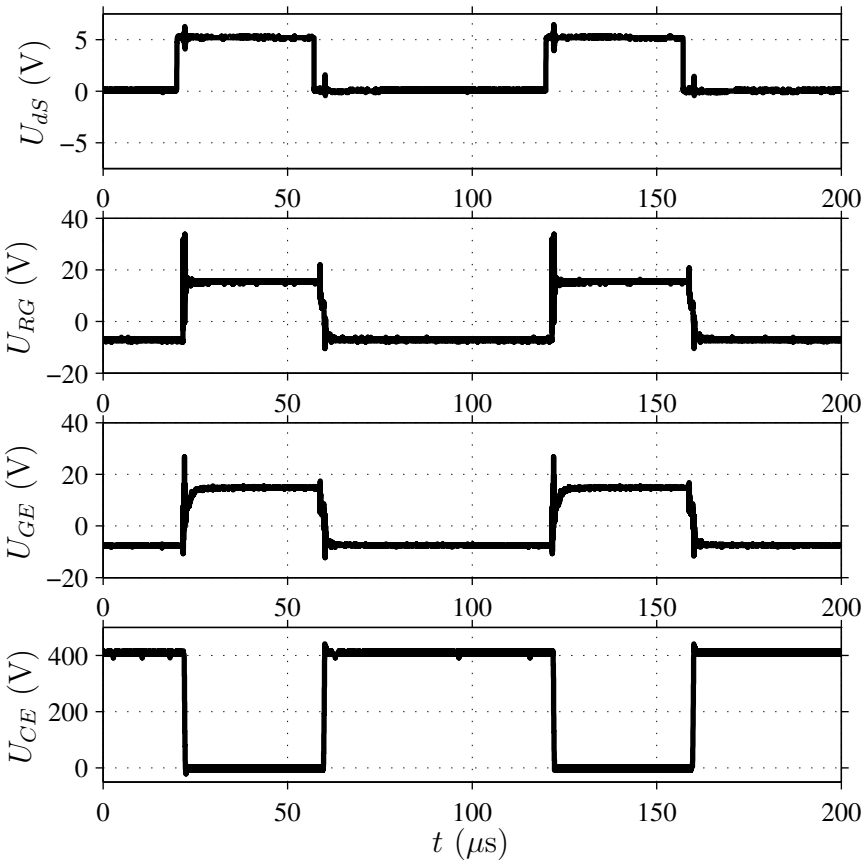

Fig. 5.13: U_{dS}, U_{RG}, U_{GE} and U_{CE} for $R_G = 7.8\ \Omega$.

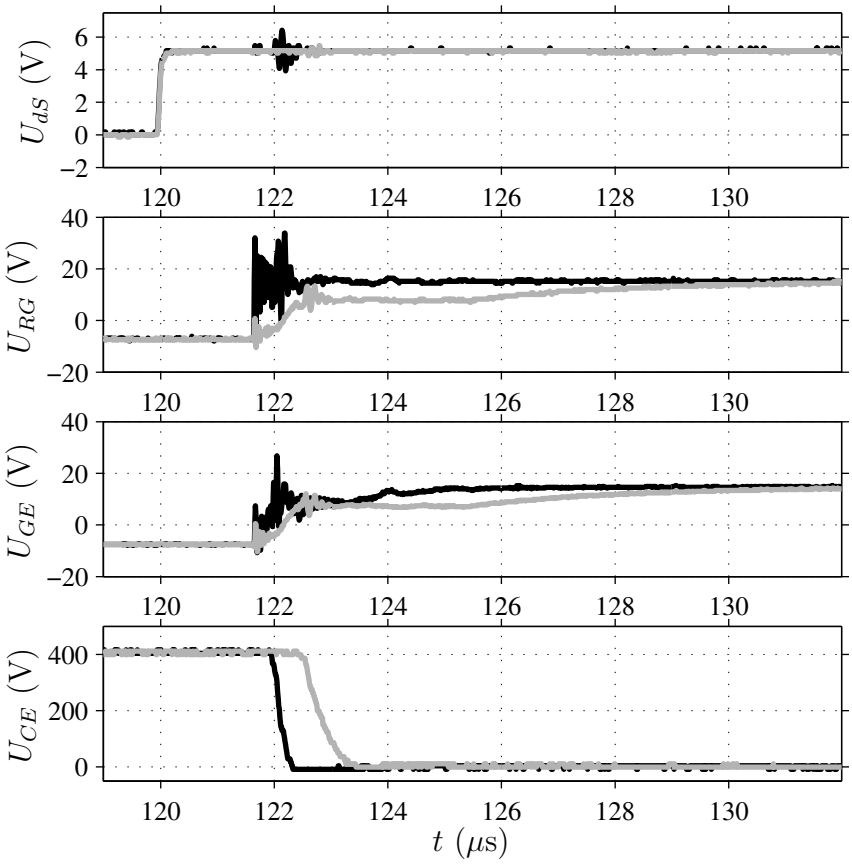

Fig. 5.14: U_{dS}, U_{RG}, U_{GE} and U_{CE} at turn on for $R_G = 22\ \Omega$ (grey) and $R_G = 7.8\Omega$ (black).

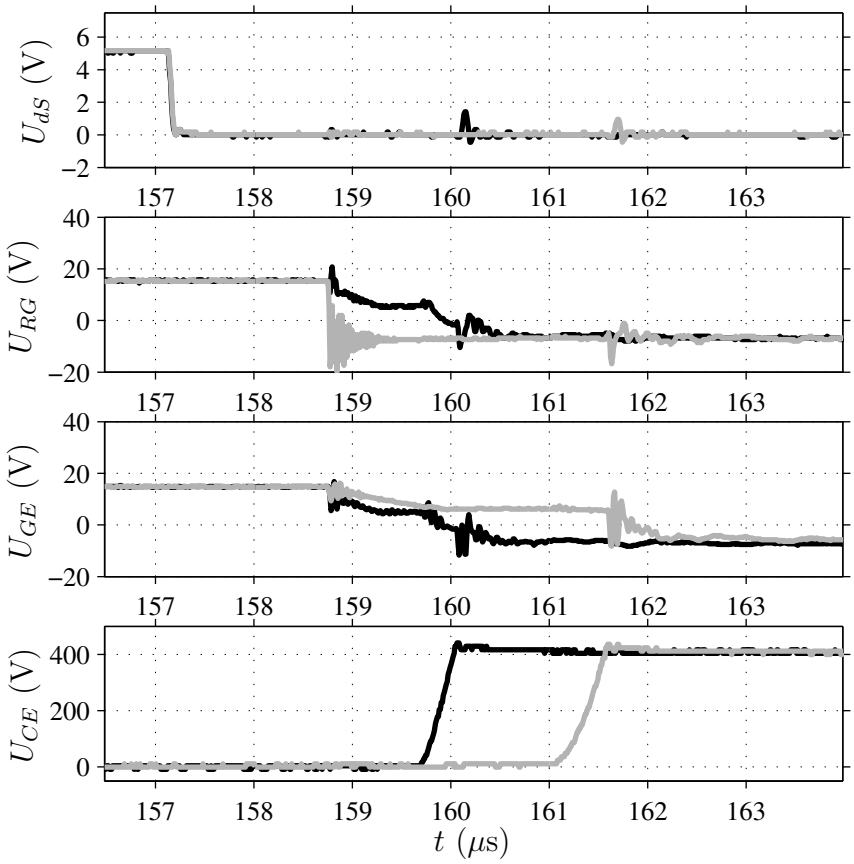

Fig. 5.15: U_{dS}, U_{RG}, U_{GE} and U_{CE} at turn off for $R_G = 22\ \Omega$ (grey) and $R_G = 7.8\Omega$ (black).

5.5.3 Current Step

Simulation and measurement are compared for a current step. The controller is both the same in the lab setup and simulation. The current measurement is sampled with 10 kHz in reality, therefore a sample and hold block has been implemented for the simulations (Appendix F). The measured and simulated current match very well. The controller shows a fast and stable behavior both for a current step from 3 to 4 A (Fig. 5.16) and 4 to 5 A (Fig. 5.17).

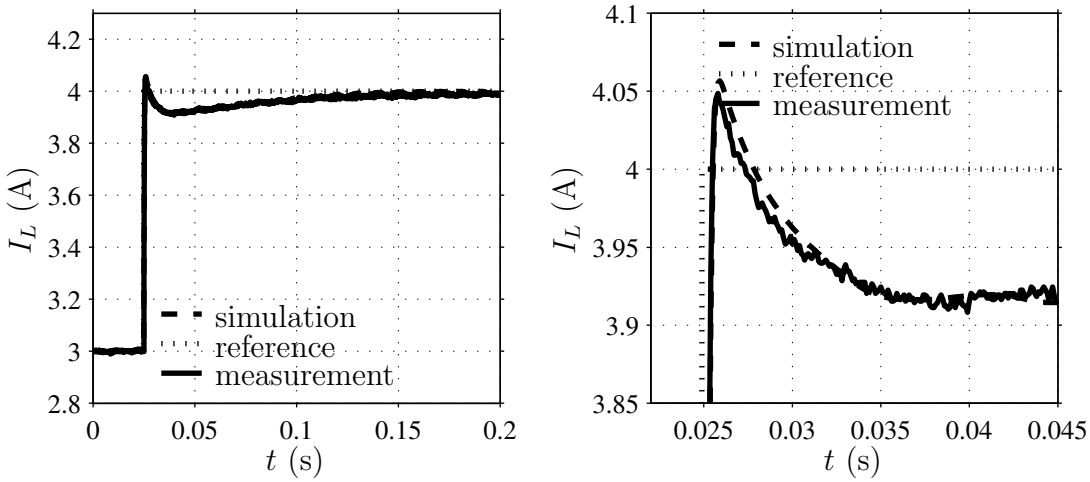

Fig. 5.16: Simulated and measured inductor current I_L of the converter. Step from 3 to 4 A.

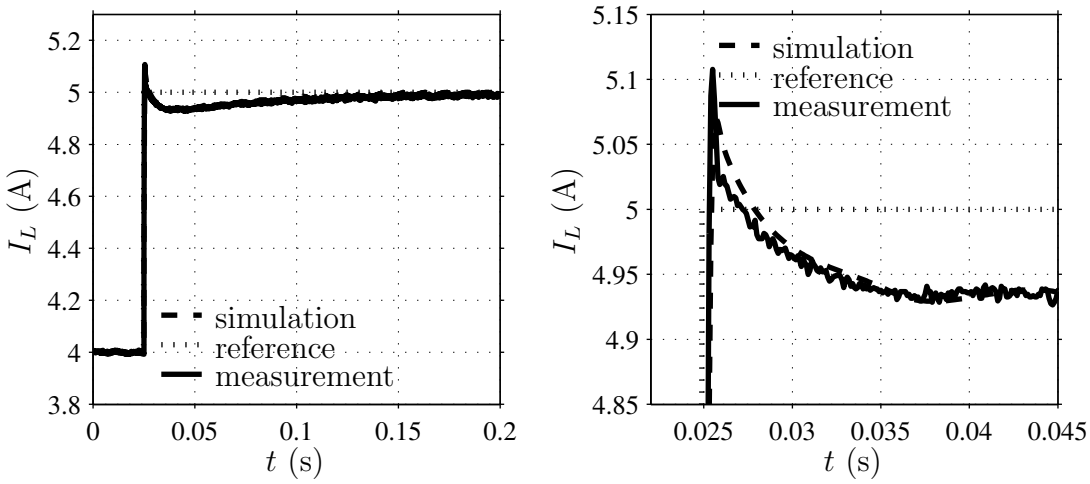

Fig. 5.17: Simulated and measured inductor current I_L of the converter. Step from 4 to 5 A.

5.6 Summary

Tests of the converter under load showed a fast step response of the current. The parameters of the PI controller, which regulates the inductor current, were obtained with state-space averaging and bode plot analysis.

Measurements of the collector-emitter voltage of the IGBT showed only a low overvoltage at turn off. Nevertheless, this issue needs to be taken into consideration if the boost converter is operated at higher currents and voltages. A snubber circuit might then be needed, which would result in additional losses and therefore lower efficiency of the converter.

Oscillations, caused by the parasitic interwinding capacitance of the inductor, occurred in the inductor current waveform. This means that for higher currents the design of the inductor is critical. There are several methods to avoid a large parasitic capacitance such as building the inductor with a single turns layer or using multiple chamber windings.

Simulations performed with Simulink/PLECS [21] matched measurements extremely well. In further work the model can be used to predict the converter behavior at higher power.

6 Experimental Lab Setup of a Wind Turbine Unit with DC Output

An experimental setup of a wind turbine unit described in Chapter 1 has been built in the laboratory (Fig. 6.1). The goals are to test the performance of such a unit, evaluate the advantages of series compensation in combination with PMSG and compare simulation and measurement. The obtained models can be used to upscale the wind turbine unit in simulation.

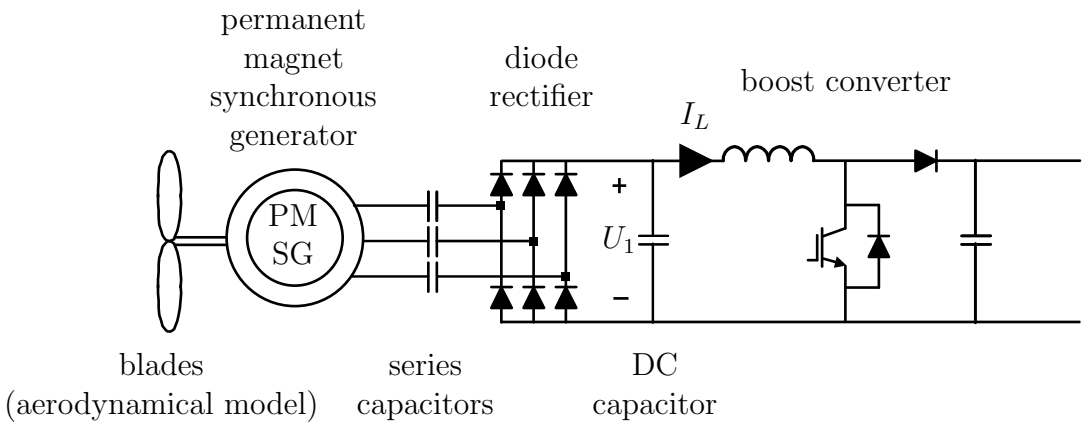

Fig. 6.1: The chosen configuration for the wind turbine unit with DC output.

6.1 System Description

6.1.1 DC Machine as Aerodynamic System

The permanent-magnet generator is driven by a DC machine. Either the speed or the armature current can be controlled. Most measurements have been carried out at constant speed. To test a whole wind turbine controller according to Chapter 2.4, the DC machine can simulate wind. For this, an aerodynamical model (Section 2.5.1) has been implemented in LabView. The torque output is adjusted considering a DC machine model (including losses). With this, the armature current reference is set.

6.1.2 PMSM

The machine used as generator is a three phase permanent-magnet synchronous machine with one pole-pair. It used to be a induction machine, but the rotor has been replaced with a permanent-magnet rotor. There was no data available such that parameters like the stator resistance, stator inductance and permanent-magnet flux linkage had to be determined first. The parameters are summarized in Table 6.1.

The flux linkage of the PMSM can be calculated with

$$\Psi_{PM} = \frac{60U_P}{\sqrt{2}\pi n_{PMSM}} \tag{6.63}$$

where

U_P	back EMF (V);
Ψ_{PM}	permanent-magnet flux linkage (Vs);
n	speed PMSM (rpm).

Measuring the back EMF at a speed of 1500 rpm leads to a value of $U_P = 164.98$V. Putting these values in equation 6.63 results in a flux linkage of Ψ_{PM}=1.48 Vs.

At ambient temperature ($\vartheta = 20$ °C), the resistance of one winding is measured to $R_{20} = 2.88\ \Omega$. The winding resistance changes with temperature ϑ,

$$R_\vartheta = R_{20}(1 + \alpha_{Cu}(\vartheta - 20^oC)) \tag{6.64}$$

where

α	temperature coefficient ($\frac{1}{^oC}$);
ϑ	winding temperature (°C).

After 15 minutes of running with a phase current of 5.3 A, the resistance is measured again and found to be 3.25 Ω. With (6.64) this leads to a winding temperature of 54.7 °C. All the measurements have been carried out on the warm machine. Therefore this resistance value has been used in the simulations.

To determine the inductance, measurements with different loads, down to short circuit have been carried out. The inductance was determined to $L = 220$ mH.

The inertia of the whole drive train (DC and permanent-magnet machine together) has been measured and is approximately J = 0.048 kgm^2.

A summary of the machine data is given in Table 6.1. Some data from the previous induction machine is included.

6.1.3 Series Compensation

For the series compensation a capacitance has been put in each phase. Each capacitance consists of eight, in parallel connected 40 μF capacitors which results in a total capacitance of $C_{\text{series}} = 240\ \mu$F. Each capacitor has a tolerance of ±10%. At full compensation, the whole voltage drop over the inductance is compensated with the capacitance:

$$\omega L = \frac{1}{\omega C_{\text{series}}}. \tag{6.65}$$

This leads to a speed with full compensation of

$$n_{\text{full compensation}} = \frac{60}{2\pi}\sqrt{\frac{1}{LC_{\text{series}}}} = 1314 \text{ rpm}. \tag{6.66}$$

Induction Machine		
rated power	P_{rated}	4 kW
number of phases	N	3
pole-pairs	p	1
rated speed	n_{rated}	2800 rpm
rated voltage	$U_{p,\text{rated}}$	380 V
rated current	I_r	8.2 A
PMSM		
inductance	L	220 mH
resistance	R	2.88 Ω
rated speed	n_{rated}	3000 rpm
rated stator frequency	$f_{s,\text{rated}}$	50 Hz
rated stator angular frequency	$\omega_{s,\text{rated}}$	314.16 $\frac{\text{rad}}{\text{s}}$
permanent-magnet flux linkage	ψ_{PM}	1.48 Vs

Table 6.1: Summary of the parameters of the previous induction machine and the permanent-magnet synchronous machine used in the lab.

6.1.4 Diode Rectifier

To generate a DC voltage from the 3 AC phases, a standard three phase diode rectifier is used. To smooth out the DC voltage, a DC capacitor of 1950 μF is placed across the DC terminals of the rectifier.

6.1.5 Boost Converter

The boost converter has been analyzed in detail in Chapter 5.

6.1.6 Output Connection

There are two possibilities output connection to the wind turbine unit:

Resistive Load The output of the boost converter can be connected to different resistances. This is the easiest way to measure.

Constant Output Voltage To test the setup for the application with constant, given output voltage, the armature terminals of two DC machines are connected in series. The DC machines are powered by induction motors coupled to the net (Fig. 6.2). The converter output voltage can be adjusted with the field current of the DC machines.

6.2 Modelling

All the modelling of the lab setup has been done in the Matlab/Simulink environment. For the electrical system, including the PMSM, the PLECS (Piece-wise Linear

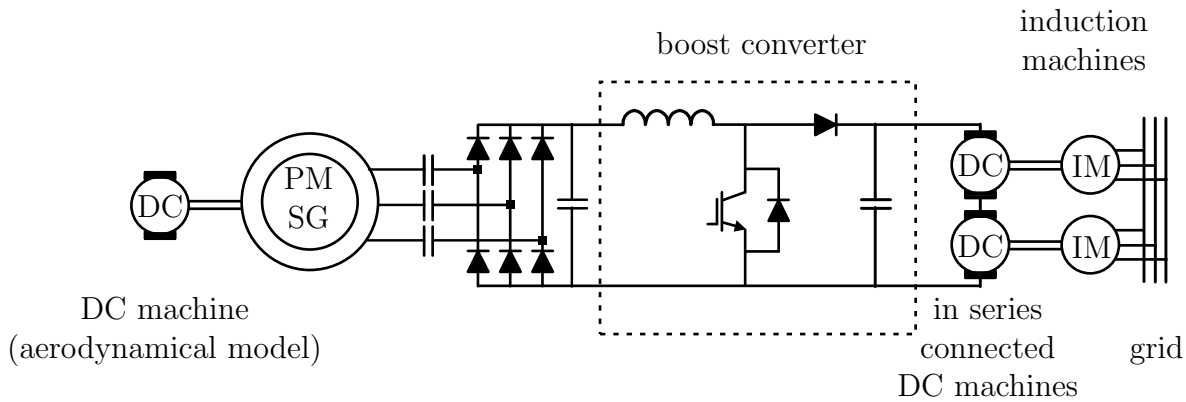

Fig. 6.2: Wind turbine unit with constant output voltage.

Electrical Circuit Simulation for Simulink) toolbox has been used [21]. With this, the electrical circuits can be integrated into a Simulink model. For the simulations with constant speed, a PI controller sets the mechanical torque of the PMSM.

The Simulink models are shown in Appendix F. The lab setup is controlled with dSpace. The PWM frequency, and therefore also the sampling rate, is 10 kHz. To be able to compare measurements and simulation results, also in the model the controllers are discrete and the measurements are sampled with the same frequency.

6.3 Comparing Simulation and Measurements

6.3.1 DC Power

The entire wind turbine unit has been simulated for DC power as function of DC current. The same has been measured on the lab setup. Without compensation the limit of the power output is clearly visible (Fig. 6.3). The peak power for different speeds is reached at the same DC current, approximately 4 A.

If the same procedure is carried out with series compensation, it can be seen that in the area of the full compensation (n = 1314 rpm), the power output is almost unlimited (Fig. 6.4).

Simulation and measurement results show good agreement. Simulation results show generally a bit higher power. Probable reasons for this are nonlinearities (inductance), uncertainties in inductance and capacitance values, harmonics and neglected losses such as iron losses and resistive losses in cables and connections.

6.3.2 Input Voltage

Running the whole setup without compensation, the measured input voltage of the converter is slightly lower than the value gained through simulations, depending on the load (Fig. 6.5). The reason for that might be the same as in Chapter 6.3.1. The uncertainty and nonlinearity of the inductance has a big influence.

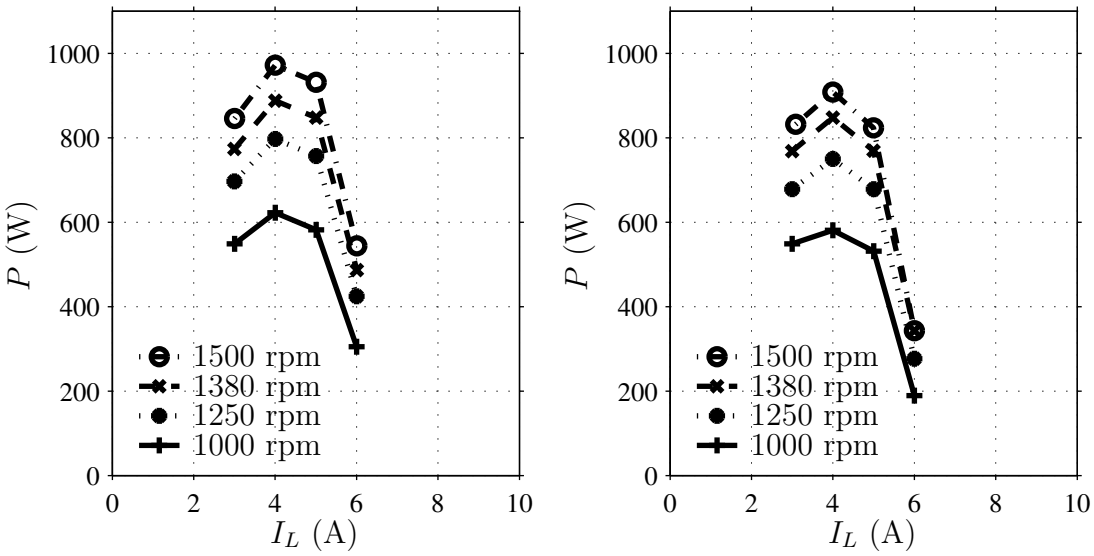

Fig. 6.3: Power output ($P = I_L U_1$) with no compensation. a) Simulation, b) measurement.

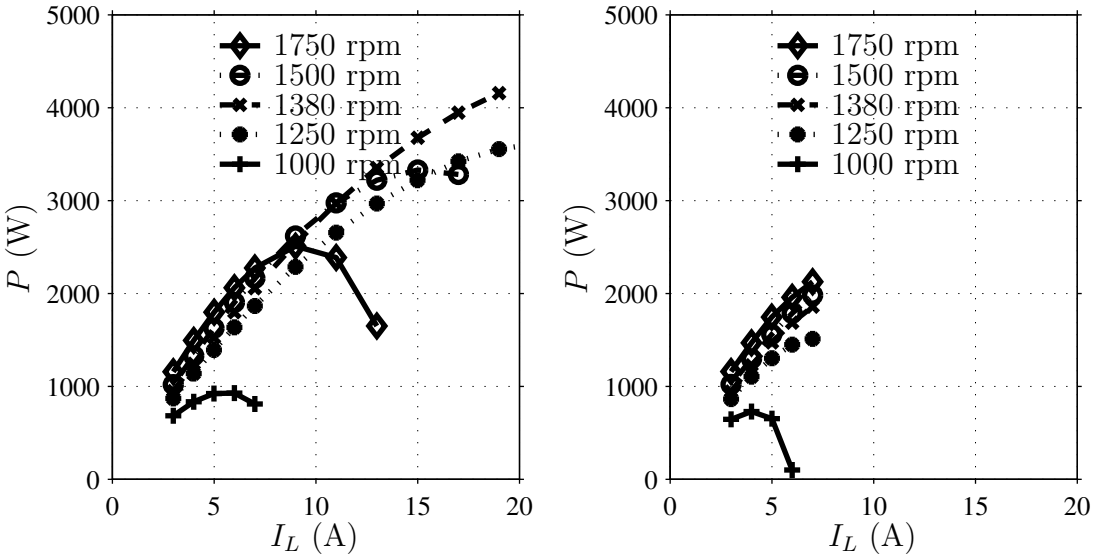

Fig. 6.4: Power output ($P = I_L U_1$) with series compensation. a) Simulation, b) measurement.

Doing the same for series compensation at the same speed leads to higher voltages. Since the speed is in the range of full compensation, the voltage is almost independent of the load (Fig. 6.6). The same phenomenon appears as without compensation, the voltage difference increases with increasing load. This probably is due to the same reasons. Furthermore it can be said that above the compensated speed, a difference in the value of the inductance, and below a difference in the capacitance, has more influence.

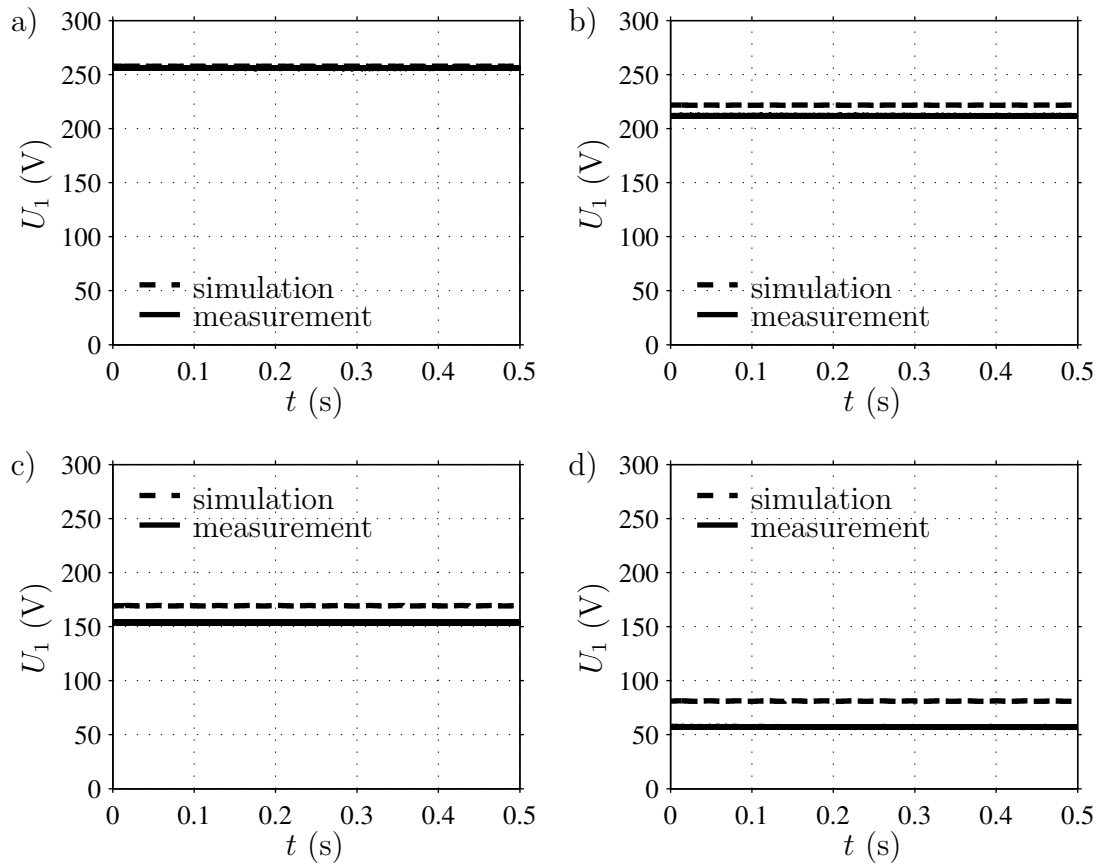

Fig. 6.5: Measured and simulated input voltage of the converter for a generator speed of 1380 rpm and no compensation. The inductor current is a) I = 3 A, b) I = 4 A, c) I = 5 A and d) I = 6 A.

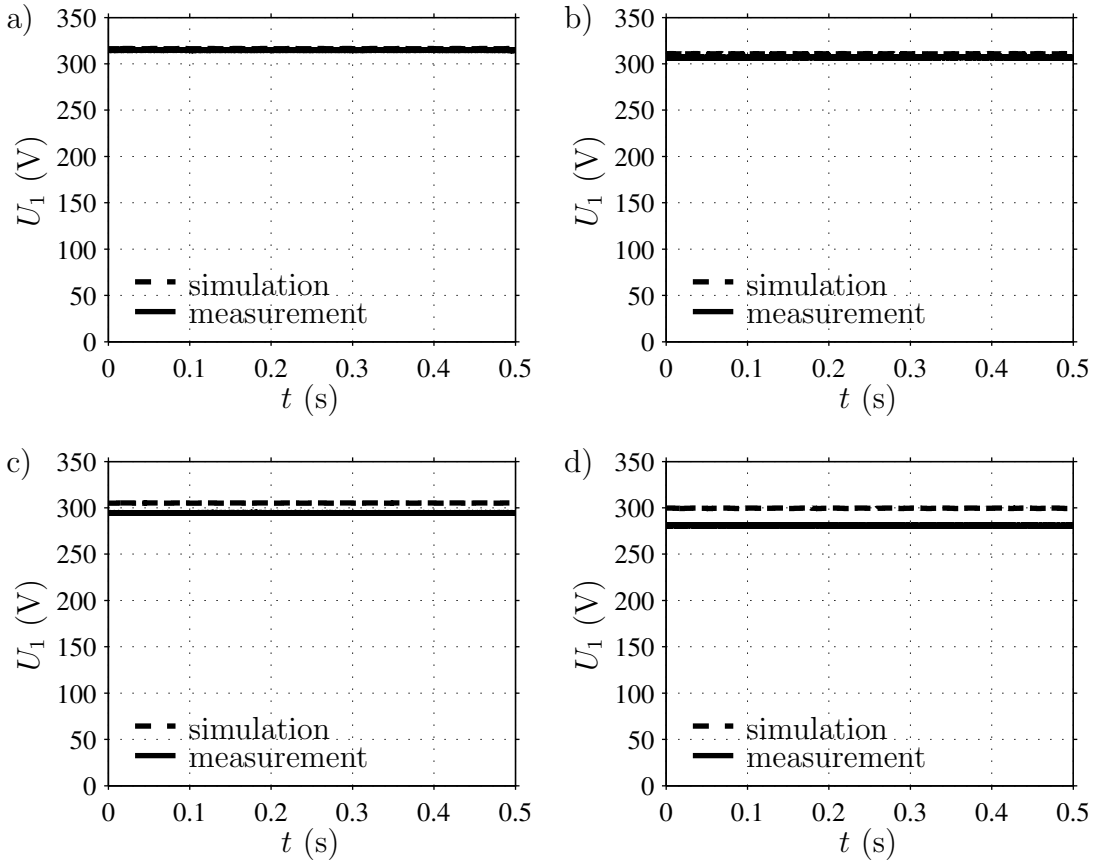

Fig. 6.6: Measured and simulated input voltage of the converter for a generator speed of 1380 rpm and series compensation. The inductor current is a) I = 3 A, b) I = 4 A, c) I = 5 A and d) I = 6 A.

6.4 Measurements for DC Link Application

One possible application for the wind turbine unit is a stall controlled variable speed wind turbine feeding a stiff DC link. The DC voltage is fixed and controlled externally. The task of the DC/DC converter is to control the torque, which is done with the input current of the boost converter. The wind turbine controller, which sets the reference current for the DC/DC converter, is built according to Chapter 2.4. The aerodynamic system is simulated with a LabView program. The blades have a radius of $r = 1$ m, and a $C_p(\lambda)$ curve according Fig. 2.1. To adjust the speed to the generator system, there is a virtual gear box with a ratio of $n_{\text{generator}}/n_{\text{blades}}$ = 1.8. The aerodynamic model is not very accurate and not designed to determine the exact power output, but to show that the wind turbine unit is feasible for wind turbine applications. The measurements show a good and expected performance over the whole speed range (Fig. 6.7). The fluctuations in the output power of the

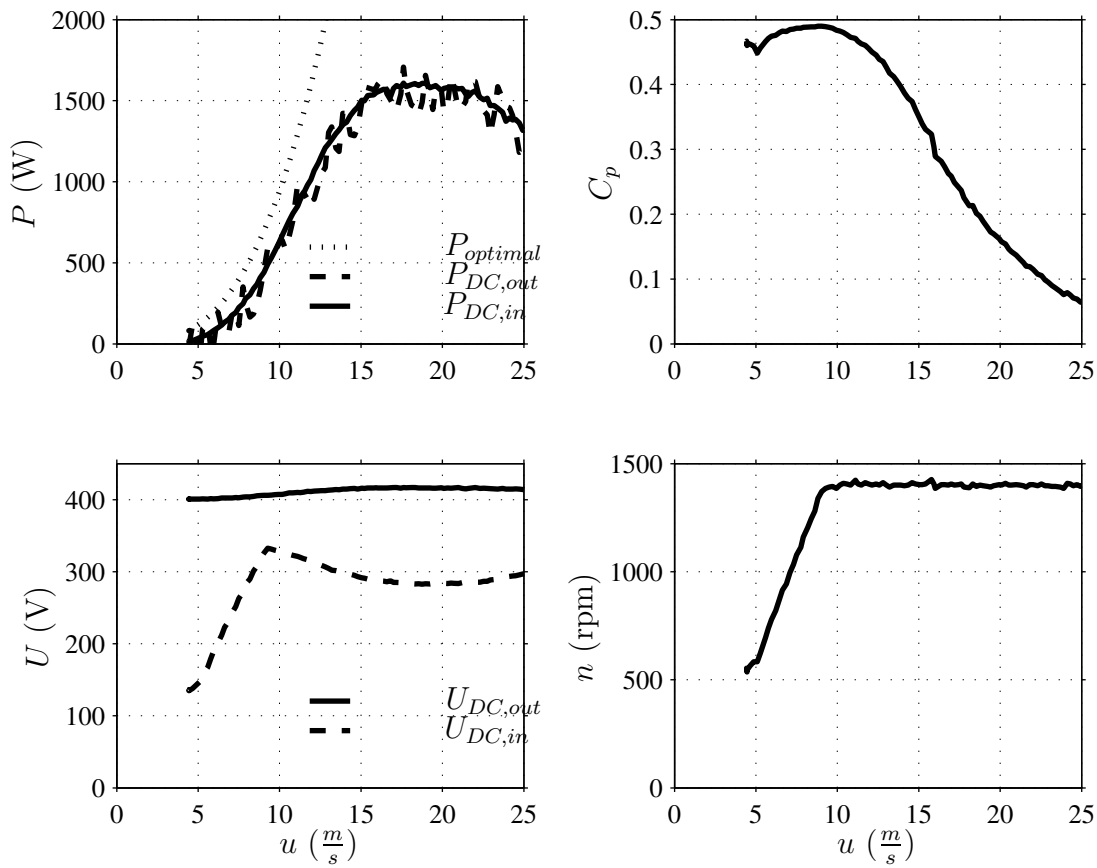

Fig. 6.7: Measurement on the lab setup as a variable speed, stall controlled wind turbine.

converter are probably due to oscillations between the output capacitance and the two in series connected DC machines. The power output is, even for the optimal C_p, much lower than the calculated optimal power. This is due to mechanical losses,

the aerodynamical model and nonlinearities in the DC machine that drives the generator.

7 Conclusion

This thesis investigated a wind turbine unit with DC output and all of its components.

Series compensation in connection with a PMSG and a diode rectifier works well for wind turbine applications. Compared to parallel compensation and no compensation the power output is increased. At the speed series compensation is designed for, the output power is just limited by the generator, not by the electrical system. Compared to a full transistor rectifier, series compensation performs almost as well for wind turbine applications and is a cheap, efficient and simple alternative.

A boost converter was built in order to investigate the entire wind turbine unit in the lab. The converter was analyzed with respect to problems that can arise in case of upscaling to higher power. The inductor has to be built carefully, a large parasitic capacitance should be avoided. This can be achieved with just one layer of windings or multi chamber windings. To limit the stress on the semiconductors, snubber circuits might be needed in case of higher power. This results in additional losses.

Simulations were carried out for both the entire wind turbine unit and the boost converter itself. In both cases, the agreement with the measurements were very good. Therefore, the models can be used to investigate the wind turbine unit in different configurations.

For the Hönö test wind turbine, a new electrical system was proposed. It increases the possible power output, has lower losses at no and low load and solves the problem with overvoltage in optimal operation of the wind turbine.

DC in wind energy is not used in industrial applications yet, but research show promising results.

7.1 Future Work

The electrical system with a PMSG, series compensation, a diode rectifier and a boost converter has been analyzed considering power output and performance in a wind turbine application. Furthermore, the wind turbine unit should be investigated with respect to losses and cost, especially compared to a full transistor rectifier.

There are interesting challenges in building a DC/DC converter in the MW range. Especially the non-ideal characteristics of the components have to be looked at closely. If the transformation ratio has to be higher, isolated DC/DC converters with a high frequency transformer have to be analyzed. A new PhD project developing and investigating DC/DC converters for wind farm applications starts soon.

The proposed new electrical system for Hönö can be installed in the test wind turbine. Then, operation experience with a series compensated system could be obtained. To increase the power output the current capability of the generator has to be determined. This is an ongoing project. FEM calculations are undertaken and the manufacturer is contacted.

A Hönö - Electrical System

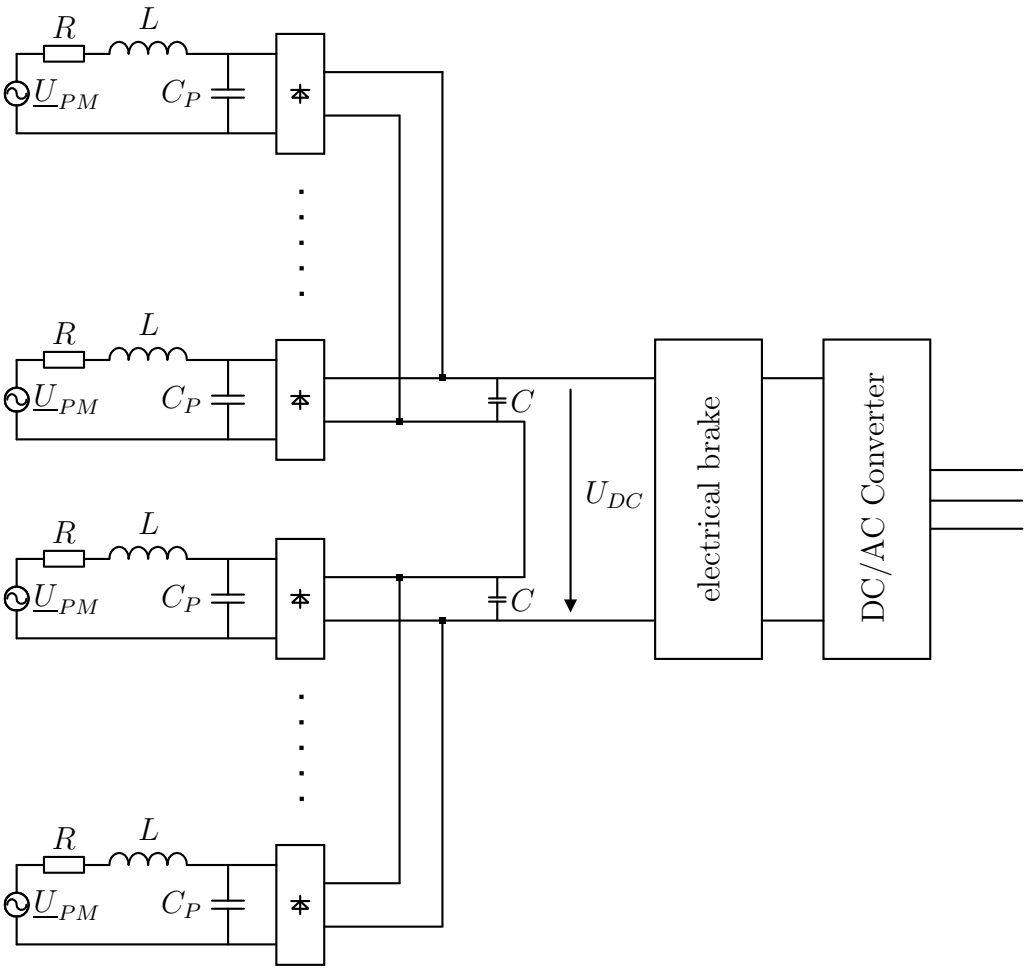

Fig. A.1: Electrical system of the Hönö wind turbine.

The upper branch consists of 14, the lower one of 13 modules. The modules in both branches are connected in parallel after the diode rectifier. Furthermore there is a 3300 μF capacitor (C) in each branch. The capacitance of C_P is 60 μF (two parallel connected capacitors of 30 μF).

B Hönö - $\mathbf{C_p}(\lambda)$ Values of the Blades

λ	C_p
2	0.014
2.25	0.016
2.5	0.022
2.75	0.032
3	0.044
3.25	0.064
3.5	0.09
3.75	0.12
4	0.15
4.5	0.218
5	0.284
5.5	0.358
6	0.408
6.5	0.44
7	0.46
7.5	0.472
8	0.482
8.5	0.488
9	0.49
9.5	0.488
10	0.484
11	0.468
12	0.444

Table B.1: $C_p(\lambda)$ values of the Hönö blades.

C Hönö - Model

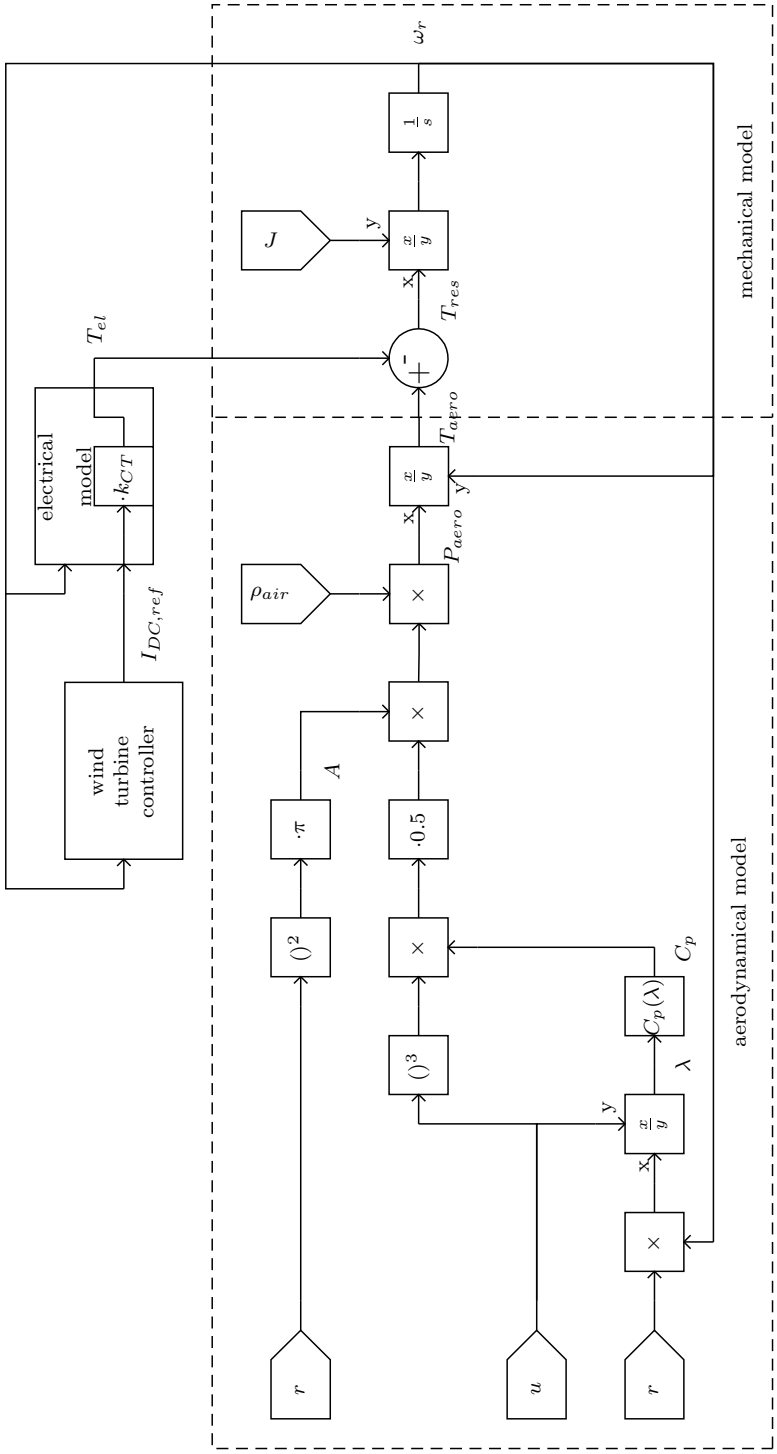

Fig. C.1: Aerodynamical, mechanical and electrical model of the Hönö wind turbine.

D Hönö - Measurements

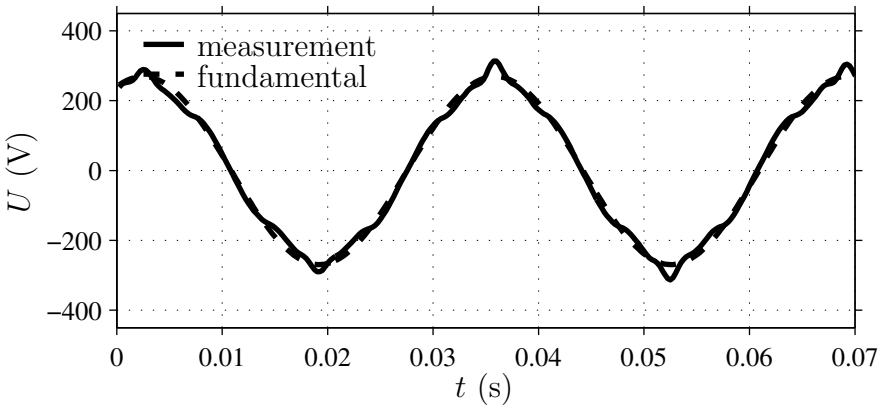

Fig. D.1: Open loop measurement on one single phase.

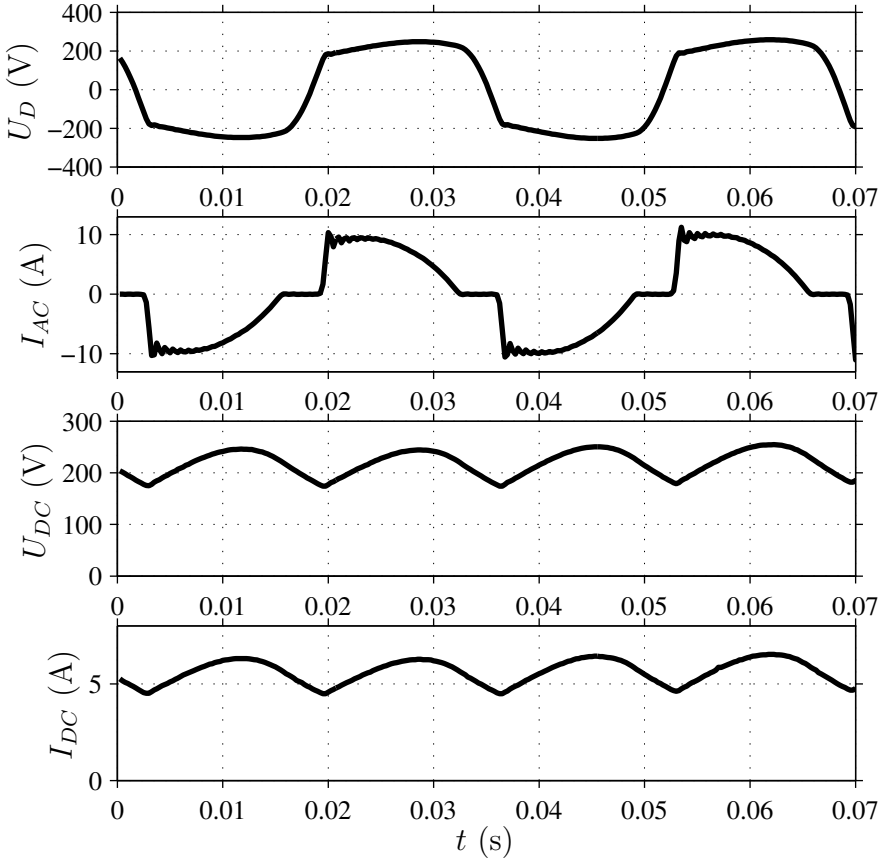

Fig. D.2: Measurements on one single phase with parallel compensation, diode rectifier and resistive DC load ($R_{DC} = 42\ \Omega$). Setup according Fig. D.3.

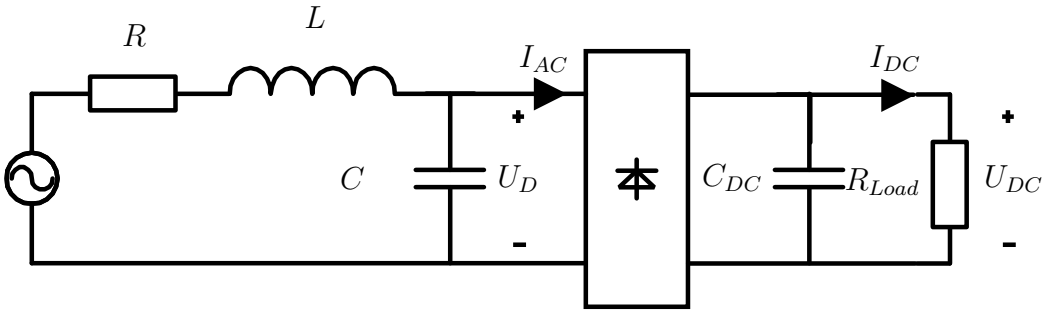

Fig. D.3: Setup for measurements on a single phase with parallel compensation, diode rectifier and resistive DC load. $C = 60\ \mu$F, $C_{DC} = 390\ \mu$F.

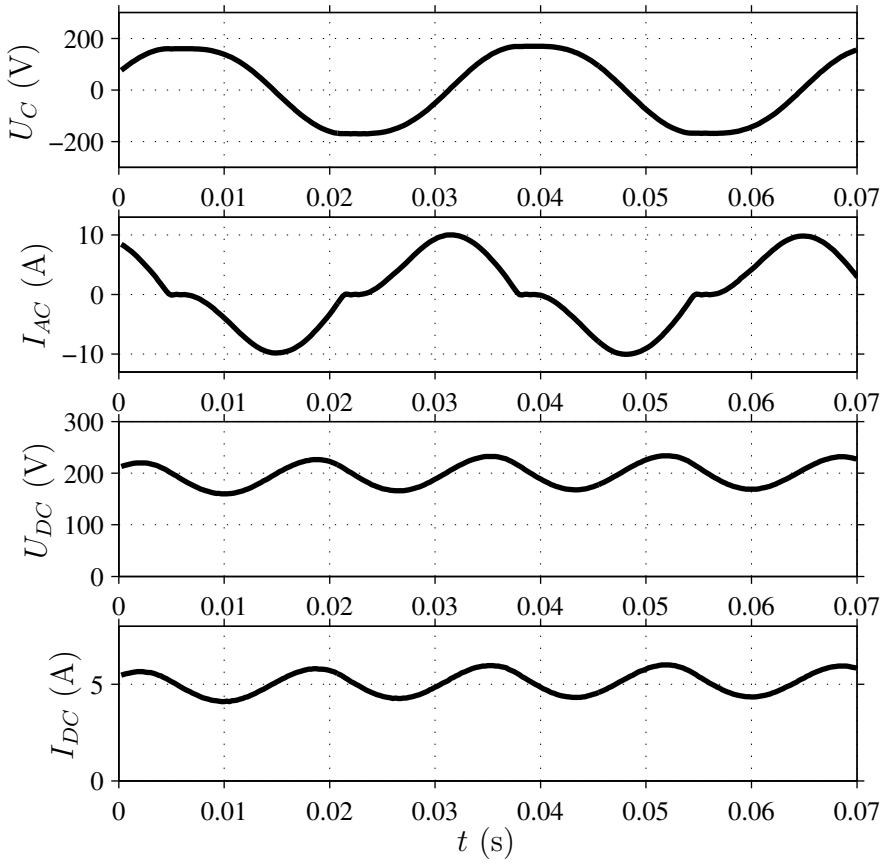

Fig. D.4: Measurements on one single phase with series compensation, diode rectifier and resistive DC load ($R_{DC} = 42\ \Omega$). Setup according Fig. D.5.

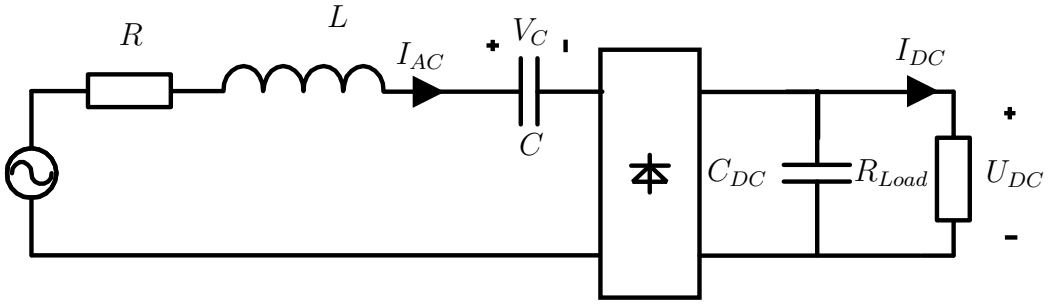

Fig. D.5: Setup for measurements on a single phase with series compensation, diode rectifier and resistive DC load. $C = 250\ \mu$F, $C_{DC} = 390\ \mu$F.

E Laboratory Setup - Overcurrent Protection

The circuit described in this section (Fig. E.1) shuts down the boost converter in case of a positive or negative overcurrent in the inductor. The output current of the LEM current transducer (LA 100-S) is flowing through a measuring resistor of 100 Ω as described in Chapter 5.3. The resulting positive or negative voltage drop across this resistor is then compared with a voltage applied to the negative input port of the two comparators (LM393). That voltage can be set with a 10 kΩ potentiometer. The voltage across the 100 Ω resistor and thus also the positive input voltage of the two comparators is 0.3 times the output current of the transducer.

SW_1 represents the overtemperature switch of the heat sink. In case the temperature of the heat sink reaches 71 °C the switch opens and causes the overtemperature error (Over Temp) to go on high (5 V). Furthermore this sets the D-flip-flop (HEF4013B) and turns the transistor on. The flip-flop can only be released by pressing the switch SW_2 which is located on the case of the boost converter. By turning on the transistor the LED lights up and indicates an error. This error signal is also read into dSpace (Main Error). The inverted main error signal is then connected to the gate driver signal of the dSpace system. In case the main error is set the input of the IGBT gate driver stays on 0 V independent of the value of the dSpace signal until the system is reset via the switch SW_2.

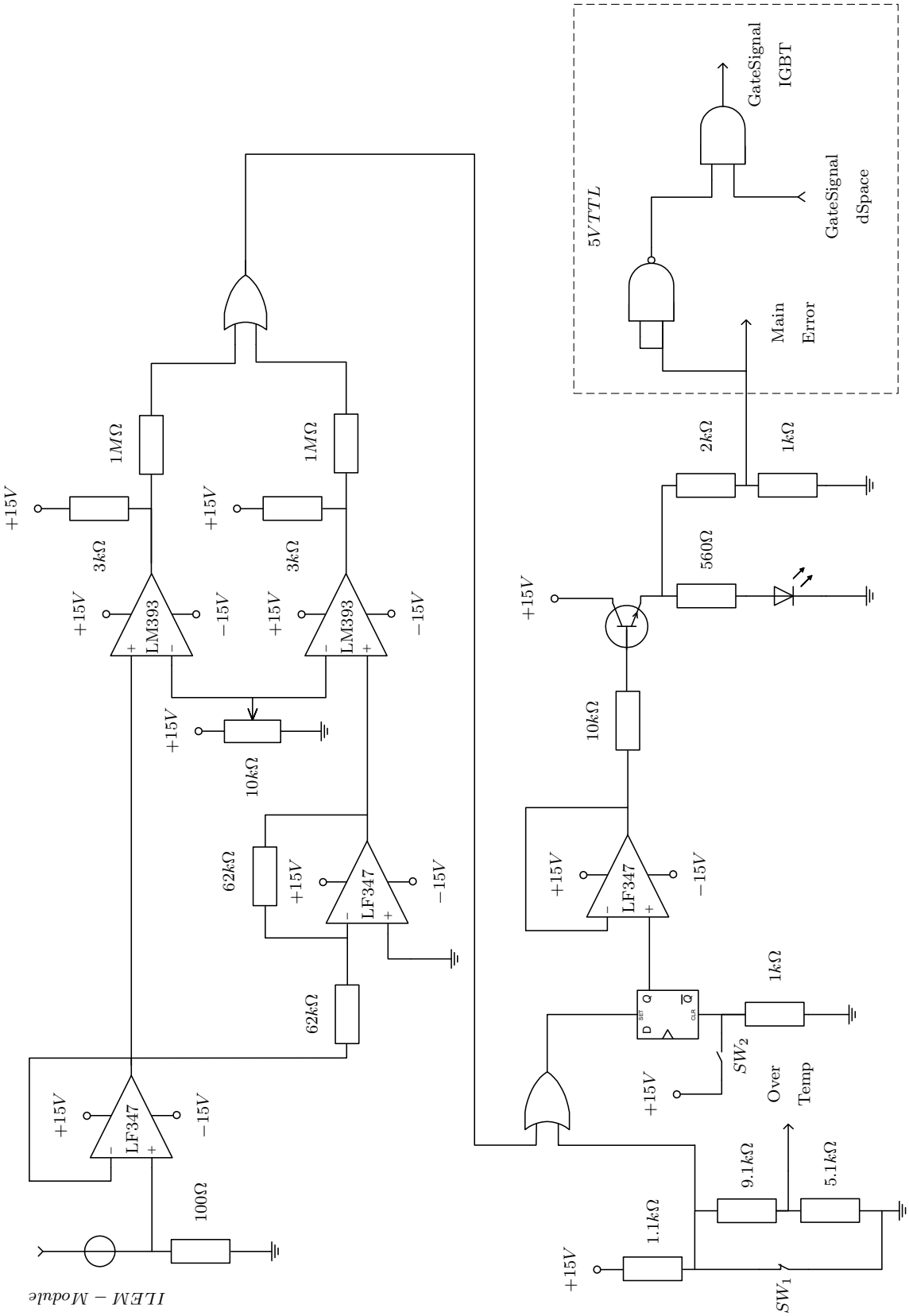

Fig. E.1: Overcurrent protection circuit.

F Laboratory Setup - Simulink Model

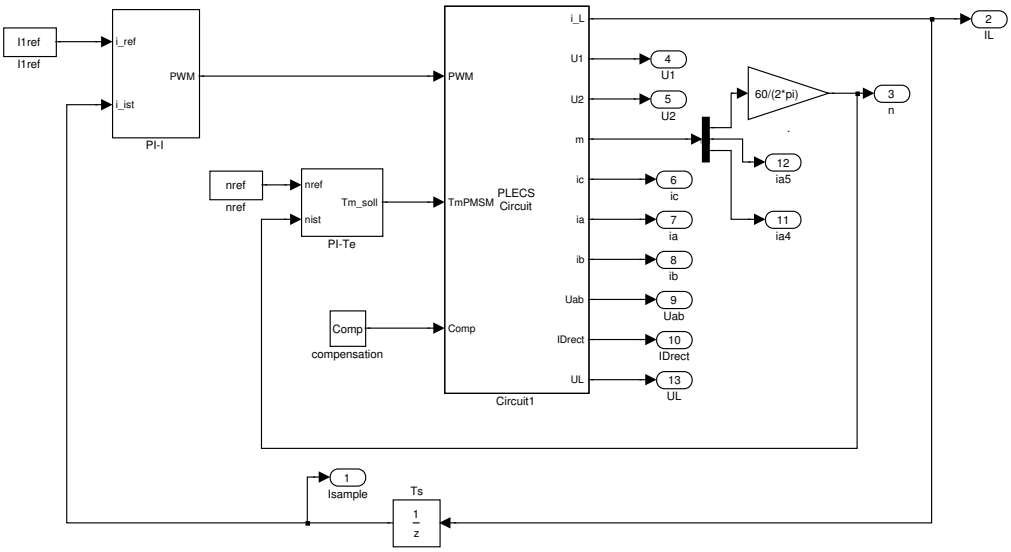

Fig. F.1: Entire Simulink model.

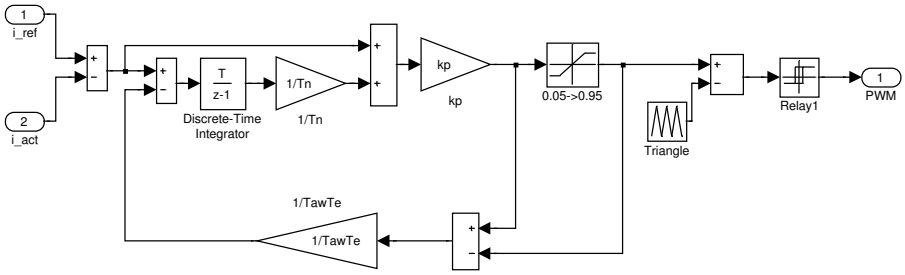

Fig. F.2: Current controller.

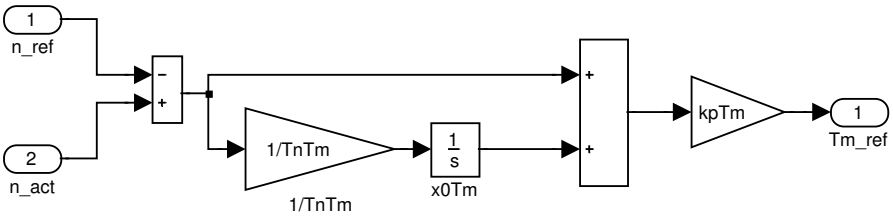

Fig. F.3: Torque controller.

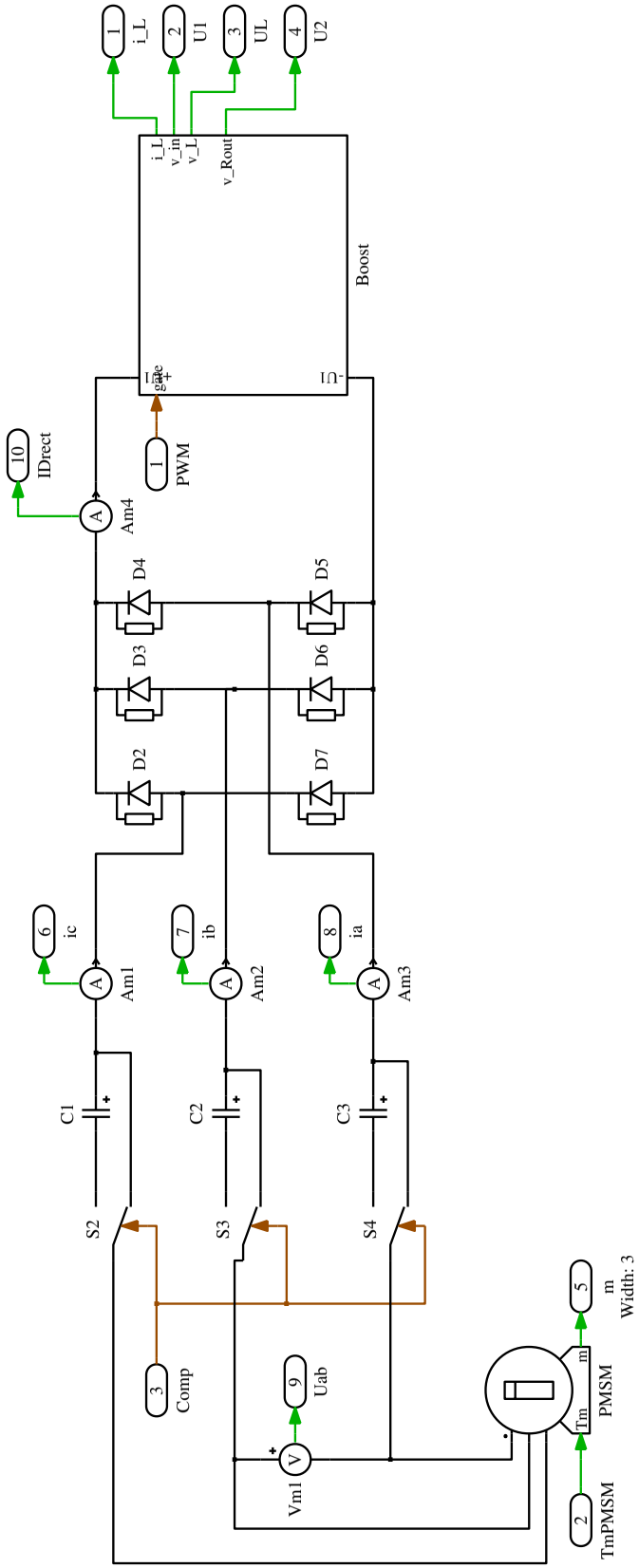

Fig. F.4: PLECS model.

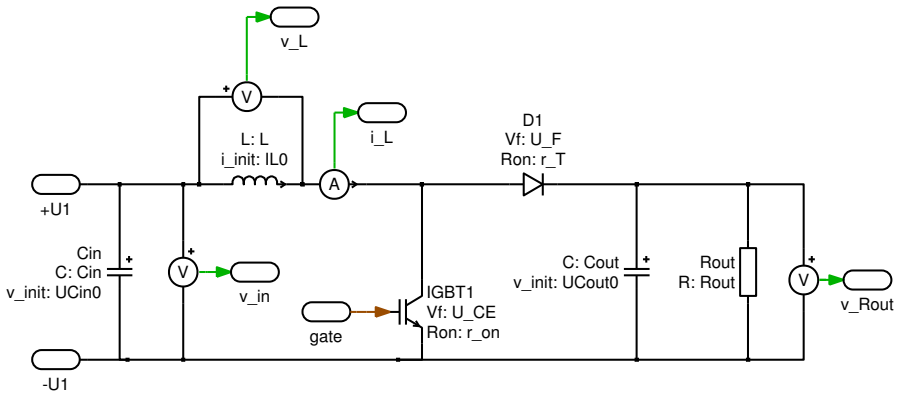

Fig. F.5: Boost model.

References

[1] D. Jorda, M. Twidell, J. Patel, F. Teofilo, R. Soin, "Remote power-integrated, customer oriented solutions", *Photovoltaic Energy Conversion, 1994*, Waikoloa, HI USA, 5-9 December 1994, pp. 747-749.

[2] L. H. Hansen, P. H. Madsen, F. Blaabjerg, H. C. Christensen, U. Lindhard, K. Eskildsen, "Generators and Power Electronics Technology for Wind Turbines", *Industrial Electronics Society, 2001 (IECON '01)*, Denver, Colorado, USA, 29 November-2 December 2001, pp. 2000-2005.

[3] S. Lundberg, "Configuration study of large wind parks", Chalmers University of Technology, Göteborg, Sweden, Licenciate Thesis 474L, 2003.

[4] O. Martander, "DC Grids for Wind Farms", Chalmers University of Technology, Göteborg, Sweden, Licenciate Thesis 443L, 2002.

[5] O. Martander, J. Svensson, "Connecting Offshore Wind Farms Using DC Cables", *Wind Power for the 21st Century*, Kassel, Germany, 25-27 September, 2000.

[6] K. J. P. Macken, L. J. Driesen, and R. J. M. Belmans, "A dc bus system for connecting offshore wind turbines with the utility system", *European Wind Energy Conference 2001*, Copenhagen, Denmark, 2-6 July, 2001, pp. 1030-1035.

[7] S. Ruin, O. Carlson, "Wind-hybrid systems with variable speed and DC-link", *Wind Power for the 21st Century*, Kassel, Germany, 25-27 September, 2000.

[8] L. N. Grimsmo, M. Korpås, T. Gjengedal, S. Møller-Holst, "A Probabilistic Method for Sizing of Isolated Wind-Electrolyzer Systems", *2004 IEEE Nordic Workshop on Power and Industrial Electronics (NORPIE/2004)*, Trondheim, Norway, 14-16 June, 2004.

[9] H. Polinder, S. W. H. de Haan, M. R. Dubois, J. G. Slootweg, "Basic Operation Principles and Electrical Conversion Systems of Wind Turbines", *2004 IEEE Nordic Workshop on Power and Industrial Electronics (NORPIE/2004)*, Trondheim, Norway, 14-16 June, 2004.

[10] A. Grauers, "Direct Driven Generators: Technology and Development Trends", *Nordic Wind Power Conference (NWPC´2000)*, Trondheim, Norway, 13-14 March, 2000, pp. 127-131.

[11] A. Grauers, "Design of Direct-driven Permanent-magnet Generators for Wind Turbines", Chalmers University of Technology, Göteborg, Sweden, PhD Thesis, 1996.

[12] A.Grauers, S. Landström, "The Rectifiers Influence on the Size of Direct-driven Generators", *Proceedings of the 1999 European Wind Energy Conference and Exhibition (EWEC'99)*, Nice, France, 1-5 March 1999, pp. 829-832.

[13] A. Grauers, A. Lindskog, "PM Generator with Series Compensated Diode Rectifier", *2000 IEEE Nordic Workshop on Power and Industrial Electronics (NORPIE/2000)*, Aalborg, Denmark, 13-16 June, 2000, pp. 59-63.

[14] S. Lundberg, "Performance comparison of wind park configurations", Chalmers University of Technology, Göteborg, Sweden, Technical Report No. 30R, 2003.

[15] H. Ganander, E. Ulén, Maria Poppen, A. Björck, M. Ellsén, O. Carlson, "Stall Control with Variable Speed at the Hönö Wind Turbine", Department of Electrical Machines and Power Electronics, Chalmers University of Technology, Göteborg, Sweden, Report No. R-92-11, January 1993.

[16] O. Carlson, A. Grauers, A. Williamson, S. Engström, E. Spooner, "Design and test of a 40 kW Permanent-Magnet Generator with a frequency converter", *EWEC´99*, March 1999.

[17] O. Carlson, Magnus Ellsén, "Control and operation experience of a 40 kW directly driven permanent magnet wind turbine generator with a frequency converter", *2001 European Wind Energy Conference (EWEC'2001)*, Copenhagen, Denmark, 2-6 July 2001.

[18] N. Mohan, T. M. Undeland, W.P. Robbins, *Power Electronics: Converters, Applications and Design*. 2nd edition, 1995, John Wiley & Sons, New York, NY.

[19] G.F. Franklin, J. D. Powell, A. Emami-Naeini, *Feedback Control of Dynamic Systems*. 3rd edition, 1994, Addison-Wesley Publishing Company, Inc.

[20] R. W. Erickson, *Fundamentals of Power Electronics*. New York: Chapman and Hall, May 1997.

[21] Plexim GmbH, *PLECS User Manual*. Zurich: Plexim GmbH, 2004.

Appendix B

Investigation of a Wind Power Generator, Part 1, Ingemar Mathiasson, Chalmers, November 2005

Investigation of a Wind Power Generator

Part 1

Ingemar Mathiasson

November 2005

Department for Energy and Environment

Division of Electric Power Engineering

Chalmers University of Technology

CONTENTS

1 INTRODUCTION 3

2 ABOUT FEM CALCULATIONS 4

2.1 GENERAL 4
2.2 THE SPECIFIC ELECTROMAGNETIC PROBLEM 4

3 FEM-ANALYSIS APPLIED ON THE GENERATOR 7

4 SIMULATION RESULTS BASED ON FEM-ANALYSIS 13

4.1 VOLTAGE – CURRENT-SIMULATIONS 13
4.1.1 Basics 13
4.1.2 No load calculations 16
4.1.3 Load calculations 16
4.2 DEMAGNETIZATION CURRENT 20
4.3 COIL INDUCTANCE 26
4.4 THE STATOR COIL WIRING NUMBER 29
4.5 THE AIRGAP BETWEEN ROTOR AND STATOR 30

5 FOURIER ANALYSIS REGARDING THE FLUX LINKAGE 34

5.1 GENERAL 34
5.2 GENERAL ABOUT DISCRETE FOURIER TRANSFORMING 34
5.3 D F T APPLIED ON THE FEM RESULT 36
5.4 CONCLUSION 40

6 FUTURE WORK 41

7 REFERENCES 42

APPENDIX (USED SOFTWARE) 42

1 INTRODUCTION

The following work is Part 1 of a study regarding a technical investigation of the wind power system at Hönö (Hönö 3, generator Morley 27/48/1). The work has different goals:

- To increase the theoretical knowledge about some important electromagnetic phenomena e.g. demagnetization, the airgap dependence, the harmonic properties of the coil current and the coil inductance
- To evaluate possibilities of increasing the active power by increasing the coil current

The work has been performed around an analysis of the PM-generator in question, where one of the important methods has been FEM-analysis. The following main parts are included in this paper:

- General about the Finite Element Method (FEM) calculations
- FEM-analysis applied on the generator
- Simulation results based on FEM-analysis
  - Voltage – Current-simulations
  - Demagnetization current
  - Coil inductance
  - The stator coil wiring number
  - The airgap between rotor and stator
- Fourier analysis regarding the flux linkage
  - General about discrete fourier transforming
  - Dft applied on the FEM result

Part 2 of this study ([1]) deals with the question about the reactive effect compensation.

2 ABOUT FEM CALCULATIONS

2.1 General

The Finite Element Method is a numerical analysis method for solving (partial) differential equations. The method is very useful in combination with complex geometry. The geometry in question is here divided into a mesh of elements consisting of triangles in 2D and tetrahedrons in 3D. The analysis is then performed separately for every single element. The result of this analysis is modeled as polynomials (one polynomial for each element) in the spatial coordinates (e.g. x, y). The finite element analysis is the solution of the set of equations for the unknown coefficients in all polynomials. By a system analysis the results from the single elements is adapted into a total system solution. This is done by matching the results of adjacent elements to each other (e.g. connect adjacent element to each other).

2.2 The specific electromagnetic problem

One important field for FEM is to solve electromagnetic problems. In this case it is of interest to solve problems in the low frequency region. This is when the electromagnetic wavelength ($\lambda = c/f$) is much larger than the geometrical dimensions.

Maxwell's equations could be stated according to the following:

(Equation 1) $$\nabla \times H = J + \frac{\partial D}{\partial t}$$ (Ampère's law)

(Equation 2) $$\nabla \times E = -\frac{\partial B}{\partial t}$$ (Faraday's law)

(Equation 3) $$\nabla \cdot D = \rho$$ (Poisson's equation)

(Equation 4) $$\nabla \cdot B = 0$$ (The condition of solenoid magnetic field)

H:	the magnetic field intensity	(A/m)
J:	current density	(A/m^2)
D:	electric flux density	(As/m^2)
E:	the electric field	(V/m)
B:	the magnetic flux density	(Vs/m^2)
ρ:	charge density	(As/m^3)

The following relations are available:

(Equation 5, Equation 6)
$$B = \mu \cdot H$$
$$D = \varepsilon \cdot E$$

μ is the material's magnetic permeability and **ε** is the coefficient of dielectricity. As the magnetic permeability **μ** for ferromagnetic materials usually is dependent on the magnetic flux density it is in this case a nonlinear problem to solve.

In this case the low frequency approximation is in question. This approximation implies that ε = 0 and the displacement current in Ampère's law could be neglected. In the FEM-calculation the magnetostatic case is assumed and take use of the following equations:

(Equation 7, Equation 8)
$$\nabla \times H = J$$
$$\nabla \cdot B = 0$$

Since $\nabla \cdot B = 0$ there exists a magnetic vector potential A such that

(Equation 9)
$$B = \nabla \times A$$

and

(Equation 10)
$$\nabla \times (\frac{1}{\mu} \nabla \times A) = J$$

As the plane case (2D) is in question the current flows are parallel to the z-axis and only the z component of **A** is present:

A = (0,0,A) and J = (0,0,J) and the equation can be simplified to the following elliptic partial differential equation

(Equation 11)
$$-\nabla \cdot (\frac{1}{\mu} \nabla A) = J$$

where $J = J(x,y)$.

(Equation 12) $$\nabla \cdot (\frac{1}{\mu}\nabla A) = \frac{1}{\mu}(\frac{\partial^2 A}{\partial x^2} + \frac{\partial^2 A}{\partial y^2})$$

and

(Equation 13) $$\frac{\partial^2 A}{\partial x^2} + \frac{\partial^2 A}{\partial y^2} = \mu \cdot J(x, y)$$

Then the magnetic flux density B could be computed as

(Equation 14) $$B = (\frac{\partial A}{\partial y}, -\frac{\partial A}{\partial x}, 0)$$

The magnetic field intensity H is given by

(Equation 15) $$H = \frac{1}{\mu} B$$

The interface condition between regions of different material properties is that $H \times n$ should be continuous. This implies the continuity of

$$\frac{1}{\mu}\frac{\partial A}{\partial n}$$

The magnetostatic potential A is on the boundary specified by the Dirichlet boundary condition.

The value on the boundary of the normal component of

$$n(\frac{1}{\mu}\nabla A)$$

is specified by the Neumann condition. This is equivalent to specify the tangential value of the magnetic field H on the boundary.

When solving the present problem the magnetostatic potential A is calculated for every single triangle (defined by the mesh of elements consisting of triangles). As mentioned in chapter 2.1 the result of this analysis is modeled as polynomials. The finite element analysis is then the solution of the set of equations for the unknown coefficients in all polynomials followed by an adaption into a total system solution where adjacent elements are adapted to each other.

3 FEM-ANALYSIS APPLIED ON THE GENERATOR

A first study of the generator is presented in [1].

The configuration of the device is shown in Figure 1. The first approximation will be to handle the device as a symmetric construction. This is not quite correct (there are 24×2 rotor poles and 27 stator E-cores). It is important to remember this approximation when using the model. This approximation makes it for example impossible to study the field in more than **one** stator E-core at the same time (same rotor position), and to compare the results).

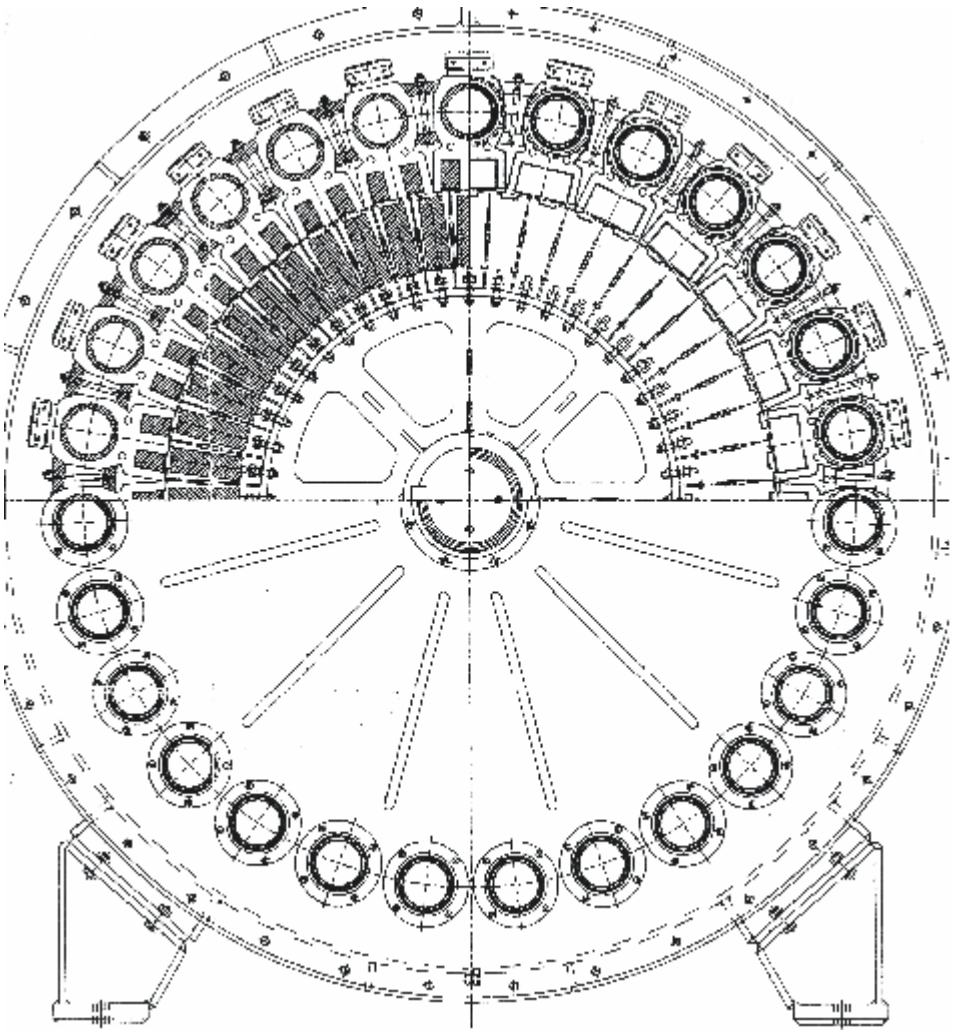

Figure 1 Configuration of the studied PM-generator consisting of 27 stator modules and 24×2 rotor poles

Figure 2 gives more in detail the configuration of the stator and rotor modules. From a circular geometry the configuration then is approximated into a rectangular geometry according to Figure 3.

The FEM-calculations have been performed by a software named “Magnet” from Infolytica Corporation. Two examples of used geometries are illustrated in Figure 4 and Figure 5. These figures correspond to different relative positions between the stator module and the rotor module. This is named “X-shift” in the figures. By calculating the coil flux linkage for different X-shift we get information about the coil flux linkage as a function of rotor position. This give us on the other hand a possibility to calculate the time derivative of the coil flux linkage and hereby the induced voltage for a given rotating speed of the generator. Figure 6 illustrates a part of the model and Figure 7 gives the corresponding flux image.

By using the method of “shifting” the stator – rotor position we have a possibility to calculate the coil inductance as a function of position.

The following points are discussed in [1] and are not treated in this paper:

- Different geometric configurations
- Air-box sizes
- Solution polynom orders
- Mesh sizes

The following main points have been treated regarding FEM-analysis:

- Voltage – Current-simulations
- Demagnetization current
- Coil inductance
- Determination of the stator coil wiring number
- The airgap between rotor and stator

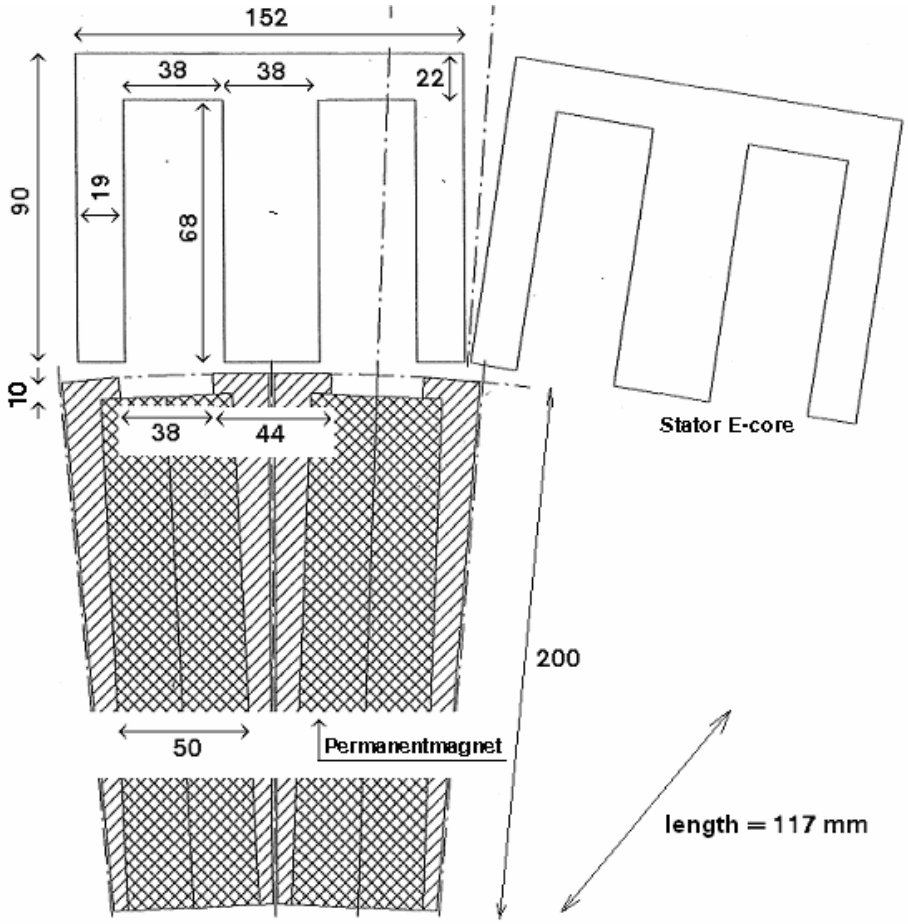

Figure 2 The stator- and rotor modules. Dimensions in mm. In the FEM-calculations we have used the following material:

- Permanent magnet: Ceramic ferrite
  B-Max: 0.4 T, Hc: $-2.7 \cdot 10^5$ A/m
- Other components: Cold rolled 1010 steel
  B-Max: 2.15 T, Hc: 0

The distance between two equivalent points of stator modules is asumed to 164 mm. See Figure 3.

The airgap between rotor and stator is 2 mm, nominal value. See chapter 4.5.

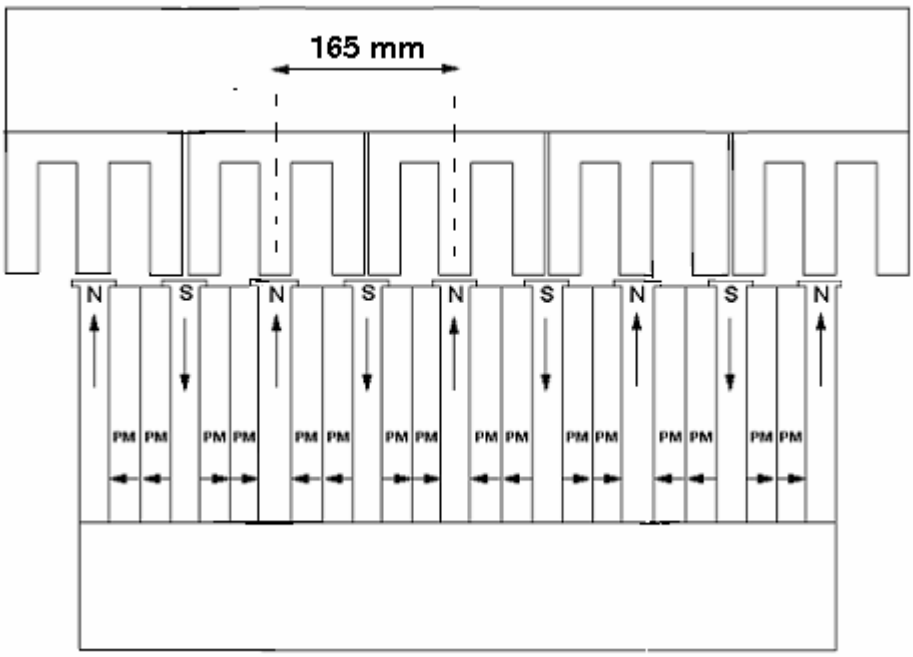

Figure 3 Model configuration for 9 poles in combination with 5 E-cores. The figure illustrates the magnetic flow direction in the rotor parts.
The distance between two equivalent points of stator modules is assumed to 165 mm

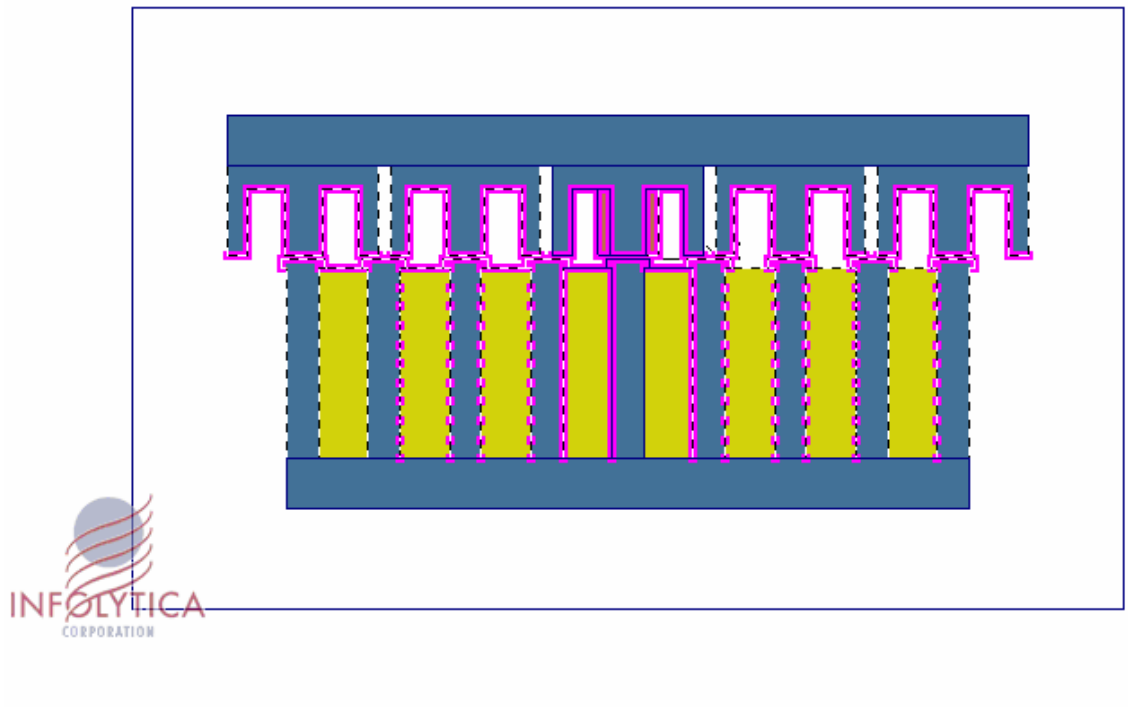

Figure 4 Geometric model used for the FEM-calculations. X-shift 0 mm

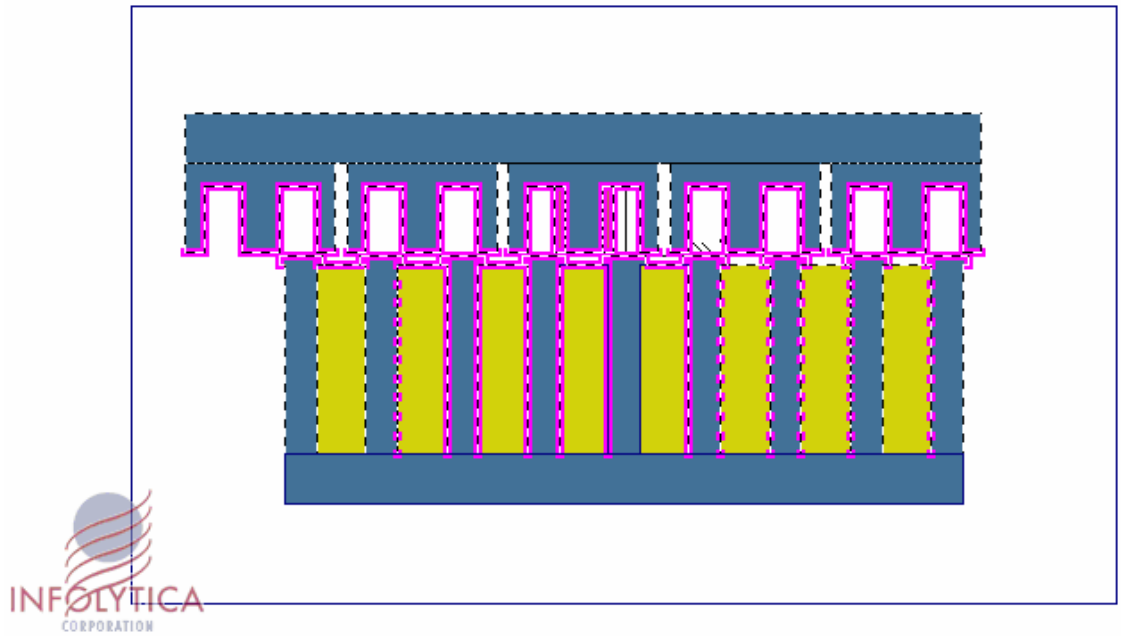

Figure 5 Geometric model used for the FEM-calculations. X-shift in this example 41 mm

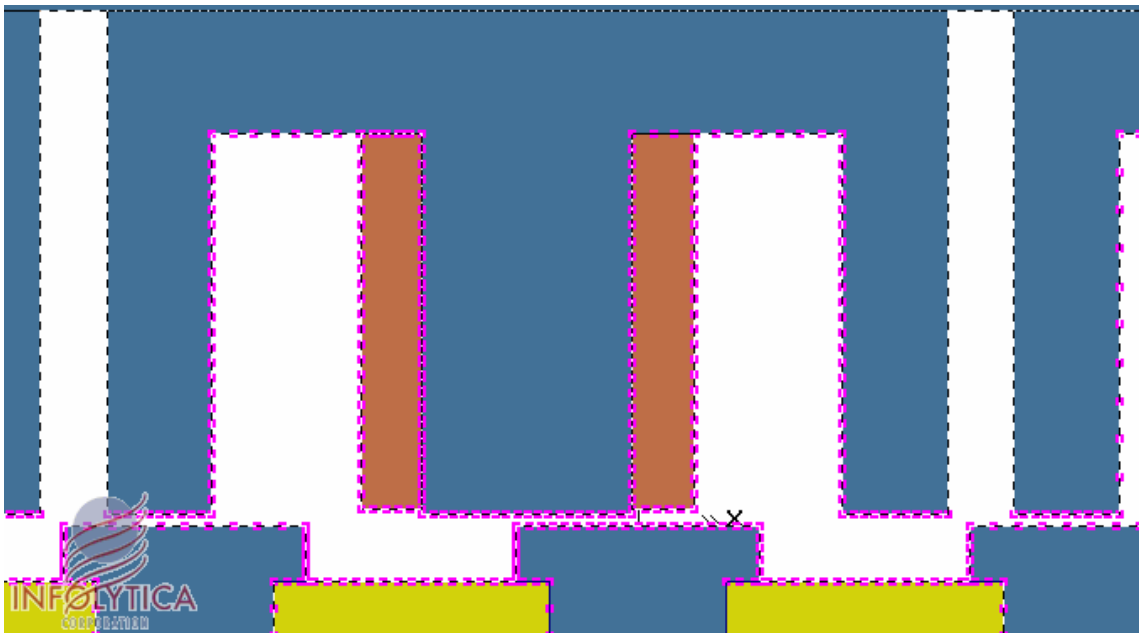

Figure 6 Part of the geometric model. X-shift in this example 20 mm. The coil is wired around the middle E-core

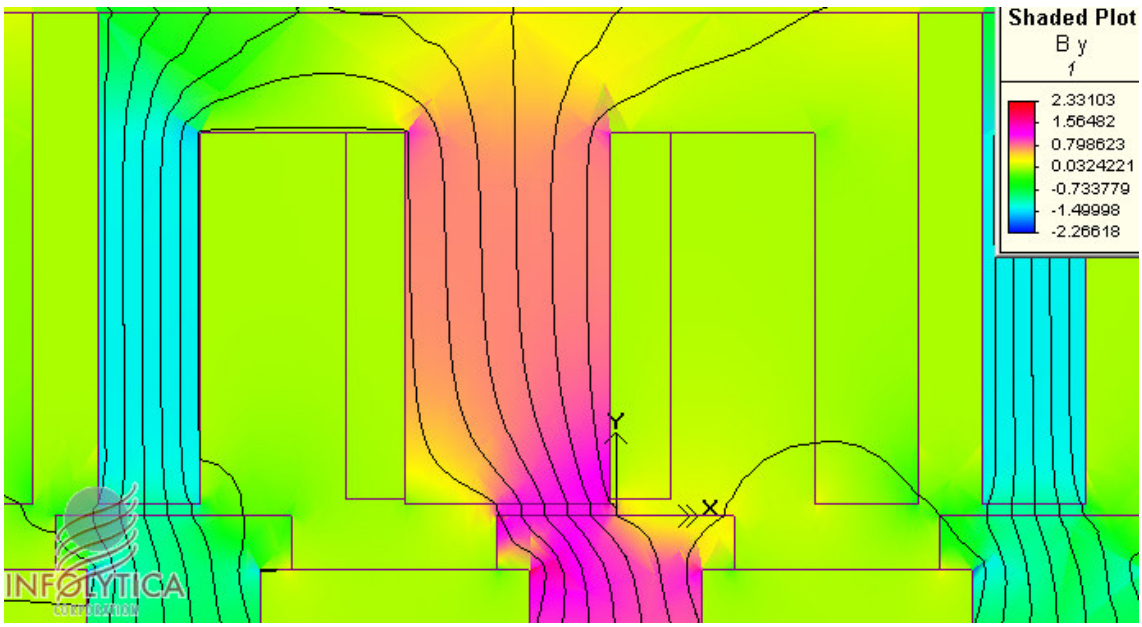

Figure 7 Calculated flux image corresponding to Figure 6

4 SIMULATION RESULTS BASED ON FEM-ANALYSIS

4.1 Voltage – Current-simulations

4.1.1 Basics

In **Table 1** we have the calculated flux linkage values for a coil with 323 turns. No current in the coil.

Shiftposition (mm)	Flux linkage (Weber)
0	-1.57463
2.5	-1.56709
5	-1.54017
7.5	-1.49872
10	-1.44704
12.5	-1.38729
15	-1.31946
17.5	-1.25001
20	-1.1811
22.5	-1.11004
25	-1.03145
27.5	-0.93993
30	-0.82634
32.5	-0.68853
35	-0.51895
37.5	-0.32085
40	-0.10013
42.5	-0.00646
45	0.134045
47.5	0.350455
50	0.543717
52.5	0.705755
55	0.837647
57.5	0.944775
60	1.031985
62.5	1.108428
65	1.177873
67.5	1.245703
70	1.315687
72.5	1.381902
75	1.440042
77.5	1.489568
80	1.528867
82.5	1.550938

Table 1 Flux linkage as a function of shift position. No current in the coil

As the distance between two equivalent points of stator modules is assumed to 165 mm we have a symmetry around a shift of 82.5 mm, 165mm + 82.5mm, 2 × 165mm + 82.5mm, ….., and so on.

Figure 8 is a plot of how the flux linkage varies when the shift is alternated.

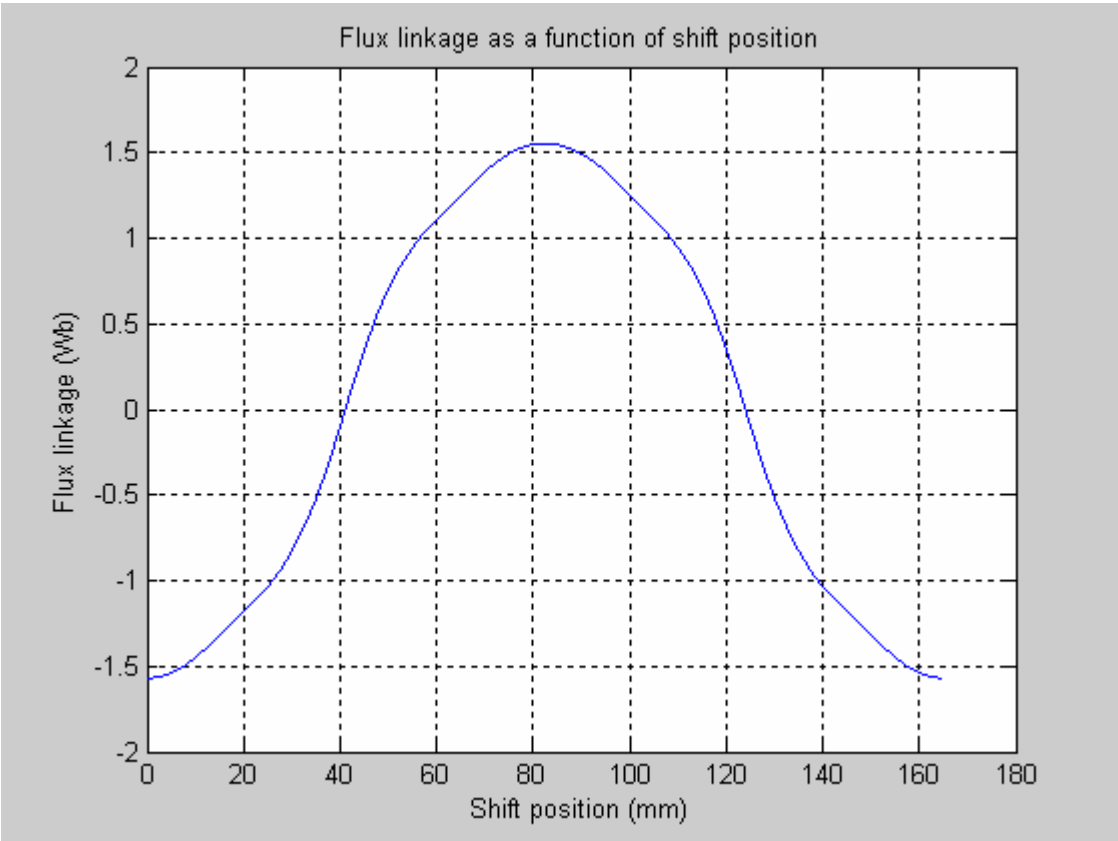

Figure 8 Flux linkage for a coil of 323 turns vs shift positon

The position dependent flux linkage according to Figure 8 could be divided into a DC-component, a fundamental frequency and a number of harmonics. This is done in chapter 5. The analysis point out the fairness to approximate the flux variation with a single sinusoidal function based on the fundamental frequency. This results in a simple expression for the corresponding induced voltage in the coil if we suppose a flux linkage variation as a result of ordinary relative movement between the rotor and the stator. Suppose the following generator parameters:

A: amplidue of the fundamental regarding flux linkage (Wb)
V_{rot}: generator rotating speed (rpm)
P: number of pole pairs in the rotor
$\phi(t)$: flux linkage (Wb)
u(t): induced voltage in the coil (V)

(Equation 16) $$\phi(t) = A \cdot \sin(\frac{Vrot \cdot P}{60} 2\pi \cdot t)$$

(Equation 17) $$u(t) = (-)\frac{d\phi(t)}{dt} = (-)A \cdot \frac{Vrot \cdot P}{60} 2\pi \cdot \cos(\frac{Vrot \cdot P}{60} 2\pi \cdot t)$$

Figure 9 gives the equivalent electrical circuit of a single stator module.

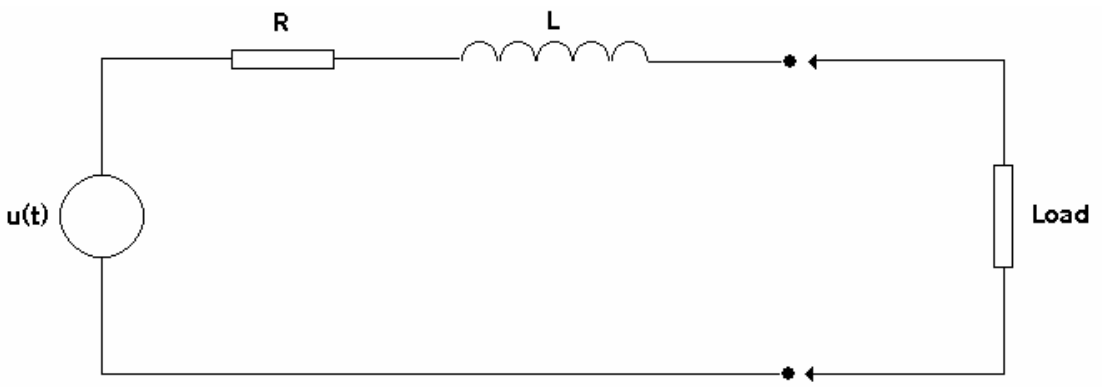

Figure 9 Equivalent circuit of the stator module

R: the coil resistance (Ω)
L: the coil inductance (H)

R and L have been measured to:

R = 1.0 Ω (20 °C)
L = 106 mH (mean value 20 °C)

P = 24

The fundamental amplidue A (based on FEM-calculations according to the above and fourier analysis according to chapter 5.3) = 1.615 Wb

4.1.2 No load calculations

Table 2 gives some examples of no load voltages (RMS), calculated by **(Equation 17**, for a stator module when the rotor speed is varied:

Rotor speed (rpm)	No load voltage, RMS (V)
50	144
70	201
80	230

Table 2 Some examples of no load voltages (RMS) for the stator module for different rotating speeds

4.1.3 Load calculations

To calculate load currents and load voltages we have used a special kind of simulation tool called "PLECS" (Piecewise Linear Electrical Circuit Simulation). The circuit according to Figure 10 corresponds to the circuit in Figure 9 with a load consisting of the ordinary "load circuit" (capacitor (C2) for reactive power compensation, diode bridge (D1 – D4), capacitor (C1) in parallel with a resistor (R1) representing the loaded DC-AC converter) for a stator module.

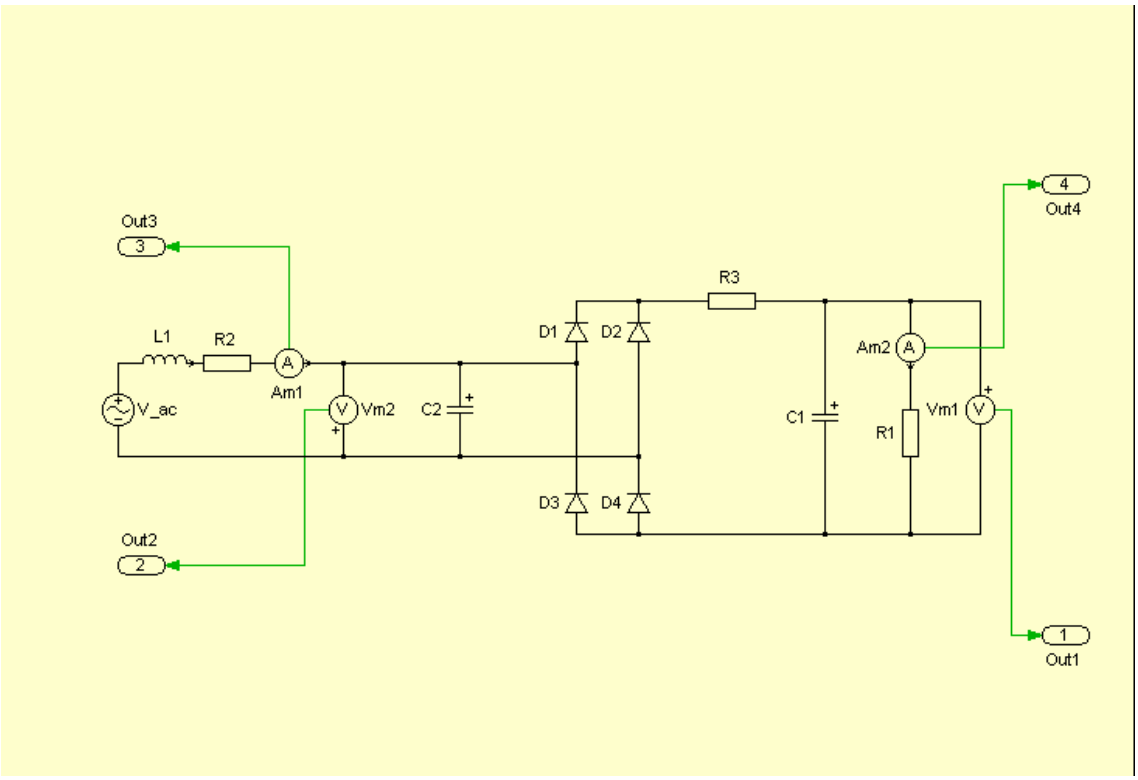

Figure 10 Used PLECS circuit for simulation

Different measurement campaigns have been realised. One of these is presented in [2]. Figure 11 and Figure 12 show some results from these measurements.

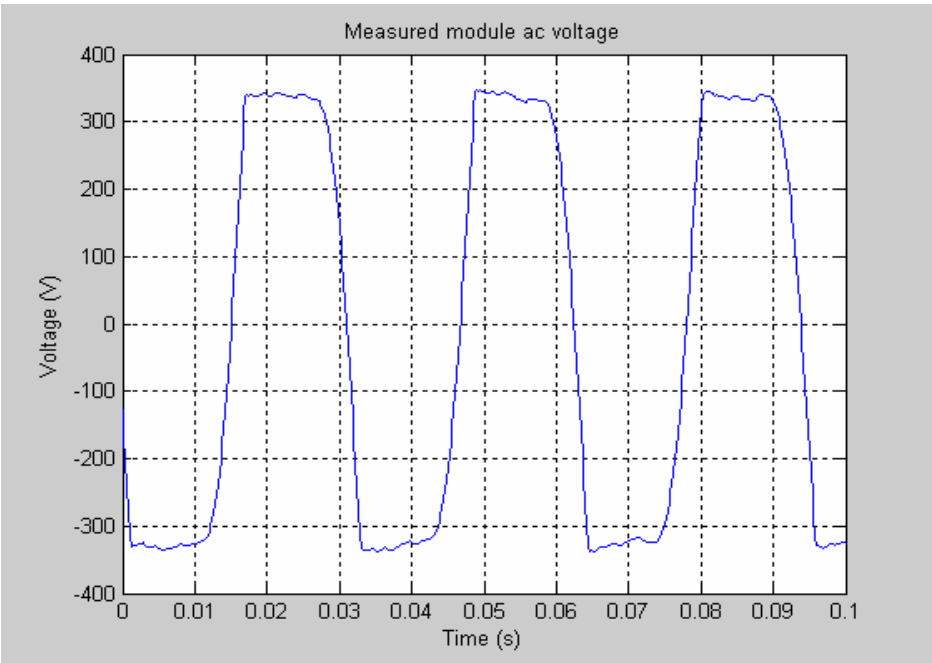

Figure 11 Measured module voltage

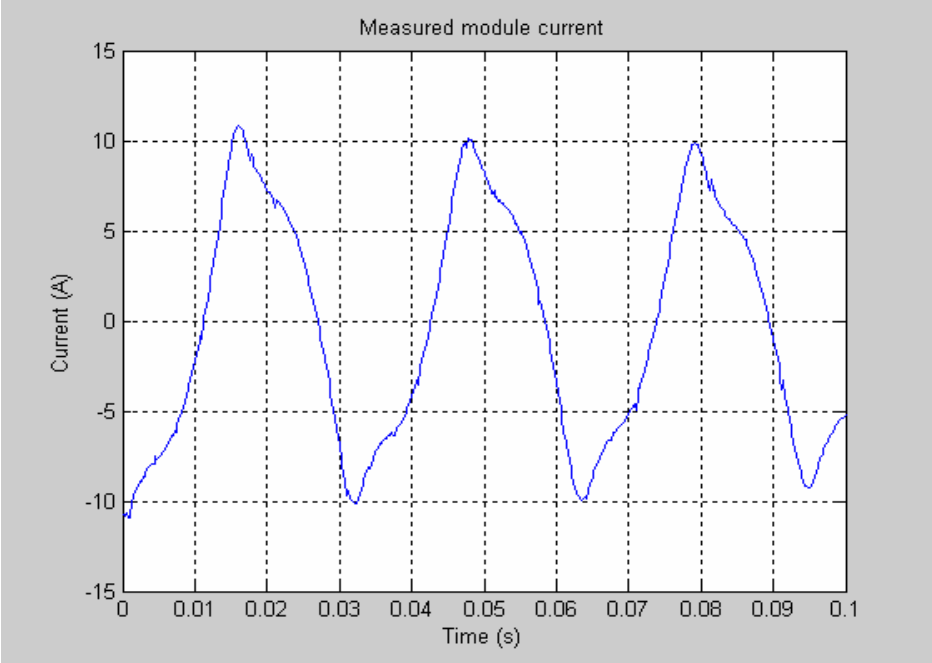

Figure 12 Measured module current

Meassured module voltage and module current according to Figure 11 and Figure 12 is based on:

- Rotor speed: 80 rpm
- Generated power 20 kW/27 per module

If we use these parameters for simulation we get the results according to Figure 13 and Figure 14.

The other parameters are (referring to Figure 10):

V_ac:	$325 \cdot \cos(2\pi \cdot 32\ t)$
L1:	106 mH
R2:	1 Ω
C2:	60 µF
D1 – D4:	forward voltage: 0V, on resistance: 0 Ω
R3:	0.1 Ω
C1:	1000 µF
R1:	200 Ω

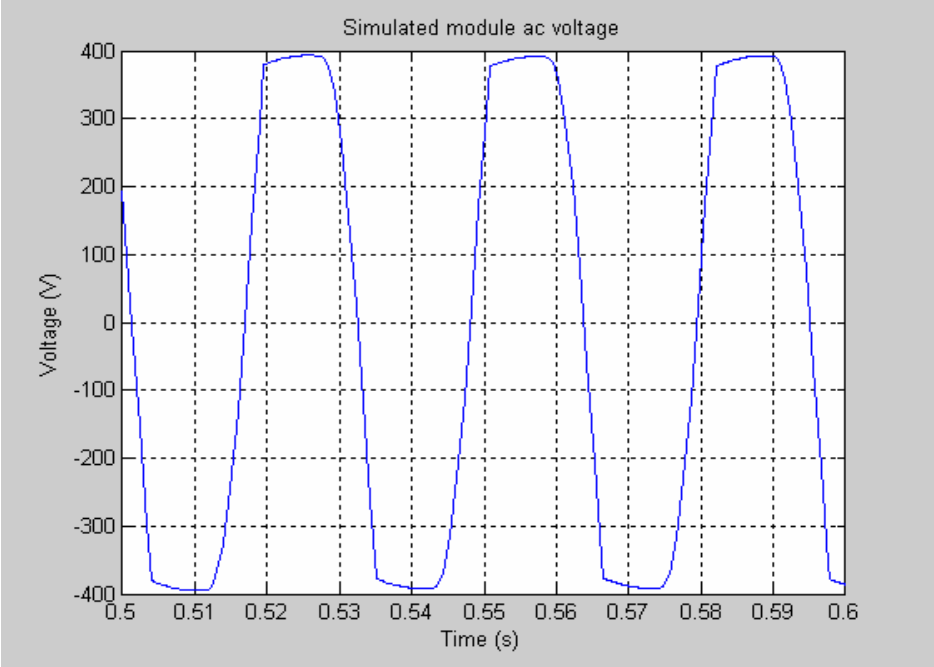

Figure 13 Simulated module voltage

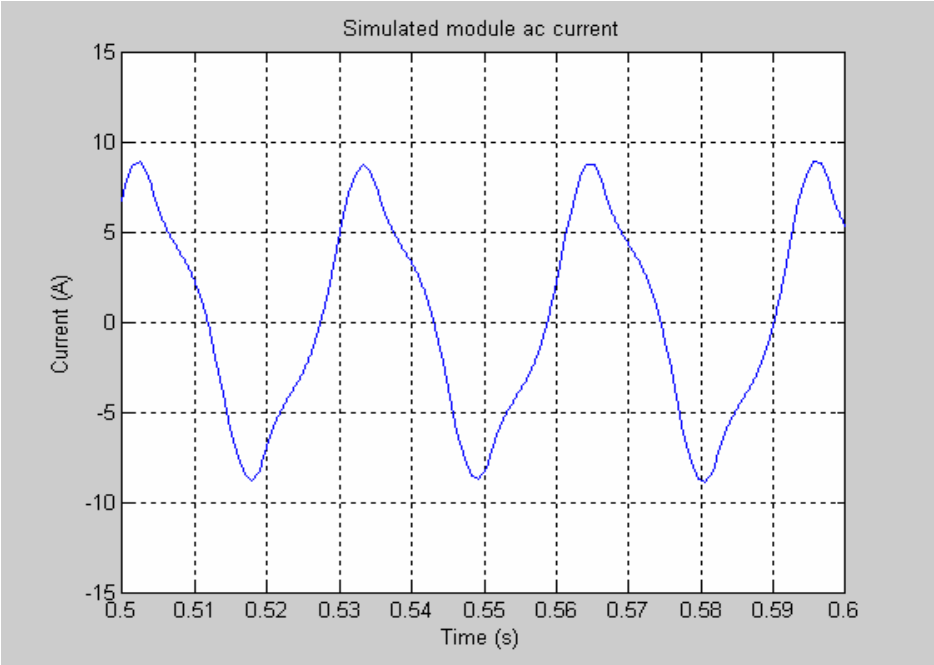

Figure 14 Simulated module current

When comparing Figure 11 (measured voltage) with Figure 13 (simulated voltage) it could be noted that the curve shapes are rather similar. The same similarity is on hand when compareing Figure 12 (measured current) with Figure 14 (simulated current). A corresponding comparison regarding the levels in question will give a **voltage difference** of about 14% **higher** top level for the simulated case compared with the measured one and a **current difference** of about 20 % **lower** top level for the simulated case compared with the measured one. However, as there are some uncertainties regarding some, for the result important, parameter values, that have been estimated, we can not expect a better agreement between simulated and measured results. There are especially two parameters that for the moment are sources for uncertainties; the coil inductance and the air gap. These parameters are treated in chapter 4.3, 4.4 and 4.5. See also chapter 6 for some suggestions of future works.

4.2 Demagnetization current

If a permanent magnet is exposed to an external magnetic field that is reversed to its own direction there is a risk for reduction of the permanent magnet capacity. Figure 15 gives an example of a part of a B-H characteristic for a certain permanent magnet. B_r corresponds to the remanence flux density and H_c is the coercivity. Suppose that a magnetic field intensity of H_1 is applied to the permanent magnet. The corresponding flux density will be B_1. If H_1 then is reduced to zero the resulting flux density in the **general case** will follow a line called the "recoil line". That means that, for the general case, we can't expect to return to the original remanence flux density, B_r, but onother one, some reduced, in the figure called B_r '. In this example we have got a partial demagnetization of the permanent magnet. The size of this demagnetization depends on the material in question and on the size of the reversed magnetic field. In "the Hönö generator" there is a similar situation. In this case the permanent magnets are exposed to the reversed magnetic fields from the stator poles. The size of the reversed field depends on the size of the coil current. Supposing that a reversed field on the permanent magnet, to some extent, will course a reduction of the remanence there is a necessity to find a limit of the coil current that is well adjusted to the induced voltage (some reduced as an effect of the remanence decreasing) in order to get an optimal total power. Relating to Figure 15, there is somewhere in between the zero point and the point corresponding to the coercivity, an optimal point resulting in an acceptable demagnetization, regarding the maximum available power. This point is marked as point 2 in Figure 15. In the case of "the Hönö generator" there is, for the moment, no information available to give a possibility to with certainty calculate the location of point 2 (the optimal point). We make temporarily the assumption that the optimal point is located somewhere in the region near the coercivity force. That imply a simple way to estimate the largest current that could be flowing in a coil without risk to seriously reduce the capacity of the permanent magnet by demagnetization. The method is to calculate the current that results in a flux that exactly balance the permanent magnet flux in the airgap. For larger currents the permanent magnet get fluxes in reversed direction with risk for seriously capacity reduction.

Figure 16 - Figure 18 illustrate the flux images with different coil currents. For a coil current of about 17 A the flux in the airgap is zero. If the current exceeds this limit the resulting flux will get a direction that is reversed to the permanent magnet.

According to this calculation we draw the conclusion that the limit current for seriously demagnetization of the permanent magnets has an amplitude of less than 17 A. (i.e. an rms value of about 12 A).

As mentioned above there is in the writing moment lack of specific information regarding the permanent magnets and their magnetizing properties in respect of demagnetization. Therefore it is recommended that further studies will be performed in order to more in detail specify the maximum acceptable coil current.

In order to get a primarily value regarding a suitable limit for uper coil current it for the moment will be suggested a current value that results in a magnetic field intensity corresponding to 85 % of the coercivity force, H_c. This is the same as 85 % of 17 A, which is about **14.5 A**. This value is used in the analysis described in [3].

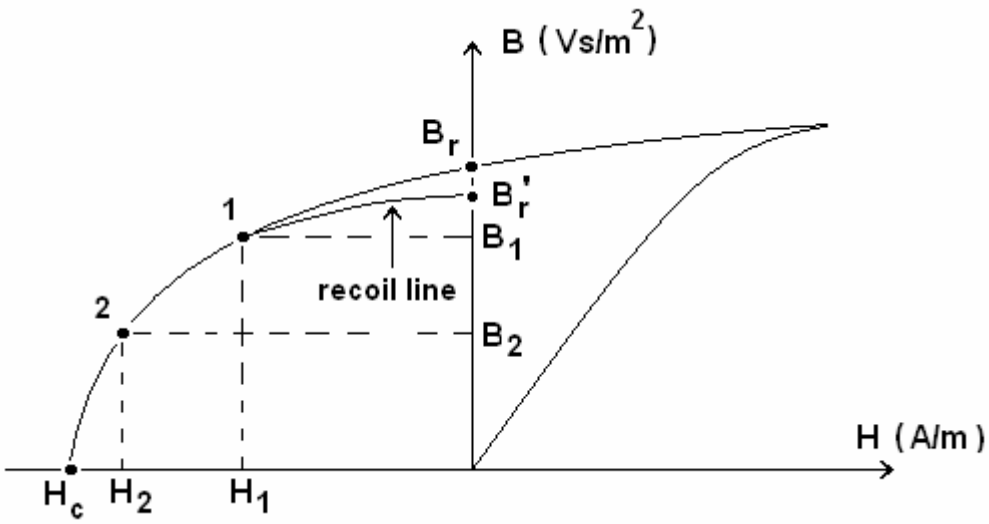

Figure 15 Portion of a B-H characteristic (example)

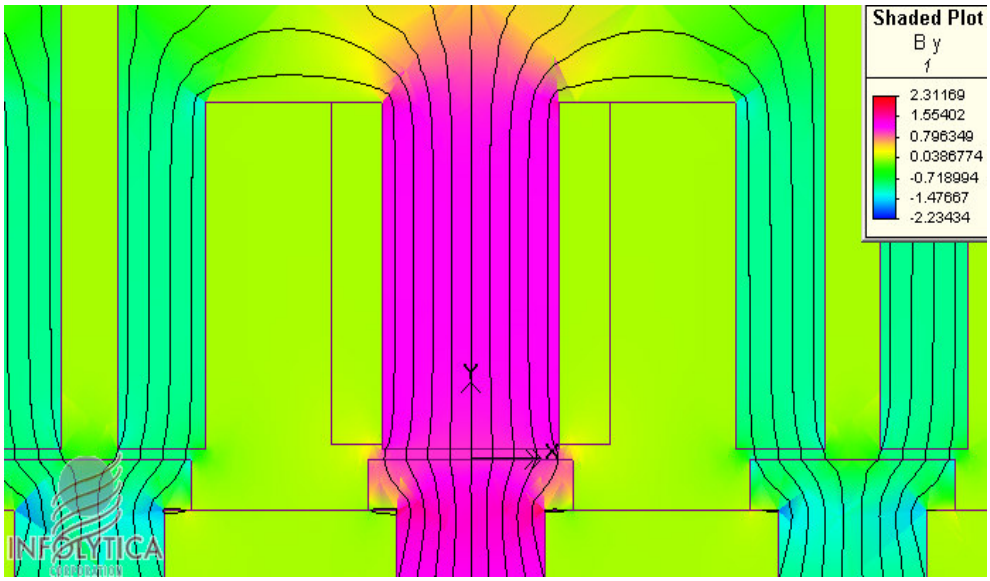

Figure 16 Flux image for a coil current of 0 A

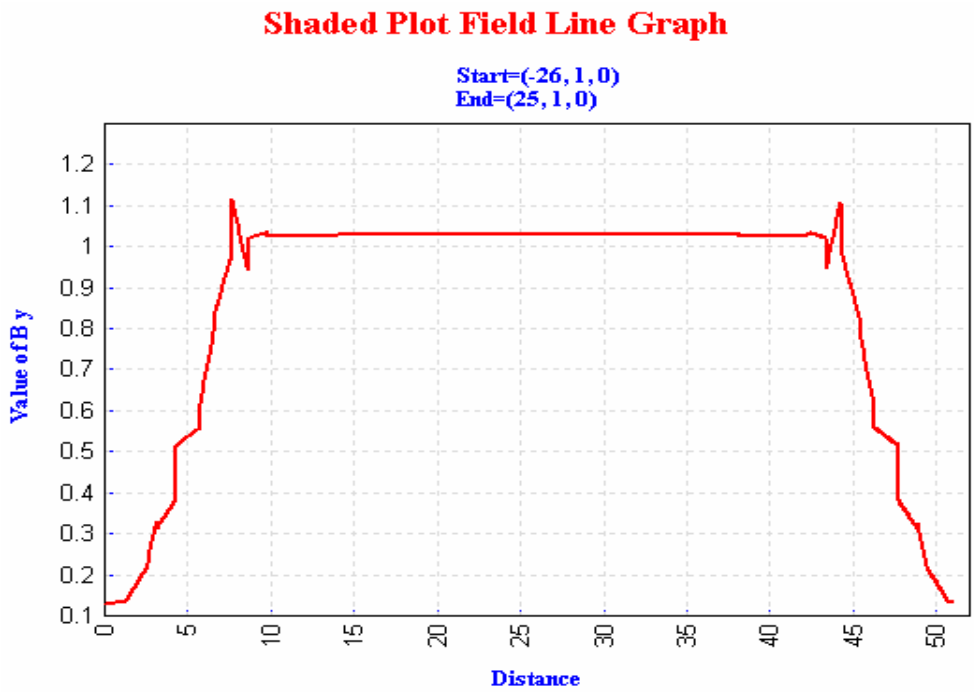

Figure 17 Airgap flux for a coil current of 0 A

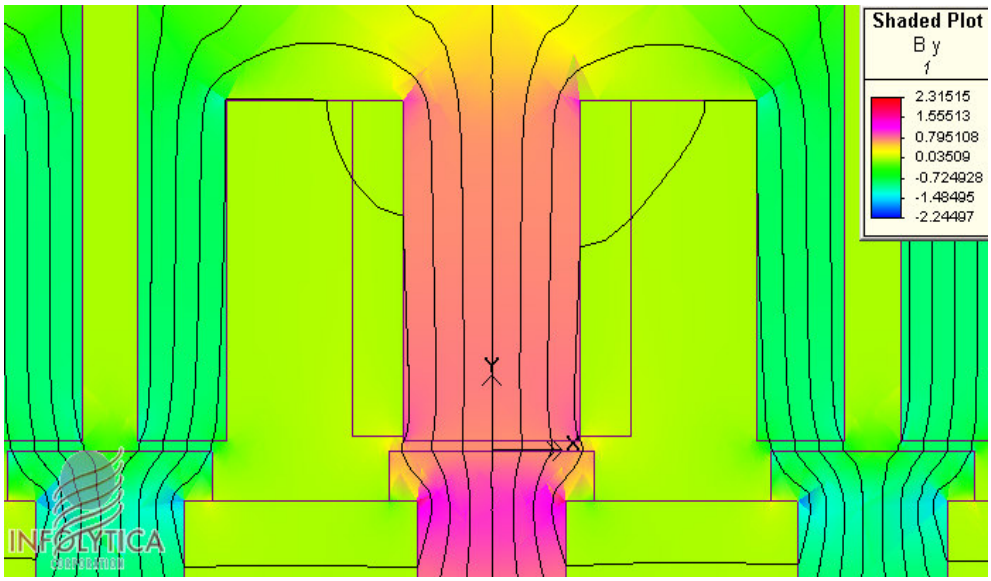

Figure 18 Flux image for a coil current of 5 A

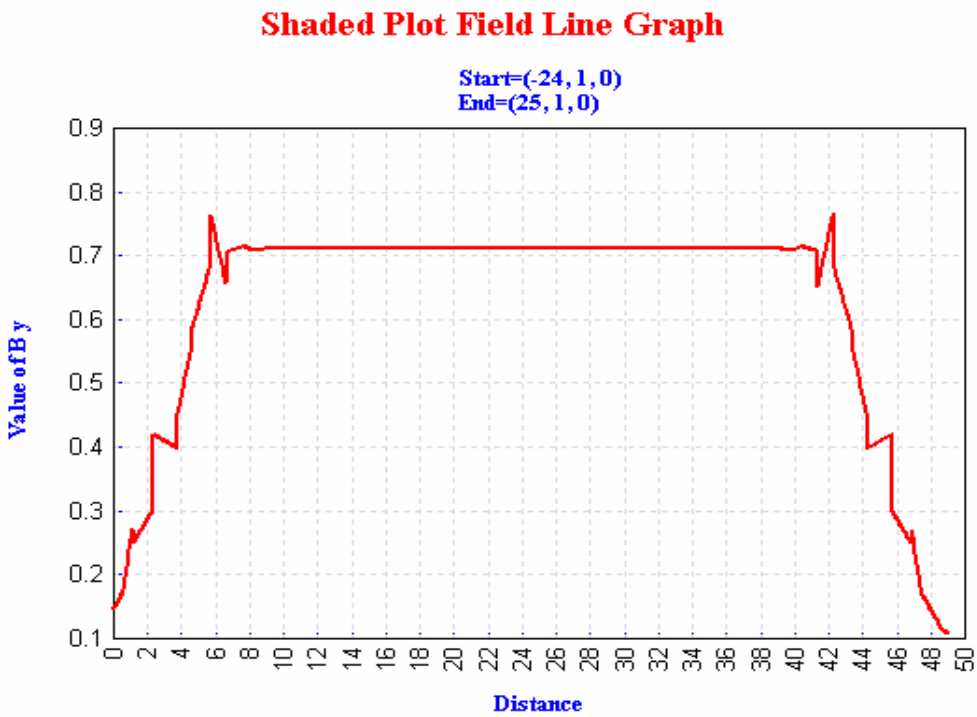

Figure 19 Airgap flux for a coil current of 5 A

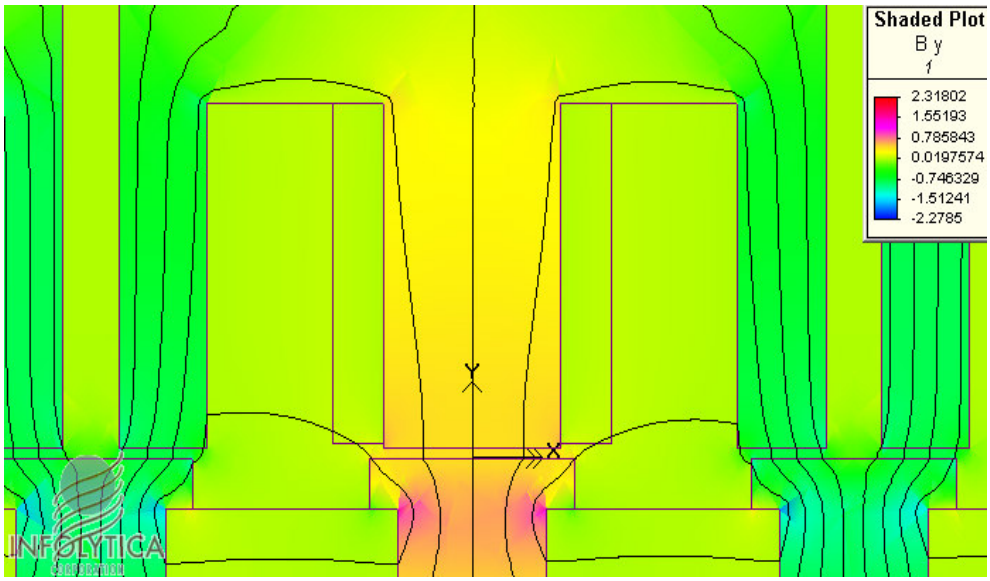

Figure 20 Flux image for a coil current of 10 A

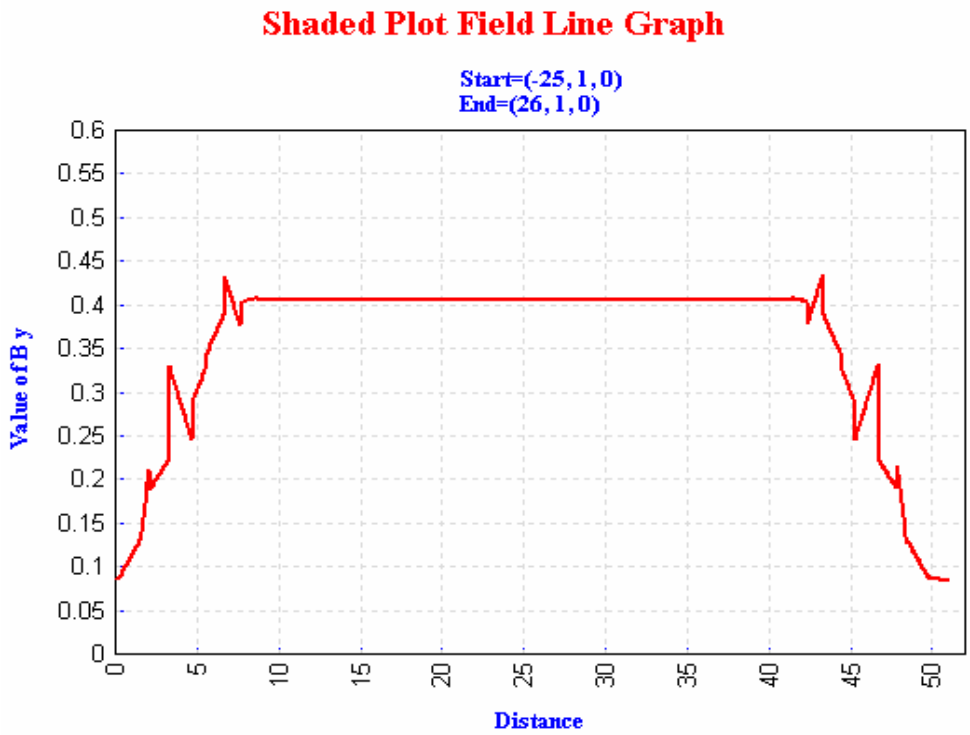

Figure 21 Airgap flux for a coil current of 10 A

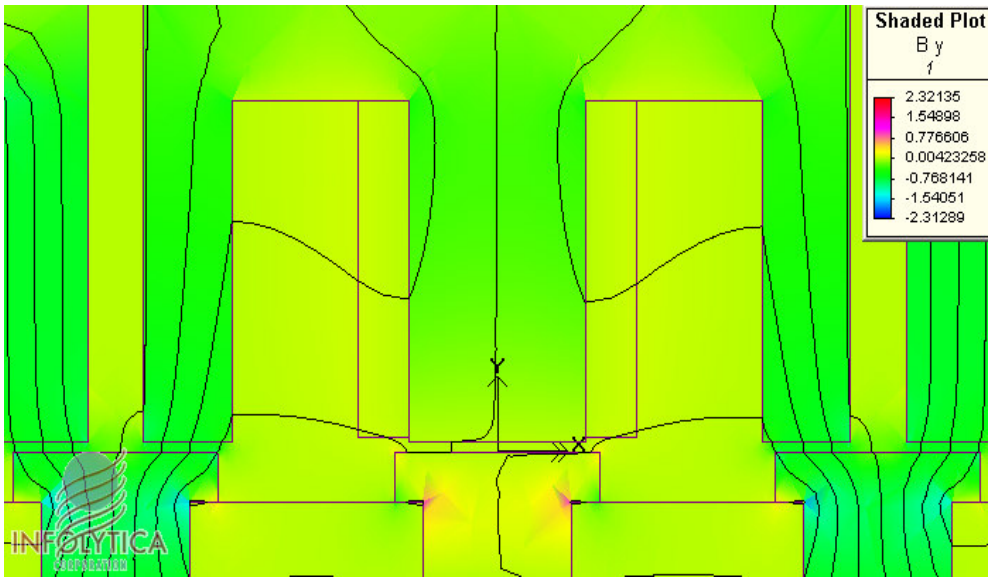

Figure 22 Flux image for a coil current of 17 A

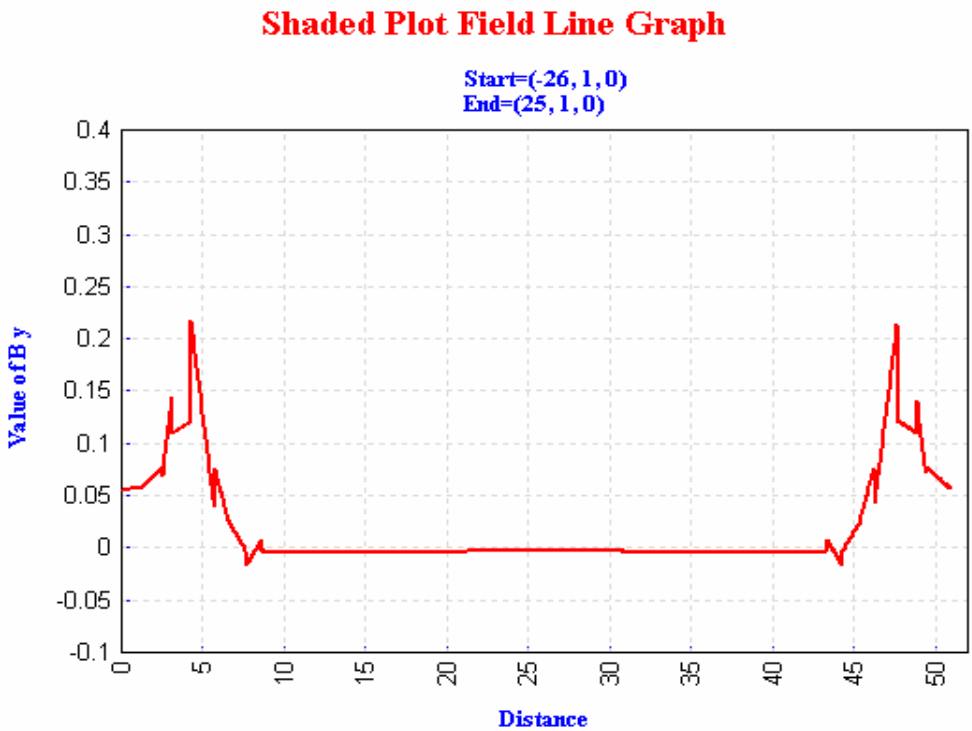

Figure 23 Airgap flux for a coil current of 17 A

4.3 Coil inductance

The coil inductance has been measured. This parameter depends on the relative position between stator and rotor. The inductance was randomly measured at different relative positions (40 positions randomly) between stator and rotor. The result was:

Mean value (measured): 106 mH
Max value (measured): 114 mH
Min value(measured): 99 mH

Total relative inductance variation $\frac{L_{\max} - L_{\min}}{L_{mean}}$ is about 14 %.

The standarddeviation: 4 mH

The mean value 106 mH is used in the calculation above.

Table 3 gives the randomly measured valus.

The coil inductance has been calculated as a function of relative position between stator and rotor. As the coil wiring number was unknown we had to estimate a reasonable value.
The first assumption, based on some data specifications of the generator, was that the coil wiring number was 600. This resulted in the values presented in Figure 24.

The principle for calculation was to calculate the flux linkage for two coil currents (+1 A and –1 A was used) and then use the definition of inductance according to the following expression: $L = \frac{\Delta\phi}{\Delta I}$, where Δϕ is the flux linkage change for a coil current change of $\Delta I = 2$ A (a change between +1 A to –1 A).

Table 4 gives the calculated flux values for the two currents and 600 turns of the coil.

Random position	Measured inductance (H)	Random position	Measured inductance (H)	Random position	Measured inductance (H)	Random position	Measured inductance (H)
1	0.112835	11	0.101982	21	0.108047	31	0.111682
2	0.108362	12	0.100742	22	0.103926	32	0.108362
3	0.10423	13	0.102945	23	0.101037	33	0.099487
4	0.110553	14	0.101037	24	0.100401	34	0.100401
5	0.114011	15	0.105947	25	0.110553	35	0.110553
6	0.101982	16	0.103245	26	0.101982	36	0.10228
7	0.106986	17	0.100109	27	0.10228	37	0.107299
8	0.111357	18	0.103926	28	0.107299	38	0.10423
9	0.111357	19	0.102945	29	0.10228	39	0.109447
10	0.104927	20	0.103926	30	0.111682	40	0.105233

Table 3 Measured inductances for different randomly positions

Shiftposition (mm)	Flux linkage + 1 A (Weber)	Flux linkage – 1 A (Weber)	Shiftposition (mm)	Flux linkage + 1 A (Weber)	Flux linkage – 1 A (Weber)
0	-3.333	-2.517	85	2.472	3.289
2.5	-3.318	-2.503	87.5	2.433	3.247
5	-3.266	-2.455	90	2.363	3.169
7.5	-3.185	-2.382	92.5	2.276	3.072
10	-3.084	-2.291	95	2.174	2.958
12.5	-2.966	-2.185	97.5	2.058	2.827
15	-2.833	-2.067	100	1.935	2.689
17.5	-2.694	-1.944	102.5	1.816	2.552
20	-2.555	-1.824	105	1.694	2.411
22.5	-2.41	-1.699	107.5	1.559	2.257
25	-2.25	-1.561	110	1.405	2.082
27.5	-2.067	-1.398	112.5	1.212	1.874
30	-1.849	-1.194	115	0.972	1.626
32.5	-1.591	-0.942	117.5	0.675	1.324
35	-1.276	-0.631	120	0.321	0.965
37.5	-0.909	-0.269	122.5	-0.078	0.569
40	-0.507	0.142	125	-0.507	0.142
42.5	-0.078	0.569	127.5	-0.909	-0.269
45	0.321	0.965	130	-1.276	-0.631
47.5	0.675	1.324	132.5	-1.591	-0.942
50	0.972	1.626	135	-1.849	-1.194
52.5	1.212	1.874	137.5	-2.067	-1.398
55	1.405	2.082	140	-2.25	-1.561
57.5	1.559	2.257	142.5	-2.41	-1.699
60	1.694	2.411	145	-2.555	-1.824
62.5	1.816	2.552	147.5	-2.694	-1.944
65	1.935	2.689	150	-2.833	-2.067
67.5	2.058	2.827	152.5	-2.966	-2.185
70	2.174	2.958	155	-3.084	-2.291
72.5	2.276	3.072	157.5	-3.185	-2.382
75	2.363	3.169	160	-3.266	-2.455
77.5	2.433	3.247	162.5	-3.318	-2.503
80	2.472	3.289	165	-3.333	-2.517
82.5	2.48	3.298			

Table 4 Calculated flux linkage as a function of shift position and with current in the coil. Two current values was used: + 1 A and – 1 A. Coil wiring number = 600

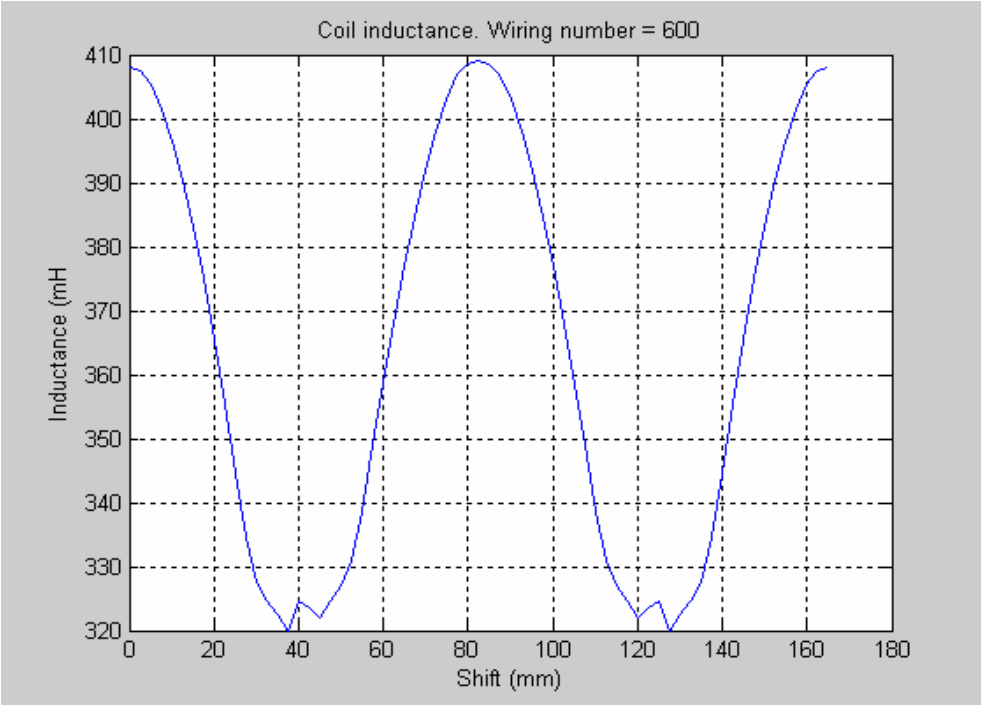

Figure 24 Coil inductance vs stator-rotor relative position. Coil wiring number = 600. The mean value of this inductances is 365 mH.

As these values were based on an estimated wiring number for the coil, here calculated inductances have to be corrected. By compareing the measured and here calculated inductances (see chapter 4.4) the wiring number is estimated to 323. By using the expression $L_{corr} = L_{first} (N_{korr} / N_{estim})^2$ new corrected inductance values are given. These values are illustrated in Figure 25.

L_{corr} : Corrected inductance values

L_{first} : 1'st calculated inductance values (Figure 24)

N_{corr} : Corrected wiring number (323)

N_{estim} : Estimated wiring number (600)

Mean value (calculation): 106 mH
Max value (calculation): 119 mH
Min value (calculation): 93 mH
The standarddeviation: 10 mH

The total relative inductance variation ($(L_{max} - L_{min}) / L_{mean}$) is about 25 %. The corresponding relative inductance variation for the measured values is 14 %.
The standarddeviation for calculated values is 10 mH, while for the measured values this parameter is 4 mH. The distribution of calculated values are consequently larger than corresponding measured distribution. The reason for this result could be an

interesting topic regarding a future work.

In the calculations according to chapter 4.1 we have regarded the coil inductance as undependent of the stator-rotor relative position. As the inductance has an influence on the resulting stator voltage, it could be a good idea to in the future, realize a more detailed analysis regarding the real effect of the inductance variation.

Regarding the coil inductance we consequently have the following topics for coming studies:

- investigation of inductance distribution (measurements and calculations)
- voltage dependent based on the inductance variation

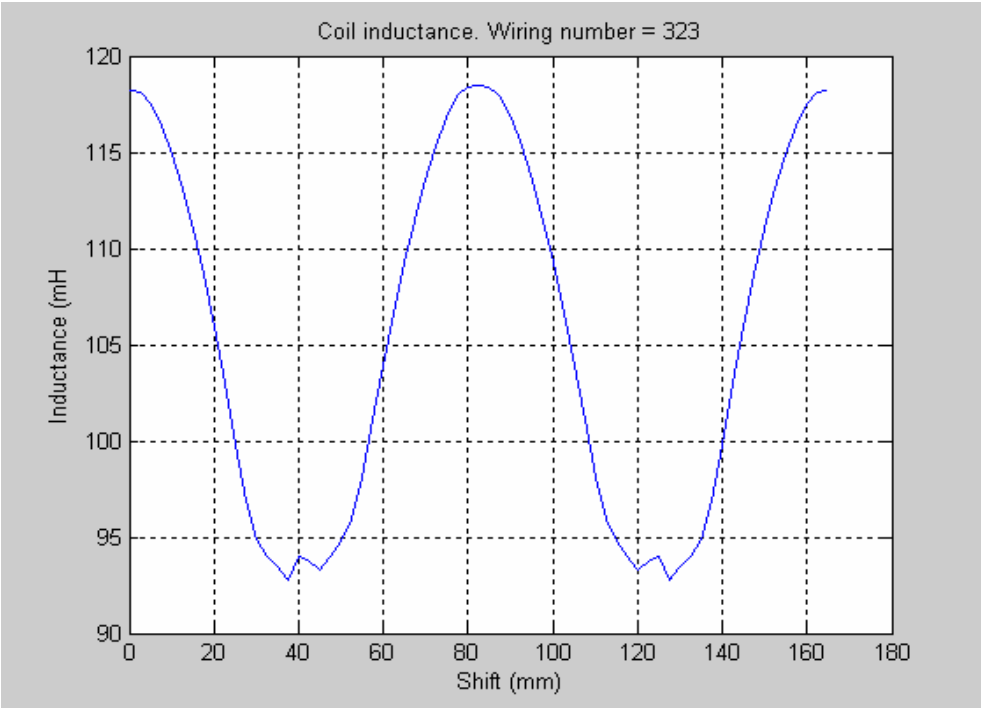

Figure 25 Corrected inductance values for a coil of 323 wiring numbers. The mean value of this inductances is 106 mH and agrees with the corresponding measured one

4.4 The stator coil wiring number

The stator coil wiring number has been estimated by using the measured coil inductance (106 mH) and the calculated coil inductance (see chapter 4.3):

Measured coil inductance (mean value): 106 mH
Calculated coil inductance (mean value) for a wiring number of 600: 365 mH

The coil inductance depends on the coil wiring number as:

$L_1 / L_2 = (N_1 / N_2)^2$

This give us the estimated wiring number as:

$N_{estimated} = N_{L=365mH} \cdot (L_{measured} / L_{calculated})^{1/2}$

$N_{L=365mH} = 600$ $L_{measured} = 106$ mH $L_{calculated} = 365$ mH

That will give us the estimated coil wiring number: 323 turns.

4.5 The airgap between rotor and stator

The airgap between rotor and stator has been assumed to 2 mm as a nominal value. As a result of mechanical imperfections this value varies during the rotation motion. This variation causes on the other hand a variation regarding the resulting flux linkage of the coil and thereby also a variation of the induced voltage. Figure 26 illustrates an example of measured "no load voltage and current" for the stator modules. The variation of the different modules is understood as an effect of varying airgap between stator and rotor vs rotor position. According to Figure 26 the following could be noted:

$V_{max} = 268$ V $V_{min} = 249$ V $V_{mean} = 255$ V

$(V_{max} - V_{mean}) / V_{mean} = 5$ % $(V_{min} - V_{mean}) / V_{mean} = -2$ %

Calculations based on FEM-analysis regarding the effect of varying airgaps have been performed. Figure 27 shows how the flux linkage alternates when the airgap varies. In Figure 28 the relative flux linkage (relative to the flux linkage value when the airgap is 2mm) is illustrated. If we make the very simple assumtion, regarding Figure 26, that the mean voltage (255 V) corresponds to an airgap of 2 mm, than it follows, comparering Figure 26 and Figure 28, that the maximum voltage (268 V, + 5 % rel mean value) corresponds to an airgap of about 1.8 mm and the minimum voltage (249 V, - 2 % rel mean value) corresponds to an airgap of about 2.1 mm. (This comparison between measured voltage and calculated flux linkage is of course relevant as we have a linearly dependence between flux linkage and induced voltage.)

The flux linkage variation (for small variations) is **approximately** linearly depending on the airgap variation. 5 % variation of the airgap results in about 5 % variation of the induced voltage and so on.

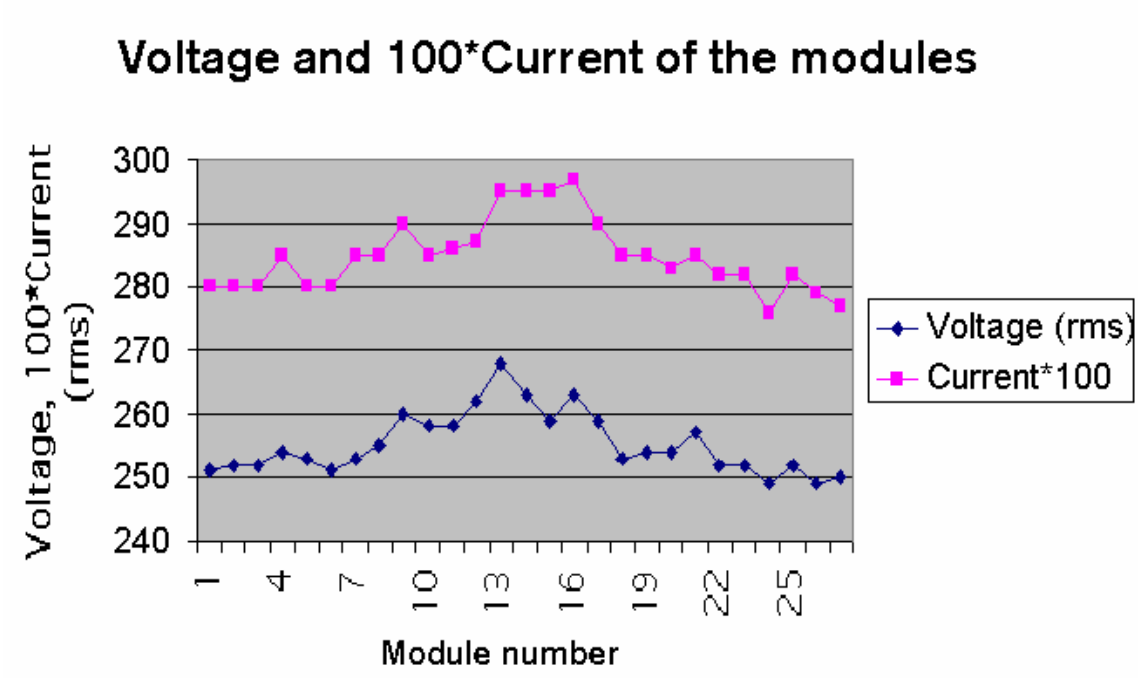

Figure 26 No load voltage and current of the modules

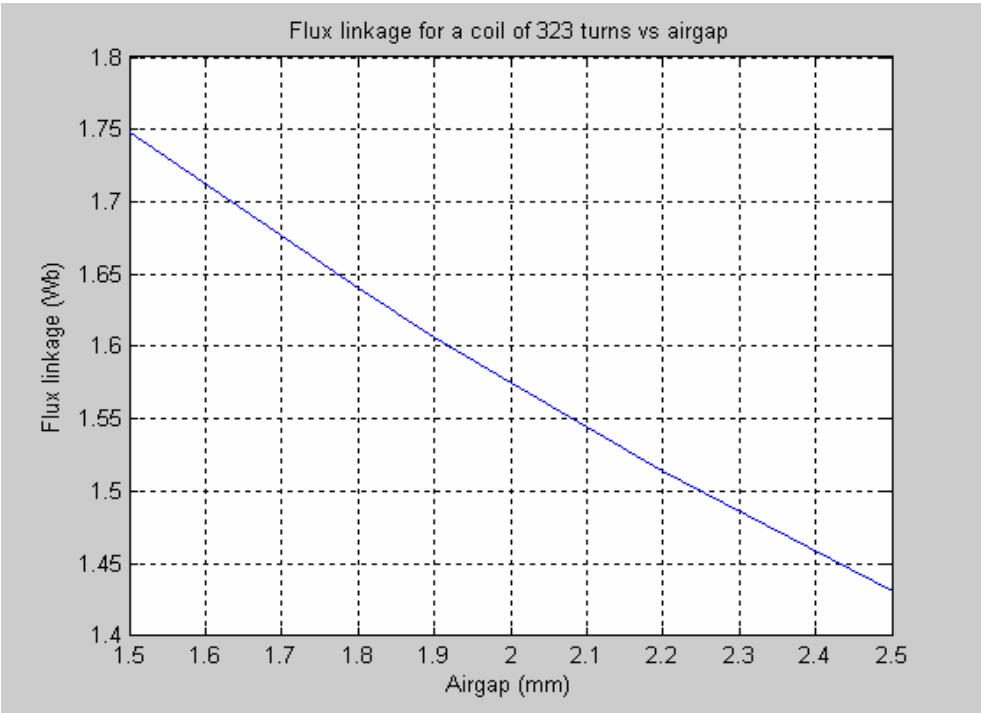

Figure 27 The resulted flux linkage (no current in the coil) vs airgap for a stator coil of 323 turns

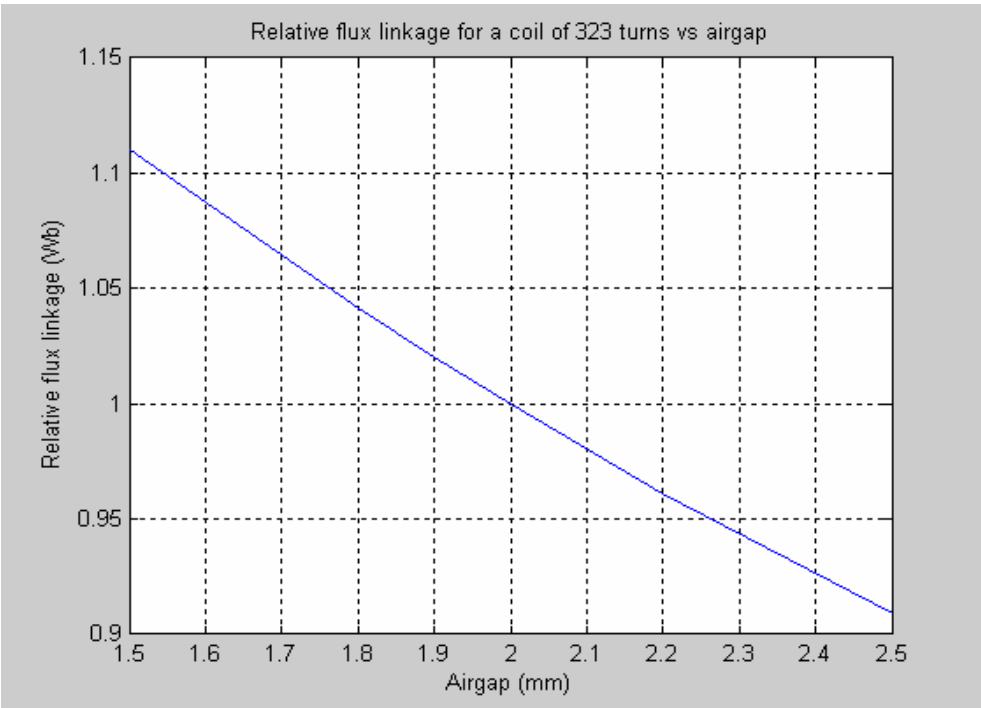

Figure 28 The relative flux linkage vs airgap. The reference is airgap = 2 mm

It is not only the induced voltage that is dependent on the airgap in question. Also the coil inductance will vary for alternating airgaps. Figure 29 illustrates the calculated coil inductance vs the airgap.

Figure 29 The coil inductance is dependent on the airgap

We have as a consequence of the discussion above two parameters, the induced voltage and the coil inductance, to take into account when analyzing the resulting effect of airgap variations. A future work that deal with this problem and that discuss the consequence on the power quality is recommended. See chapter 6.

5 FOURIER ANALYSIS REGARDING THE FLUX LINKAGE

5.1 General

A special kind of system analysis regarding the calculated flux linkage is realized by using the discrete calculated values as sample inputs to a discrete fourier analysis. Totally 66 calculated values give 66 sample points. The analysis results in a series of sine formed functions that together will modelle the flux linkage in question.

5.2 General about discrete fourier transforming

Suppose a continuous and real function v(t) that is repeated with a periodic time T. This function could be divided into an infinite number of components according to:

(Equation 18) $$v(t) = V_0 + \sum_{k=1}^{\infty} v_k(t)$$

(Equation 19) $$v_k(t) = \sqrt{2} V_k \cos(k 2\pi f_0 t + \phi_k)$$

(Equation 20) $$V_k = \frac{\sqrt{2}}{T} \int_0^T v(t) \exp(-jk 2\pi f_0 t) dt$$

(Equation 21) $$V_0 = \frac{1}{T} \int_0^T v(t) dt$$

(Equation 22) $$f_0 = \frac{1}{T}$$

Suppose a time dependent signal, e.g a voltage v(t), that is sampled with N uniformed distributed samples in a measurement window T. Then we have the following time points: $t_n = \frac{nT}{N}$, for $n = 0,1,.....,N-1$

If we transform the expression " $V_k = \frac{\sqrt{2}}{T} \int_0^T v(t) \exp(-jk 2\pi f_0 t) dt$ " above into a discrete expression we get:

(Equation 23) $$V_k = \frac{\sqrt{2}}{N} \sum_{n=0}^{N-1} v(\frac{nT}{N}) \exp(-j \frac{2\pi}{N} kn)$$

The so called discrete Fourier transform X is defined according to:

(Equation 24) $$X_k = \sum_{n=0}^{N-1} x_n W_N^{kn}$$

x_n is the voltage value at time point n

(Equation 25) $$W_N = \exp(-j\frac{2\pi}{N})$$

<u>Return to the the voltage v(t) and applying the defined discrete Fourier transform:</u>

The DC-level:

(Equation 26) $$V_0 = \frac{1}{N} X_0$$

The different harmonics:

(Equation 27) $$V_k = \frac{\sqrt{2}}{N} X_k \qquad k = 1,2,....., N-1$$

The RMS values of the harmonics:

(Equation 28) $$V_{k,RMS} = |V_k|$$

The phase angles of the harmonics:

(Equation 29) $$\varphi_k = \arctan(\frac{\beta_k}{\alpha_k})$$

where β_k is the **imaginary** part and α_k is the **real** part of V_k.

The frequency of the harmonics:

(Equation 30) $$fm = \frac{m}{T} \qquad m = 1,2,3....., \frac{N}{2}$$

Appendix A 3 gives a ”mat-lab”- program based on the expressions above.

5.3 D f t applied on the FEM result

Table 4 gives the calculated flux linkage values for a coil with 600 turns. The total shift interval corresponds to a total shift of one stator module. Figure 30 illustrates the flux linkage wave form for a coil with 323 turns when the rotor moves a shift of one stator module. Figure 31 illustrates the flux linkage vs time for a rotor speed of 80 rpm. As can be observed the wave form differs from a perfect sine curve. If we make a fourier analysis of the curve, using the program routine according to Appendix A3 (66 sample points corresponding to each calculated value are used) we get the result presented in Table 6. As could be noted the fundamental (base) harmonic (e.g 32 Hz for a rotating speed of 80 rpm) is quite dominating. Figure 32 and Figure 33 illustrate the difference between the original calculated curve and the corresponding curve approximated with sine functions. In Figure 32 there is a comparison between the original calculated values and a sine function based on the fundamental frequency ($0.4 \cdot V_{rot} \cdot 1$, where V_{rot} : rotor speed (rpm)). As could be observed the flux function with a fair accuracy could be approximated with a single sine function. Figure 33 gives the corresponding result with 3 sine functions (1st , 3rd and 5th harmonics) taken into account. Here we can see that the two curves are very closed together.

Shiftposition (mm)	Flux linkage (Weber)	Shiftposition (mm)	Flux linkage (Weber)
0	-1.57463	85	1.550938
2.5	-1.56709	87.5	1.528867
5	-1.54017	90	1.489568
7.5	-1.49872	92.5	1.440042
10	-1.44704	95	1.381902
12.5	-1.38729	97.5	1.315687
15	-1.31946	100	1.245703
17.5	-1.25001	102.5	1.177873
20	-1.1811	105	1.108428
22.5	-1.11004	107.5	1.031985
25	-1.03145	110	0.944775
27.5	-0.93993	112.5	0.837647
30	-0.82634	115	0.705755
32.5	-0.68853	117.5	0.543717
35	-0.51895	120	0.350455
37.5	-0.32085	122.5	0.134045
40	-0.10013	125	-0.10013
42.5	0.134045	127.5	-0.32085
45	0.350455	130	-0.51895
47.5	0.543717	132.5	-0.68853
50	0.705755	135	-0.82634
52.5	0.837647	137.5	-0.93993
55	0.944775	140	-1.03145
57.5	1.031985	142.5	-1.11004
60	1.108428	145	-1.1811
62.5	1.177873	147.5	-1.25001
65	1.245703	150	-1.31946
67.5	1.315687	152.5	-1.38729
70	1.381902	155	-1.44704
72.5	1.440042	157.5	-1.49872
75	1.489568	160	-1.54017
77.5	1.528867	162.5	-1.56709
80	1.550938	165	-1.57463
82.5	1.555245		

Table 5 Calculated flux linkage as a function of shift position. No current in the coil

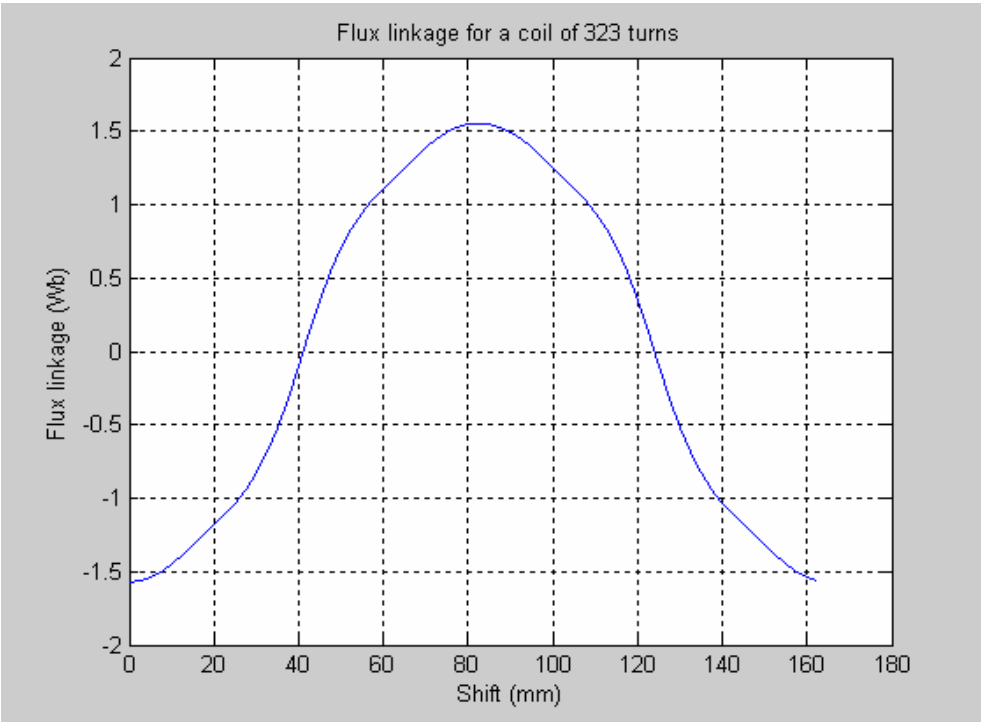

Figure 30 Flux linkage for a coil of 323 turns vs shift positon. Total shift interval corresponds to one stator module.

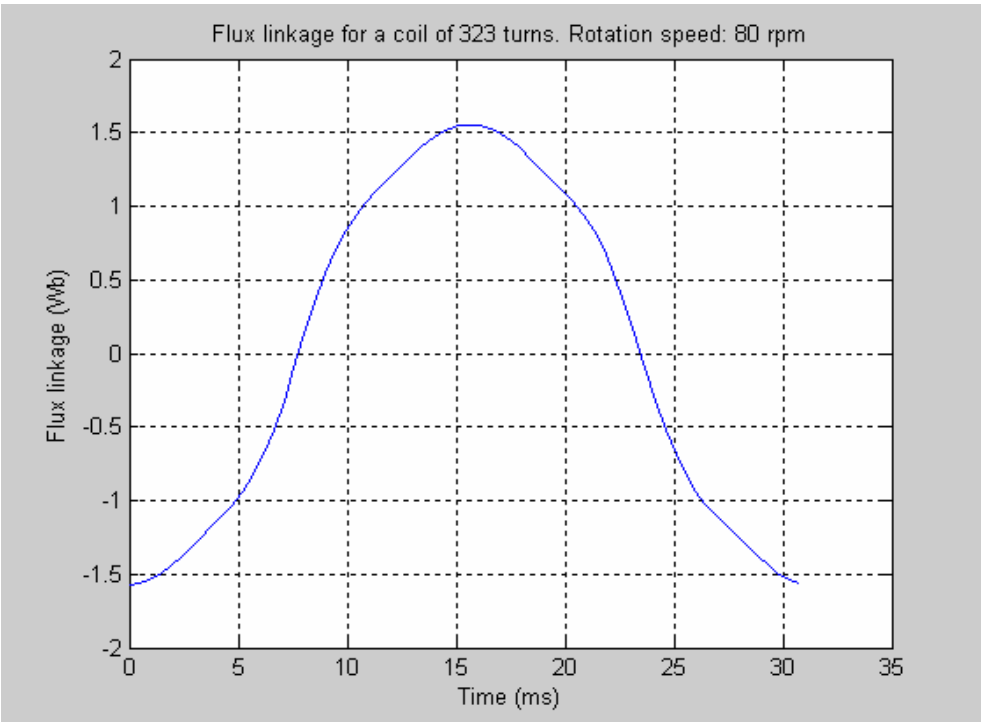

Figure 31 Flux linkage for a coil of 323 turns vs time.
Rotation speed: 80 rpm

Parameter	Frequency (hz)	Amplitude (Wb)	Phase angle (rad)	Relation to 1 harmonic
Mean level	0	0.0015	-	0.1 %
1 harmonic (base)	$0.4 \cdot V_{rot} \cdot 1$	1.6166	π	1
2 harmonic	$0.4 \cdot V_{rot} \cdot 2$	0.0098	π	0.6 %
3 harmonic	$0.4 \cdot V_{rot} \cdot 3$	0.1076	0	6.7 %
4 harmonic	$0.4 \cdot V_{rot} \cdot 4$	0.0029	0	0.2 %
5 harmonic	$0.4 \cdot V_{rot} \cdot 5$	0.0696	π	4.3 %

Table 6 The result of fourieranalysis. V_{rot} : Rotor speed (rpm)

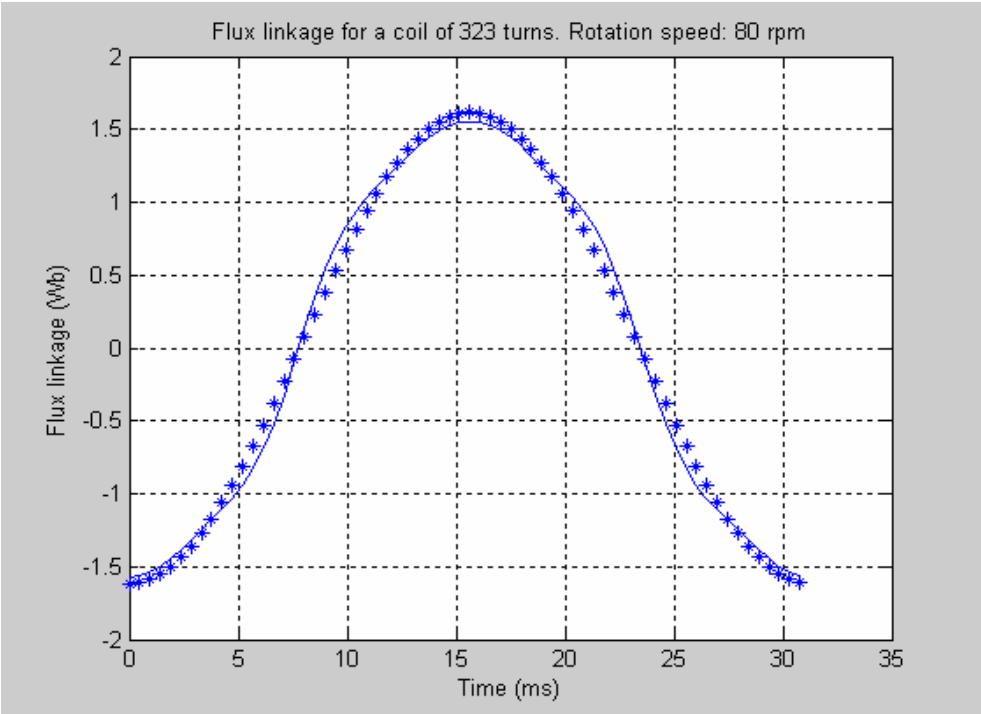

Figure 32 Flux linkage for a coil of 323 turns vs time. Rotation speed: 80 rpm
__ : original function **: 1 sine function (1st harmonic)

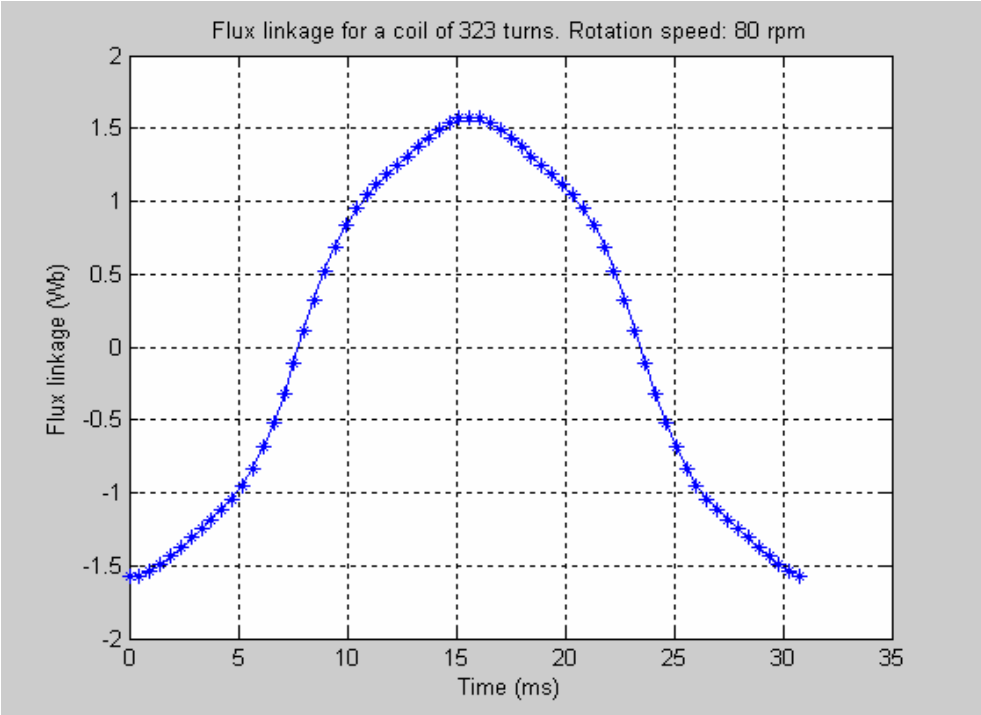

Figure 33 Flux linkage for a coil of 323 turns vs time. Rotation speed: 80 rpm
__ : original function **: 3 sine functions (1st , 3rd and 5th harmonics)

5.4 Conclusion

According to the fourieranalysis of the calculated flux function the flux vs time could be described by using 3 sine functions with frequencies corresponding to 1st , 3rd and 5th harmonics:

$$\phi(t) = A_1 \cdot \cos(\omega_1 t + \alpha_1) + A_3 \cdot \cos(\omega_3 t + \alpha_3) + A_5 \cdot \cos(\omega_5 t + \alpha_5)$$

$A_1 = 1.6166$	$A_3 = 0.1076$	$A_5 = 0.0696$
$\omega_1 = 2\pi \cdot 0.4 \cdot \Omega \cdot 1$	$\omega_3 = 2\pi \cdot 0.4 \cdot \Omega \cdot 3$	$\omega_5 = 2\pi \cdot 0.4 \cdot \Omega \cdot 5$
$\alpha_1 = \pi$	$\alpha_3 = 0$	$\alpha_5 = \pi$

Ω = Rotor speed (rpm)

At this step we limit the description by using the first term.

i.e.: $\phi(t) = A_1 \cdot \cos(\omega_1 t + \alpha_1)$

As is illustrated in **Figure 32**, this results in a fair good approximation. However, in a future work, it could be of interest to more in detail investigate the contents of harmonics and its dependence of e.g mechanical design and the resulted effect on power quality. This is mentioned in chapter 6.

6 FUTURE WORK

The performed investigation of the Hönö generator has resulted in a number of interesting questions. The following ones are of immediate importance:

- The question regarding demagnetizing current. A more detailed study to define an appropriate upper current limit for the stator coils is recommended. See chapter 4.2.

- In the calculations according to chapter 4.1 we have regarded the coil inductance as undependent of the stator-rotor relative position. However according to chapter 4.3 the inductance will vary as a function of relative position between stator pole and rotor pole. As the inductance has an influence on the resulting stator voltage, it could be a good idea to in the future, realize a more detailed analysis regarding the real effect of the inductance variation. Regarding the coil inductance we consequently have the following topics for coming studies:
    - complementary investigation of inductance distribution (measurements and calculations)
    - voltage dependent based on the inductance variations

7 REFERENCES

[1] APPLIED COMPUTATIONAL ELECTROMAGNETICS
EXTRA PROJECT WORK
INVESTIGATION OF A GENERATOR MODEL
Chalmers, Juli 2003, Ingemar Mathiasson

[2] Laboratory Measurements of a 40 kW Permanent Magnet Generator
Chalmers, December 1998, Ola Carlson and Anders Grauers

[3] Investigation of a Wind Power Generator. Part 2
Chalmers, Januari 2005, Ingemar Mathiasson

APPENDIX (USED SOFTWARE)

A 1 FEM-analysis

The FEM-calculations have been performed by a software named “Magnet” from Infolytica Corporation. The version of Magnet that have been used is limited to 2 dimensions and static calculations (2D Magnetostatic version).

A 2 Circuit Simulation

Circuit simulations have been performed by a software named “PLECS” ((Piecewise Linear Electrical Circuit Simulation). See chapter 4.1.

A 3 Discrete Fourier Calculations

A matlab-routine called ”dft_1” has been used to perform discret fourier analysis. The base theory is described in chapter 5.2.

```
%

%   Program dft_1

%

%   Programmet genomför beräkning av den diskreta fouriertransformen för en samplad
signal

%

%       Ingemar Mathiasson      6/6 - 04

%

%



%   Den diskreta fouriertransformen beräknas enligt uttrycket:

%   X(k+1)=DFT(Xn) = summa(x(n+1)*W_N^(k*n)),      n=0,,, till N-1, där N

%   är antalet sampel inom mätfönstret

%   W_N=exp(-j*2*pi/N);     x(j): samplad signal sampel j;

%   Följande gäller för den spektralanalyserade signalen: Medelnivå (likriktad
komponent): V0 = 1/N * X(1)

%

%   RMS-värden för grundton och övertoner: Vk = qrt(2)/N * abs(X(k)),    k= 2, 3, ...,
N,

%   OBS! Det är endast de första N-1 elementen som innebär ny information.

%   Resten av elementen är en "spegling" map realaxeln

%

%   Frekvenser: f(k) = 1/T, 2/T, ..., N/2T

%
```

```
%   Fasvinklar: FI(k) = arctan(b(k)/a(k)), där b(k) är imaginärdelen och a(k) är realdelen
an X(k)

%

%

%

%

   clear

%

%    load s_fil     % alternativ lagringsfil

%

%    load s_fil_2   % alternativ lagringsfil

%


%    load s_fil_flux_linkage     % alternativ lagringsfil. Användes för lagring av
beräknade avlänkningsflöden. Antal spolvarv = 600

%

     load s_fil_flux_linkage_2   % alternativ lagringsfil. Användes för lagring av
beräknade avlänkningsflöden. Antal spolvarv = 323

%

   N=length (signal_s);    % antal sampel

%

   W_N=exp(-j*2*pi/N);

%

   n_ton=6;    % antal delkomponenter som skall analyseras (inkl DC-komponent)

%

   for k=0:n_ton-1

%
```

```
   Xk(k+1)=0;
%
      for n=0:N-1
         x(n+1)=signal_s(n+1);
         Xk(k+1)=Xk(k+1)+x(n+1)*W_N^(k*n);
      end
%
   end
%
   Xk(1)=Xk(1)/N;      % DC-komponent
   for k=1:n_ton-1

   Xk(k+1)=Xk(k+1)*sqrt(2)/N;
   End

%
   Xk_2=abs(Xk);       % ger sinussignalernas RMS-värden. Första elementet i vektorn
är DC-nivån
   Xk_3=sqrt(2)*Xk_2;  % ger sinussignalernas toppvärden. Första elementet i vektorn
är ej relevant
   fas_vinkel=angle(Xk);   % ger de olika komponenternas fasvinkel i radianer
%
%
%   STOP
```

Appendix C

Investigation of a Wind Power Generator, Part 2, Ingemar Mathiasson, Chalmers, November 2005

Investigation of a Wind Power Generator

Part 2

Ingemar Mathiasson

November 2005

Department for Energy and Environment

Division of Electric Power Engineering

Chalmers University of Technology

CONTENTS

1 INTRODUCTION 3

2 SERIES- AND PARALLELL COMPENSATION. 3

3 PARALLEL COMPENSATION 4

4 SERIES COMPENSATION 8

5 COMPARISON BETWEEN PARALLEL AND SERIES COMPENSATION 10

6 PRESENT DESIGN 18

7 CONCLUSIONS 23

8 FUTURE WORK 24

9 REFERENCES 24

APPENDIX (USED SOFTWARE) 25

1 INTRODUCTION

The following work is Part 2 of a study regarding a technical investigation of the wind power generator at Hönö (Hönö 3, generator Morley 27/48/1). This work deals with the question of the differences between the two principles to make reactive power compensation; parallel compensation and series compensation.

Part 1 of this study ([3]) deals with FEM-analysis applied on the generator and consequences based on this FEM-analysis

2 SERIES- AND PARALLELL COMPENSATION.

The electrical power from the single stator module could in an ordinary way be expressed according to:

(Equation 1) $S = P + jQ$, where

S: the complex apparent power, P: the active power, Q: the reactive power

The reactive power from the stator module is in the first place an effect of the stator coil inductance. It is of interest to reduce the reactive power consumption as much as possible. There are two different suitable main methods present; the parallel compensation (a capacitor parallel with the stator coil) and the series compensation (a capacitor in series with the stator coil). See below in Figure 1 and Figure 2. Referring to the symbols in the figures:

U(t): the induced voltage, R: the coil resistance, L: the coil inductance, C: a capacitor to reduce the reactive power and Load: represents the load in question

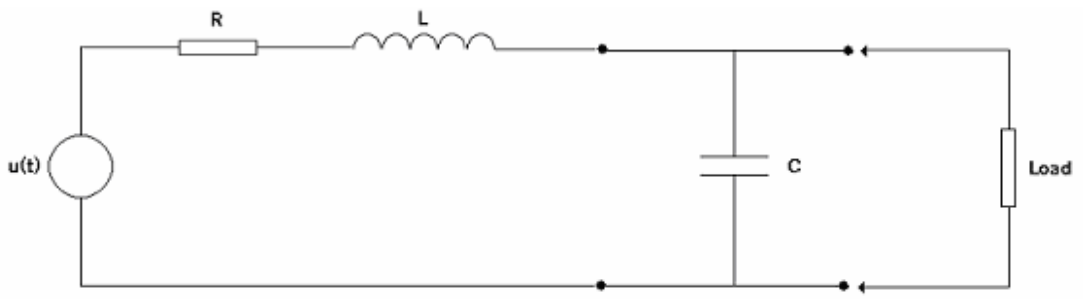

Figure 1 The principle for parallel compensation.

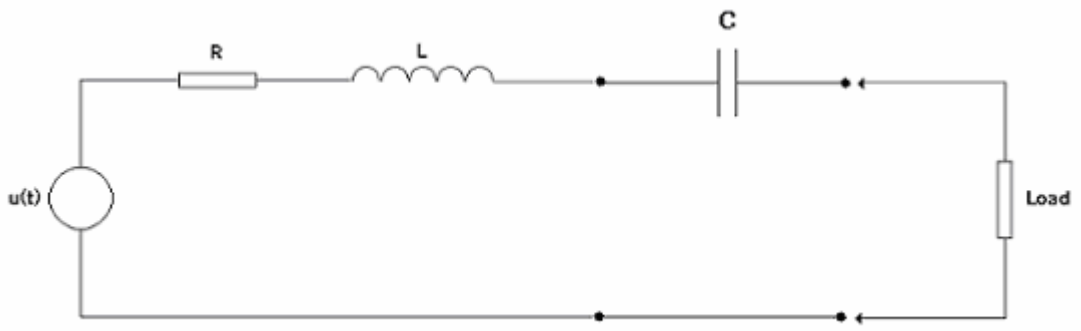

Figure 2 The principle for series compensation

The following is an analysis to find out some important differences between the two compensating methods.

The correlation between the electric angle speed, ω, and the rotating speed (rpm), V_{rot}, is:

(Equation 2) $$\omega = \frac{V_{rot} \cdot 2\pi \cdot P}{60}$$ where P = 24 is the number of pole pair.

3 PARALLEL COMPENSATION

The following is a circuit analysis regarding the equivalent circuit of a stator coil in combination with parallel compensation. The question that should has it's answer is: "what conditions should be fulfilled to get maximum active power from the stator coils".

Figure 3 gives the circuit principle for the parallel compensation.

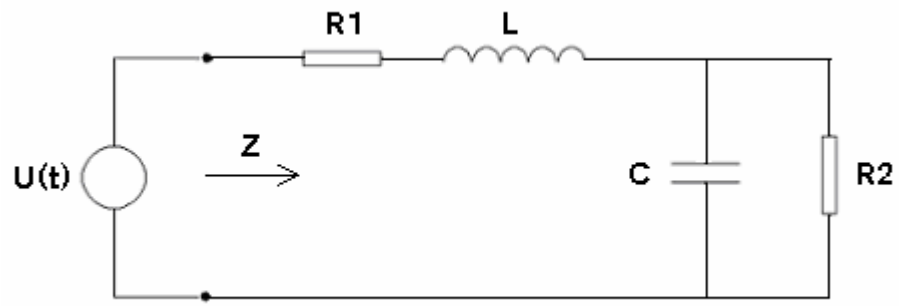

Figure 3 The principle of the parallel compensation.
U(t): induced voltage in the coil, R1: coil resistance, R2: load resistance (it is assumed a resistive load), L: coil inductance, C: capacitance for compensation

The impedance Z in the circuit is:

(Equation 3)
$$Z = R_1 + j\omega L + \frac{\frac{1}{j\omega C} \cdot R_2}{\frac{1}{j\omega C} + R_2}$$

For maximum compensation the phase angle of Z should be zero.

Developing of (Equation 3) gives:

$$Z = \frac{R_1 + R_2 - \omega^2 LCR_2 + j\omega(L + CR_1R_2)}{1 + j\omega CR_2} = \frac{|A| \cdot e^{j\varphi 1}}{|B| \cdot e^{j\varphi 2}} = |C| \cdot e^{j(\varphi 1 - \varphi 2)}$$

(Equation 4)
$$Z = |C| \cdot e^{j(\varphi 1 - \varphi 2)}$$

(Equation 5)
$$\varphi 1 = \arctan \frac{\omega(L + CR_1R_2)}{R_1 + R_2 - \omega^2 LCR_2}$$

(Equation 6) $\varphi 2 = \arctan \omega C R_2$

For maximum compensation Z is quite resistive and φ1 = φ2. That gives:

(Equation 7) $$\omega C R_2 = \frac{\omega(L + C R_1 R_2)}{R_1 + R_2 - \omega^2 L C R_2}$$

or:

(Equation 8) $$C^2 - C\frac{1}{\omega^2 L} + \frac{1}{\omega^2 R_2{}^2} = 0$$

This gives the following solution:

(Equation 9) $$C = \frac{1}{2\omega^2 L} \pm \sqrt{\left(\frac{1}{2\omega^2 L}\right)^2 - \frac{1}{\omega^2 R_2{}^2}}$$

As C has to be real (passive components are suggested) the following has to be satisfied:

(Equation 10) $$\left(\frac{1}{2\omega^2 L}\right)^2 \geq \frac{1}{\omega^2 R_2{}^2}$$

Looking for the maximum load for perfect compensation, than R_2 should be chosen as low as possible. That means:

(Equation 11) $$\left(\frac{1}{2\omega^2 L}\right)^2 = \frac{1}{\omega^2 R_2{}^2}$$ or

(Equation 12) $$R_2 = 2\omega L$$

and

(Equation 13) $$C = \frac{1}{2\omega^2 L}$$

This is the condition that has to be fulfilled to get maximum active power from the voltage source in question. Then there is no reactive power from the voltage source (Z is quite resistive) and R_2 is as low as possible.

Putting (Equation 12) and (Equation 13) into (Equation 3) gives:

$$Z = R_1 + j\omega L + \frac{\frac{1}{j\omega C}\cdot R_2}{\frac{1}{j\omega C} + R_2} = R_1 + j\omega\cdot\frac{R_2}{2\omega} + \frac{\frac{R_2}{j\omega\cdot\frac{1}{2\omega^2\frac{R_2}{2\omega}}}}{\frac{1}{j\omega\cdot\frac{1}{2\omega^2\frac{R_2}{2\omega}}} + R_2}$$

and after some simplifications:

(Equation 14) $$Z = R_1 + \frac{R_2}{2}$$ or assuming $R_1 << R_2$

(Equation 15) $$Z \approx \frac{R_2}{2}$$

Conclusion regarding parallel compensation:

Compensation capacitans: $C = \frac{1}{2\omega^2 L}$ (according to (Equation 13))

Where ω is the electric angle speed according to (Equation 2) and L is the stator coil inductance. If (Equation 13) is satisfied then the stator coil load is quite resistive according to (Equation 14) or (Equation 15).

4 SERIES COMPENSATION

The following is a circuit analysis regarding the equivalent circuit of a stator coil in combination with series compensation. The question that should has it's answer is: "what conditions should be fulfilled to get maximum active power from the stator coils".

Figure 4 gives the principle for the series compensation.

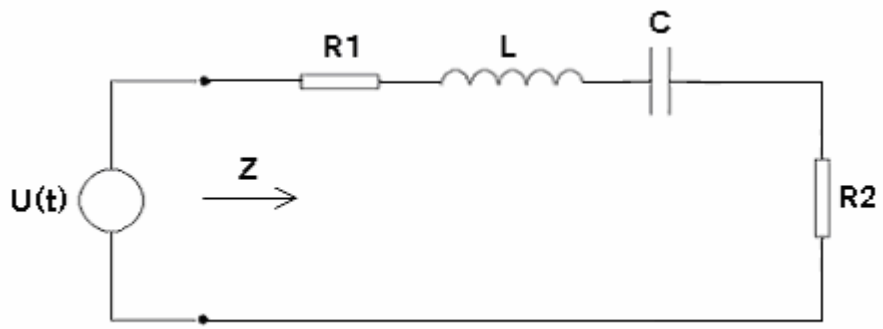

Figure 4 The principle of the series compensation. U(t): induced voltage in the coil, R1: coil resistance, R2: load resistance (it is assumed a resistive load), L: coil inductance, C: capacitance for compensation

The impedance Z in the circuit is:

(Equation 16) $$Z = R_1 + R_2 + j\omega L + \frac{1}{j\omega C}$$

For maximum compensation the phase angle of Z should be zero.

This implies $$j\omega L + \frac{1}{j\omega C} = 0$$ or

(Equation 17) $$C = \frac{1}{\omega^2 L}$$

If (Equation 17) is satisfied the impedance Z is quite resistive according to

(Equation 18) $$Z = R_1 + R_2$$

<u>Conclusion regarding series compensation</u>:

Compensation capacitans: $$C = \frac{1}{\omega^2 L}$$ (according to (Equation 17))

Where ω is the electric angle speed according to (Equation 2) and L is the stator coil inductance. If (Equation 17) is satisfied then the stator coil load is quite resistive according to (Equation 18).

5 COMPARISON BETWEEN PARALLEL AND SERIES COMPENSATION

A comparison is done between the two compensation principles by the following assumption:

- Power parameters are compared during different rotating speeds

- Complete compensation by a rotating speed, below named V_{rot}, of 80 rpm. This rotating speed is below named $\mathbf{V_{rot_comp}}$.

- The current amplitude in a coil is for each rotating speed adapted to a maximum value with an upper limit. The adaption is performed by altering the value of the resistance R2, the load. The goal of the study is to get the maximum power available from the generator. Therefore the current amplitude is adjusted to a value that is not allowed to exceed that value, which was predicted in [3] (demagnetization current). If this value is exceeded there is a risk for damaging the permanent magnets by demagnetization. In [3] a maximum recommended value of about 14.5 A (amplitude) was predicted. As a limit for the calculations in this chapter a current amplitude of **14.5 A** therefore is chosen. This current limit is below named $\mathbf{I_{max}}$.

- The following circuit parameters are used:

  - R1: 1 Ω
  - R2: Controlled to get maximum allowed current
  - L: 106 mH
  - C: parallel compensation 116,7 µF (adapted for 80 rpm)
    series compensation 233,4 µF (adapted for 80 rpm)

- The induced voltage is calculated according to the result presented in [3]
  i.e. $u(t) = A \cdot \omega \cdot \cos \omega t$, where A is 1,615 (Vs) and $\omega = \frac{V_{rot} \cdot 2\pi \cdot P}{60}$
  ω is the electric angle speed, V_{rot} is the generator rotating speed (rpm) and P is the number of pole pairs (24) in the rotor. See Figure 17

- The impedance is calculated according to above (chapter 3 and chapter 4)

- Simulations have been performed by mathlab routines in accordance with A 3
  Some results of simulations are presented in Figure 5 to Figure 17. The following could be noted:

- For low rotating speeds the P-comp (parallel compensation) is more effective than the S-comp (series compensation). See Figure 5. Mean value over the interval is about 6.5. For V_{rot} < about 56 rpm the P-comp is more effective than S-comp
- For low rotating speeds it could be a problem to reach I_{max} when using S-comp. See Figure 6, Figure 7 and Figure 8
  - Figure 6: For V_{rot} < about 56 rpm it is not possible to get I_{max} by S-comp
  - Figure 7**:** For V_{rot} < about 56 rpm the load resistance is zero for S-comp
- Within a sertain interval of rotating speed, below V_{rot_comp}, S-comp is more effective than P-comp. See Figure 9. In this example ($60 \leq V_{rot} \leq 80$) the active power relation between P-comp and S-comp is about 0,6. This means assuming a rectangular probability distribution in between the V_{rot} region in question, that in this case there is an increasing of active power by more than 60 % by using S-comp instead of P-comp
- For $V_{rot} > V_{rot_comp}$ it is impossible to limit the current by increasing the load resistance, when using P-comp. This effect depends on the parallel capacitor that take more and more over the total current when the frequency is increasing. See Figure 14 and Figure 15. In Figure 16 it can be observed how the the real part of the impedance is decreasing when $V_{rot} > V_{rot_comp}$ in spite of increased resistive load. The capacitor take more and more over when the frequency is increasing

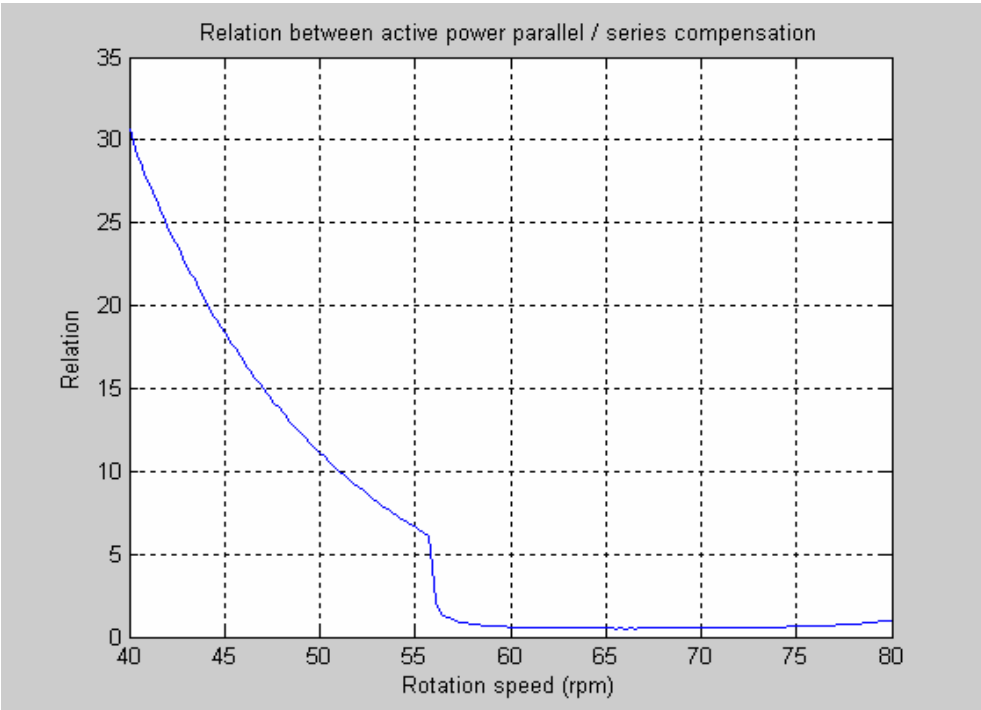

Figure 5 Relation between active power for P-comp/S-comp
Mean value over the interval is about 6.5
For V_{rot} < about 56 rpm the P-comp is more effective than S-comp

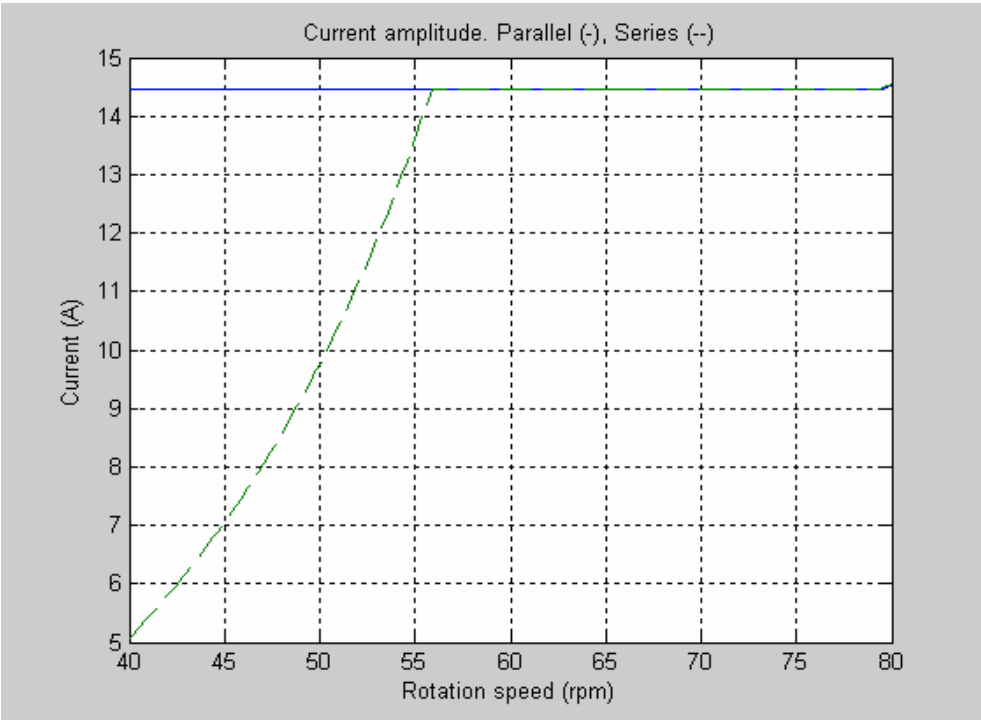

Figure 6 Current amplitude for P-comp and S-comp (- -)
For V_{rot} < about 56 rpm it is not possible to get I_{max} by S-comp

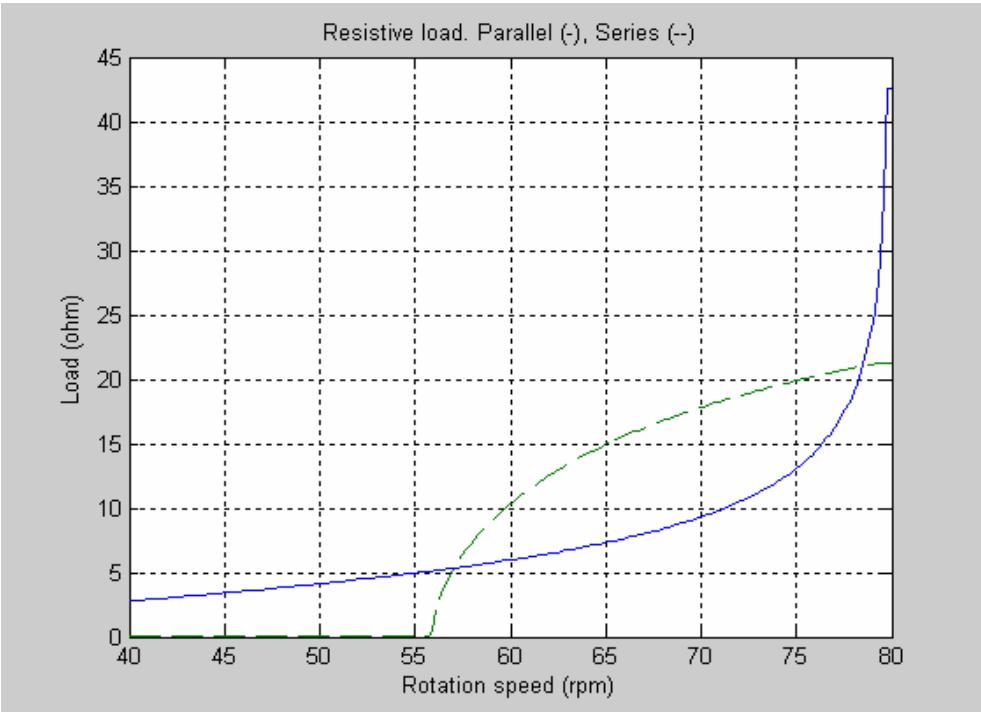

Figure 7 Adjusted load (resistive) for P-comp and S-comp (- -)
For V_{rot} < about 56 rpm the load resistance is zero for S-comp

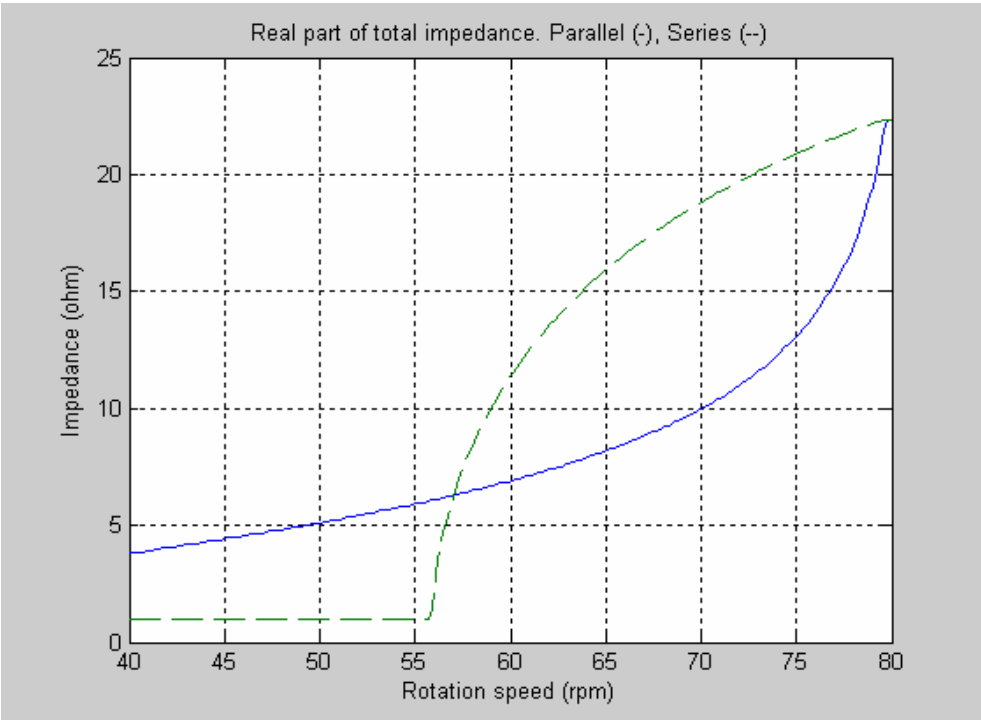

Figure 8 Real part of the total impedance for P-comp and S-comp (- -)

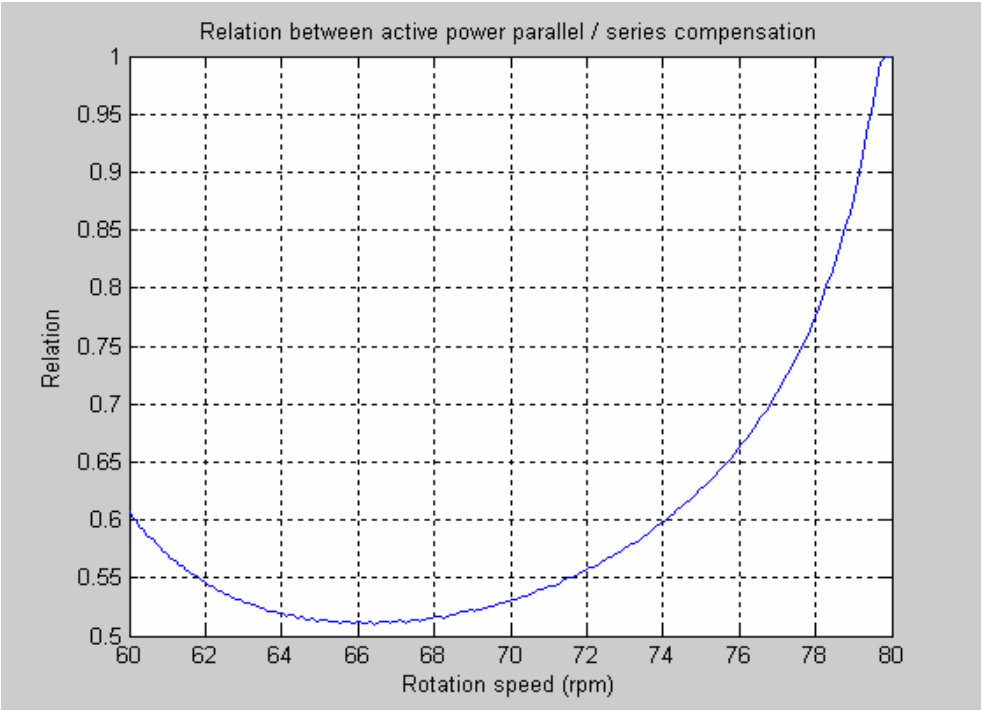

Figure 9 Relation between active power for P-comp/S-comp
Mean value over the interval is about 0.60
For V_{rot} < 80 rpm the S-comp is more effective than P-comp

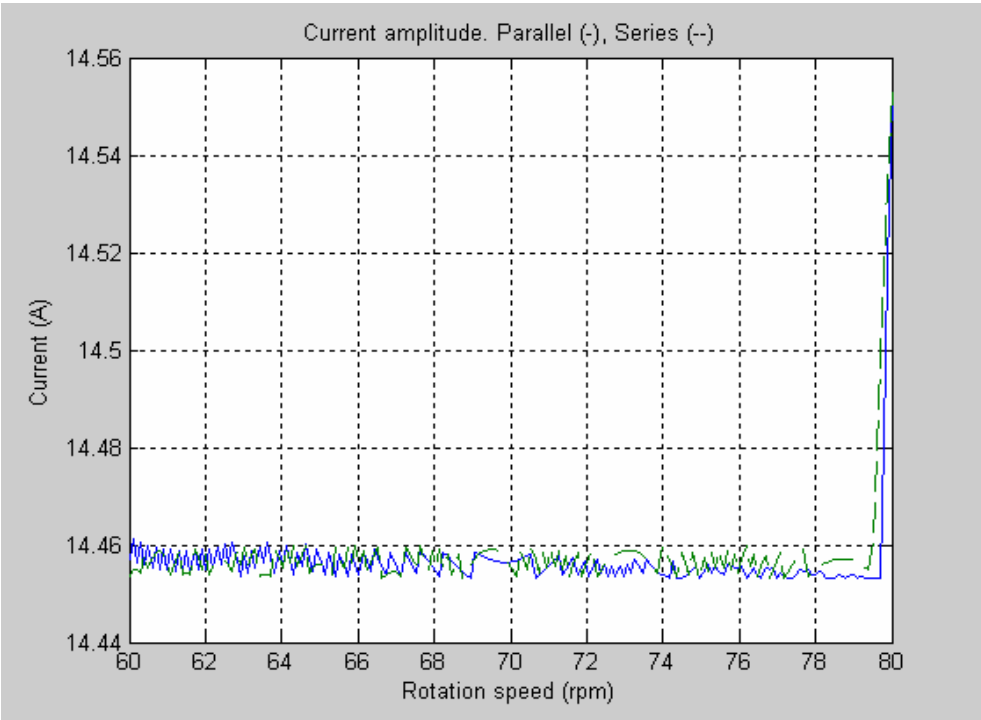

Figure 10 Current amplitude for P-comp and S-comp (- -). The current is adjusted to a value of about 14.5 A (amplitude)

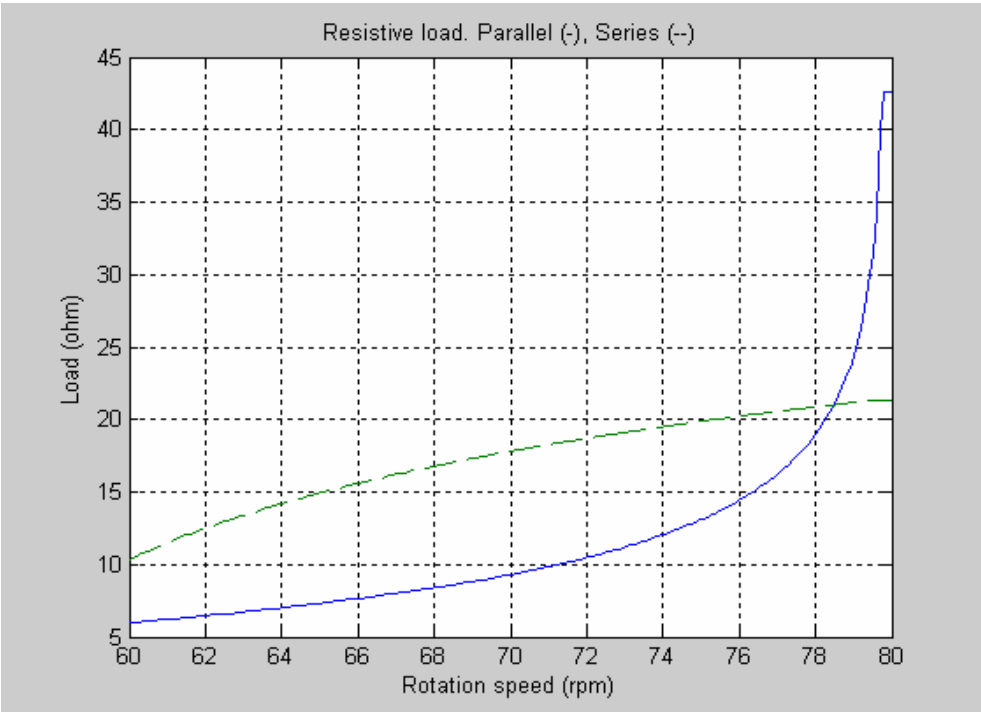

Figure 11 Adjusted load (resistive) for P-comp and S-comp (- -). The load is adjusted to result in a current of about 14.5 A (amplitude)

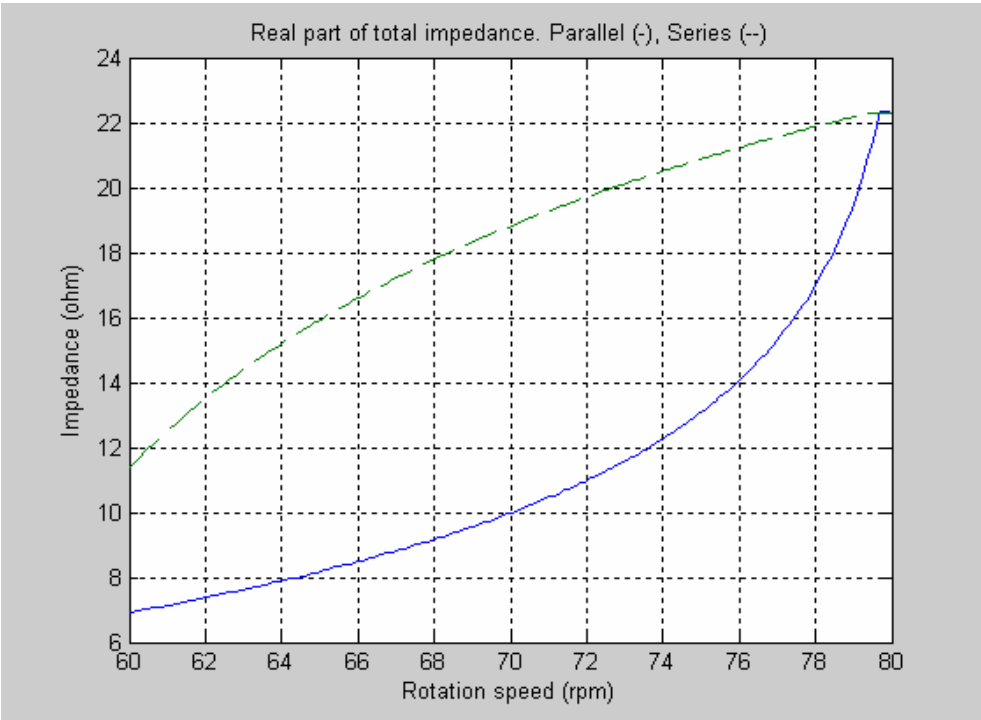

Figure 12 Real part of the total impedance for P-comp and S-comp (- -)

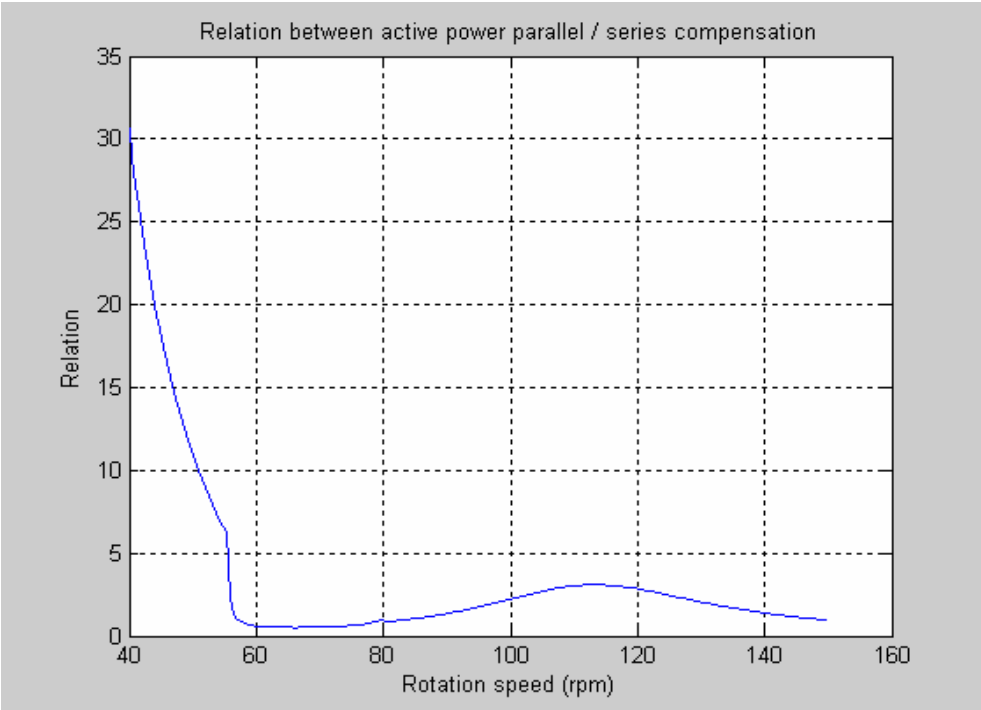

Figure 13 Relation between active power for P-comp/S-comp
For V_{rot} > about 80 rpm it is impossible to limit the current with P-comp

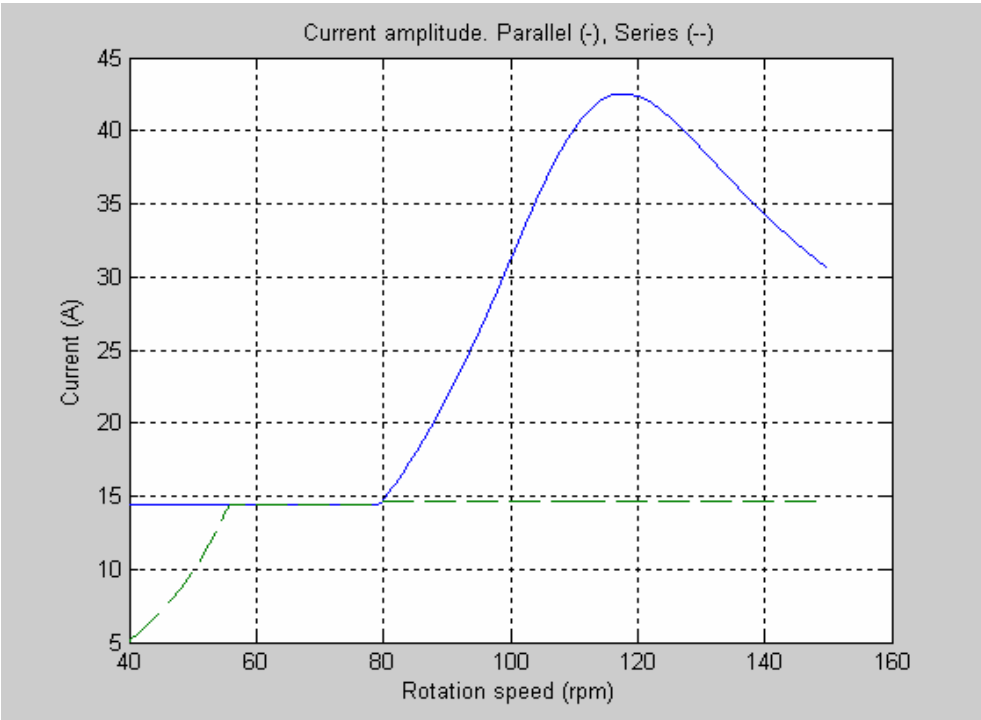

Figure 14 Current amplitude for P-comp and S-comp (- -)
For V_{rot} > about 80 rpm it is impossible to limit the current with P-comp

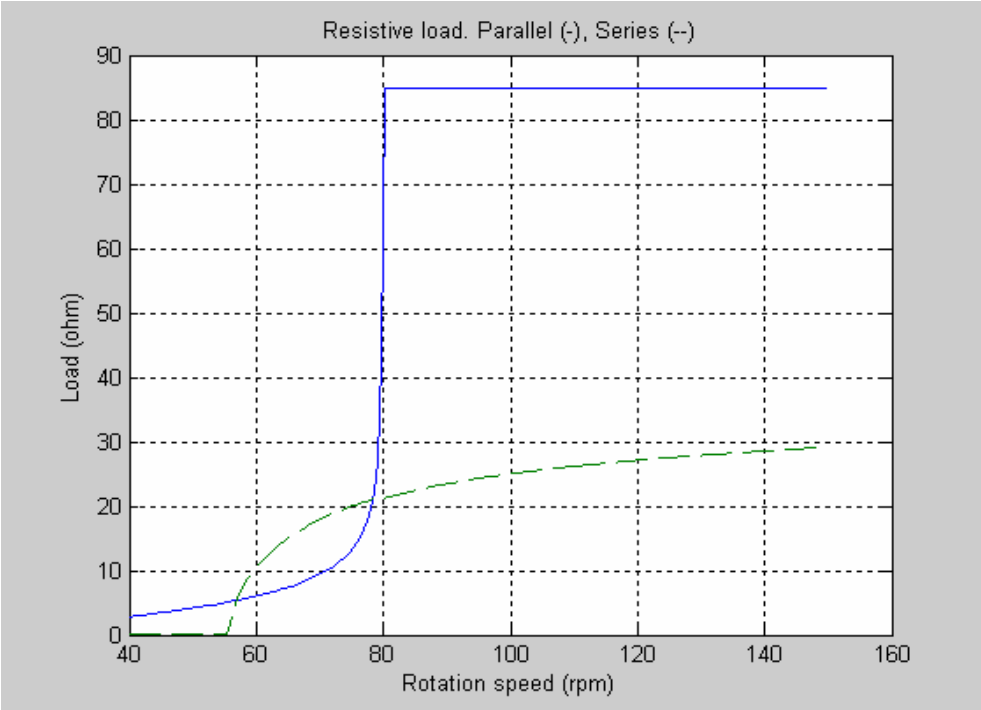

Figure 15 Adjusted load (resistive) for P-comp and S-comp (- -)
For V_{rot} > about 80 rpm it is impossible to limit the current with P-comp

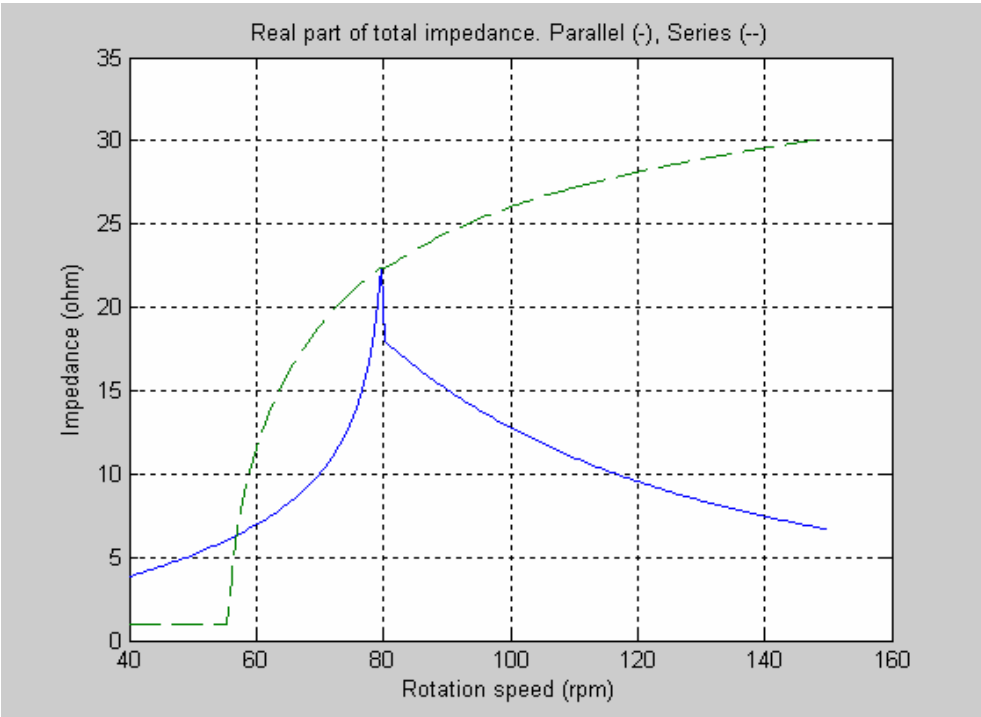

Figure 16 Real part of the total impedance for P-comp and S-comp (- -)
The real part is for the P-comp decreasing when V_{rot} > about 80 rpm, in spite of strongly increased resistive load

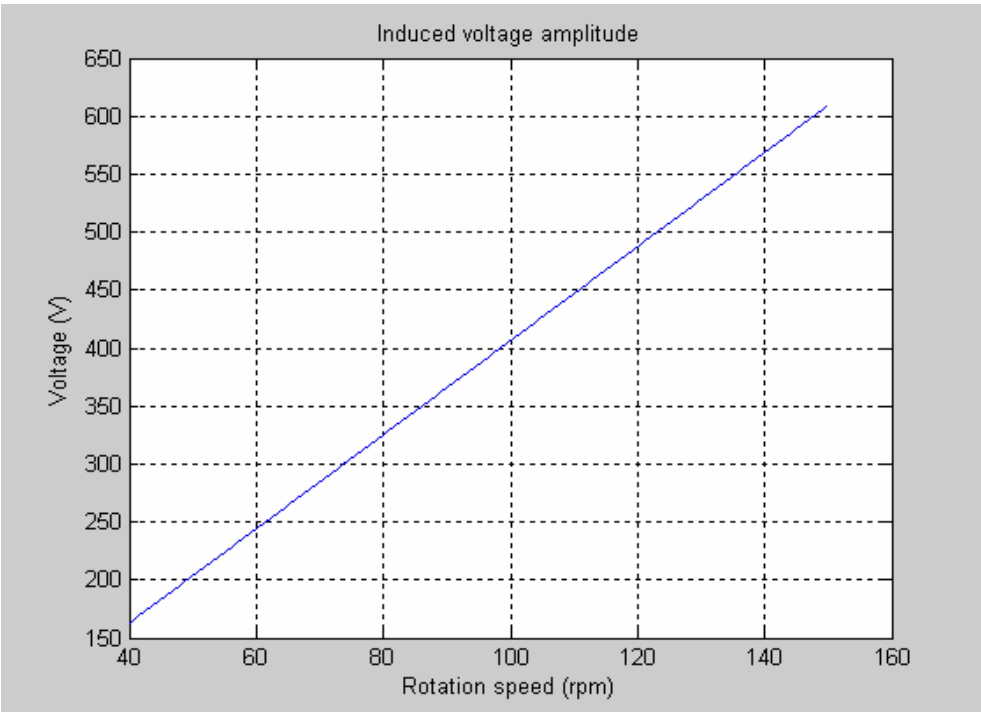

Figure 17 Induced voltage amplitude vs rotation speed

6 PRESENT DESIGN

The present generator design, that is based on parallel compensation, has a compensation capacitor of 60 µF. For a parallel compensation circuit there is a complete compensation at:

$$\omega = \frac{1}{\sqrt{2LC}}$$

That means a complete compensation at a rotation rate of:

$$V_{rot} = \frac{\omega \cdot 60}{2\pi \cdot P} = \frac{60}{2\pi\sqrt{2LC}\,24}$$

L = 0.106 H and C = 60 µF give

$V_{rot} \approx 112$ rpm

Figure 18 - Figure 25 illustrate some simulation results based on C and L parameters according to the present design (with P-comp) and by adapting R2 (the load) to get maximum allowed current amplitude (if possible), I_{max}, for each rotating speed. Note! In the present simulations and when compareing with the corresponding results with series compensation, V_{rot_comp} (complete compensation) for <u>S-comp</u> has been chosen to the same value as in chapter 5, i.e. at V_{rot_comp} = 80 rpm (the compensation capacitor is 233,4 µF). The following could then be noted:

- For P-comp it is now possible to limit the current amplitude to I_{max}, by adjusting the load resistance, if $V_{rot} \leq$ about 112 rpm. See Figure 19 and Figure 20. In Figure 21 it can be observed how the real part of the impedance is increasing up to V_{rot_comp} (112 rpm)
- If V_{rot} is studied in the interval 60 rpm to 80 rpm an extremely increasing of the effectivity for S-comp compared with P-comp can be noticed. See Figure 22. The result is, assuming a rectangular work distribution in between the V_{rot} region in question, that in this case there is a possibility to get 2,5 times more active power by using S-comp (note! V_{rot_comp} = 80 rpm for S-comp in this case) instead of P-comp (note! V_{rot_comp} = 112 rpm for P-comp in this case)

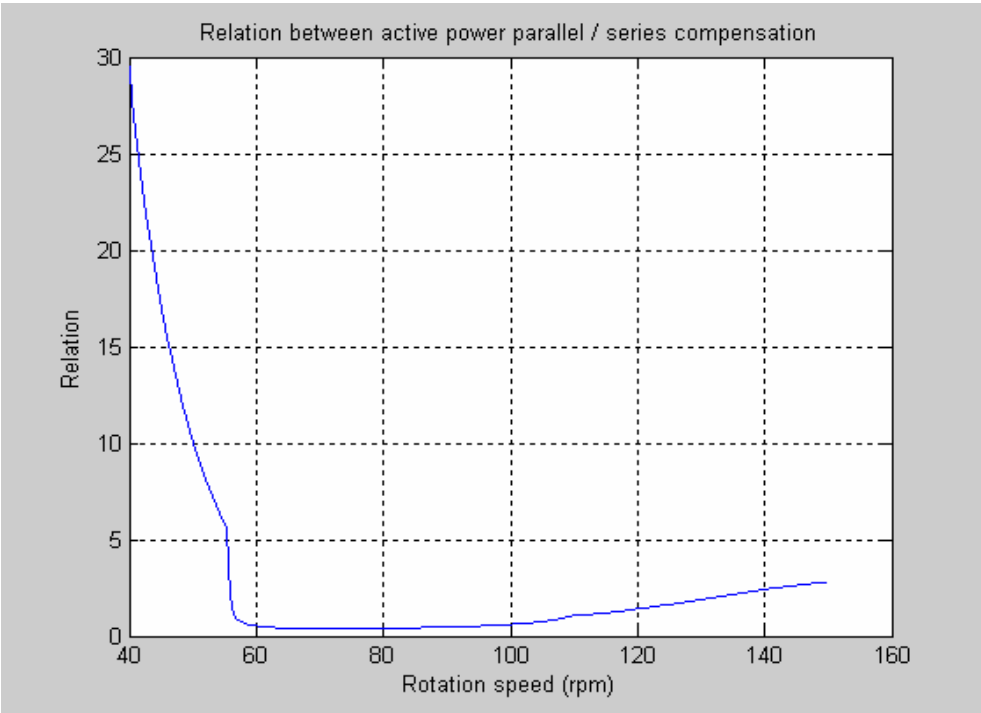

Figure 18 Relation between active power for P-comp/S-comp
For P-comp it is now possible to limit the current if $V_{rot} \leq$ about 112 rpm

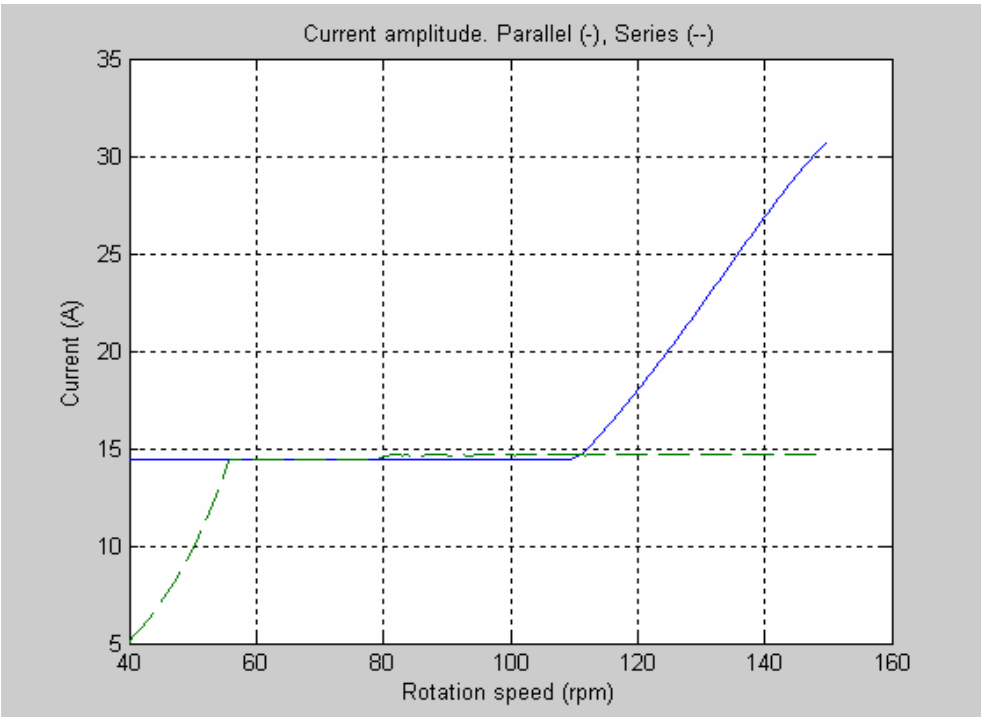

Figure 19 Current amplitude for P-comp and S-comp (- -)
For P-comp it is now possible to limit the current if $V_{rot} \leq$ about 112 rpm

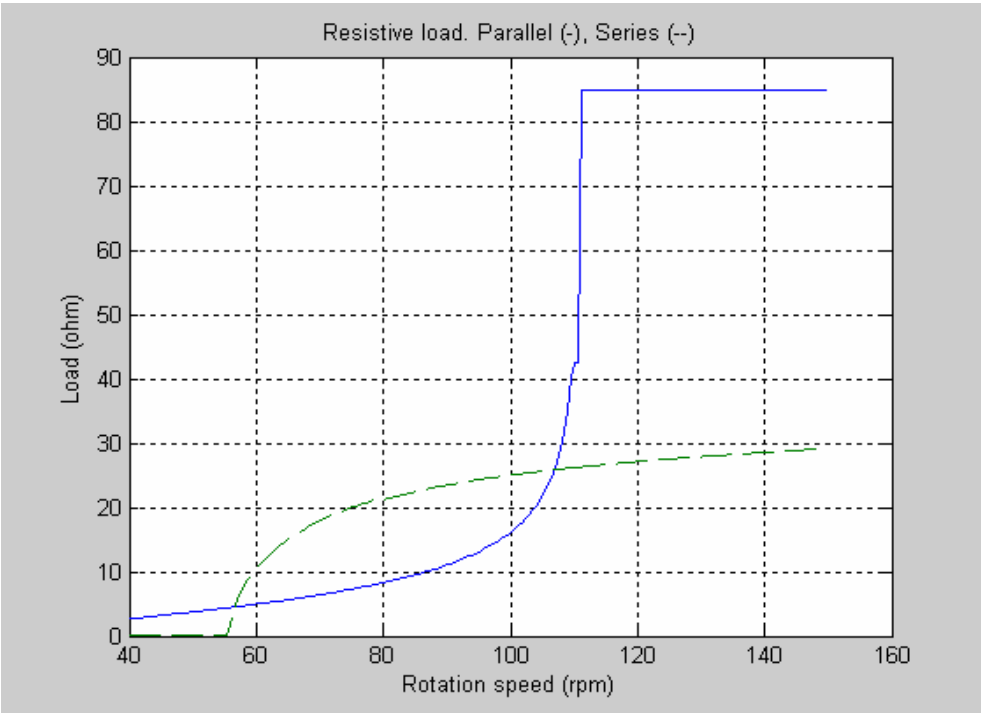

Figure 20 Adjusted load (resistive) for P-comp and S-comp (- -)
For P-comp it is now possible to limit the current for $V_{rot} \leq$ about 112 rpm

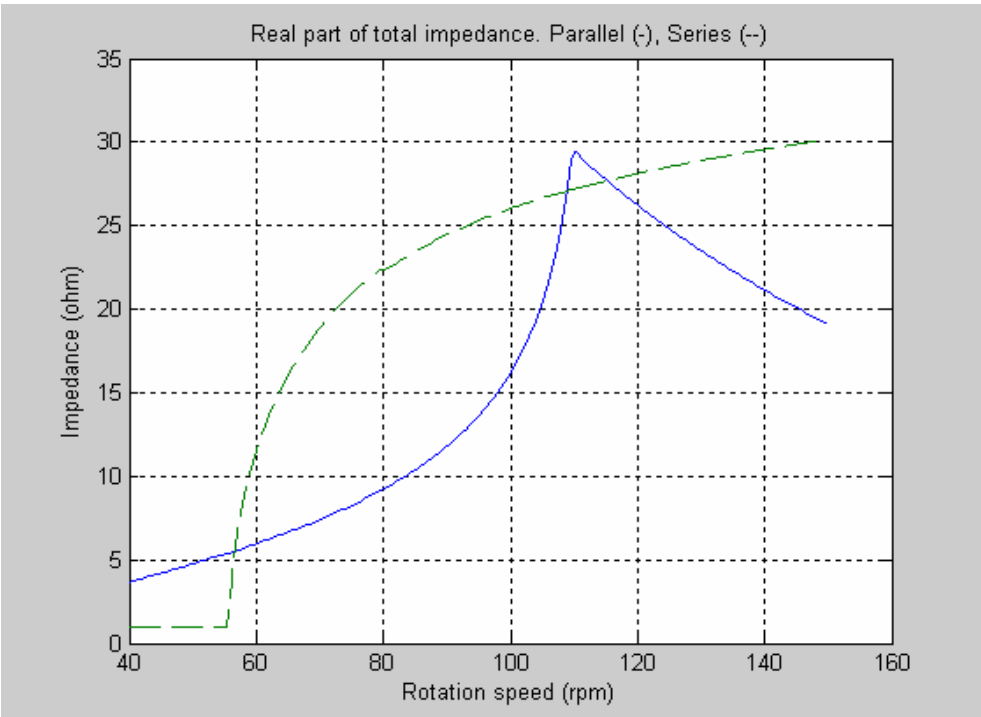

Figure 21 Real part of the total impedance for P-comp and S-comp (- -)
The real part is for the P-comp decreasing when $V_{rot} >$ about 112 rpm, in spite of strongly increased resistive load

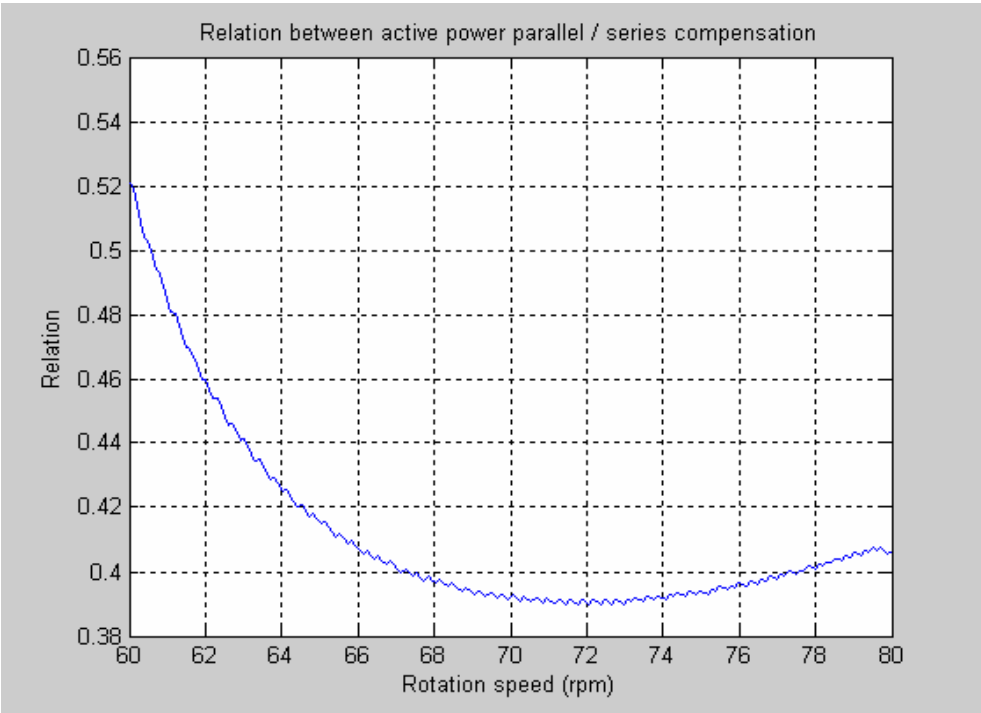

Figure 22 Relation between active power for P-comp/S-comp
Mean value over the interval is about 0.4

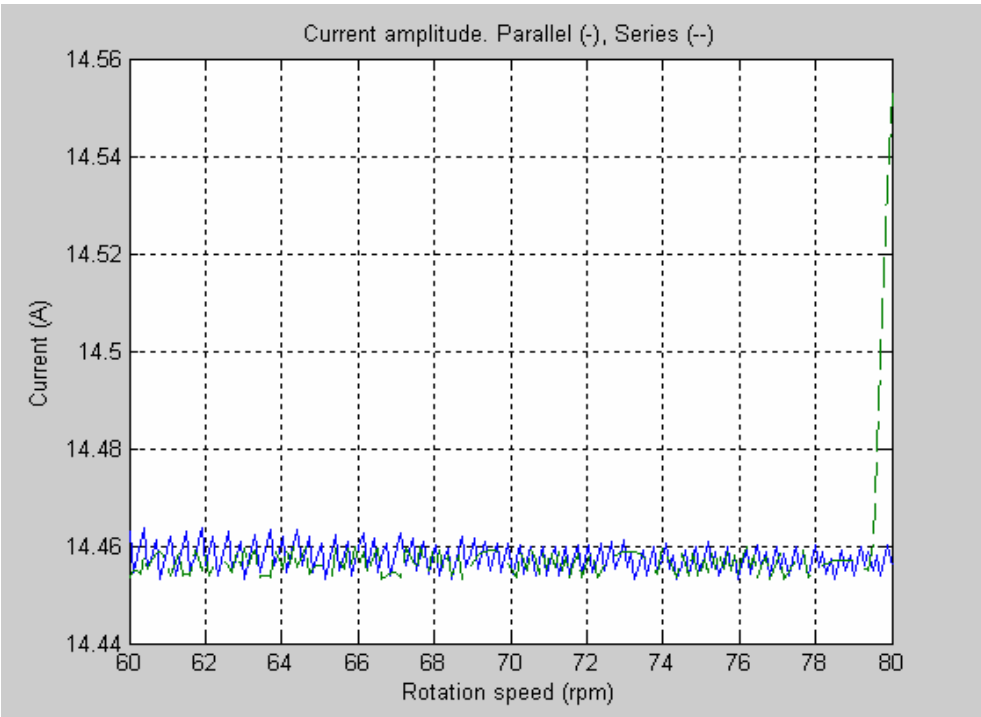

Figure 23 Current amplitude for P-comp and S-comp (- -)

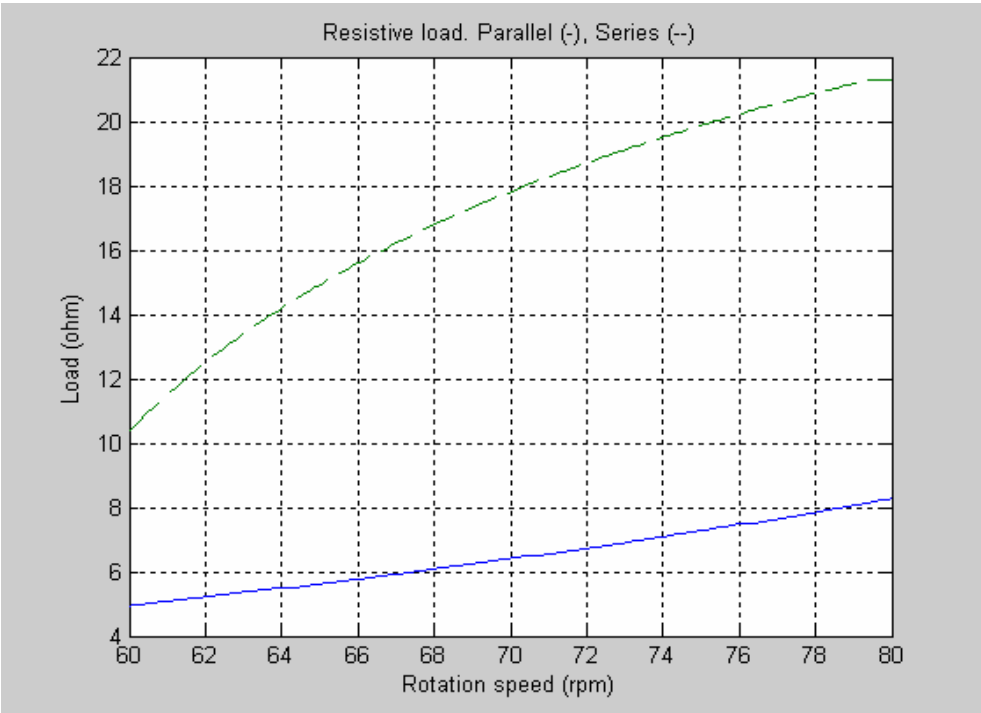

Figure 24 Adjusted load (resistive) for P-comp and S-comp (- -)

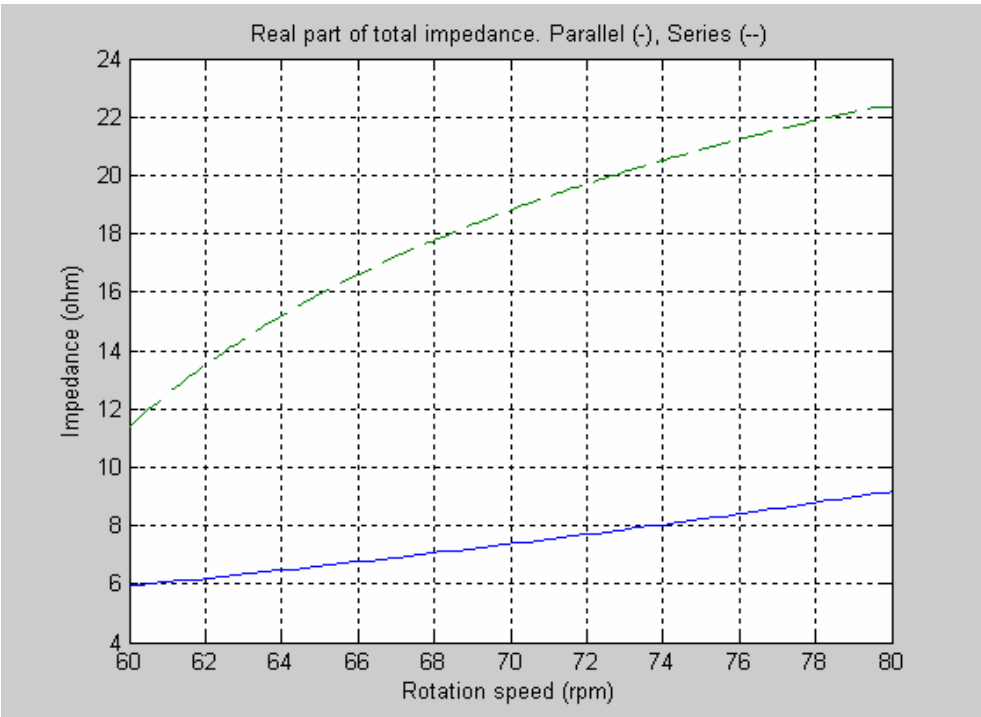

Figure 25 Real part of the total impedance for P-comp and S-comp (- -)

7 CONCLUSIONS

The following conclusions could be taken as a result of the analysis above:

- For large working areas in respect of V_{rot}*) it could be a problem to adjust the current amplitude by using the load. S-comp (series compensation) could result in problems for small V_{rot} values (problem to reach the wanted level) and P-comp (parallel compensation) could give problem for large V_{rot} values (problem to limit the wanted level). To get a basis for optimization of the best V_{rot_comp}**) and thereby choice of the compensating capacitors, furher studies regarding the probability distribution of the V_{rot} values have to be done. See chapter 8
- Depending on the choice of V_{rot_comp} , choice of working area in respect of V_{rot} and the probability distribution of the V_{rot} values in that working area, we could get very different answers with respect to the question of: "which compensating principle is the best one, S-comp or P-comp". The results above give a hint that <u>probably</u> the S-comp is to prefere. But more studies regarding the probability distribution of the V_{rot} values have to be done before we have a more specific answer. See chapter 8
- The used example in chapter 5 resulted among other things in: "Within a sertain interval of rotating speed, <u>below V_{rot_comp}</u>, we have that S-comp is more effective than P-comp. See Figure 9. In this example ($60 \leq V_{rot} \leq 80$) the active power relation between P-comp and S-comp is about 0,6. This means, if we assume a rectangular probability distribution in between the V_{rot} region in question, that we in this case have an increasing of active power by more than 60 % by using S-comp instead of P-comp".

*) V_{rot}: rotation speed of the generator (rpm)

**) V_{rot_comp}: the rotation speed that, with respect to compensation principle in question, gives perfect reactive compensation (no reactive power)

8 FUTURE WORK

Above there is suggested a study to investigate the statistical work/probability distribution of the different V_{rot}. This future work should include:

- Statistical studies regarding the wind speed
- Adapting the wind speed distribution to an optimal working area for V_{rot} with respect to λ-C_p and V_{rot_comp} for P-comp and S-comp

9 REFERENCES

[1] APPLIED COMPUTATIONAL ELECTROMAGNETICS

EXTRA PROJECT WORK
INVESTIGATION OF A GENERATOR MODEL
Chalmers, Juli 2003, Ingemar Mathiasson

[2] Laboratory Measurements of a 40 kW
Permanent Magnet Generator
Chalmers, December 1998, Ola Carlson and Anders Grauers

[3] Investigation of a Wind Power Generator. Part 1
Chalmers, Januari 2005, Ingemar Mathiasson

APPENDIX (USED SOFTWARE)

A 1 Software. Parallel compensation

A matlab-routine called ”medel_p_kp_Dlast” has been used to simulate the circuit for parallel compensation. The routine controls the current amplitude to a specific value in between the rotation speed region that is to be studied. The control is realized by adapting the load (resistive) to an appropriate level. Some parameters are loaded in the file "fil_parkomp" for later use.

```
%

%   medel_p_kp_Dlast

%


%   Reglerar utgående strömamplitud från en generatormodul till önskad

%   nivå inom valfritt varvtalsintervall. Reglering sker genom att anpassa


%   lasten som förusätts resistiv. Kompensering map reaktiv effekt sker med

%   parallellkompensation. Lagring av vissa beräkningsparametrar görs i

%   filen "fil_parkomp"

%

%

%   Ingemar Mathiasson,  Januari 2005

%

%

   clear

%

   R1=1.;       % spolresistans

%    R2=39.9611;      % lastresistans anpassad för 75 rpm

   R2=42.6251;      % lastresistans anpassad för 80 rpm
```

```
L=0.106;    % spolinduktans
%    C=1.3276e-004;  % kompensationskapacitans anpassad för 75 rpm
%   C=1.1668e-004;   % kompensationskapacitans anpassad för 80 rpm
C=60.e-006;      % kompensationskapacitans enligt dagens design
A=1.615;    % amplitud för avlänkat spolflöde
%    Imax=15.2360;   % maximalt tillåten spolström
Imax=14.5530;   % maximalt tillåten spolström
%    Imax=12.;   % maximalt tillåten spolström
DR2=0.05;        % stegning av R2 vid anpassning av last

%
rpm=75;     % rotationshastighet (nominell)
rpm=60;     % rotationshastighet
%
N_sampel=200;       % antal rotationssampel
%
rpm_min=60;   % lägsta rotationsfrekvens
rpm_max=80;   % högsta rotationsfrekvens
%
rpm_steg=(rpm_max-rpm_min)/(N_sampel-1);    % sampelsteg
%
for k=1:N_sampel
rpm(k)=rpm_min+(k-1)*rpm_steg;     % aktuell rotationsfrekvens
w(k)=rpm(k)/60*24*2*pi;   % vinkelfrekvens för inducerad spänning
R2=42.6251;      % lastresistans anpassad för 80 rpm
%    R2=39.9611;      % lastresistans anpassad för 75 rpm
```

```
%    R2_var(k)=2*w(k)*L;   % varierbar lastresistans anpassad till aktuell
rotationsfrekvens

   C_var(k)=1/(2*w(k)*w(k)*L);  % varierbar kompensationskapacitans anpassad till
aktuell rotationsfrekvens

%

   U(k)=A*w(k);      % inducerade spänningens ampliud

%

   for m1=1:5000

%

   Z(k)=R1+j*w(k)*L+(R2/(j*w(k)*C))/(1/(j*w(k)*C)+R2);     % Impedans


   I(k)=U(k)/abs(Z(k));

   if I(k) < Imax-0.1

       R2=R2-DR2;

       if R2 < 0, R2=0.01;, end

   else

      break

   end

   end

%

   for m1=1:5000


  Z(k)=R1+j*w(k)*L+(R2/(j*w(k)*C))/(1/(j*w(k)*C)+R2);     % Impedans

   I(k)=U(k)/abs(Z(k));

   if I(k) > Imax+0.1

       R2=R2+DR2;

       if R2 > 85, R2=85;, end
```

```
    else
        break
    end
    end
%
    I(k)=U(k)/abs(Z(k));     % amplitud för utgående ström
    R2_var(k)=R2;            % resistiv last
    Z_var(k)=Z(k);           % total impedans
    Z_var_R(k)=real(Z(k));     % reell del av total impedans

    fi(k)=atan(imag(Z(k))/real(Z(k)));     % kretsens fasvinkel
    P(k)=U(k)^2/abs(Z(k))/2*cos(fi(k));     % aktiv effekt enskild statormodul
    Q(k)=U(k)^2/abs(Z(k))/2*sin(fi(k));     % reaktiv effekt enskild statormodul
    Ptot(k)=27*P(k);                 % aktiv effekt enskild statormodul
    Qtot(k)=27*Q(k);                 % reaktiv effekt enskild statormodul
%
    end
%
    save fil_parkomp Ptot Qtot I R2_var Z_var_R rpm       % lagra aktiv och reaktiv
effekt i filen "fil_parkomp"
%
    figure(1)
    plot(rpm,P), grid
%
%   Sök medeleffekter
%
```

```
   Pmedel=mean(P);        % medeleffekt för modul

   Ptot_medel=mean(Ptot);      % medeleffekt för generator

%

%

%   STOP
```

A 2 Software. Series Compensation

A matlab-routine called ”medel_p_ks_Dlast” has been used to simulate the circuit for series compensation. The routine controls the current amplitude to a specific value in between the rotation speed region that is to be studied. The control is realized by adapting the load (resistive) to an appropriate level. Some parameters are loaded in the file "fil_parkomp" for later use.

```
%

%   medel_p_ks_Dlast

%

%   Reglerar utgående strömamplitud från en generatormodul till önskad

%   nivå inom valfritt varvtalsintervall. Reglering sker genom att anpassa

%   lasten som förusätts resistiv. Kompensering map reaktiv effekt sker med

%   seriekompensation. Lagring av vissa beräkningsparametrar görs i

%   filen "fil_serkomp"

%

%

%   Ingemar Mathiasson,  Januari 2005

%

%

   clear

%
```

```
   R1=1.;       % spolresistans
%    R2=39.9611/2;      % lastresistans anpassad för 75 rpm
   R2=42.6251/2;      % lastresistans anpassad för 80 rpm
   L=0.106;    % spolinduktans
%    C=2.6552e-004;  % kompensationskapacitans anpassad för 75 rpm
   C=2.3336e-004;   % kompensationskapacitans anpassad för 80 rpm

%    C=120.e-006;      % kompensationskapacitans med motsv kompensations frekvens
som dagens design
   A=1.615;    % amplitud för avlänkat spolflöde
%    Imax=15.2360;   % maximalt tillåten spolström
    Imax=14.5530;   % maximalt tillåten spolström
%    Imax=9.;   % maximalt tillåten spolström
   DR2=0.01;        % stegning av R2 vid anpassning av last
%
   rpm=75;     % rotationshastighet (nominell)
   rpm=30;     % rotationshastighet
%
   N_sampel=200;       % antal rotationssampel
%
   rpm_min=60;   % lägsta rotationsfrekvens
   rpm_max=80;   % högsta rotationsfrekvens
%
   rpm_steg=(rpm_max-rpm_min)/(N_sampel-1);    % sampelsteg
%
   for k=1:N_sampel
```

```
   rpm(k)=rpm_min+(k-1)*rpm_steg;     % aktuell rotationsfrekvens

   w(k)=rpm(k)/60*24*2*pi;   % vinkelfrekvens för inducerad spänning

%    R2=39.9611/2;      % lastresistans anpassad för 75 rpm

   R2=42.6251/2;      % lastresistans anpassad för 80 rpm

%    R2_var(k)=2*w(k)*L;   % varierbar lastresistans anpassad till aktuell
rotationsfrekvens



   C_var(k)=1/(w(k)*w(k)*L);  % varierbar kompensationskapacitans anpassad till
aktuell rotationsfrekvens

%

   U(k)=A*w(k);      % inducerade spänningens ampliud

%

   for m1=1:5000

%

   Z(k)=R1+j*w(k)*L+1/(j*w(k)*C)+R2;     % Impedans

   I(k)=U(k)/abs(Z(k));

   if I(k) < Imax-0.1

      R2=R2-DR2;

      if R2 < 0, R2=0.01;, end

   else

     break

   end

   end

%

   for m1=1:5000
```

```
  Z(k)=R1+j*w(k)*L+1/(j*w(k)*C)+R2;     % Impedans
   I(k)=U(k)/abs(Z(k));
   if I(k) > Imax+0.1
      R2=R2+DR2;
      if R2 > 85, R2=85;, end
  else

       break
   end
   end
%
   I(k)=U(k)/abs(Z(k));     % amplitud för utgående ström
   R2_var(k)=R2;            % resistiv last
   Z_var(k)=Z(k);           % total impedans
   Z_var_R(k)=real(Z(k));     % reell del av total impedans
   fi(k)=atan(imag(Z(k))/real(Z(k)));     % kretsens fasvinkel
   P(k)=U(k)^2/abs(Z(k))/2*cos(fi(k));     % aktiv effekt enskild statormodul
   Q(k)=U(k)^2/abs(Z(k))/2*sin(fi(k));     % reaktiv effekt enskild statormodul
   Ptot(k)=27*P(k);                  % aktiv effekt enskild statormodul
   Qtot(k)=27*Q(k);                  % reaktiv effekt enskild statormodul
%
   end
%
   save fil_serkomp Ptot Qtot I R2_var Z_var_R rpm       % lagra aktiv och reaktiv
effekt i filen "fil_serkomp"
%
```

```
figure(1)
plot(rpm,P), grid
%
%   Sök medeleffekter
%
Pmedel=mean(P);         % medeleffekt för modul

Ptot_medel=mean(Ptot);      % medeleffekt för generator
%
%
%   STOP
```

A 3 Software. Comparison Parallel / Series Compensation

A matlab-routine called ” komp_par_ser” has been used to compare the performance between parallel compensation and seires compensation. The routine uses parameters that are loaded in the files "fil_parkomp" (performance of parallel compensation) and "fil_serkomp" (performance of series compensation). This routine is preceded by the routines ”medel_p_kp_Dlast” and ”medel_p_ks_Dlast”.

```
%
%   komp_par_ser
%
%   Gör olika jämförelser rörande prestanda hos parallell- resp
%   seriekompensering. Utnyttjar filerna "fil_parkomp" resp "fil_serkomp".
%   Programmet föregås av körningar med programmen "medel_p_kp_Dlast" resp
%   "medel_p_kp_Dlast"
%
%   Ingemar Mathiasson,  Januari 2005
%
```

```
%
   clear
%
   load fil_parkomp        % hämta aktiv och reaktiv effekt avseende
parallellkompensering
   Ptot_par=Ptot;

   Qtot_par=Qtot;
   I_par=I;
   R2_var_par=R2_var;
   Z_var_R_par=Z_var_R;
%
   clear Ptot Qtot I R2_var Z_var_R
%
   load fil_serkomp        % hämta aktiv och reaktiv effekt avseende seriekompensering
   Ptot_ser=Ptot;
   Qtot_ser=Qtot;
   I_ser=I;
   R2_var_ser=R2_var;
   Z_var_R_ser=Z_var_R;
%
   Prel=Ptot_par./Ptot_ser;      % relation mellan aktiv effekt för par-komp och ser-komp
   Qrel=Qtot_par./Qtot_ser;      % relation mellan reaktiv effekt för par-komp och ser-
komp
   Irel=I_par./I_ser;            % relation mellan ström för par-komp och ser-komp
%
   Prel_medel=mean(Prel);        % medelvärde över aktuellt rotationsintervall
```

```
   Qrel_medel=mean(Qrel);        % medelvärde över aktuellt rotationsintervall

   Irel_medel=mean(Irel);        % medelvärde över aktuellt rotationsintervall

%

   figure(1)

   plot(rpm,Prel), grid, title('Relation between active power parallel / series
compensation'), xlabel('Rotation speed (rpm)'), ylabel('Relation')


%    figure(2)

%    plot(rpm,Qrel), grid, title('Relation between reactive power parallel / series
compensation'), xlabel('Rotation speed (rpm)'), ylabel('Relation')

%    figure(3)

%    plot(rpm,Irel), grid, title('Relation between current parallel / series compensation'),
xlabel('Rotation speed (rpm)'), ylabel('Relation')

   figure(4)

   plot(rpm,I_par,'-',rpm,I_ser,'--'),grid, title('Current amplitude. Parallel (-), Series (--)'),
xlabel('Rotation speed (rpm)'), ylabel('Current (A)')

   figure(5)

   plot(rpm,R2_var_par,'-',rpm,R2_var_ser,'--'),grid, title('Resistive load. Parallel (-),
Series (--)'), xlabel('Rotation speed (rpm)'), ylabel('Load (ohm)')

   figure(6)

   plot(rpm,Z_var_R_par,'-',rpm,Z_var_R_ser,'--'),grid, title('Real part of total
impedance. Parallel (-), Series (--)'), xlabel('Rotation speed (rpm)'), ylabel('Impedance
(ohm)')

%

%

%   STOP
```

Appendix D

Preliminärt beräkningsunderlag för generatorn 05-11-1996

DESIGN AND PERFORMANCE OF MODULAR PERMANENT-MAGNET DIRECT-DRIVE, VARIABLE-SPEED WIND TURBINE GENERATOR

DATE 05-11-1996

40 kW 75.0 rpm

HONO
Single Magnet Design
AIR COOLED

27 Modules
48 Poles.

TURBINE DIAMETER	m	10.0
DESIGN MAX SPEED	rpm	75.0
POWER COEFFICIENT	%	45.0
POWER AT NOMINAL WIND SPEED	kW	42.3
SHAFT TORQUE	kN.m	5.4
AIRGAP	mm	3.3
MAGNET BLOCK LENGTH	mm	101.6
MAGNET BLOCK WIDTH	mm	152.4
MAGNET BLOCK THICKNESS	mm	50.8
MAGNET BLOCKS PER MODULE		1
ROTOR MODULE OVERALL WIDTH	mm	80.0
MAX LAM WIDTH AT BOTTOM OF MAGNET	mm	4.0
POLE FACE TOTAL WIDTH	mm	45.0
POLE TIP GAP	mm	35.0
POLE TIP DEPTH (inc bridge if used)	mm	6.0
AIR PATH LEAKAGE	%	14.9
STATOR MMF TO DEMAGNETISE	Amp.Turn	%12198
ROTOR MODULE MASS	kg	7.8 (A)
includes magnets, poles, plates, & tapping bar		
MODULE E-CORE WIDTH	mm	150
MODULE radius at airgap surface	mm	1
MODULE E-CORE DEPTH (magnetic)	mm	84
SLOT DEPTH	mm	65.0
SLOT WIDTH	mm	37.5
TURNS PER COIL		526
WIRE DIAMETER	mm	1.80
PARALLEL WIRES		1.00
MEAN TURN LENGTH	mm	541
RESISTANCE AT RATED TEMPERATURE	Ohm	2.730
THERMAL RESISTANCE	K/W	0.478
RATED COPPER TEMPERATURE	Deg C	130
COOLING AIR TEMPERATURE	Deg C	40
RATED RMS CURRENT	Amp	8.134
IRON LOSS AT RATED FREQUENCY	W	9.3
MASS OF COPPER	kg	6.440
MASS OF INSULATION	kg	1.975
MASS OF LAMINATIONS	kg	6.763
APPROX TOTAL MASS OF MODULE	kg	15.644 (B)
POLE NUMBER		48
ROTOR DIAMETER	m	1.287
ROTOR MODULE GAP	mm	4.2
STATOR MODULES PER RING		27
STATOR MODULE GAP	mm	0.5
POLE PITCH REFERRED TO MEAN GAP	mm	84.44

40 pF FLη = 93.2%
Torque ratio 1.31

60 pF FLη ≃ 89.5%
Torque ratio 1.70

80 pF FLη 81.8%
Torque Ratio 2.12

6.14 A	40 pF
7.68 A	60 pF
10.41 A	80 pF

Use 40 - 50 pF

ACTIVE MASS
48 × A + 27 × B = 796 kg

— Acceptable beam loss with m.steel beams.

MAGNETIC CIRCUIT CALCULATIONS

Displacement	Magnet flux	Coil Linkage	Self induc	Left mut	Right mut

mm	mWeber	mWeber	mH	mH	mH
0.0	1.99	-2098	148.7	-14.9	-14.9
7.0	1.84	-2048	145.8	-15.1	-16.3
14.1	1.72	-1889	142.0	-15.0	-17.6
21.1	1.66	-1624	140.2	-15.2	-20.3
28.1	1.73	-1241	148.4	-17.0	-23.2
35.2	1.77	-744	152.0	-18.2	-23.5
42.2	1.73	-0	159.3	-22.0	-22.0

Displacement mm	Rotor rad F N	Rotor tang F N	Rotor twist N.m	
0.0	1325	-87	7.7	0
7.0	1233	-103	13.0	0
14.1	1044	-390	1.1	0
21.1	700	-396	-35.3	0
28.1	464	-210	-30.5	0
35.2	424	197	16.9	0
42.2	589	381	45.0	0

Displacement mm	Stat rad F N	Stat tang F N	Stat twist N.m
0.0	2258	1	-2169.7
7.0	2176	371	-2112.3
14.1	2012	413	-1998.9
21.1	1907	133	-1924.4
28.1	2045	13	-2101.5
35.2	2239	143	-2304.5
42.2	2420	0	-2557.5

COIL FLUX, EMF AND SELF INDUCTANCE COMPONENTS (Emf Vrms at rated F)

HARMONIC	FLUX LINKAGE		E (Vrms)	L (mH)
1.0	2.2	291.8	0.0	
2.0	0.0	-4.5		
3.0	-0.1	-51.4	0.0	
4.0	0.0	5.0		
5.0	0.0	23.6	0.0	
6.0	0.0	0.3		

MEAN SELF INDUCTANCE (excl leakage) mH 148.1
MEAN EFFECTIVE INDUCTANCE (INC MUT, EXC LEAKAGE) mH 120.2
MEAN MUTUAL INDUCTANCE TO ADJACENT COILS mH -18.2
SLOT LEAKAGE INDUCTANCE mH 53.31

MAGNETIC EQUIVALENT CIRCUIT FOR EXTERNAL EFFECTS:
STATOR CORE PEAK POTENTIAL (A) 552.1
SERIES RELUCTANCE (kA/Weber) 332.6
MEAN RAD FORCE FOR NOMINAL GAP (N) 2339.104
MEAN RAD FORCE FOR NOMINAL GAP (N) 0
MAGNETIC OVALISING STIFFNESS (MN/m) 2759199

module emf	Vrms	291.8016
module inductance	mH	173.4638
module resistance	Ohm	2.729624
module rated current	Arms	8.133928
module S/C current	Arms	8.893436
demagnetisation current	Arms	16.39741
resonant capacitance	muF	162.2515
optimum capacitance	muF	80.02223
maximum overspeed	%	20

overspeed resonant C	muF	112.6747
CHOSEN CAPACITANCE	muF	50.0
giving -----		
terminal voltage	Vrms	395.4414
rated input power	W	2365.265
rated output power	W	2184.671
peak output power	W	3102.587
no-load current	Arms	9.675437
overspeed NL current	Arms	.3570376

MODULES PER BEAM 1

STRUCTURAL DESIGN

SIMPLE CYLINDRICAL BEAMS ----------
CANTILEVER SUPPORT ONE END ----------
MODULES NOT LINKED TOGETHER ----------

STATOR RING EXTERNAL DIAMETER	m	1.538
STATOR RING INTERNAL DIAMETER	m	0.500
STATOR RING THICKNESS	mm	25.0
STATOR RING MASS (EACH)	kg	325.9
STATOR INNER RING COMPRESSION	mm	0.021
STATOR OUTER RING EXTENSION	mm	0.015
STATOR RING OVALISING STIFFNESS	MN/m	%8017.777
STATOR OVALISING STIFFNESS	MN/m	%542.388
ROTOR CYLINDER OUTER DIAMETER	m	0.919
ROTOR CYLINDER THICKNESS	mm	5.0
NUMBER OF ROTOR DISCS		1
ROTOR DISC INSIDE DIAMETER	m	0.709
ROTOR CYLINDER MASS	kg	13.0
ROTOR CYLINDER AND DISC MASS	kg	22.9
ROTOR RADIAL EXPANSION	mm	0.020
ROTOR OVALISING STIFFNESS	MN/m	26.93
TOTAL OVALISING STIFFNESS	MN/m	25.66
SHAFT OUTER DIAMETER	mm	120
SHAFT INNER DIAMETER	mm	100
SHAFT LENGTH	mm	955
SHAFT MASS	kg	26

MASS OF LEADS BEARINGS ETC approx kg 108

screening rings

STRUCTURE LOSS FOR COMPLETE MACHINE

FREQUENCY Hz	BEAMLOSS kW	RINGLOSS kW	pk BEAM FLUX mW
6.000	0.048	0.000	0.000
12.000	0.093	0.000	0.000
18.000	0.133	0.000	0.000
24.000	0.169	0.000	0.000
30.000	0.203	0.000	0.000
36.000	0.234	0.000	0.000

OK

STEP BY STEP SIMULATION OF RECTIFIER CIRCUIT
INCLUDING STATOR SATURATION

steps per half cycle 180 simulated cyles 4
winding temperature 100

Appendix E

Ola Carlson, Anders Grauers, “Laboratory Measurements of a 40kW Permanent Magnet Generator”, Department of Electric Power Engineering, Chalmers University of Technology, December 1998.

Laboratory Measurements of a 40 kW Permanent Magnet Generator

Ola Carlson and Anders Grauers

December 1998

Department of Electric Power Engineering
Chalmers University of Technology

Content

1 SUMMARY 1

2 INTRODUCTION 1

3 ELECTRICAL SYSTEM DESIGN 1

4 MEASUREMENT RESULTS 2

4.1 GEARBOX LOSSES 4

4.2 STATIONARY OPERATION 4

4.2.1 No load operation 5

4.2.2 Resistive load operation 7

4.2.3 Converter load operation 9

4.2.4 Wind turbine operation 11

4.2.5 Short circuit operation 12

5 TIME SERIES MEASUREMENT 13

5.1 LOAD PERFORMANCE 13

6 LABORATORY DOCUMENTATION 17

7 CONCLUSIONS 22

8 REFERENCE 22

1 Summary

This work has been carried out within the Joule project No JOU2 CT 93-0297.

The electrical system for a variable speed directly driven permanent magnet wind generator has been designed, built up and tested out.

The laboratory tests of the generator show that it works acceptably. The results show a lower peak power than expected.

The important and extensive work with redesigning and adapting the test wind turbine for the direct driven generator is almost finished. Only tests of the control systems in the laboratory remain before the turbine will be erected on the Hönö site.

2 Introduction

This report has been carried out within the Joule project No JOU2 CT 93-0297.

The electrical system for a variable directly driven permanent magnet wind generator has been designed, built up and tested out.

The generator design is carried out by Ed Spooner at Durham University and Alan Willianson at UMIST. The generator is manufactured at Morley Electrical Engineering. The converter design is carried out at Chalmers University of Technology. Previous work within this project is described in [1,2]. Nordic Windpower AB is the technical coordinator of the project.

This report describes the tests and measurements of the 40 kW PM generator. The efforts of the technical staff of the department are hereby gratefully acknowledge. Magnus Ellsén for his very well done design of the measurement system and electrical connection boards. Bo Lagerkvist for his mechanical works with the adaptation of the generator to the nacelle and the reconstruction of the nacelle. Conny Larsson, Per Ekelund, Ulrik Johansson, Robert Karlsson have also been a part of the construction group involved in the project.

3 Electrical system design

The generator stator consists of 27 modules. The outputs of each module are separately connected to a phase compensating capacitor circuit and a full diode bridge rectifier. The modules in the generator is divided in two groups and connected in parallel within the group. These two groups are series connected to the DC-link. This connection is done due to the demand of low current in the DC-link and converter.

The DC-bus interfaces a thyristor based DC/AC-converter via one smoothing inductor. The DC/AC-converter is connected to the grid through a transformer, which makes it possible to operate the converter on a 500 V level.

In case of a control system failure or loss of grid, two independent brake systems are implemented to able braking of the turbine shaft, including the case of an internal system signal failure. The brake function is obtained without access to the grid. The brake systems are realised as one mechanical and one electrical system, [2]. The electrical brake system is acting directly on the DC-bus output.

4 Measurement results

Laboratory tests of the permanent magnet generator with converter have been carried out. The generator test set-up was realised as a DC-motor and the PM-generator, with a gearbox connected in between. The tests are focused on the following parts:

1. power-speed performance of the direct-driven generator with converter or resistive load
2. stability of the system
3. efficiency measurements

The following 9 functional parts build up the test system see Figure 4.1

1. DC motor supplied by an AC/DC rectifier, speed-regulated into chosen speed
2. shaft speed transducer
3. torque transducer for high speed revolution
4. gearbox with conversion ratio of 21:1
5. modular 40 kW PM generator
6. rectifier system
7. DC-current and voltages measurements.
8. thyristor DC/AC-converter
9. transformer for adaptation to grid voltage

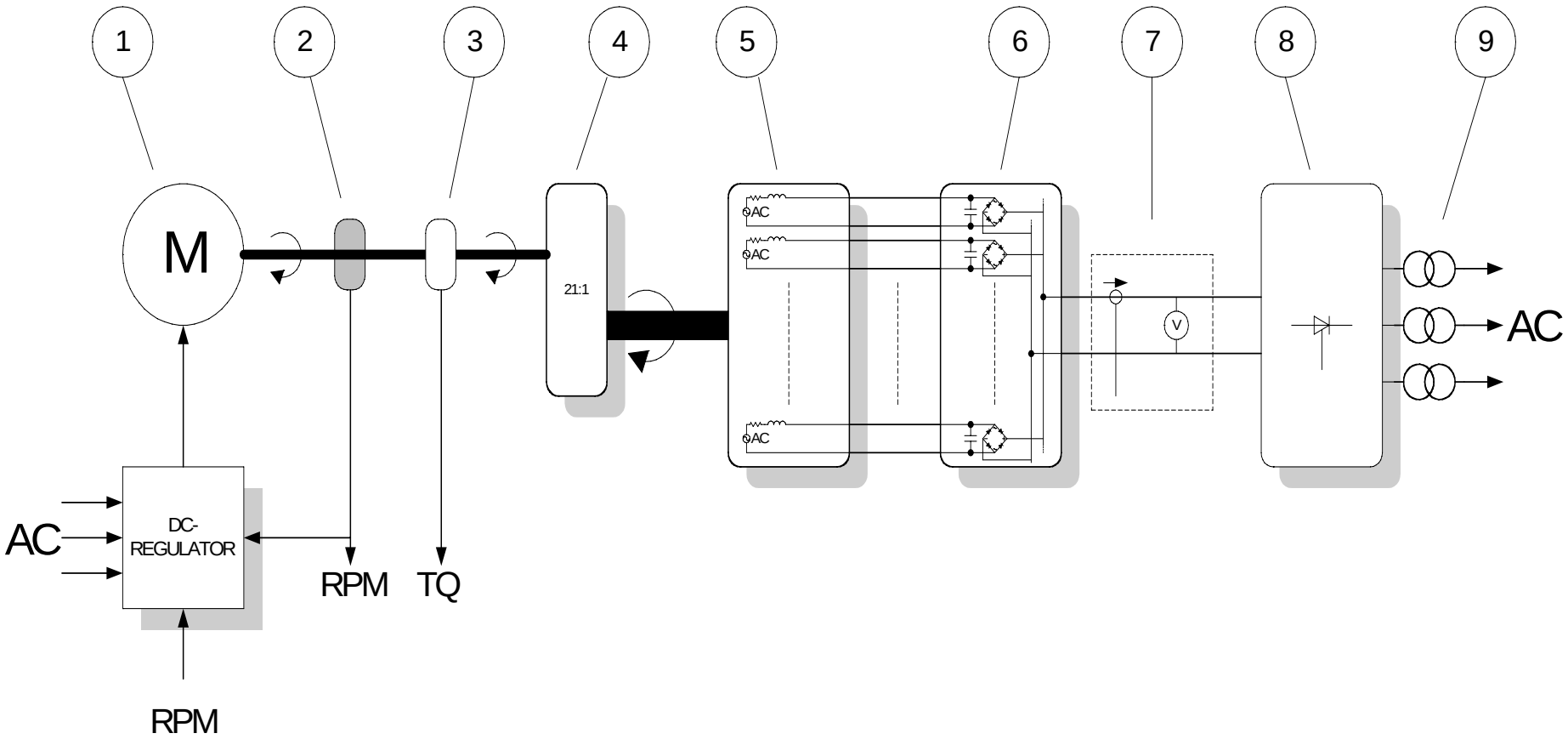

Figure 4.1: Generator test set-up.

4.1 Gearbox losses

To achieve a low speed and a high torque performance for testing of the generator the test set-up was realised with a gearbox and a DC-motor. The input torque of the gearbox was measured at the high-speed shaft of the gearbox. The low speed torque of the generator was calculated by extracting the gearbox losses from the high-speed shaft torque measurements. The power loss of the gearbox was measured and was estimated as stated in equation 1. The measurement result is shown in Figure 4.1.

$$P_{Gearloss} = 0.0013 * (N_{Gen})^{1.6} + 0.04 * P_{in}$$

$$\begin{aligned} &Where: \\ &P_{Gearloss} = Gearloss(kW) \\ &N_{Gen} = Speed(rpm) \\ &P_{in} = InputPower(kW) \end{aligned} \qquad (1)$$

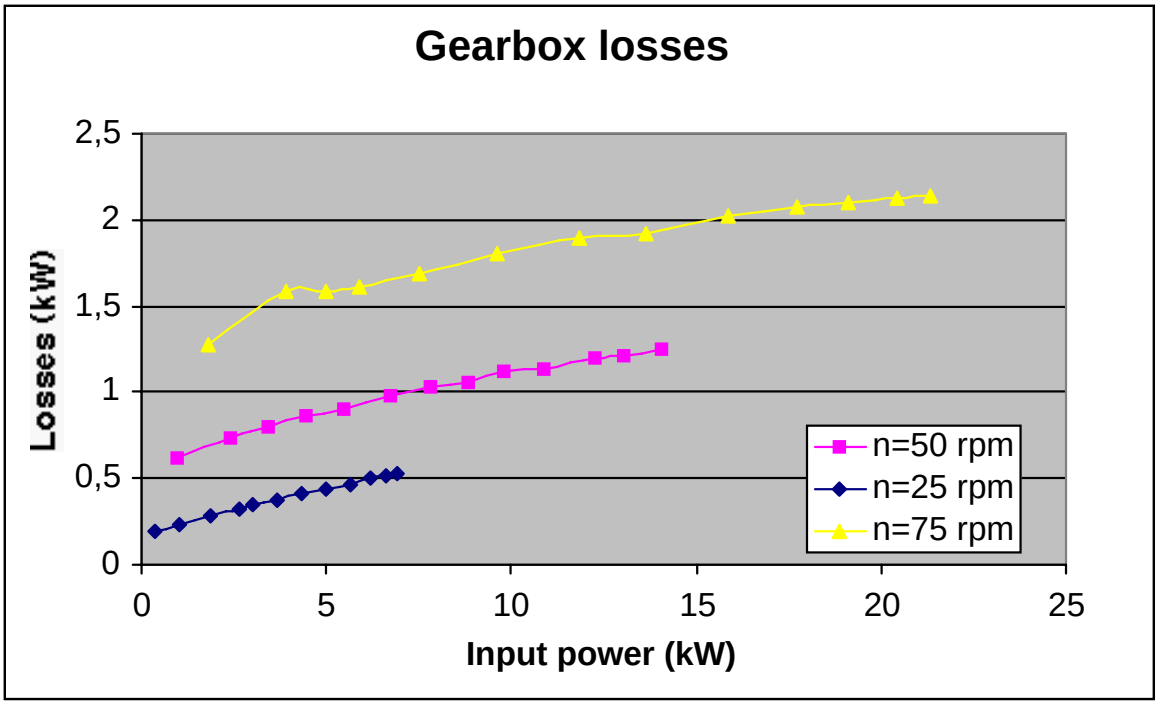

Figure 4.1: Gearbox losses

4.2 Stationary operation

Stationary operation has been performed with no load, resistive load and converter load of the generator with rectifier.

4.2.1 No load operation

Measurements have been carried out on a single coil and on the complete generator. During the measurements on the complete generator the two rectified parts of the generator were connected in series.

The no-load voltage show a characteristic, which is special for this generator type, see Figure 4.2. On synchronous generators the no-load voltage is linear with the speed. Because compensating capacitors are used in this generator, and since the modules have a high inductance, resonance phenomena's occur. The theoretical resonance frequency is slightly higher than the rated frequency and it can be seen that the no-load voltage increase more than linearly with the speed for speeds higher than 60 rpm.

However, also at speeds close to 30 rpm the no-load voltage is much higher than the induced voltage. That resonance phenomenon depends on the rectifier and is excited at one third of the capacitor-inductance resonance frequency. As soon as the generator is loaded the resonance at low speed will disappear.

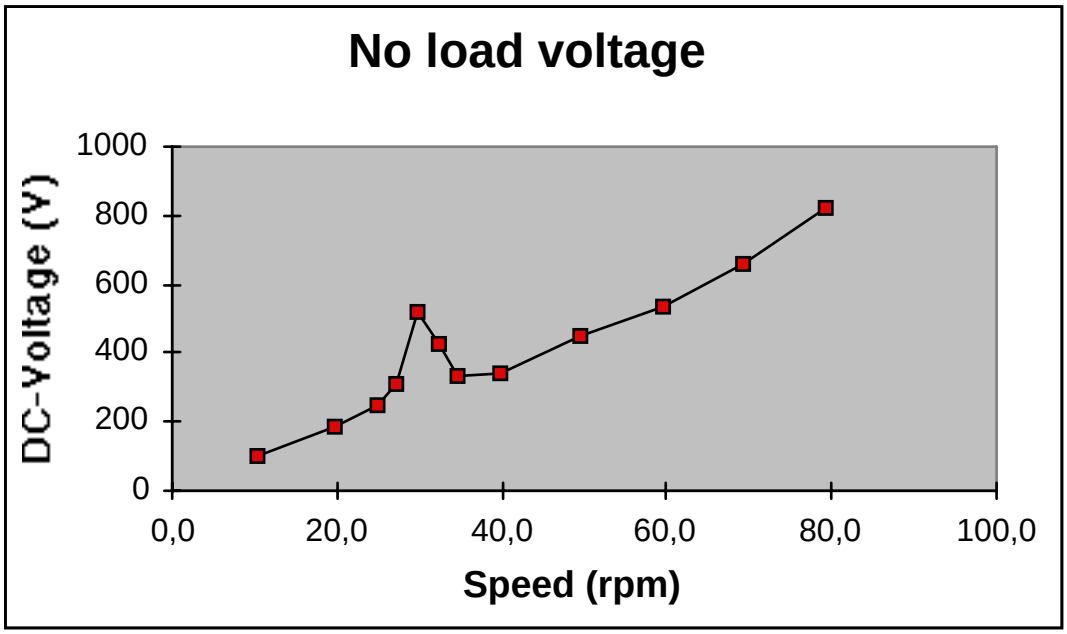

Figure 4.2: No load dc-voltage.

In every individual module of the generator the no load current and voltages have been measured. As can be seen in Figure 4.3 there are some differences between the modules. During the test, the speed of the generator was held constantly at 75 rpm. The voltage, and thereby the current of a single module, depends mainly on the distance to the rotor, the value of the capacitor connected to the module and the speed of the rotor. The difference between the modules is likely to depend on a not perfectly round stator.

The no load power losses of the generator with capacitors were calculated from measurements of the torque and speed on the high-speed shaft of the gearbox. The loss of the gearbox was calculated as described in part 4.1. The loss at rated speed is 2.0 kW as can be seen in Figure 4.4.

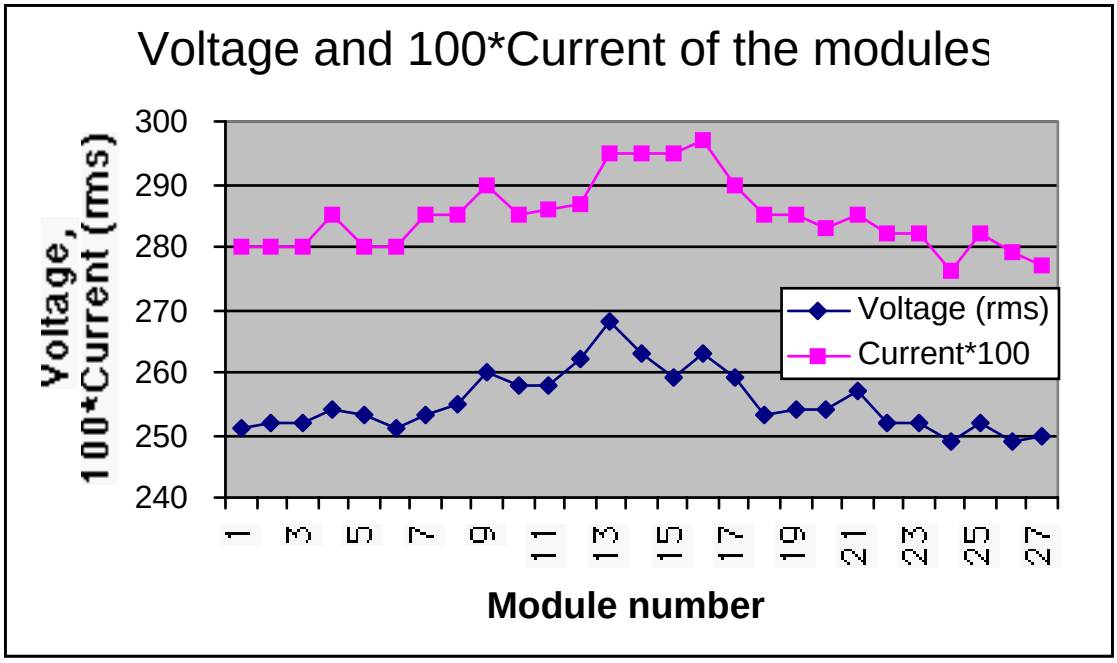

Figure 4.3: No load voltage and current of the modules.

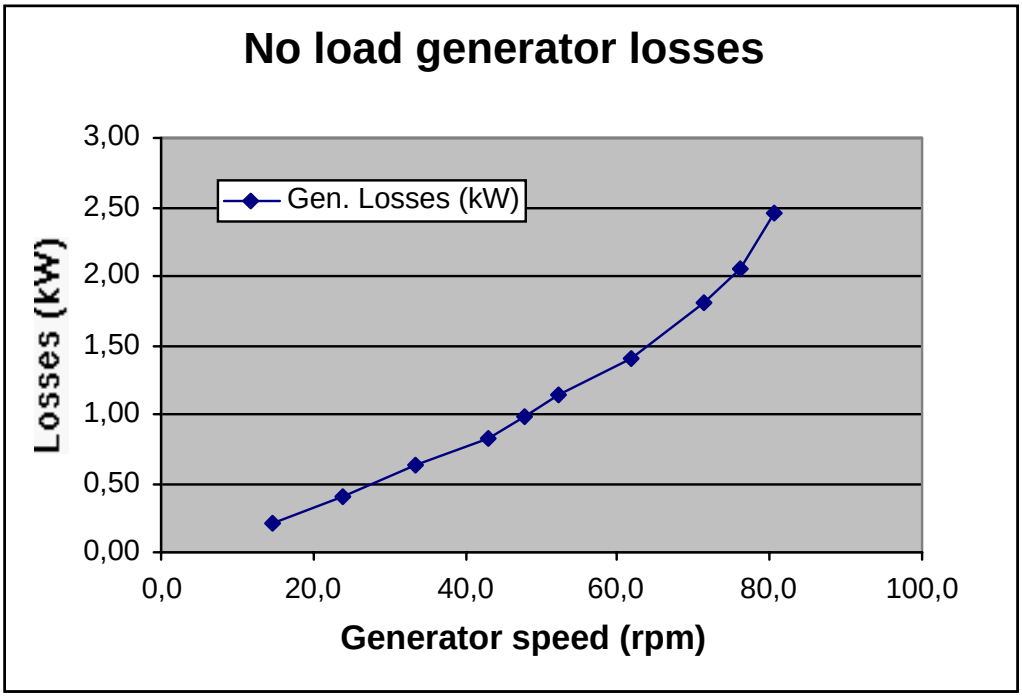

Figure 4.4: The no load losses of the generator with capacitors.

4.2.2 Resistive load operation

The modules in the generator are divided into two groups and are connected in parallel within the group. The current of each module can be seen in Figure 4.5. Since the generator has an odd number of modules the two series connected groups of modules are not equal. One of the groups consists of 13 modules and the other of 14. This lead to an unequal division of the current between the modules. This reduces the efficiency and the peak power of the generator.

To reduce this effect, the two groups of modules will be equipped with one smoothing capacitor each. These capacitors will lead to the same effect as if the number of modules were much higher.

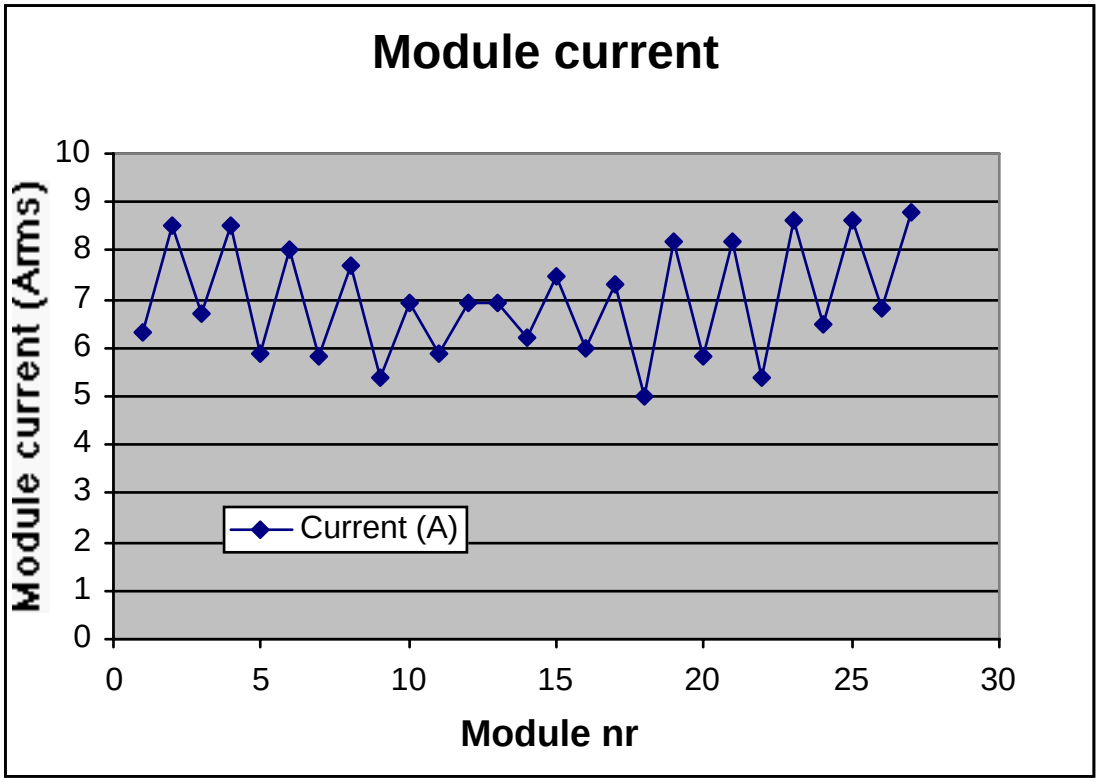

Figure 4.5: Load current of the modules of the generator.

The generator performance with resistive load at the dc-link was measured as shown in Figure 4.6 and Figure 4.7. During these tests 18 modules were connected to the dc-link. The power and torque in the figure are the test results multiplied by a factor of 1.5. The reason to limit the test power was that lack of power from the DC-motor drive.

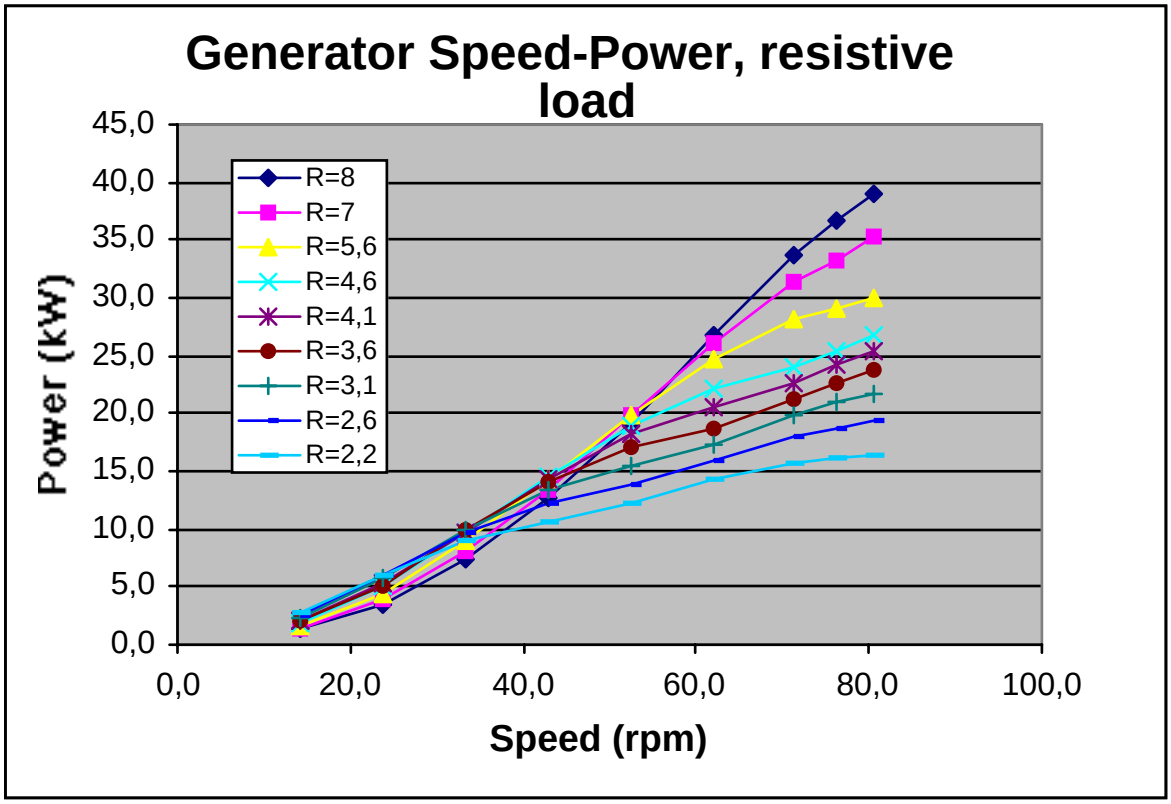

Figure 4.6: Generator power performance with resistive load.

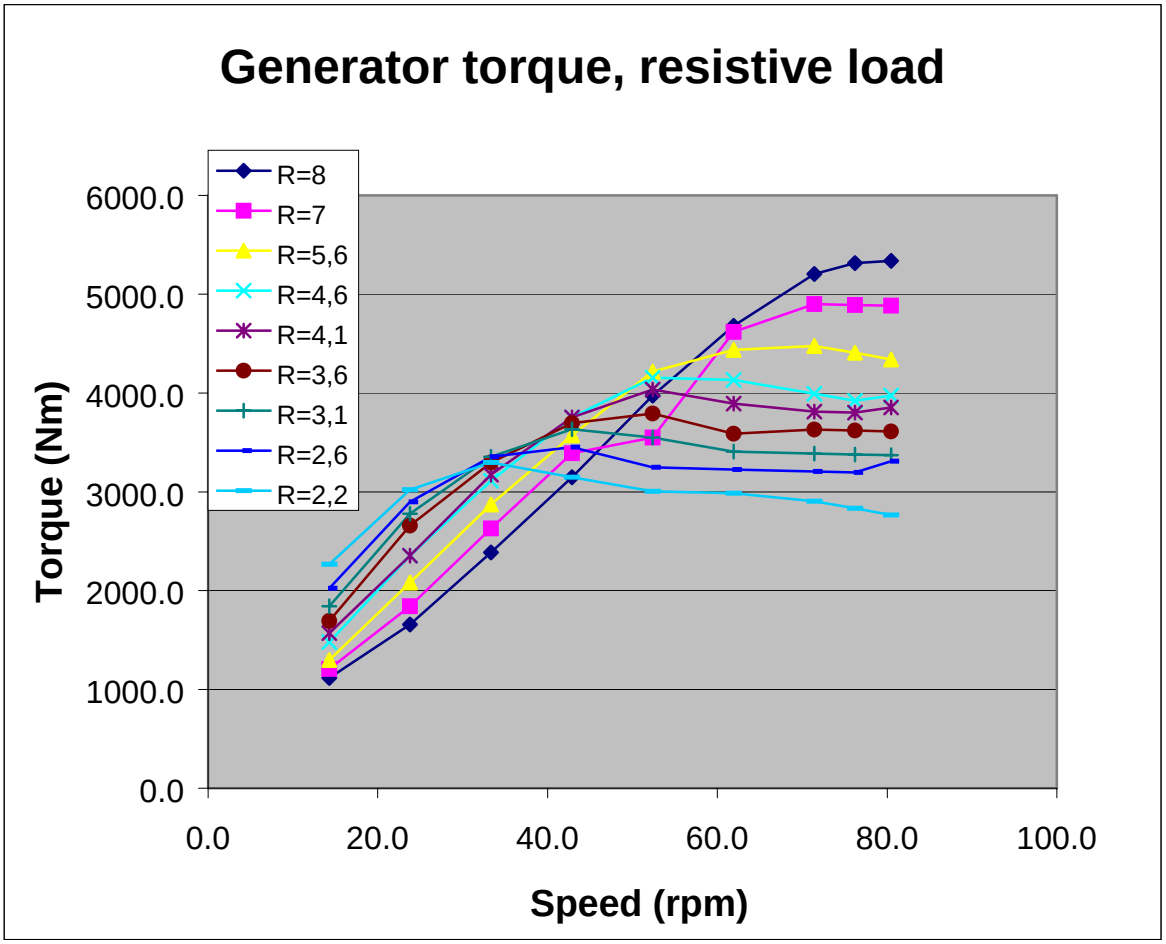

Figure 4.7: Generator torque performance with resistive load.

4.2.3 Converter load operation

The generator with rectifier is connected to a grid-commutated converter in this wind turbine operation. Measurements have been carried out with converter operation. Stationary operation gives the following operation points, see Figure 4.8 and Figure 4.9. The maximum DC-power at rated speed is 32 kW.

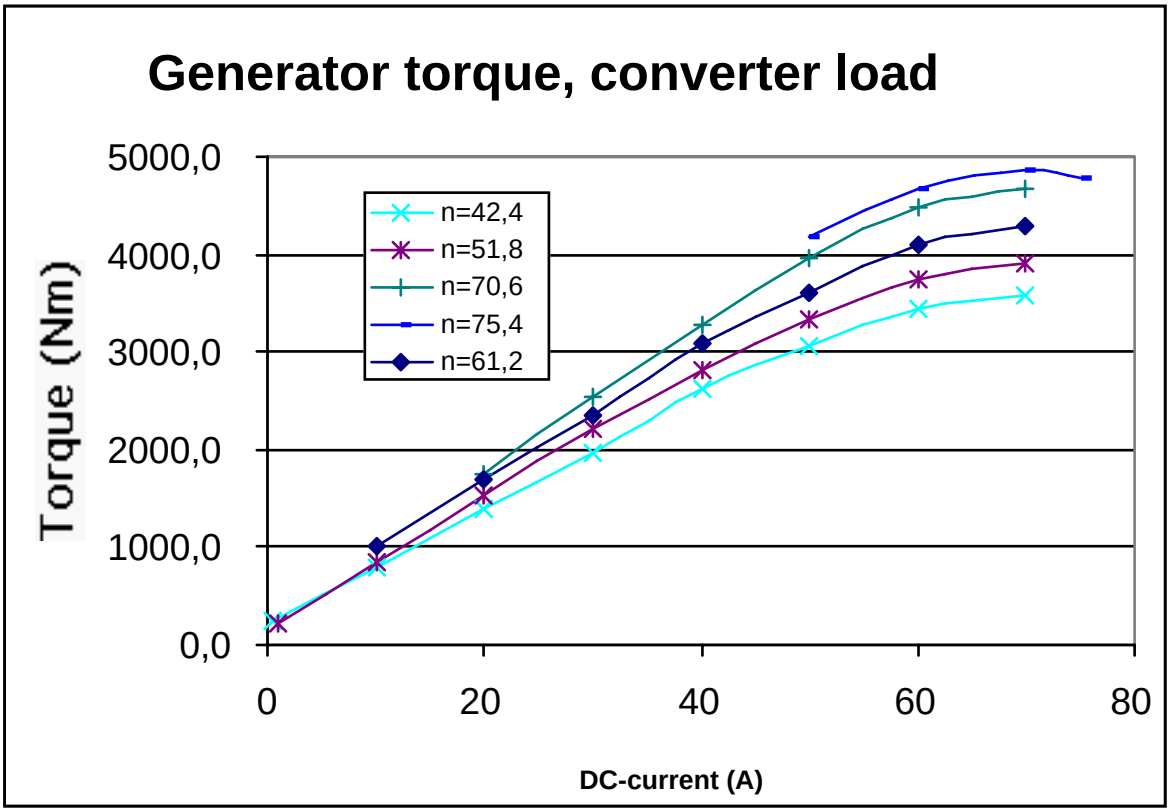

Figure 4.8: Generator torque with converter load.

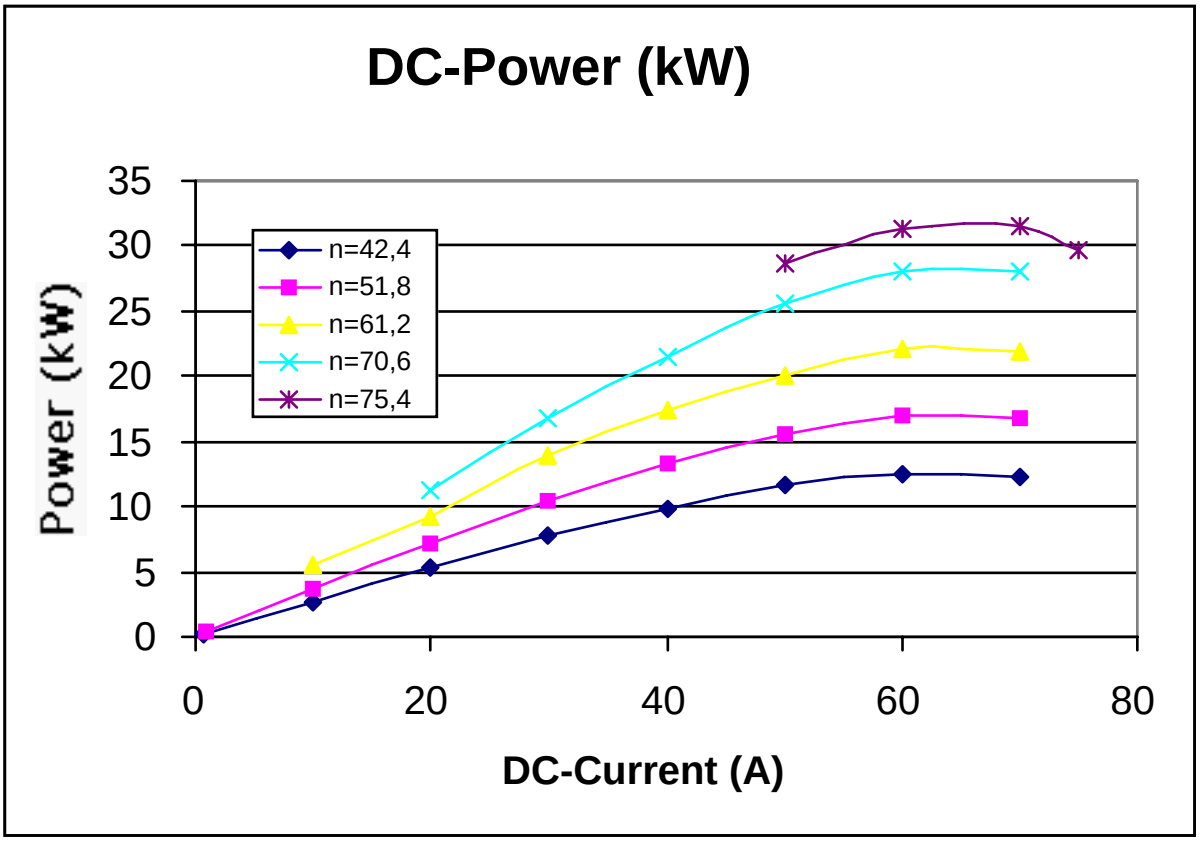

Figure 4.9: Generator dc-power with converter load.

4.2.4 Wind turbine operation

During wind turbine operation it is important that the generator torque always has the possibility to be larger than the aerodynamic torque. Figure 4.10 shows that the maximum aerodynamic torque is always less then the generator torque. The aerodynamic torque will increase with the speed and be larger than the generator torque if a high over speed situation occurs. For a given turbine speed can the maximum torque value just be reached at specific wind speed.

The margin between available turbine torque and generator torque is low at rated speed, 75 rpm. The operation of the wind turbine at high wind speed and rated turbine speed should be done with caution.

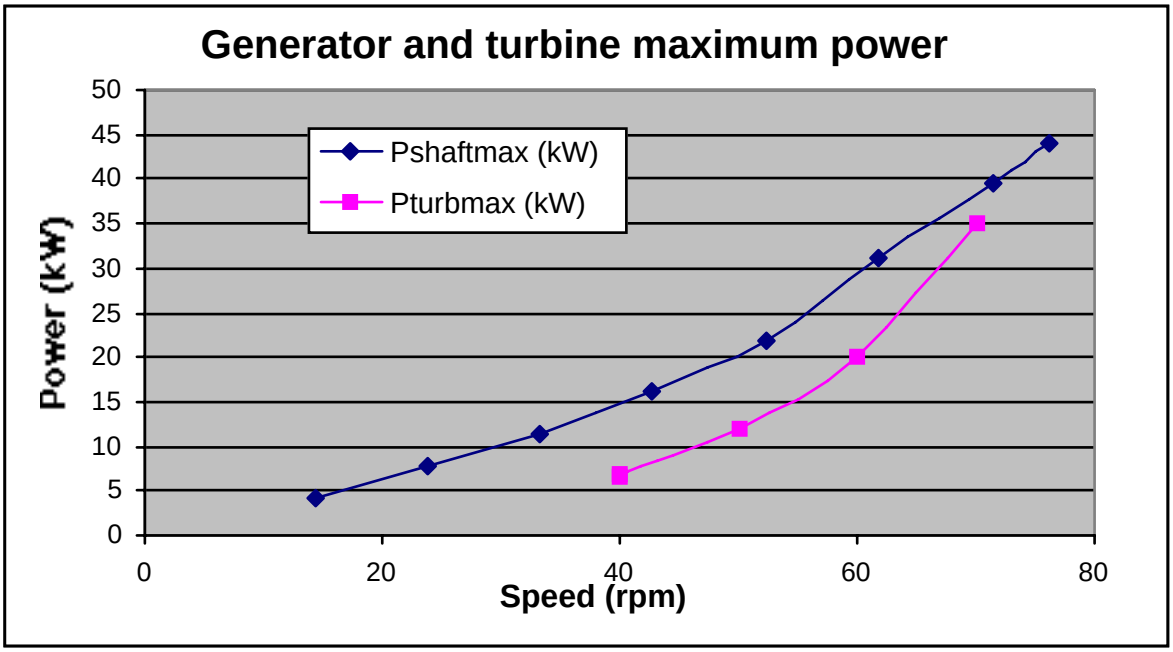

Figure 4.10: Turbine and generator maximum power.

4.2.5 Short circuit operation

The short circuit torque of the generator was measured. During the test the dc-link was short circuit. The torque and current was measured at different speeds. The stationary short circuit torque is 20 % of the rated torque, see Figure 4.11.

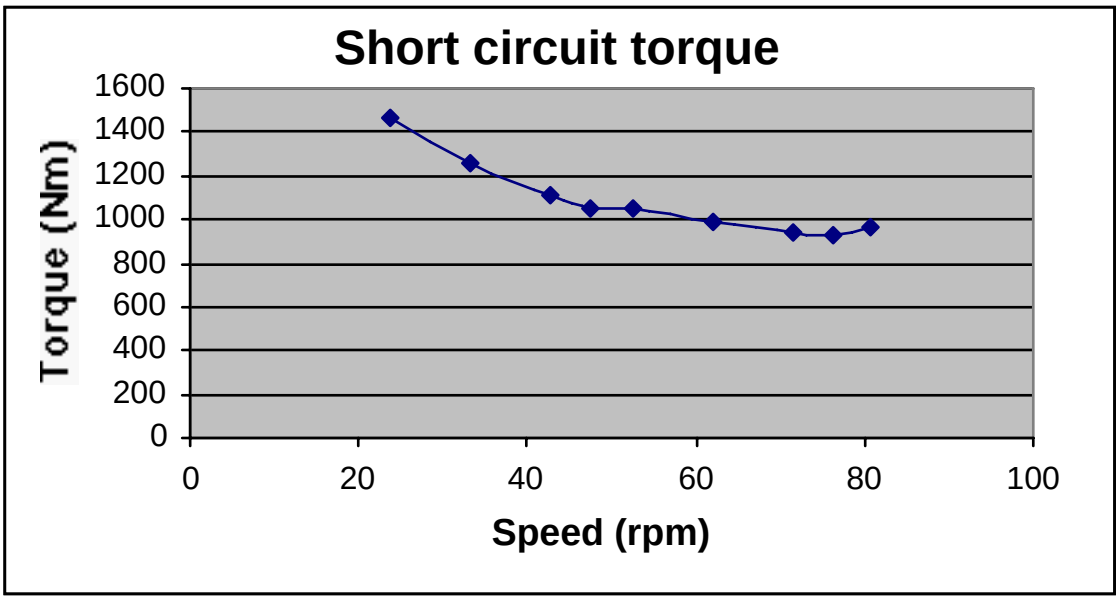

Figure 4.11: Stationary short circuit torque.

5 Time series measurement

A number of time series measurements have been performed to evaluate the performance of the generator. Currents and voltages of individual modules were stored, as well as dc-link voltage and speed of the generator. The sampling rate was 5 kHz and a low-pass filter with 2 kHz bandwidth was connected.

Description of the measurement system are as follow: PC-computer, sample and hold, filter, current probes, voltages measurements with AD210J, speed sensor with 16834 pulses per revolution of the generator.

Both measurements with all modules in parallel and the modules divided in two groups and series connected were performed. The load of the generator was resistive during all time series measurements presented in part 5 of this report.

5.1 Load performance

The voltage and current of module 11 at the speed of 80 rpm and at the power of 20 kW are presented in Figure 5.1 and 5.2. As can be seen, the current in the coil is not sinusoidal and the voltage is limited due to the diodes and the dc-link voltages. During this measurements all modules were in parallel operation.

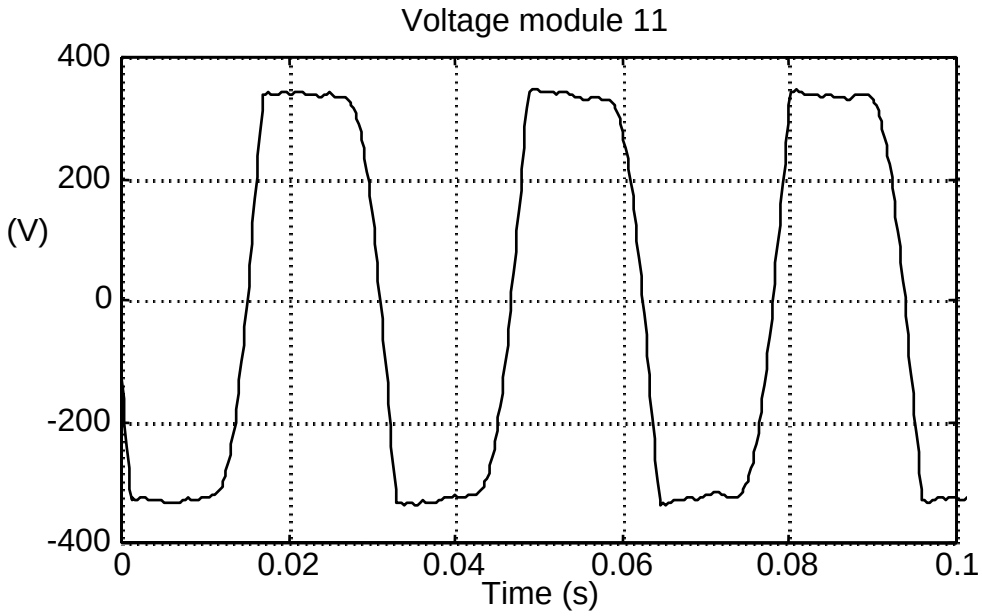

Figure 5.1: Voltage of module 11.

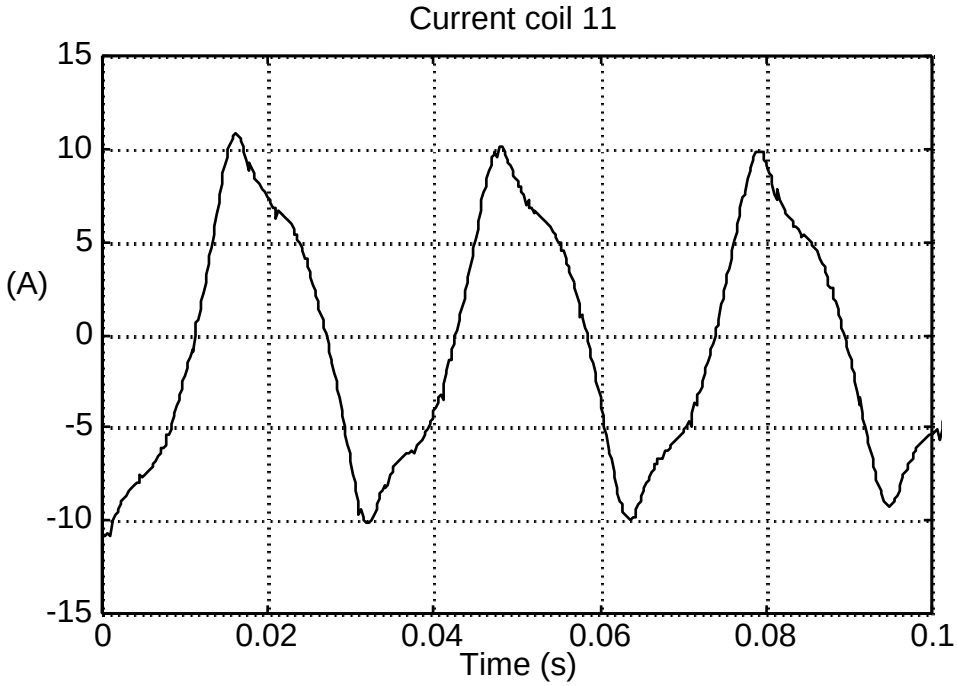

Figure 5.2: Current of module 11.

The generator can be connected in two different ways, with all modules in parallel or the modules divided in two groups and series connected. With all modules in parallel the dc-link voltage and current will be more smoothed out, but for the operation of the generator there is no problem with some ripple on the dc-link. The output voltage will be twice as high in series connection compared with parallel connection. The opposite will occur for the current. For comparison see Figure 5.3 for parallel connection with the power of 12.4 kW and speed of 70 rpm and Figure 5.4 for series connection with the power of 18.6 kW and speed of 71 rpm.

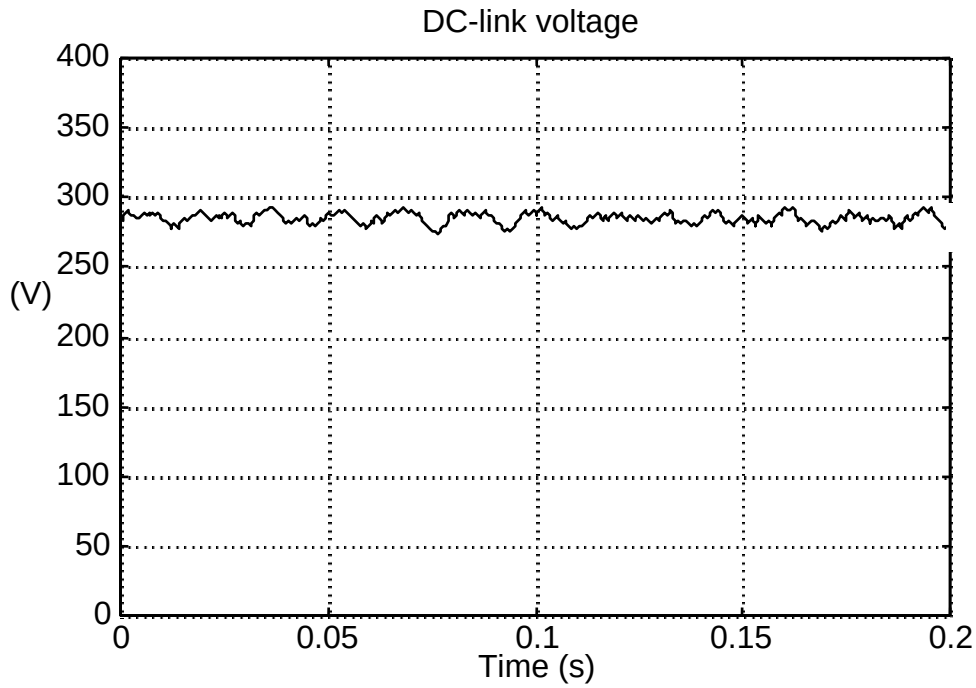

Figure 5.3: DC-link voltage, all modules in parallel.

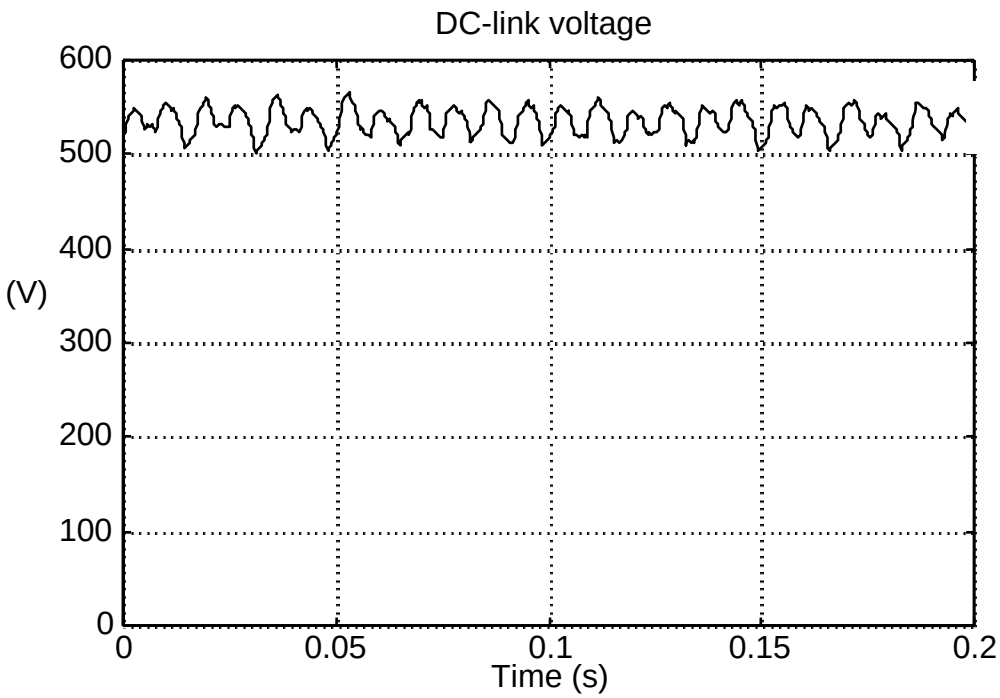

Figure 5.4: DC-link voltage, modules in two groups in series.

One interesting question about this generator is, how much will the modules influence each other with respect to the voltage. To find this out, measurements were carried out in the following way; Module #1was short circuited and the voltage of #2 and #13 were measured. In Figure 5.5 and in Figure 5.6 the voltages are shown.

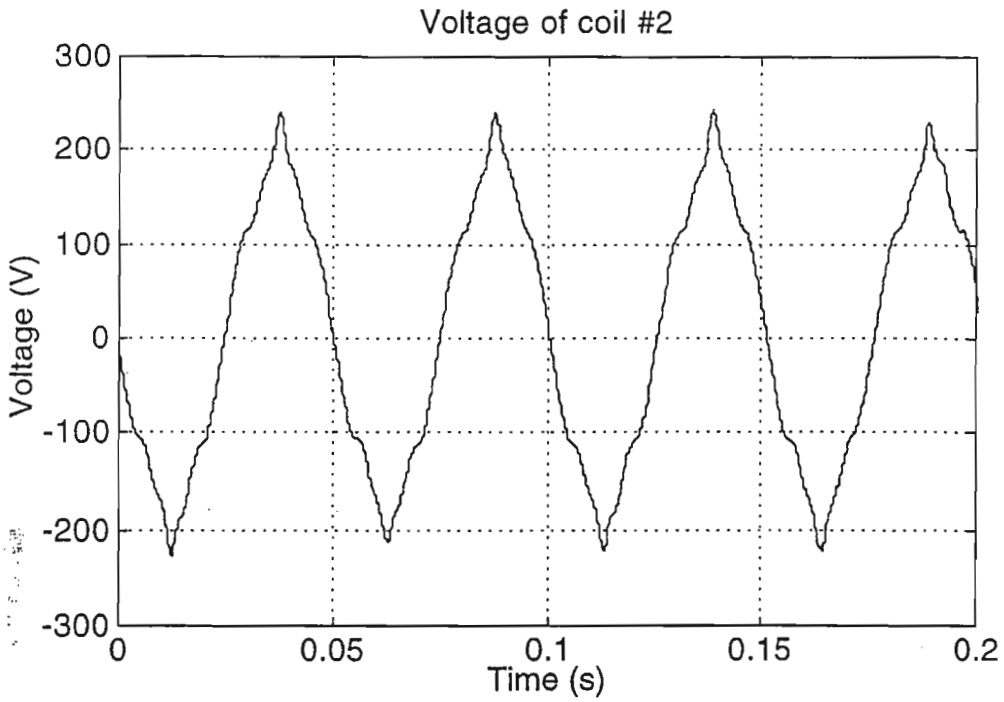

Figure 5.5: Voltage of module #2.

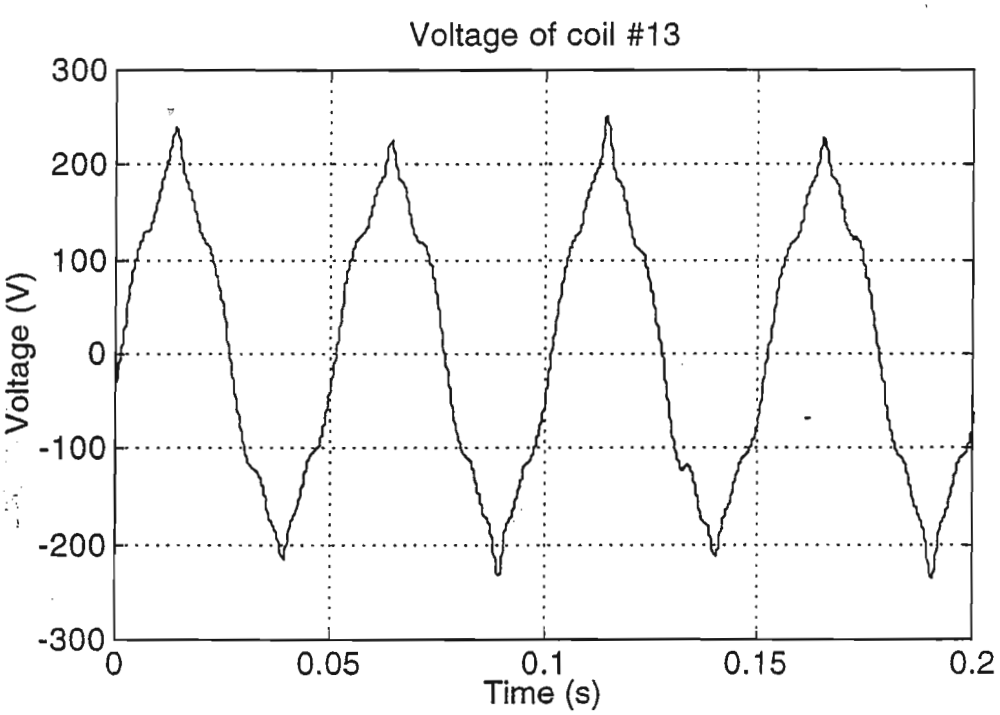

Figure 5.6: Voltage of module #13.

As can be seen, no significant difference occur between the two measured voltages, and it is possible to conclude that the coils are operating independently of each other. During these tests no capacitors or rectifiers were connected to the modules. Module #2 is placed next to module #1 and module #13 is placed as far away as possible from module #1.

1 Laboratory documentation

The redesign of the nacelle and the connection boards for both power connection and measurements has been far more extensive than the original plans. On the other hand the results are very good. The generator has a stable operation and the measurements signals have few disturbances. In parallel to this project the computer system has also been redesigned. Today a PC-based control computer is installed and the control program is written in the C++ language. The Figure 6.1 to 6.5 shows the generator, wind turbine simulator and electrical hard ware such as rectifier, electrical brake and converter.

Figure 6.1: PM-generator and wind turbine nacelle.

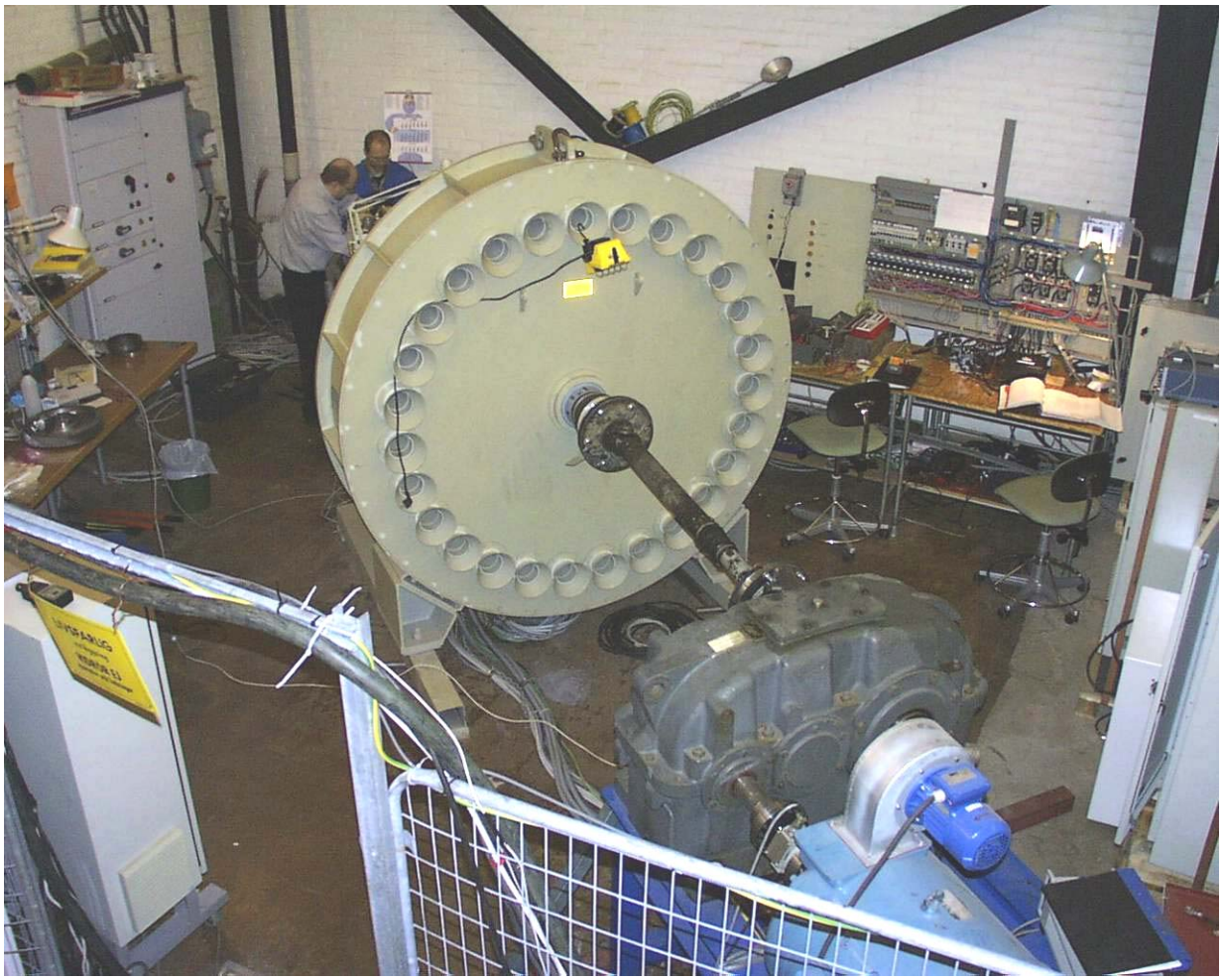

Figure 6.2: Laboratory set-up with PM-generator, gearbox and DC-motor.

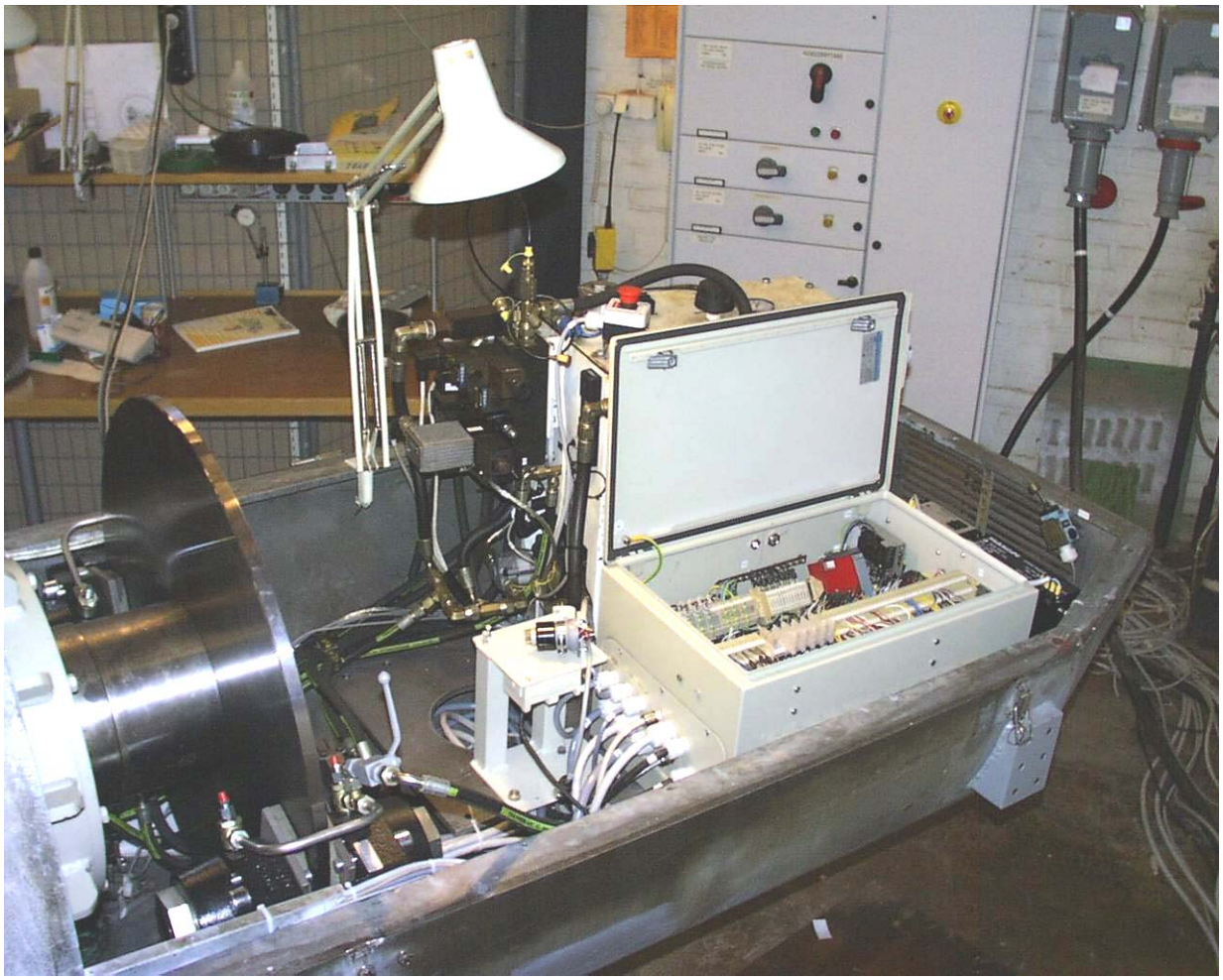

Figure 6.3: Close look in the wind turbine nacelle, on the left side, the mechanical brake and on the right side, the connections box for the sensors in the nacelle.

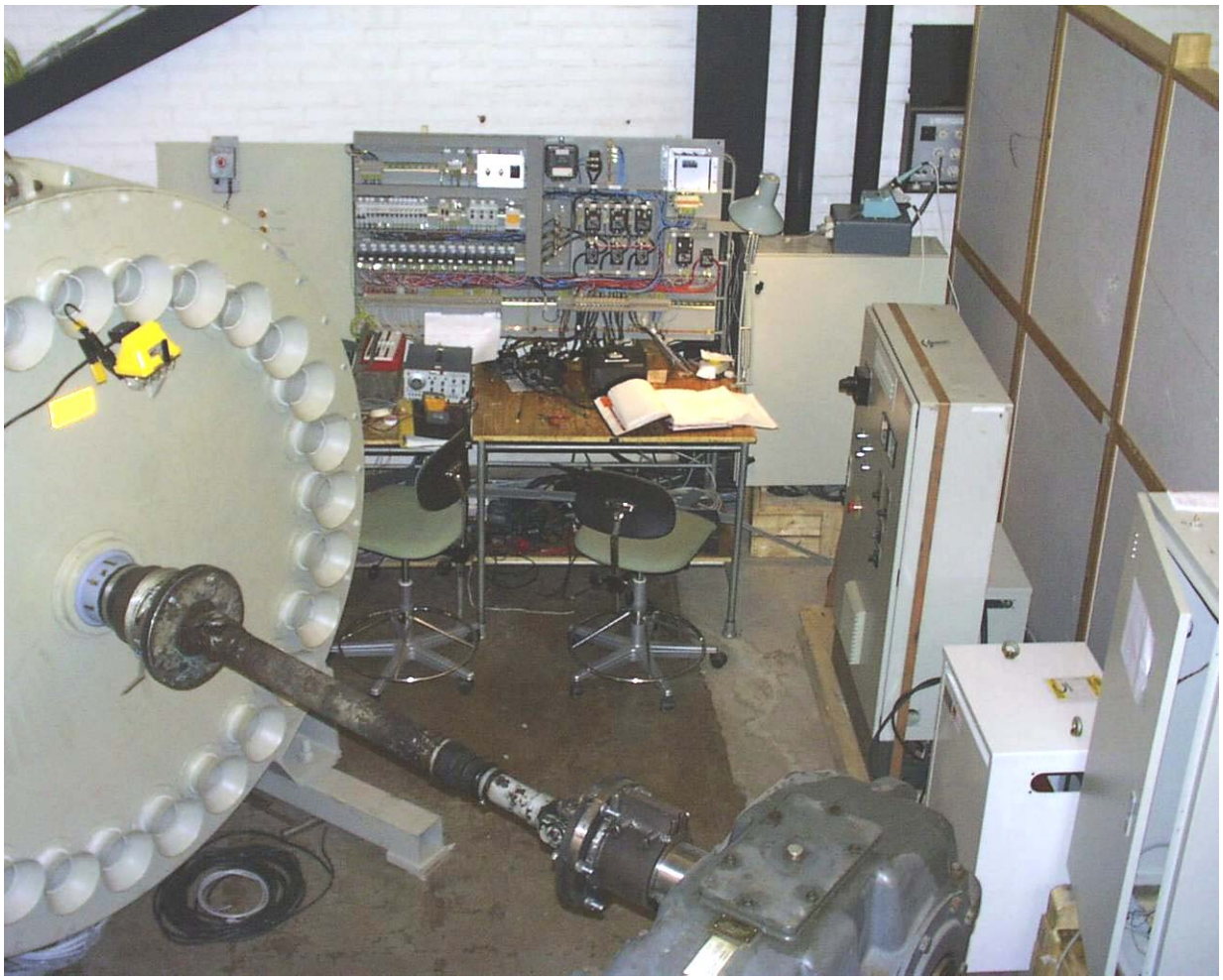

Figure 6.4: The generator with the main shaft. On the right side are the electrical brake, DC-choke, transformer, DC/AC-converter and rectifier. The connection board is seen in the middle of the picture.

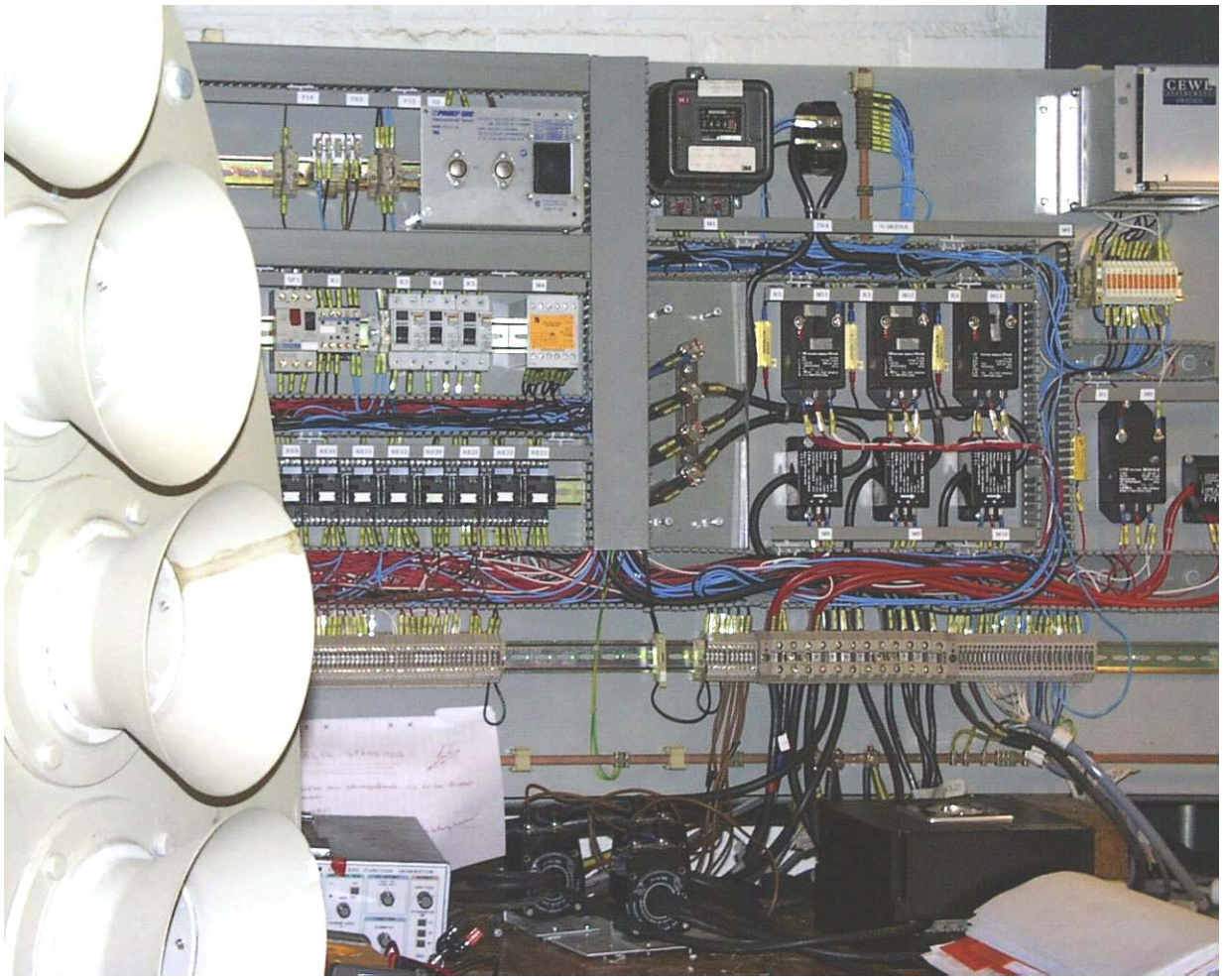

Figure 6.5: The connection board for the power with current and voltage transducers.

2 Conclusions

The laboratory tests of the generator show that it works acceptably. The results show a lower peak power than expected.

The important and extensive work with redesigning and adapting the test wind turbine for the direct driven generator is almost finished. Only tests of the control systems in the laboratory remain before the turbine will be erected on the Hönö site.

3 Reference

[1] Williamson A. C., "Directly Driven Wind Turbine Generator, Final Report". England, Manchester, UMIST, 3 February 1998.

[2] Högberg E., Lundmark P., "Design and Test of an Electrical System for a Direct-Driven Permanent-Magnet Generator for a Wind Turbine". Sweden, Göteborg, Chalmers University of Technology, Department of Electric Power Engineering, Report No. 16E, October 1997.

Appendix F

Carlson, O., Grauers, A., Williamson, A., Engström S., Spooner, E., "Design and Test of a 40 kW Directly Driven Permanent-Magnet Generator with a Frequency Converter" *European Wind Energy Conference and Exhibition* (EWEC ´99), Nice, France, March 1-5, 1999.

DESIGN AND TEST OF A 40 kW DIRECTLY DRIVEN PERMANENT-MAGNET GENERATOR WITH A FREQUENCY CONVERTER

O. Carlson[1], A. Grauers[1], A. Williamson[2], S. Engström[3], E. Spooner[4]

1. Department of Electric Power Engineering
Chalmers University of Technology
S-412 96 Göteborg, Sweden
Phone: +46-31 772 16 37
E-mail: ola.carlson@elkraft.chalmers.se
E-mail: anders.grauers@elkraft.chalmers.se

2. Department of Electrical Engineering and Electronics
UMIST, PO Box 88, Sackville St.
Manchester M60 1QD, United Kingdom
Phone: +44-161 200 4735
E-mail: ACW@fs5.ee.umist.ac.uk

3. Nordic Windpower AB, Box 968,
191 29 Sollentuna, Sweden
Phone: +46-8 767 75 88
E-mail: agir@algonet.se

4. School of Engineering, University of Durham
South road, Durham DH1 3LE, United Kingdom
Phone: +44-191 374 3920
E-mail: edward.spooner@durham.ac.uk

ABSTRACT: This paper presents the design and test evaluation of a 40 kW, directly driven, permanent-magnet generator with a frequency converter. The electrical system is designed for a turbine with a diameter of 12 m and stall regulation. The generator design is characterised by modular rotor and stator elements that may be produced in quantity without any large-scale facilities. The magnets are of the ferrite type furnished with laminated iron flux concentrators. The stator elements consist of an E-core lamination with a single coil. The main shaft and bearings are integrated into the generator design. The converter system consists of diode rectifiers and a thyristor inverter. Although this paper is concerned with a 40 kW pilot scale test unit, a detailed design study for a 500 kW machine has been carried out and the construction is such as to lend itself to designs for much higher outputs.
Laboratory tests of the generator with a frequency converter are being carried out. These tests cover the whole speed and power range. The tests focus on the power-speed performance, stability of the system and efficiency measurements.
Keywords: Converters, Electricity Generators, Variable-Speed Operation

1. INTRODUCTION

The development of permanent-magnetic material and the reduction of costs of the power electronic components have opened the possibility of designing cost-effective wind turbines with a directly driven generator. However, the directly driven generator needs damping, either with mechanical springs and dampers or preferably with an electrical damping, i.e. variable speed operation. With directly driven generators, which are optimised for low speed operation, the performance (efficiency, reliability) of the systems can be improved whilst the cost can be reduced. The design of the drive train is also greatly simplified compared with a conventional drive train with gears and a high-speed generator.

This paper presents the design and test evaluation of a 40 kW, directly driven, permanent-magnet generator with a frequency converter. The electrical system is designed for a turbine with a diameter of 12 m and stall regulation. Although this paper is concerned with a 40 kW pilot scale test unit, a detailed design study for a 500 kW machine has been carried out and the principle is such as to lend itself to designs for much higher outputs.

Laboratory tests of the generator with a frequency converter are being carried out.

On the basis of several years of design experiences, the design of the generator has been evaluated and its performance has been compared with the theoretical predictions. The evaluation has particularly been concerned with parameter values, losses and peak power.

The work has been carried out within the Joule Project No JOU2 CT 93-0297.

3. THE ELECTRICAL SYSTEM

The electrical system is characterised by the variable speed operation of the low speed permanent-magnet generator and the converter. The system also includes an electrical brake and a DC-current breaker, see Figure 1.

3.1 The Generator

The generator design is characterised by a modular arrangement whereby modules of a set size, for both the permanent-magnet rotor and the stator, may be assembled to produce a machine of any required rating within a wide range. At the higher ratings, for example 1MW, the slow speed of rotation associated with a direct-couple generator requires that the diameter be very large - perhaps of the order of 4m - yet the modules required to produce such an assembly can be manufactured with quite modest facilities. The modular philosophy and initial small (1kW) proving tests are described in [1]. The modules for the machine of this paper are of a more modern and commercial design, yet still employ ferrite magnets in the rotor modules and a simple concentric coil, in a basic 'E-core' stamping for the stator.

The machine tested has 48 rotor modules, arranged to give 24 pole-pairs with a rotor diameter of 1.287 m. The stator is comprised of 27 modules placed in a ring to give an air gap of 3.25 mm. This relatively small number of modules results in a curvature which is about the minimum possible for the module design. To set the rating to about 40 kW, to match the existing turbine, the active length of the modules was set to 0.1 m. The length is only 2/3 the pitch of the stator modules, and this has resulted in

end effects assuming much more significance than they would in a machine using modules of greater length (which is easily achieved) for higher powers and so, in this respect, the machine is atypical.

Mechanically, the generator was designed to include all bearings necessary to carry the turbine, mounted upwind on the shaft. This resulted in an overall diameter of 2.11m, and length (not including the front bearing) of 0.712m with a total mass of 4500 kg.

Each stator coil was designed to give an open-circuit voltage of 211V rms at the nominal speed of 75 rev/min. The relatively high inductance of each coil requires that it be tuned with a capacitor, placed across the terminals of individual rectifier bridges, connected in parallel, so as to achieve full potential output into a DC-link, over the working range of speed. Post-production problems with respect to current capabilities of available equipment forming the power conditioning and connection to the grid required that the modules be arranged into two groups, connected in parallel within each group, and then the two groups connected in series to form the DC-link. This is not the ideal mode of connection for the number of modules existing, but it is believed that it will not have a serious effect upon performance.

3.2 The Frequency Converter and Electrical Brake

The DC-bus interfaces a thyristor based DC/AC-converter via one smoothing inductor. The DC/AC-converter is connected to the grid through a transformer, which makes it possible to operate the converter on a 500 V level.

In case of a control system failure or loss of grid, two independent brake systems are implemented for braking the turbine shaft, even in the case of an internal system signal failure.

The brake function is obtained without access to the grid. The braking systems are realised as one mechanical and one electrical system [2]. The electrical brake system acts directly on the DC-bus output.

In order to control the braking torque several methods can be used. Three different methods of electrical braking of a variable speed wind energy converter can be used. The simplest solution is to connect a resistor to the frequency converter DC-link. When activating the brake, the resistor is connected to the DC-link resulting in a braking current proportional to generator voltage and, hence, the turbine speed. This implies an optimal braking torque only within a small speed range. Using a higher value of the resistance makes the brake more efficient at higher speeds and vice versa.

To increase the speed range, in which the resistor brake is efficient, two or more resistors can be used. The switches connected to the resistors are then to be switched in order to decrease the total resistance as the turbine speed decreases.

The brake for this system is based on the third method, where the brake current is held at a constant level independent of the generator voltage. This is achieved by switching the resistor on and off and will result in maximum torque control.

In Figure 1, the main circuit of the DC-link is shown. The transistors T1, T2 and T3 are insulated gate bipolar transistors (IGBT). Directly after the diode rectifier, electrolyte capacitors are connected in order to stabilise the DC-voltage. Without capacitors the voltage will rise uncontrolled when opening the breaker, due to the high inductance in the armature windings of the generator.

Besides the components shown in Figure 1, the circuit is equipped with protection devices against over-voltages, which could damage the transistors.

A schematic drawing of the electrical brake is shown in the middle part of Figure 1. The idea is to keep the braking current from the generator at an almost constant value by switching T2 on and off. When the brake is activated, T1 is switched on and kept in the conducting state throughout the braking procedure.

In the DC-link, between the brake and the smoothing inductance, a DC-breaker is placed.

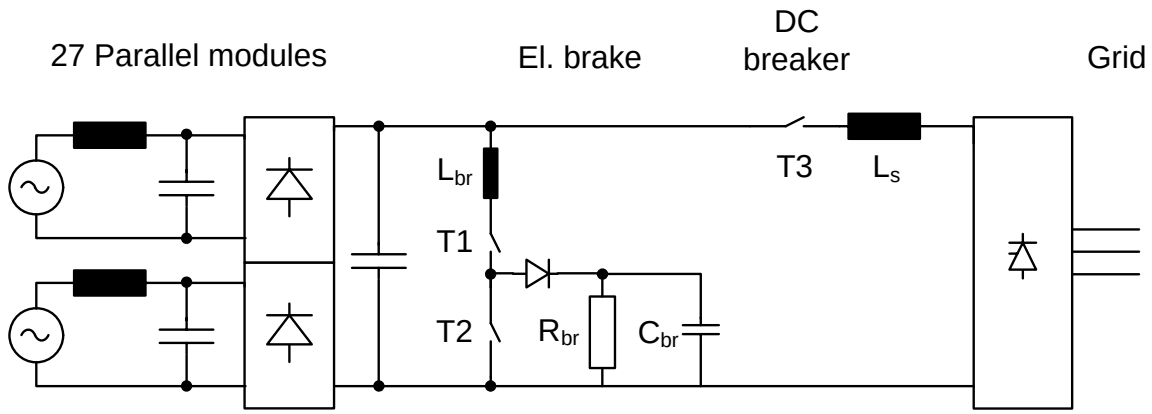

Figure 1: Electrical system with generator, rectifier, brake, DC-breaker and inverter.

The breaker consists of a transistor, T3, which can break DC currents up to 200 A. When the electrical brake is activated this breaker will, at the same time, break the current through the thyristor inverter. The transistor is turned on again when the control computer of the wind energy converter sends a reset signal to the control system of the brake.

In some cases of grid failure, the grid will act as a short-circuit to the inverter. This results in a large current through the inverter and in a blown fuse. This fuse must be replaced manually. The breaker will, however, open the DC-link at a grid loss, thereby reducing the need for service.

4. PERFORMANCE

Laboratory tests of the generator with a frequency converter are being carried out. These tests cover the whole speed and power range. The tests focus on the following aspects:

1. system parameter identification
2. power-speed performance of the directly driven generator with converter
3. efficiency measurements
4. stability of the system

The laboratory system and tests of the generator are reported in more detail in [3].

4.1 Laboratory Set-up

During the laboratory tests a 40 kW DC-machine drives the generator. The nominal speed of the DC-machine is 1500 rpm and, therefore, a gearbox of the ratio 21:1 is mounted between the generator and the DC-machine. The generator shaft speed and torque are measured, and, thereby the input power. In addition, the generator armature voltage, current and active power are measured with a DC power meter.

4.2 Results of Measurements

The resistance of each coil was measured and all were very close to 0.97 Ω at 19 deg. C. The inductance of each coil was determined to be 119 mH. This is close to the value of 112 mH estimated from 3-D field plots at the design stage. The inductance value is important, as indicated in Section 3.1, because it gives high internal impedance which retricts the maximum power output, unless it is tuned by capacitance. It is obviously desirable to be able to estimate the inductance value with reasonable accuracy at the design stage. The same is true for the induced, open-circuit voltage of the coils, and the value of 203 V rms measured at 75 rev/min is close to the value of 211 V rms predicted at the design stage.

Figure 3 shows the DC -power as a function of the DC-current at five rotational speeds. The power increases almost linearly with increasing current as the DC-current increases from 0 to about 60 A. At high currents the voltage drop becomes so high, due to the armature impedance that the power decreases. This drop limits the power. At 75 rpm the power maximum is 32 kW at a DC-current of 65 A, for the generator prototype.

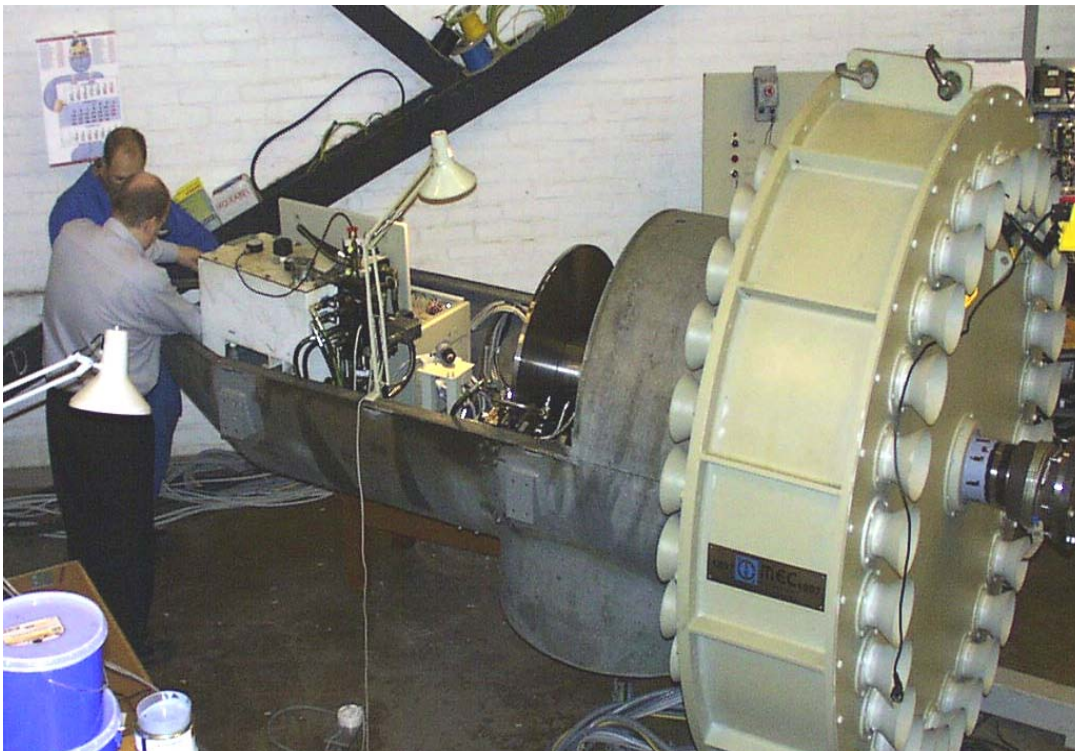

Figure 2: The generator (right) mounted on the wind turbine nacelle for laboratory tests.

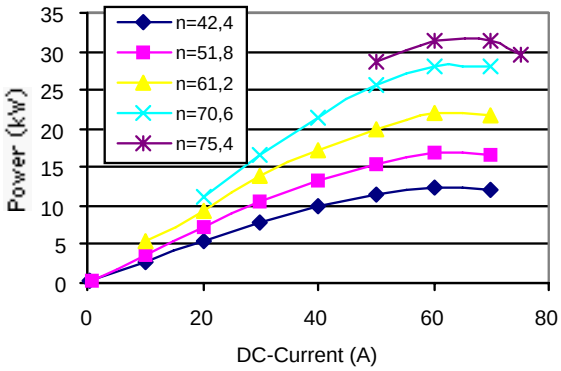

Figure 3: DC-power as a function of DC-current at different speeds.

The torque of the generator is shown in Figure 4. As can be seen, the maximum torque at different speeds is reached at the same current, approximately 70 A.

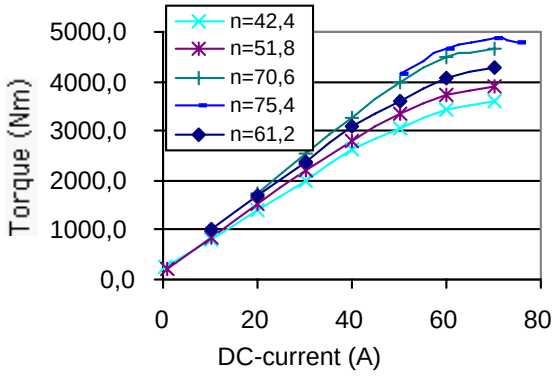

Figure 4: Generator shaft torque as a function of DC-current at different speeds.

The efficiency of the generator with diode rectifiers is approximately 85% at maximum power, and, what is more important, close to 90% at partial load. Moreover, the efficiency is high at low power since the generator then operates at a low speed see Figure 5.

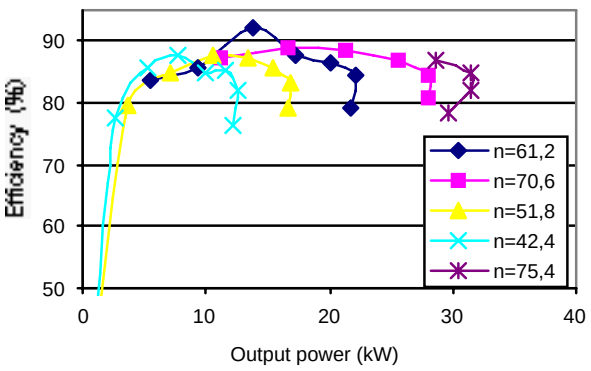

Figure 5: Efficiency of the generator operated with diode rectifiers at selected rotational speeds.

The step response of the DC-current shows a fast and stable operation of the generator and converter system. Thereby, the torque control of the wind turbine will also be good, see Figure 6.

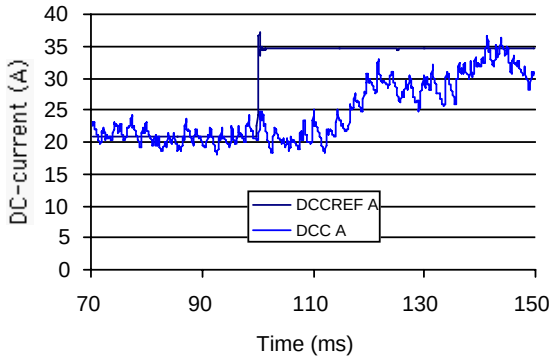

Figure 6: Step response of the DC-current.

7. CONCLUSIONS

The results of the measurements and the theoretical evaluation reveal good system performance and efficiency. The peak power performance at rated speed is within the operational envelope of the wind turbine.

The project also demonstrates that a wind turbine system with a directly driven permanent-magnet, low-speed generator and a frequency converter is well suited for up-scaling today's commercial sized wind turbines.

8. ACKNOWLEDGEMENTS

The financial support given by the EC is gratefully acknowledged. The authors would also like to thank Magnus Ellsén, Per Lundberg, Ulrik Johansson, Conny Larsson and Bo Lagerkvist for their valuable laboratory work.

9. REFERENCES

[1] Spooner E, Williamson A.C. and Catto G. "Modular Design of Permanent-Magnet Generators for Wind Turbines", IEE Proc. EPA, Vol 143, No.5, Sept 1996, pp 388-395.

[2] Högberg E. and Lundmark P. "Design and Test of an Electrical System for a Direct-Driven Permanent-Magnet Generator for a Wind Turbine". Chalmers University of Technology, M.Sc. Thesis No. 16E, Göteborg, Sweden, October 1997.

[3] Carlson O. "Laboratory Measurements of a 40 kW Permanent Magnet Generator", Chalmers University of Technology, Department of Electric Power Engineering, Göteborg, Sweden, March 1999.

Appendix G

Ola Carlson, Magnus Ellsén, “Control and Operation experience of a 40 kW Directly Driven Permanent Magnet Wind Turbine Generator with a Frequency Converter”, Department of Electrical Power Engineering, Chalmers University of Technology, Sweden. *Presented at 2001 European Wind Energy Conference (EWEC 2001), Copenhagen, Denmark, 2-6 July 2001*.

CONTROL AND OPERATION EXPERIENCE OF A 40 KW DIRECTLY DRIVEN PERMANENT MAGNET WIND TURBINE GENERATOR WITH A FREQUENCY CONVERTER

Ola Carlson and Magnus Ellsén
Department of Electrical Power Engineering
Chalmers University of Technology
S-412 96 Göteborg, Sweden
Phone: +46 31-772 16 37, +46 31-772 8517, Fax: +46 31-772 16 33
E-mail: ola.carlson@elteknik.chalmers.se magnus.ellsen@elteknik.chalmers.se

ABSTRACT: The development of permanent-magnet materials and the decrease in costs for power electronics have made it possible to design a cost-effective wind turbine with a direct driven generator. Overall efficiency and reliability can be improved and costs can be reduced compared with a standard generator and a gearbox. The absence of a gearbox also leads to a less complex assembly.

The purpose of this work is to present the experience of the operation of a 40 kW direct driven permanent magnet wind turbine generator with a frequency converter. The generator together with the electrical system is in operation at the Chalmers test wind turbine. The maximum allowable speed of the turbine is regulated by a PID-controller, which makes it possible to tune the stall speed. The objective has been to tune up the stall speed in order to reach maximum power without loosing control over turbine speed. The rated stall speed is found when the torque peaks from the wind turbine are close to, but not greater than the maximum generator torque. The conclusion from the operation of this new type of generator is that it works properly, but there is a need to match the control very closely with the design to optimise the use of the generator.

Keywords: Control, Converters, Generators, Stall, Variable speed operation

1. INTRODUCTION

The development of permanent magnet materials and decreasing costs for power electronics have made it possible to design a cost-effective wind turbine with a direct driven generator. Overall efficiency and reliability can be improved and cost can be reduced compared with a standard generator and a gearbox. The lack of a gearbox also leads to a less complex assembly.

This paper presents the design and test evaluation of a 40 kW, direct driven, permanent-magnet generator with a frequency converter. The electrical system is designed for a turbine with a diameter of 13.5 m and stall regulation. Although this paper is concerned with a 40 kW pilot scale test unit, a detailed design study for a 500 kW machine has been carried out and the principle is such as to lend itself to designs for much higher outputs.

Laboratory tests and wind turbine operation of the generator with a frequency converter are being carried out. The turbine is stall regulated and operates with variable speed.

Previous parts of this work has is being carried within the Joule Project No JOU2 CT 93-0297.

2. THE ELECTRICAL SYSTEM

The electrical system is characterised by the variable speed operation of a low speed permanent magnet generator and converter. The system also includes an electrical brake and a DC-current breaker, see Figure 1. The components have been chosen to achieve good operation characteristics with special emphasis on high efficiency in the electrical system. The main parts, which achieve low losses, are the permanent magnets, the diode rectifier and the thyristor inverter.

2.1 The Generator

The generator design is characterised by a modular arrangement whereby modules of a set size, for both the permanent-magnet rotor and the stator, may be assembled to produce a machine of any required rating within a wide range. At higher ratings, for example 1 MW, the slow speed of rotation associated with a direct-couple generator requires a very large diameter - perhaps of the order of 4m - yet the modules required to produce such an assembly can be manufactured with quite modest facilities. The modular philosophy and initial small (1 kW) proving tests are described in [1]. The modules for the machine of this paper are of a more modern and commercial design, yet still employ ferrite magnets in the rotor modules and a simple concentric coil, in a basic 'E-core' stamping, for the stator.

The machine tested has 48 rotor modules, arranged to give 24 pole-pairs with a rotor diameter of 1.287 m. The stator is comprised of 27 modules placed in a ring to give an air gap of 3.25 mm. This relatively small number of modules results in a curvature, which is about the minimum possible for the module design. To set the rating to about 40 kW, to match the existing turbine, the active length of the modules was set to 0.1 m.

Mechanically, the generator was designed to include all bearings necessary to carry the turbine, mounted upwind on the shaft. This resulted in an overall diameter of 2.11 m, and length (not including the rear end bearing) of 0.712 m with a total mass of 4500 kg.

Each stator coil was designed to give an open-circuit voltage of 211 V rms at a nominal speed of 75 rev/min. The relatively high inductance of each coil requires that it be tuned with a capacitor, placed across the terminals of individual rectifier bridges, connected in parallel, so as to achieve full potential output into a DC-link over the working range of speed. Post-production problems with respect to current capabilities of available equipment forming the power conditioning and connection to the grid required that the modules be arranged into two groups, connected in parallel within each group, and then the two groups connected in series to form a DC-link. This is not the ideal mode of connection for the number of existing modules, but it is believed that it will not have any serious effect on performance.

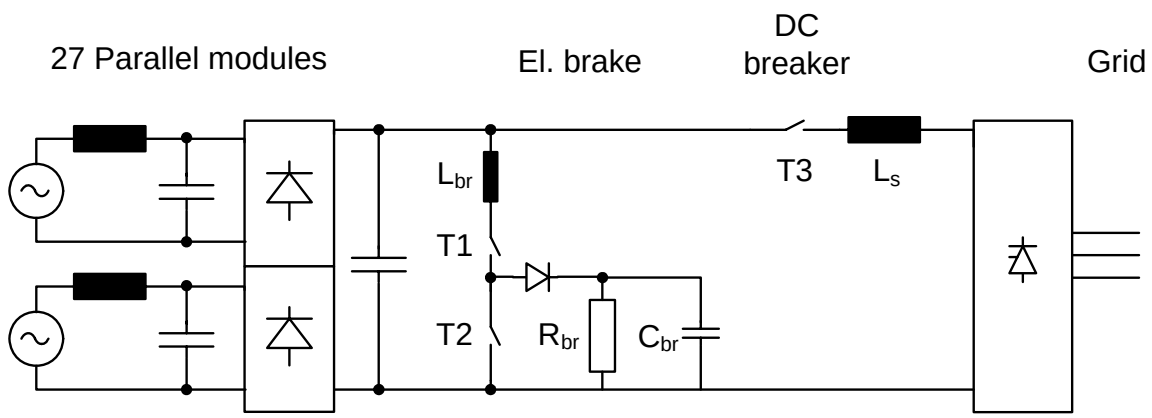

Figure 1: Electrical system with generator, rectifier, brake, DC-breaker and inverter.

2.2 The Frequency Converter and Electrical Brake

The DC-bus interfaces a thyristor based DC/AC inverter via one smoothing inductor. The DC/AC inverter is connected to the grid through a transformer, which makes it possible to operate the converter on a 500 V AC level or 600 V DC level.

In case of a control system failure or loss of grid, two independent brake systems have been implemented for braking the turbine shaft, even in the case of an internal system signal failure. The brake function is obtained without access to the grid. The braking systems are realised as one mechanical and one electrical system [2]. The electrical brake system acts directly on the DC-bus output. The brake current is held at a constant level independent of the generator voltage. This is achieved by switching the resistor on and off and will result in maximum torque control.

Figure 1 shows the main circuit of the DC-link. The transistors T1, T2 and T3 are insulated gate bipolar transistors (IGBT). Electrolyte capacitors are connected directly after the diode rectifier, in order to stabilise the DC-voltage. Without capacitors the voltage will rise uncontrolled when opening the breaker, due to the high inductance in the armature windings of the generator.

In the DC-link, between the brake and the smoothing inductance, a DC-breaker is placed. The breaker consists of a transistor, T3, which can break DC currents up to 200 A. When the electrical brake is activated this breaker will, at the same time, break the current through the thyristor inverter and, thereby, avoid high currents in the inverter.

3. PERFORMANCE

Laboratory tests and wind turbine operation of the generator with a frequency converter are being carried out. These tests cover the whole speed and power range. The tests focus on the following aspects:

1. power-speed performance of the direct driven generator with converter and wind turbine
2. control of the turbine by control of the current of the generator
3. stability of the system

The laboratory system and tests of the generator are reported in more detail in [2,3].

3.1 Operation of the wind turbine

The wind turbine is equipped with a stall regulated turbine. As is well known, the maximum power of a stall regulated turbine is proportional to the speed of the turbine. To obtain good control of the wind turbine, it is necessary that the available generator power is always higher than the turbine power. As can be seen in Figure 2, this is true for the wind turbine up to about 75 rpm. The maximum turbine power, at every rotational speed, was calculated at the most efficient wind speed. The shaft power of the generator was measured in the laboratory.

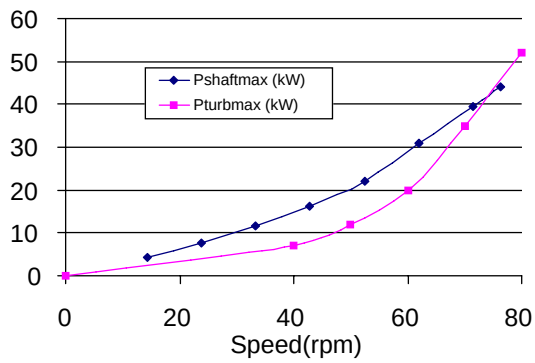

Figure 2: Maximum turbine and maximum generator shaft power as a function of shaft speed.

3.2 Performance of the electrical system

The generator operation characteristics are as follows:

1. The voltage output increases with speed and decreases with increasing current. This is due to the Faraday law of induced voltages and the armature reactions in the stator coils. The unexpected high values for no load voltages at 42 and 52 rpm is due to resonances between the capacitors and the coils in the stator circuit. See Figure 3.
2. The generator torque is proportional to the current and increases slightly with speed, and the maximum torque at different speeds is reached at the same current, approximately 70 A. See Figure 4.

Due to the operation characteristics of the thyristor inverter, the DC-voltage has to be limited to 600 V. In case of higher voltages, the over voltage protection system will activate the electrical brake and stop the turbine.

As can be seen from the above described characteristics, they are influencing each other. Higher turbine speed gives higher turbine torque and, thereby, power, but the higher speed also gives higher voltages. Too high voltages will stop the generator. Higher aerodynamic torque from the turbine requires higher electrodynamic torque and, thereby higher current from the generator, which will decrease the voltages. The conclusion is that there is a

narrow path to follow with increased speed, increased torque, increased current and, consequently, a limited increase in voltage.

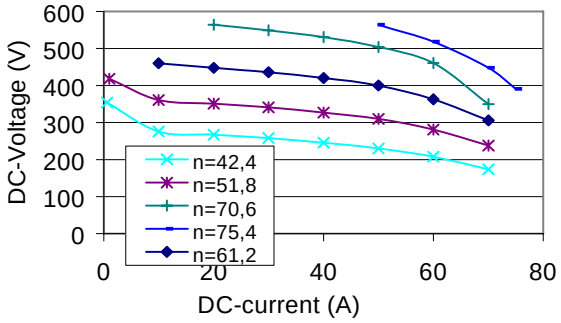

Figure 3: Generator DC-Voltage as a function of DC-current at different speeds.

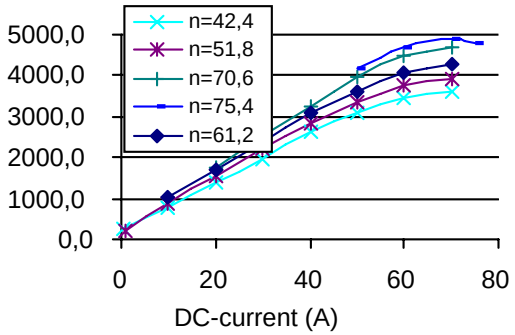

Figure 4: Generator shaft torque as a function of DC-current at different speeds.

3.3 Control of the wind turbine

The experimental experience has been taken from the operation of the wind turbine at Chalmers test station. See Photo 1.

Due to the PM-generator, diode bridges and stall regulation, only the magnitude of DC-current can be directly controlled. The control of the wind turbine is carried out according to the control scheme in Figure 5. The torque reference is translated to a current reference by a model of the electrical system. The control can be divided into different modes of operation.

- **Standby:** The wind turbine is waiting for the right conditions to start up. The turbine cannot start to rotate from aerodynamic forces. A hydraulic system will start the rotation and spin the turbine up to 40 rpm, at which point the wind forces take over. No load is applied below 50 rpm.
- **Ramp up:**. Softly increases the load until it reaches the optimal curve.
- **Optimal:** Within the optimal control there is a standard optimal regulator, which sets the torque reference value by a constant multiplied by the square of the rotor speed. To prevent fast changes in the rotor speed there is also a part influencing the torque reference due to speed changes.
- **Stall:** In Stall mode the turbine stalls and the maximum output power depends on the turbine speed. The operator sets the reference speed. The stall speed controller is a PID-controller with a low pass filter.
- **Retardation:** In the retardation mode, the speed of the turbine is slowed down in a controlled way. At high speed, the current is set to give a maximum generator torque and as the speed slows down, the torque reference is set down. A low pass filter is used to smooth out current changes.

Photo 1: The experimental wind turbine at Chalmers test station.

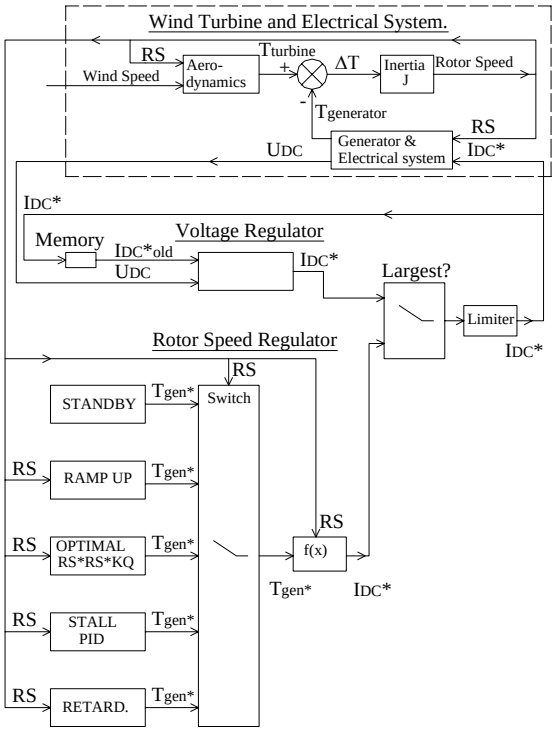

Figure 5: The layout of the different control modes in the wind turbine controller.

The control criteria can be visualised as in Figure 6. The control of the generator dc-current has to follow the black line in the figure to obtain optimal operation between 55 and 71 rpm and to have no over voltage between 71 and 74

rpm and finally limit the speed to 74 rpm to avoid too high power. The different limits are also shown in the figure; Ramp up, Optimal current-speed curve, DC-Voltage controller(current), Maximum torque current limit and stall speed limit.

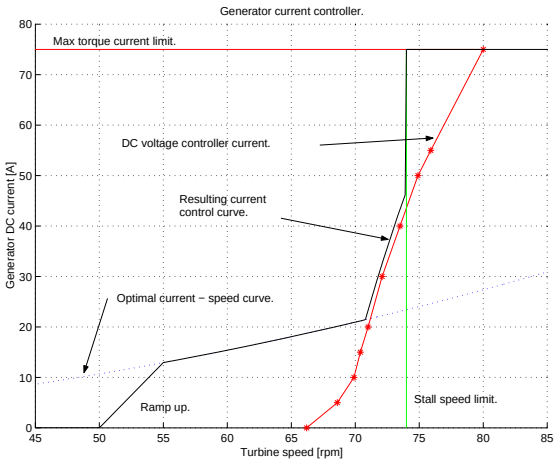

Figure 6: Generator current as a function of the generator speed in different control modes. Theoretical layout.

Figure 7 shows the wind turbine operation results. As can be seen, the electrical control, i.e., the DC-link current, agrees with the theoretical outlines rather well. The electrical brake current control can also be seen in the figure as current varies between 70-80 A. The measured data have been obtained from the operation of the wind turbine for a couple of minutes, including a start and a braking with the electrical brake, at wind speeds around 10-14 m/s.

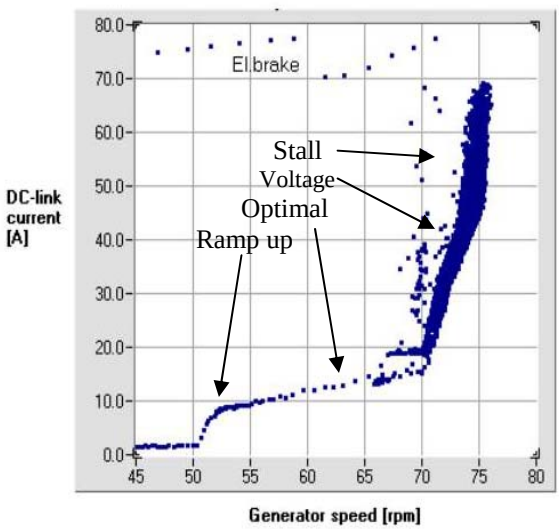

Figure 7: Generator DC-current as a function of the generator speed in different control modes. Results from operation of the wind turbine.

Temperature measurements have been carried out and they show a stable temperature of 48 ^{o}C in the winding of one stator coil. During the single day of operation, the average output power was about 28 kW, the ambient temperature was 12 ^{o}C and the wind speed was between 11 and 14 m/s.

4. CONCLUSIONS

The results of the measurements and the theoretical evaluation reveal good system performance, but there is a need to match the control very closely with the design to optimise the use of the generator.

Due to the diode rectifier and thyristor inverter a DC-current breaker is introduced and due to the absence of aerodynamic brakes it is necessary to have an electric brake. Furthermore, this system with a PM-generator, diode rectifier and stall regulation makes a rather complex control system.

The project also demonstrates that a wind turbine system with a direct driven permanent magnet, low-speed generator and a frequency converter is well suited for up-scaling today's commercial sized wind turbines.

5. FUTURE WORK

The work with the control algorithms will be continued to achieve safe operation and high energy production.

The heating of the generator will be investigated at high power operation.

The voltage change due to speed and power changes is significant in this configuration with parallel capacitors. It will be further investigated if there can be an improvement made by connecting the capacitors in series with the stator coils. Another interesting solution of the problem is to introduce active transistor rectifiers at each stator coil.

6. ACKNOWLEDGEMENTS

The financial support given by the National Energy Administration of Sweden and Göteborg Energi is gratefully acknowledged. The authors would also like to thank Staffan Engström, Alan Williamson, Ed Spooner and Lennart Hansson for their valuable collaboration during the design and laboratory phases of the project.

7. REFERENCES

[1] Spooner E, Williamson A.C. and Catto G. "Modular Design of Permanent-Magnet Generators for Wind Turbines", IEE Proc. EPA, Vol 143, No.5, Sept 1996, pp 388-395.

[2] Carlson O. "Laboratory Measurements of a 40 kW Permanent Magnet Generator", Chalmers University of Technology, Department of Electric Power Engineering, Göteborg, Sweden, March 1999.

[3] Carlson O., Grauers A., Williamson A., Engström S., Spooner E, Design and test of a 40 kW Permanent-Magnet Generator with a frequency converter", EWEC-99, March 1999.

Appendix H

Magnus Ellsén, ”RESEBERÄTTELSE IMTS 2003 PÅ GOTLAND.”, Chalmers tekniska högskola, Göteborg, 2003.

RESEBERÄTTELSE IMTS 2003 PÅ GOTLAND.

Årets Informal Meeting of Test Stations, det 21: a i ordningen, hölls den 24: e till 25: e september i Vattenfalls byggnad på Näsudden, Gotland. Mötet arrangerades på ett föredömligt sätt av Göran Ronsten, FOI.

Mötet samlade 24 deltagare från 8 länder.

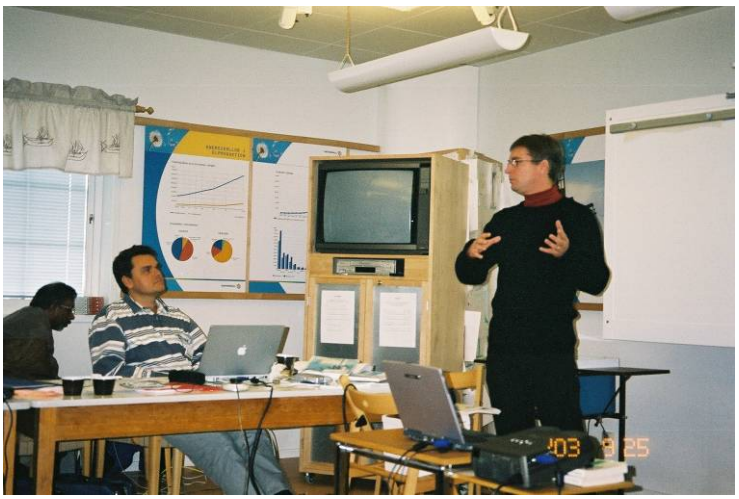

Göran Ronsten, FOI och Mikael Magnusson, SMHI

Mötet inleddes med att Helena Andersson på Gotlands kommun berättade om det omfattande miljöarbetet på Gotland. Man har som långsiktig målsättning att införa kretsloppstänkande och använda sig av enbart förnyelsebar energi. Eko-strategin visar sig till exempel i miljöundervisning redan från daghemsstadiet och uppåt. Högskolan på Gotland har kurser i t.ex. vindkraftteknik. Andra exempel är miljöanpassade hus, biobränslen och biogas i fjärrvärmenätet samt tankstationer med rapsolja (RME) för fordon.

Problemet med tillräckligt noggranna vindmätare belystes av bland annat Jan-Åke Dahlberg, FOI. Han har gjort noggranna undersökningar på skålkorsanemometrar i vindtunnel. Det visade sig att den från anemometern avlästa vindhastigheten varierade så mycket att det krävdes medelvärdesbildning över åtminstone 100 s för att få ett korrekt värde. Som referens användes en specialtillverkad propelleranemometer. Mätningar visade att det inte var hög turbulensintensitet i vindtunneln som gav den instabila avläsningen. Snarare berodde det på den komplexa strömningen runt skålkorset. Standarden för anemometerkalibrering kommer troligen att justeras med hänsyn till de nya rönen.

Jenny Trumars från Chalmers presenterade sitt påbörjade arbete med studier av våglaster på vindkraftverk till havs. Mätningar av våghöjden och mekaniska laster görs på ett av Bockstigen-verken utanför Näsudden.

M.P. Ramesh från The Centre for Wind Energy Technology, C-WET, Indien berättade om deras verksamhet. Provstationen är belägen i staden Chennai i södra Indien. Man har 40 anställda och jobbar med kartläggning av vindresurser, forskning & utveckling, certifiering, testning och informationsspridning.

Från England rapporterades att NEG-Micon har tagit i bruk en stor bladtestanläggning på Isle of Wight. Här testar man sina egna vingar av upp till 40 meters längd. Statiska och dynamiska test utförs.

Förberedelser för båtfärd till Bockstigen vindkraftpark.

Ett nytt center kallat NaREC, New and Renewable Energy Centre, är under uppbyggnad på ett hamnområde i Blyth i nordöstra England. Det är ett stort projekt med bl.a. bladtesthall för blad upp till 70 m längd. Av speciellt intresse är att de håller på att bygga upp ett helt nytt elkraftlaboratorium. Laboratoriet skall inrymma ett ”Low Power Network” Det är nu under uppbyggnad. På längre sikt planerar man även ett ”High Power Network” Exempel på komponenter i LPN är olika typer av generatorer med drivmaskin, svänghjulsenergilager med omriktare, dieselgenerator, vindkraftverk, solcellanläggning och vågkraftverk. Dessa kan kopplas ihop i olika konfigurationer via nätmodeller och transformatorer med lindningskopplare till olika laster. De bilder jag såg på presentationen visade elektriska maskiner på gissningsvis ca 25 kW.

De bygger också upp en testrigg med dubbelmatad asynkronmaskin på ca 25 kW. Syftet är att utveckla reglersystemet. Man är också intresserad av felfall och transientbeteende.

Troels Friis Pedersen från Risö berättade om deras nyetablerade provstation på Jylländska västkusten.

Erwin Werkhoven från ECN berättade om ett nyutvecklat moduluppbyggt distribuerat mätsystem, Dante, som är speciellt lämpat för utvärdering av vindkraftverk. Maximala samplingshastigheten är dock begränsad till 128 Hz vilket gör att det inte är tänkt för elkvalitémätningar.

Hans Ganander, Teknikgruppen AB, berättade om mätsystemet på Bockstigen havsbaserade vindkraftpark.

Petteri Antikainen från VTT, Finland, tog upp frågan om behovet av en provstation i kallt klimat.

Magnus Ellsén, Chalmers presenterade institutionen för eltekniks arbete på vindkraftverks nätinverkan, samt berättade om institutionens provstation.

I samband med mötet gjordes studiebesök i vindkraftverket Näsudden II. Verket har världsrekord i antal producerade kWh. Vi fick även se HVDC light-stationen på Näsudden. Den utgör ena änden av en likströmsförbindelse med Visbytrakten på 80 MW.

Flertalet deltagare följde även med på en båttur ut till de havsbaserade vindkraftverken vid Bockstigen. En ny lejdare med gummirep, konstruerad av Sten Dahlman, Teknikgruppen AB, demonstrerades i de relativt höga vågorna. Idén är att lejdarens nedre ände fastgörs i båten, så att faromomentet att komma i och ur båten minskas.

Mötet avslutades med en diskussion om reglerna för IMTS. Det beslöts att behålla mötets informella karaktär. En lagom storlek är runt 20 – 30 personer. Proceedings kommer endast att göras tillgängliga för deltagare.

C-WET, Indien och Risö, Danmark har erbjudit sig att arrangera nästa möte. En omröstning resulterade i att nästa möte kommer att arrangeras av Risö. Även NaREC erbjöd sig att arrangera ett möte i framtiden.

Kväll på Näsudden.